Biodegradable polymers
based on trimethylene carbonate
for tissue engineering applications

Ana Paula Gomes Moreira Pêgo

Committee

Chairman:	Prof. dr. P.J. Gellings	(U. Twente, The Netherlands)
Promotor/Secretary:	Prof. dr. J. Feijen	(U. Twente, The Netherlands)
Promotor:	Prof. dr. E. Marani	(U. Twente, The Netherlands)
Assistant *Promotor*:	Dr. D.W. Grijpma	(U. Twente, The Netherlands)
Referee:	Dr. A.A. Poot	(U. Twente, The Netherlands)
Members:	Prof. dr. C.A. van Blitterswijk	(U. Twente, The Netherlands)
	Prof. dr. M. Wessling	(U. Twente, The Netherlands)
	Prof. dr. M.A. Barbosa	(U. Porto, Portugal)
	Prof. dr. L.H. Koole	(U. Maastricht, The Netherlands)
	Dr. M.J.A. van Luyn	(U. Groningen, The Netherlands)

Cover design: João Pedro Pêgo
Cover: An extra dimension! Stereogram of a nerve guide.

BIODEGRADABLE POLYMERS BASED ON TRIMETHYLENE CARBONATE FOR TISSUE ENGINEERING APPLICATIONS

DISSERTATION

to obtain

the doctor's degree at the University of Twente,

on the authority of the rector magnificus,

prof. dr. F.A. van Vught,

on account of the decision of the graduation committee,

to be publicly defended

on Wednesday, 27th November 2002 at 13:15

by

Ana Paula Gomes Moreira Pêgo

born on the 30th September 1973

in Porto, Portugal

This dissertation has been approved by:

"Viver por alguém
é deixar partir quem quer ir mais além!
Viver por alguém
é querer apenas que o outro fique bem!"
Viver por alguém, Luís Pedro Silva

To all the ones that let me go in the
pursuit of my dreams….

…. and in memory of my friend Carlos (How I wish you were here...).

Acknowledgements

thank you for the discussions, help, fun and friendship throughout these years. I also learned a lot from you!

To all the members of the graduation committee I would like to leave here a special word of appreciation for accepting the (literally) heavy task of going through my thesis.

I would like to express my sincere gratitude to the ones whose contribution is not evident when reading throughout the thesis but in one way or the other contributed to it by making my life in the lab much easier. Namely to:

- the other staff members of the group for their availability to help me whenever I needed some advice or assistance. In particular I would like to thank Karin for always answering to my "small questions", Hetty for the valuable help in all computer 'crises' and the technical staff - John and Zlata - for the hundred of small things I asked you 'for yesterday' (of course!) and you made your best to have them on time.

- Clemens Padberg, my 'white knight' in technical matters as GPC, DSC, microscopy… I cannot imagine my work without your help! And Mark Smithers for all the SEM sessions in which we spent hours 'searching for THE pores' and where you tried to ease my frustration towards the 'non-porous' structures with a nice cup of coffee!

- my colleagues also performing research, not only in our group but also in the RBT, STEP and MTP groups, for their support (so many times technical) and willingness to help whenever I came with another question, need for translation, request, emergency, crisis, accident, etc, but above all for creating a great working atmosphere. Naming just a few… Audrey, Dries, Eva, Francesca, Laura, Louis, Margie, Meike, Menno, Ralf, Wilco, Ype, Zheng and Zhiyuan…. Without you I would never have had so much to tell in this thesis but also I would not have had so much fun in the many coffee/tea breaks and BBQs and 'learning' how to ice-skate, how to get lost in a triathlon, how to organize a triathlon, how to play tennis and so on…

- Miriam, Cláudia and Zheng for handling so well the challenging task of sharing an office with me, surviving to my very unorganized organization!

But these words of thanks would be incomplete if there was not a space dedicated to the ones that shared my life outside my working hours and were my source of energy when I thought I gave it all – my friends and family.

Nowadays I also feel 'at home' in the Netherlands because of friends like Alby, Cléver, Eva, Fréderic, Kathrin, Kelen, Laura, Laurent, Louis, Marcos, Margie, Meike, Miechel, Vlora among others. Thank you for sharing your lives, traditions and experiences with me, for the moments of fun, for listening (I know myself when I start complaining…) and for supporting me all along!

And there were also those friends that from a distance always kept their fingers crossed for me. Your names are not here but they are in my heart. Thank you. I just want to make an exception to my old friends Gi and Mo. Girls you were great! Thanks for frequently

checking if I was 'alive and kicking', your trust in 'my work capabilities', support and energy were vital!

Audrey and Menno, I dedicate a paragraph to you – my colleagues, friends and *paranimfen* – because you were really involved in nearly every important moment of this Ph.D. By helping me carry the 'burden' of the lab work, the problems, the corrections of the thesis, my health problems, my losses, etc, things were a bit easier to coupe with. And because of you, I will take with me loads of good memories of parties, trips and endless conversations about nothing or everything… What a trio we are of stubborn, arguing, tempered and always critical persons! Eh! Eh! Thanks a lot for everything!

I cannot find words enough to express how much I am grateful to all my family for their support, unconditional love and trust during all these years. You mean the world to me!

Mãe you taught me so much… to not be 'afraid' of asking "Why?", to always look to the bright side of life, to be me, to be… along with so many other little (so useful) things like your passion for the chemistry that surrounds all the moments of our lives. That made all the difference to this adventure, you know? Thank you for being much more than a mother.

Pai your correctness and dedication towards your work are characteristics that served as an inspiration throughout the years. And did you know that by taking me to your work in the years you performed research (I was 2 or 3??) you are responsible for my first memories of being (and feeling well) in a lab?!

João and Zé thank you for being my guardian angels. Your friendship, care, infinite patience and a number of small things, that words cannot describe, helped me in making this dream come true. I am the luckiest sister in the world for having you, such wonderful persons, as brothers!

Avó Alice, Avô Abílio e tio Zé obrigado por serem meus fãns incondicionais!

Macielito, the last words are for you. We made it! Thank you for being (literally) here for me when I needed you the most, for understanding my silences and for reading between the lines when I was feeling down, for cherishing me and for always cheering me up. Above all thanks for respecting my choices and loving me as I am.

Ana Paula

Contents

PART IV - Concluding Remarks

PART I

INTRODUCTION

"Thus, the task is, not so much to see what no one has yet seen; but to think what nobody has yet thought, about that which everybody sees."
Erwin Schrödinger (1887-1961)

CHAPTER 1

Introduction

Biodegradable polymers have great potential in the field of tissue engineering. For many applications, an essential stage of the process is the design and fabrication of three-dimensional scaffolding structures[1,2]. In general, the scaffold should be prepared from a biocompatible material that degrades and resorbs at a controlled rate to match cell and tissue growth *in vitro* and/or *in vivo*. The material should be processable into porous three-dimensional structures with interconnected pores in a variety of shapes and sizes. The mechanical properties of these structures should allow the scaffold to provide the correct micro-stress environment for the cells to develop into the desired tissue. The scaffold should initially act as an adhesive substrate and a physical support for the cells. During proliferation of the cells and production of extracellular matrix, the scaffold should degrade leaving in its place a new patch of tissue.

In the past few years much attention has been given to the use of natural materials like collagen[3,4] and synthetic materials like poly(lactide) (poly(LA)), poly(glycolide) (poly(GA)) and their copolymers[5-8] for the preparation of porous scaffolds. However, these materials have limitations for use in tissue engineering. Collagen has some disadvantages associated with polymers obtained from a natural source such as large batch-to-batch variations upon isolation from biological tissues, as well as restricted versatility in designing devices with specific mechanical properties. Poly(LA) and poly(GA) are rather stiff and brittle materials that can have inappropriate degradation rates for certain applications[9]. In engineering tissues for soft-tissue applications synthetic elastic scaffolds with tunable degradation properties are desirable. Such structures should perform well under long-term cyclic deformation conditions. Degradation during cellular ingrowth of such an elastic scaffold would provide the transfer of stress to occur gradually from the synthetic matrix to the developing tissue.

AIM AND STRUCTURE OF THE THESIS

In this thesis biodegradable, elastomeric porous structures that can serve as scaffolds in soft tissue engineering are prepared. Poly(1,3-trimethylene carbonate) (poly(TMC)) – a rubbery and amorphous polymer – has been taken as a starting point in the design of an alternative synthetic material. In order to obtain materials with suitable mechanical properties and degradation rates, TMC has been copolymerized with either D,L-lactide (DLLA) or ε-caprolactone (CL).

Based on their mechanical properties, degradation rates and the adhesion and proliferation of the appropriate cell types, (co)polymers have been selected and processed into porous scaffolds. Their suitability for heart tissue engineering and peripheral nerve regeneration has been investigated.

This thesis is divided in four parts. In the introductory part, **Chapter 2** provides the reader with an overview of the literature on the tissue engineering approach to nerve reconstruction and cardiomyoplasty. The requirements of these systems and the motivations behind the selection of biodegradable, elastomeric materials for the preparation of scaffolds for these applications are discussed. The potential advantages of TMC-based elastomers over previously described degradable elastomers are also addressed.

The second part of this thesis concerns the synthesis and characterization of TMC based (co)polymer systems. In **Chapter 3** and **Chapter 5** the synthesis of TMC-CL and TMC-DLLA (co)polymers is described, respectively. Statistical copolymers have been obtained by ring-opening polymerization in the melt, using stannous octoate as catalyst. The effect of copolymer composition on the thermal and mechanical properties of the polymers as well as on their hydrophobicity is discussed.

The influence of the catalyst/initiator system and polymerization conditions on the microstructure and physical properties of copolymers of equimolar amounts of TMC and CL is addressed in **Chapter 4**. The two catalyst systems used are stannous octoate and yttrium isopropoxide.

The effect of comonomer type and copolymer composition on the *in vitro* hydrolytic degradation of selected TMC-CL and TMC-DLLA copolymers is reported in **Chapter 6**. The degradation of melt-pressed copolymer films in phosphate buffered saline at pH 7.4 and 37°C has been followed for a period of over two years. The water uptake, molecular weight, weight loss, composition and the

thermal and mechanical properties of the different copolymers have been evaluated as a function of degradation time.

The *in vivo* biodegradation and the tissue response evoked by a TMC-DLLA and a TMC-CL based copolymer as well as that of poly(TMC) is described in **Chapter 7**. Poly(TMC-DLLA) (48:52 mol%) and poly(TMC-CL) (11:89 mol%) have been selected as potential materials for the development of flexible heart constructs and artificial nerve guides, respectively. Polymer disks have been subcutaneously implanted in the back of rats and the tissue reaction at the site of implantation, the implant dimensions as well as mass loss, molecular weight, composition and thermal properties of the polymers have been monitored and evaluated as a function of implantation time.

Poly(TMC), has been often regarded as a rubbery polymer that can not be applied in the biomedical field due to its poor dimensional stability, tackiness and inadequate mechanical properties. In **Chapter 8** we show that very high molecular weight poly(TMC), besides being very flexible, is also tough and shows rubber-like properties despite being totally amorphous and not cross-linked. The dependence of the mechanical properties on the molecular weight of the polymer is discussed. The stress-strain behavior in cyclic loading and the creep behavior of this polymer have been investigated. Finally, in view of possible use of poly(TMC) based implants in the clinic, the possibility to sterilize the scaffolds by means of a standard sterilization method has been studied.

The developed polymers are evaluated with regard to their applicability in tissue engineering in the third part of this thesis.

Based on their mechanical properties and degradation rates, TMC-CL (co)polymers were found suitable for the preparation of artificial nerve guides. The aim of the work presented in **Chapter 9** is to evaluate how variations in polymer composition affect the adhesion, proliferation and morphology of human Schwann cells (SCs) on TMC and CL (co)polymer substrates, with the final goal of using these materials in the preparation of artificial nerve grafts seeded with SCs.

In a preliminary study, poly(CL) has been used as a model polymer to set-up the preparation methods of pliable, two-ply permeable conduits for guided tissue regeneration and to study the effect of the tube structure on the mechanical performance of the conduits. The results of this study are presented in **Appendix A**.

In **Chapter 10** the design of biodegradable and highly flexible two-ply nerve conduits based on elastomeric (co)polymers of TMC and CL is described. This study addresses the effectiveness of permeable conduits in the improvement of

nerve regeneration compared to the performance of comparable non-permeable nerve guides. The *in vivo* performance of these nerve guides has been evaluated in the correction of 6 mm gaps in the rat sciatic nerve model.

The first attempts to further improve guided nerve regeneration by filling the nerve guides with a Schwann cell-containing ECM-derived protein gel are discussed in **Appendix B**.

The TMC-DLLA copolymers were found to degrade faster than TMC-CL copolymers. They can be totally resorbed in approximately one year, fitting the requirements for the preparation of scaffolds for heart tissue engineering better than TMC-CL copolymers. In **Chapter 11** the potential use of copolymers of TMC and DLLA to produce flexible three-dimensional scaffolds for heart tissue engineering is evaluated. Cell-material interactions have been evaluated in terms of adhesion and proliferation of endothelial cells and cardiomyocytes. This study also addresses the preparation and characterization of highly porous structures based on these elastomeric materials. The dimensional stability and degradation of the prepared scaffolds under hydrolytic conditions is also presented.

In the last part of this thesis some concluding remarks and possible directions for further research are given.

Most of the work described in this thesis has been published[10] or will be published in the near future[11-18].

REFERENCES

[1]   Langer R, Vacanti JP. Tissue Engineering. *Science* 1993; 260: 920-926.

[2]   Marler JJ, Upton J, Langer R, Vacanti JP. Transplantation of cells in matrices for tissue regeneration. *Adv Drug Deliv Rev* 1998; 33: 165-182.

[3]   Compton CC, Butler CE, Yannas IV, Warland G, Orgill DP. Organized skin structure is regenerated *in vivo* from collagen-GAG matrices seeded with autologous keratinocytes. *J Invest Dermatol* 1998; 110: 908-916.

[4]   Ceballos D, Navarro X, Dubey N, Wendelschafer-Crabb G, Kennedy WR, Tranquillo RT. Magnetically aligned collagen gel filling a collagen nerve guide improves peripheral nerve regeneration. *Exp Neurol* 1999; 158: 290-300.

[5]   Matsumoto K, Ohnishi K, Sekine T, Ueda H, Yamamoto Y, Kiyotani T, Nakamura T, Endo K, Shimizu Y. Use of a newly developed artificial nerve conduit to assist peripheral nerve regeneration across a long gap in dogs. *ASAIO J* 2000; 46: 415-420.

[6]   Niklason LE, Gao J, Abbott WM, Hirschi KK, Houser S, Marini R, Langer R. Functional arteries grown *in vitro*. *Science* 1999; 284: 489-493.

[7]   Vacanti JP, Morse MA, Saltzman WM, Domb AJ, Perez-Atayde A, Langer R. Selective cell transplantation using bioabsorbable artificial polymers as matrices. *J Pediatr Surg* 1988; 23: 3-9.

[8]   Mooney DJ, Sano K, Kaufmann PM, Majahod K, Schloo B, Vacanti JP, Langer R. Long-term engraftment of hepatocytes transplanted on biodegradable polymer sponges. *J Biomed Mater Res* 1997; 37: 413-420.

[9]   Folliguet TA, Rucker-Martin C, Pavoine C, Deroubaix E, Henaff M, Mercadier JJ, Hatem SN. Adult cardiac myocytes survive and remain excitable during long-term culture on synthetic supports. *J Thorac Cardiovasc Surg* 2001; 121: 510-519.

[10]   Pêgo AP, Poot AA, Grijpma DW, Feijen J. Copolymers of trimethylene carbonate and ε-caprolactone for porous nerve guides: synthesis and properties. *J Biomater Sci Polym Ed* 2001; 12: 35-53. Chapter 3 of this thesis.

[11]   Pêgo AP, Zhong ZY, Dijkstra PJ, Grijpma DW, Feijen J. Influence of catalyst and polymerization conditions on the properties of 1,3-trimethylene carbonate and ε-caprolactone copolymers. *(submitted to Macromol Chem Phys, 2002)* Chapter 4 of this thesis.

[12]   Pêgo AP, Poot AA, Grijpma DW, Feijen J. Physical properties of high molecular weight 1,3-trimethylene carbonate and D,L-lactide copolymers. *(submitted to J Mater Sci: Mater Med, 2002)* Chapter 5 of this thesis.

[13]   Pêgo AP, Poot AA, Grijpma DW, Feijen J. *In vitro* degradation of trimethylene carbonate based (co)polymers. *Macromol Chem Phys (accepted for publication)*. Chapter 6 of this thesis.

[14]   Pêgo AP, van Luyn MJA, Brouwer LA, van Wachem PB, Poot AA, Grijpma DW, Feijen J. *In vivo* behavior of poly(1,3-trimethylene carbonate) and copolymers of 1,3-trimethylene carbonate with D,L-lactide or ε-caprolactone. Degradation and tissue response. *(submitted to J Biomed Mater Res, 2002)* Chapter 7 of this thesis.

[15]   Pêgo AP, Grijpma DW, Feijen J. Extraordinary properties of very high molecular weight poly(1,3-trimethylene carbonate). *(submitted to Macromolecules, 2002)* Chapter 8 of this thesis.

[16]   Pêgo AP, Vleggeert-Lankamp CLAM, Deenen M, Lakke EAJF, Grijpma DW, Poot AA, Marani E, Feijen J. Adhesion and growth of human Schwann cells on trimethylene carbonate (co)polymers. *(submitted to J Biomed Mater Res, 2002)* Chapter 9 of this thesis.

[17]   Pêgo AP, Poot AA, Grijpma DW, Feijen J. Biodegradable elastomeric scaffolds for soft tissue engineering. *J Control Release* (in press).

[18]   Pêgo AP, Siebum B, Gallego y van Seijen XJ, van Luyn MJA, Poot AA, Grijpma DW, Feijen J. Preparation of degradable porous structures based on 1,3-trimethylene

carbonate and D,L-lactide (co)polymers for heart tissue engineering. *(submitted to Tissue Eng, 2002)* Chapter 11 of this thesis.

CHAPTER 2

The need for biodegradable elastomers in tissue engineering

TISSUE ENGINEERING

Every year millions of persons suffer from tissue loss, tissue or organ mal-function or end-stage organ failure as a consequence of trauma, disease, aging or genetic deficiencies. Tissue engineering aims at developing biological substitutes for the restoration, maintenance or improvement of tissue/organ function[1]. Therefore, this interdisciplinary field that applies the principles of engineering and the life sciences, has great potential in increasing the patients' quality of life, overcoming the shortage of donor tissues and organs as well as in reducing the costs of health care.

Tissue engineering involves the development of a functional living tissue using cells, which are normally associated in one way or another with a matrix or scaffolding to guide tissue development[2]. Such matrices or scaffolds can be natural[3-7], artificial[8,9], or a combination of both[10]. Living cells can migrate into the implant after implantation[11,12] or can be incorporated into the matrix under cell culturing conditions prior to implantation[13]. Such cells can either be isolated as fully differentiated cells of the tissue they will recreate[14,15] or be derived from stem cells induced to differentiate into a certain cell type[16,17].

Potentially all mammalian tissues can be engineered. The list of tissue or organ structures under research has grown exponentially in the past few years[18]. Among others, these include bone[19,20], liver[21], intestine[22,23], skin[15,24], cartilage[25,26], peripheral nerves[27-29] and cardiovascular structures[14,30].

We have focused on the engineering of soft tissues, in particular in peripheral nerve reconstruction and cardiac muscle engineering. Both subjects will be discussed separately in the following sections.

ARTIFICIAL NERVE GUIDES

Nerve Reconstruction – Relevance to Health Issues

In 1995, there were more than 50,000 peripheral nerve repair procedures performed in the US. However, these data probably underestimate the number of nerve injuries observed, as not all surgical or traumatic lesions can be repaired[31].

Peripheral nerve injuries can either result from mechanical, thermal or chemical causes or congenital or pathological etiologies. Failure to restore these damaged nerves can lead to the loss of muscle function, impaired sensation and painful neuropathies.

A nerve itself consists of numerous axons, which conduct the action potentials. Axons can be myelinated by Schwann cells or non-myelinated. Schwann cells are the neuronal satellite cells of the peripheral nervous system. These cells have as main functions to serve as supporting elements and to insulate the axons by forming the myelin sheath, which greatly enhances the conduction of the electrical signals. The nerve fibers, in turn, are surrounded by several layers of supporting connective tissue sheaths. In the context of nerve regeneration, the most important structures in these layers are the tubes constituted by the basal lamina, which directly surround the (myelinated) axon and Schwann cells. Nerve lesions can be systematically classified into two types: one in which the basal lamina tubes are still intact and one in which they are severed. The latter may include total nerve disruption[32]. Following injury, Wallerian degeneration is triggered[33]; the (myelinated) axon distal to the lesion degenerates and the content of the basal lamina tube is phagocytosed. Re-establishment of continuity occurs by elongation of the axons proximal to the lesion, of which the cell bodies were not affected. Functional recovery is possible when axons are guided to the target organ by their original basal lamina tubes. When the basal lamina tubes are disrupted, outgrowing axons fail to find their way resulting in neuroma formation. In such cases recovery can only be expected after surgical reconstruction of the anatomical continuity.

Strategies

For centuries, achieving surgical repair of nerves has been the aim of many physicians and surgeons[31,33]. The currently available techniques include the end-to-end coaptation of the nerve ends by suturing and the correction of the nerve defect by means of grafting with an autologous nerve graft, when the extension of the nerve gap prevents the direct approximation of the nerve ends. Several harvest

sites are used to obtain these donor nerve grafts, including the sensory nerves in the lower extremity (e.g. sural nerve). However, the use of an autograft has important side effects, such as the loss of function at the donor graft site and secondary deformities. Furthermore, this approach has limitations in terms of tissue availability and possible mismatch between the damaged nerve and graft dimensions.

The use of allografts is an option, but the obtained results are still inferior to the ones obtained with nerve autografts[34]. Furthermore, when allografts are applied immunosuppression is required[35].

Autologous blood vessels[36-39] and muscle grafts[40-42] have also been used with minor levels of success.

A method of nerve repair that would minimize surgical trauma and operation time, preventing scar tissue formation and which allows manipulation of the regenerative capacity of the proximal stump will be a welcome addition to peripheral nerve surgery. It is worthwhile noticing that, even with the currently applied techniques for the clinical repair of peripheral nerve injuries, the success of regeneration is variable and functional recovery is rarely complete[43]. So there is the need to not only overcome the side effects associated with the use of autologous nerve grafts, but also to improve the outcome of the regeneration process.

Artificial Nerve (Axon) Guides

Much research has been undertaken to use readily available conduits as axon guides, instead of nerve autografts, for bridging gaps in peripheral nerves. The idea behind the use of a nerve guide, i.e. tubulation, is to prevent or reduce the ingrowth of undesirable connective tissue at the site of injury and to bridge the gap, providing directional guidance to the regenerating axons[44].

A variety of conduits have been used[45]. Both biological and synthetic materials are available for structure-supported axonal migration. Among the ones from biological sources [46-48], collagen shows the greatest potential as it can promote migration of the axons and support-cells such as Schwann cells. Synthetic materials are an attractive choice due to the controlled manner in which they can be manufactured and the possibility of tuning their structure, degradation rates and mechanical properties.

Because of its inert and elastic properties, silicone tubing was one of the first and most commonly used synthetic nerve conduits. In 1982, the silicone tube model was introduced and since then has been a tremendously useful tool for studying the basic

biological mechanisms underlying nerve regeneration[49,50]. When a silicone tube was used in rats to bridge a 10-mm gap of the sciatic nerve, the result was the spontaneous formation of a new nerve trunk of more or less normal appearance bridging the defect inside the tube (Figure 1).
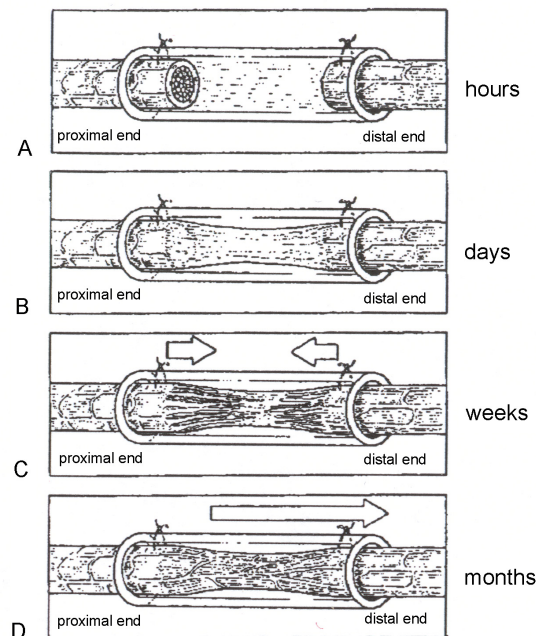
Figure 1. Structural and cellular events in a silicone tuber following implantation. A) Within hours there is accumulation of fluid containing neurotrophic factors and various inflammatory cells. B) Within days a well-organized fibrin matrix containing macrophages is formed between the nerve ends. C) Within weeks the fibrin matrix is invaded by Schwann cells, fibroblasts and microvessels from proximal and distal segments and axons are growing out towards the distal end. D) Within months the nerve fibers mature and the extracellular matrix becomes well organized, resembling a normal, well-vascularized nerve structure (from Dahlin and Lundborg[51]).

It was found that the nature and quality of this structure were related to the distance between the nerve ends. When this distance exceeded 10 to 15 mm, no or inferior regeneration occurred in the tube[49]. The tube was found to be a useful all-or-nothing model for axonal growth, where the effect of various manipulations to the system could be tested[52,53]. Supplementing the silicone conduits with growth factors or extracellular matrix (ECM) proteins, many of which are produced by Schwann cells, improved the regeneration over a 15 mm gap. These stimulating factors include laminin, collagen, fibronectin, nerve growth factor (NGF) and acid and basic fibroblast growth factors[54-57].

Silicone nerve guides have been successfully applied in patients for the correction of different peripheral nerve defects[58]. However, this approach has been criticized due to reports of inflammation and chronic nerve compression after longer implantation periods[59]. In these cases a second operation was required to remove the non-degrading silicone nerve conduits. Nerve guides that degrade upon nerve regeneration and maturation are, therefore, a preferred alternative. Several polymers have been examined for the preparation of degradable nerve guides (Table 1).

Table 1. Biodegradable polymers used in the preparation of peripheral nerve guides

Material	References
Poly(glycolic acid) (PGA)	[60-62]
Poly(lactic acid) (PLA)	[29,63-65]
Copolymers of glycolic cid (GA) and lactic acid (LA)	[65-67]
Copolymers of LA and ε-caprolactone (CL)	[68-71]
Copolymers of GA and trimethylene carbonate (TMC)	[27,72]
Copolymers of TMC and CL	[73]
Poly(phosphazene)s	[74]
Poly(urethane)s	[75,76]
Poly(orthoester)s	[77]
Poly(phosphoester)s	[78]
Poly(hydroxybutyrate)s (PHB)	[79]

From these, only PGA conduits (PGA mesh or PGA crimped conduit) have been used with some success to repair short (<3 cm) nerve gaps in patients[62]. However, for the repair of nerve gaps over clinically relevant distances refinement of these systems is required[27,80].

Regarding the graft material, the polymer should not show a too high degree of swelling or too rapid degradation[81,82]. It is important to select a material as well as processing conditions that will result in a graft that degrades in accordance with the nerve regeneration and maturation rates. The time required for regeneration will be a function of the nerve location, the species, the age of the patient and the gap length. Based on information gained from the silicone tube model, a biodegradable graft for a 10-mm gap in the rat sciatic nerve should maintain its shape and mechanical properties for eight weeks or longer in order to ensure that axons have entered the distal stump and have been myelinated. In humans nerve regeneration proceeds more slowly and often, in the clinical situation, longer nerve gaps need to

be reconstructed. Furthermore, the resorption process should not induce a strong inflammatory tissue response[51] that can lead to unrestricted macrophage invasion and fibrosis. The nerve guide should be flexible, since it will be subjected to flexing during the grafting procedure and during the implantation period, but relatively strong and easy to handle in microsurgery. Non-kinking behavior is another important requirement, as upon bending the graft should not occlude and compress the regenerating nerve[27,62,81,83,84].

Enhancing Nerve Regeneration by Optimizing Guide Design

The studies using polymeric nerve guides suggest that nerve regeneration is influenced by the selected polymer system and that it should not be considered as a passive layer. Manipulation of the physical, chemical and electrical properties of the conduits allows control over the regeneration environment and can result in an enhancement of the regeneration process. Furthermore, mimicking the natural regeneration environment, by incorporating molecular constituents involved in the regeneration process, can also improve the effectiveness of nerve conduits. Figure 2 gives an overview of different refinements to nerve guides that are currently under investigation. The following features will be discussed in detail: permeability, incorporation of support cells and inclusion of ECM constituents.

<u>Permeability</u>

A key physical property of the nerve guide wall is its permeability, as it affects the diffusion of soluble factors into and out of the regeneration environment. A semi-permeable nerve guide allows nutrient exchange across its wall and the transport of tissue fluids outwards avoiding compression of the tissue. However, the tube should allow retention of trophic or growth factors secreted by the severed nerves within the lumen while serving as a barrier to fibroblast infiltration into the regeneration site. Therefore, pore size and porosity are important factors to consider when designing a nerve conduit.

Aebischer et al. reported that semi-permeable silicone tubes with a molecular weight cutoff of 50 kDa showed improved regeneration when compared to impermeable tubes. On the other hand, semi-permeable tubes with a molecular weight cutoff of 100 kDa resulted in impaired nerve regeneration[85,86]. Also with biodegradable systems, studies show that nerve regeneration and reinnervation were considerably improved in semi-permeable tubes when compared to impermeable ones[80,87,88].
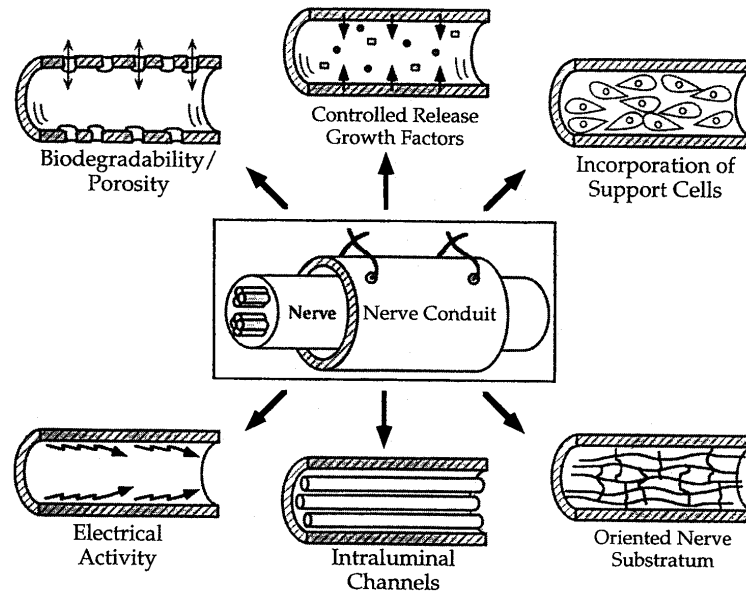
Figure 2. Possible refinements to nerve guidance channels (adapted from Schmidt et al.[89]). Clockwise, from top left: (1) tuning of degradation rates and transmural permeability (see text) (2) the incorporation or the controlled release of growth-promoting molecules[90,91]; (3) the incorporation of support cells (see text); (4) the inclusion of internal-oriented matrices[48]; (5) the incorporation of intraluminal channels/filaments to mimic the fascicular structure of the nerve[92,93]; and (6) use of electrically conductive polymers[94-96] for the preparation of nerve guides.

Nowadays it is recognized that a good incorporation of the implant in the body and enhanced wound healing can be achieved when the porous structure allows in- or overgrowth of tissue[97] with sufficient vascularization[98].

In the development of an effective artificial nerve graft, the guide can have a two-ply structure[75], of the same or different materials, to achieve the desired retention, support and integration properties. A thin, inner layer will function as the primary permeability barrier. A thicker, macroporous external layer would provide the nerve guide with dimensional stability and ensure the strength and toughness of the graft, without compromising its flexibility. This outer layer should be highly porous with interconnected pores to provide a low resistance to in- and out-flowing fluids and to promote ingrowth of tissue.

Seeding of nerve guides with support cells

Peripheral nerve injury triggers a sequence of events in which Schwann cells (SCs) play a critical role in creating a permissive environment for regrowth of injured nerves[99-102]. These cells undergo mitosis in response to nerve trauma, and are

found in nerve gaps following injury in the early stages of nerve regeneration[103]. The alignment of SCs into cords, the bands of Büngner, appears to be a critical step for axon outgrowth[104]. These cords serve as scaffolds for regenerating axons, providing directional orientation by expressing adhesion molecules on the SC plasma membrane. SCs also produce structural and adhesive extracellular matrix molecules such as laminin and collagen and secrete a range of neurotrop(h)ic factors such as NGF. SCs are also responsible for myelination of axons. The incorporation of SCs into a nerve guide, with a few exceptions[105,106], already proved to have a positive effect on the overall regeneration process, increasing peripheral nerve growth, myelination and functional recovery[28,107-111].

Considering the seeding of nerve guides with SCs prior to implantation, it is important to address the isolation procedures of these cells. Unless autologous cells are used, immunosuppression is required, at least in the initial stages of the process. It is possible to isolate and propagate SCs from adult human tissue retrieved at the injury site, although the process takes a few weeks[112]. In this case additional surgery will be necessary to harvest the cells and there would be a time delay between injury and graft implantation[113]. Another approach would be the use of genetically engineered cells (e.g. fibroblasts) modified to produce nerve growth factors[114-116] or bone-marrow stromal cells that can be induced to differentiate into cells with SCs characteristics[117].

Inclusion of extracellular matrix components

Different molecules found on neural cell membranes and in the ECM are known to be involved in nerve regeneration, having important effects on axonal guidance and outgrowth. Several studies show that specific manipulations of the microenvironment of regenerating axons can have a positive effect on the rate and extent of nerve regeneration *in vivo*. Nerve guides containing laminin, fibronectin, collagen and other ECM proteins were tested for the enhancement of nerve repair and compared with results obtained with empty tubes[54,55,98,118-120]. It is important to take into consideration the concentration of ECM elements that are employed, as for example dense protein gels were found to impede regeneration in semi-permeable tubes[121].

The application of functionalized gels with immobilized peptides (RGD sequences) have also been shown to support nerve regeneration *in vivo*[122].

The aim of this thesis with regard to artificial nerve guides is to design biodegradable and highly flexible two-ply nerve conduits for the reconstruction of peripheral nerve defects, based on elastomeric (co)polymers of TMC and CL. The effectiveness of permeable conduits in the improvement of nerve regeneration is compared to the performance of non-permeable comparable nerve guides. The *in vivo* performance of the prepared nerve guides is evaluated in the correction of 6 mm gaps in the rat sciatic nerve model. In addition, the effect of supplementing the nerve conduits with SCs seeded in an ECM protein-based gel is assessed. In line with this concept, the adhesion and proliferation of human SCs on the surface of TMC and CL based (co)polymers is also evaluated.

TISSUE ENGINEERING APPROACH TO CARDIOMYOPLASTY

Congestive Heart Failure and Congenital Heart Defects – Relevance to Health Issues

When a heart attack (myocardial infarction) is not immediately fatal, the damage can still lead to heart failure after some time. Post-ischemic heart failure is a major medical issue in western countries. In 2002 an estimated 1,100,000 Americans will have a heart attack[123]. About 650,000 of these will be first attacks and 450,000 will be recurrent attacks. Over 45% of the people who experience a coronary attack in a given year will die from it[123]. In Figure 3 it can be seen how myocardial ischemia, due to blocking of coronary arteries, can lead to damage of heart tissue.
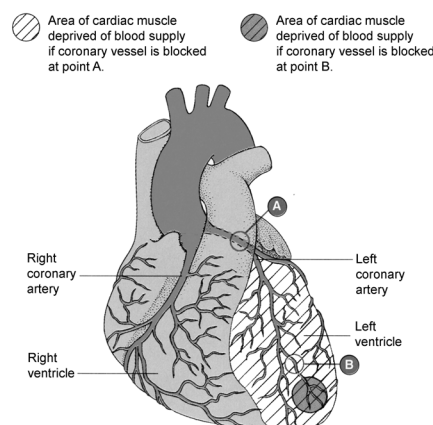
Figure 3. Damage to heart tissue as a result of partial or total blockage of arteries (adapted from[124]). Note that obstruction of a large artery (A) results in a larger damaged area than obstruction of a small artery (B).

Even after the blood supply is (surgically) restored to the affected area, the heart muscle tissue is not able to regenerate. In contrast to long-standing dogma, there is now evidence that supports some proliferation *in vivo* of post-natal mammalian cardiomyocytes, especially after damage to the heart[125]. Clinically however, this level of cardiomycocyte proliferation seems to be unable to rescue damaged muscle[125]. The affected areas heal by scar formation, accompanied by enlargement of the remaining contractile tissue to compensate for the loss of cardiac musculature. Although scar tissue is dynamic, cellular, vascularized, metabolically active and contractile, its different tonus contributes to the congestive dysfunction[126].

Congenital heart defects are part of a number of pathologies that can be present from the time of birth. More deaths occur as a consequence of cardiac defects than as a result of any other birth defect[127]. The incidence of congenital heart diseases, reported in different studies, varies from about 4/1,000 to 50/1,000 live births[128].

Strategies

In spite of improved therapies to avoid ventricle remodeling and stiffening, the prognosis for patients with heart failure due to extensive heart damage is poor. Coronary interventions (bypass) and drugs limit scar formation, but are temporary solutions[129]. Heart transplantation remains the most accepted option in the treatment of heart failure conditions, despite a shortage of donor organs and the required immunosuppressants to avoid rejection of the foreign organ[30,130]. The use of a mechanical ventricular assist device is still restricted to short time periods, bridging the time to transplantation[131].

Several experimental techniques that might provide a more permanent solution are being investigated. In dynamic cardiomyoplasty, latissimus dorsi muscle is mobilized from the chest wall, wrapped around the left and right ventricles and stimulated to contract by means of a pacemaker. The procedure produced inconsistent and moderate effects[132] and interest in it has diminished in recent years[133]. Another technique, molecular myoplasty, aims at the transformation of non-myogenic cells into contractile cells or to induce cardiomyocytes to reenter the cellular cycle. At the moment there is still very little experimental evidence of the feasibility of this technique[132]. A third possibility is cellular myoplasty, which involves grafting myogenic cells into the damaged myocardium[132]. There have been several reports of cell transplantation studies with a variety of cell types[134]. Ventricular and atrial myoblasts[135,136], skeletal myoblasts[137,138] and bone

marrow cells have been demonstrated to engraft in the infarcted myocardium[139-141] and to improve myocardium function with different levels of success. However, injection of cell suspensions may be of little benefit in cases where the local scar tissue is missing or seriously damaged. Especially in case of larger scar areas, implantation of tissue engineered cardiac muscle constructs is thought to be a promising alternative to improve heart function.

Newly grown cardiac tissue can also be used in the treatment of congenital heart defects. Several graft materials, such as expanded poly(tetrafluoroethylene) or glutaraldehyde-treated xenopericardium, are available for surgery of congenital heart defects but their long-term results have been compromised by material related failure and lack of remodeling potential. Other significant factors are their thrombogenicity and lack of contractility[142]. Cell injection is not possible in case of congenital heart defects. An autogenous and contractile bioengineered graft would be ideal for the surgical repair of congenital heart defects, as the living tissue patch is probably able to remodel and therefore to keep up with growth.

Engineering Cardiac Muscle

In the tissue engineering approach to cardiomyoplasty, the appropriate cells are incorporated into a scaffold that is implanted in or onto the scar tissue. The scaffold should initially act as an adhesive substrate and a physical support for the cardiac cells. During proliferation of the cells and production of extra cellular matrix, the scaffold should degrade leaving in its place a new patch of tissue.

Scaffolds

For the preparation of degradable, three-dimensional scaffolds into which cells are incorporated, materials from natural origin, such as collagen and alginates have been the materials of choice[30,135,142-145]. Although results are promising, there are still questions that need to be addressed. These include the improvement of the integration of the newly grown tissue with the host myocardium and the critical mass of 'myocardial' tissue that should be implanted[30]. However, important conclusions were already drawn in terms of material properties. In order to allow the development of myocardial tissue, the scaffold should be made from a biocompatible material that can be reproducibly processed into three-dimensional highly porous structures that are dimensionally stable under physiological conditions. Furthermore, the mechanical properties of the scaffolding material should be adequate to provide the correct micro-stress environment for the cells to

develop the required phenotype and orientation. Therefore, the scaffold should be very flexible and elastic in order to allow the contraction of the growing tissue and to withstand the contractions of the surrounding myocardium after implantation, with no risk of enlargement of the heart compartment(s). When the cells organize, proliferate and produce their own extra cellular matrix the scaffold should degrade to make place for the growing tissue, without inducing a severe tissue reaction. The time period is not yet established during which the maintenance of the shape and the mechanical strength of the scaffolds is required for the reconstruction of the myocardium in humans. In the rat animal model a period of at least 8 weeks seems to be adequate[30].

The use of a synthetic, biodegradable polymer for the preparation of the scaffolds has potential advantages over materials from natural origin. The former allow more possibilities of tuning the macrostructure, mechanical properties and degradation profile of the material. Furthermore, the preparation of scaffolds from synthetic materials is much more versatile. It was proposed that inappropriate sizing of the grafts interferes with the contractility of the viable myocardium[142].

In the class of synthetic degradable polymers only PGA[146,147] and a copolymer of GA and LA (Vicryl)[148] have been used for cardiac muscle engineering. Experiments were only conducted *in vitro*. These polymers can have important drawbacks for use in the preparation of scaffolds for heart tissue engineering such as incompatible mechanical properties, too high rates of degradation and being poor substrates for cell adhesion[147,148].

Cells

The establishment and survival of engineered cardiac grafts based on the use of fetal and neonatal rat cells has been reported. For clinical strategies, however, the use of (autologous) multipotent bone marrow derived cells is necessary.

Although there is now evidence that post-natal mammalian heart cells can proliferate *in vivo*, it remains a challenge to achieve significant proliferation of such cells[125]. An attractive alternative is the use of stem cells to generate new cardiomyocytes. Cells derived from various sources, such as bone marrow derived stem cells, human endothelial progenitor cells or embryonic stem cells may in the future replace lost tissue or malfunctioning specialized cells[125,149,150].

Appropriate vascularization[151] and innervation[152] of cardiac muscle replacement tissue are other issues that will have to be addressed.

The aim of this thesis regarding cardiac muscle engineering is to evaluate the potential use of elastomeric (co)polymers of TMC and DLLA in the preparation of biodegradable and highly flexible scaffolds for cardiac muscle tissue engineering. The cell-material interactions will be evaluated in terms of the adhesion and proliferation of endothelial cells and the growth of cardiomyocytes. This study also addresses the preparation and characterization of highly porous structures based on these elastomeric materials. The dimensional stability and degradation under hydrolytic conditions is also investigated.

BIODEGRADABLE ELASTOMERS

The most widely used synthetic polymers in tissue engineering have been the aliphatic polyesters PGA, PLA and copolymers of GA and LA (PLGA)[9,18,153]. In engineering tissues for soft-tissue applications degradable elastic scaffolds are desirable as discussed in the previous sections. Such materials should perform well under long-term cyclic deformation conditions. Degradation of such an elastic scaffold during cellular ingrowth would provide the opportunity for stress transfer to gradually occur from the synthetic matrix to the tissue components.

While the use of elastomers for medical devices is widespread, going back in time when the rubber industry itself started[154,155], there are relatively few reports on synthetic biodegradable elastomeric polymers that would be suitable for such applications.

Poly(urethane)s

Segmented poly(urethane)s have been employed as elastomeric biomaterials because of their tunable mechanical properties, processability and biocompatibility[155]. Their high mechanical strength and elastomeric properties are attributed to an aggregated semicrystalline structure of hard segments and an amorphous structure of soft segments. Segmented poly(urethane)s are normally used in non-degradable devices[154,155], but their degradation rates can be accelerated to levels relevant for tissue engineering applications by introducing hydrolytically labile segments into the polymer backbone. Degradable poly(ester) soft segments, such as PLA and PCL, have been used for this purpose[156-160]. Alternatively, labile groups can be introduced in the hard segment, through the use of appropriate chain extenders [161,162].

Poly(ester) elastomers

In the class of random poly(ester)s high molecular weight copolymers of L-lactide and CL (50:50 mol%) have been proposed as tough degradable elastomers[163]. The good mechanical properties of the material can be ascribed to the non-random distribution of monomer sequences, resulting in the presence of crystallizable L-lactide sequences. In order to increase the rate of degradation of this copolymer the formation of the slowly degrading crystalline L-lactide domains were prevented by the introduction of D-lactide units[164]. However, this leads to a decrease in the tensile strength of the polymer[165].

Poly(ether ester)s

Multi-block copolymers based on poly(ethylene glycol) (PEG) and poly(butylene terephthalate) (PBT) (PEOT/PBT) are thermoplastic elastomers[166,167]. Variation of the PEOT/PBT block copolymer composition and the molecular weight of the used PEG allow the synthesis of a family of copolymers with a wide range of mechanical properties, degradation profiles and biological behavior [168-171]. Recently, poly(ether ester amide)s (PEEA) have also been proposed as interesting thermoplastic elastomers for tissue engineering[172-174]. In the latter polymers a more hydrolytically labile ester-amide unit replaces the teraphthalate unit.

Poly(hydroxyalkanoate)s

Poly(hydroxyalkanoate)s (PHAs) are a class of natural poly(ester)s that are produced by numerous organisms. Typically, PHAs with short pendant groups are hard crystalline materials, while PHAs with longer pendant groups are elastomeric[175]. From this family of polymers, the most studied elastomers for biomedical applications have been poly(hydroxybutyrate) (PHB) and poly(hydroxybutyrate-co-valerate) (PHBV)[79,175-177].

Poly(phosphazene)s

Poly(phosphazene)s are highly flexible chains of alternating phosphorous-nitrogen (P-N) atoms with two substituents attached to the P-N backbone[155]. Because of the vast array of molecules that can be attached to the polymer backbone via macromolecular substitution on the polymeric intermediate (poly(dichlorophosphazene)), polymers with a wide range of properties can be synthesized. For example, introduction of an amino acid ester side group confers hydrolytic instability to the resultant polymer[178,179], whereas introduction of p-

methylphenoxy side groups increases the hydrophobicity of the poly(phosphazene)[180]. Examples of applications of these polymer systems include nerve guides for nerve regeneration[74] and porous scaffolds for skeletal tissue engineering[181].

<u>Poly(glycerol sebacate)</u>

An elastomeric copolymer of glycerol and sebacic acid has been reported which features a small number of cross-links and hydroxyl groups directly attached to the polymer backbone[182]. Both cross-linking and hydrogen-bonding interactions between the hydroxyl groups contribute to the mechanical properties of the elastomer. The polymer is biocompatible and resorbs completely within 2 months, which makes it an interesting candidate for short-term biomedical applications.

TRIMETHYLENE CARBONATE BASED (CO)POLYMERS

Poly(1,3-trimethylene carbonate) (poly(TMC)) (Figure 4), an aliphatic polycarbonate with a low glass transition temperature of approximately –15ºC[183], has long been known[184].
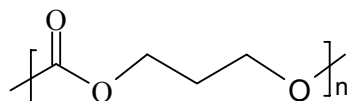
Figure 4. Chemical structure of poly(1,3-trimethylene carbonate) (poly(TMC)).

Poly(TMC) degrades very slowly in an aqueous medium, showing limited molecular weight decrease and mass loss. The *in vivo* degradation of poly(TMC) is still a matter of debate. In one study no decrease of the molecular weight or mass loss of poly(TMC) samples ($\overline{M}_n$ =75,100) was observed after six months of subcutaneous implantation in rats[185]. Another study with poly(TMC) of relatively low molecular weight ($\overline{M}_n$ =19,100) revealed higher degradation rates in comparison with the *in vitro* hydrolysis, suggesting surface degradation with the contribution of enzymatic activity[183].

The suitability of poly(TMC) for the preparation of biomedical implants has been previously evaluated[186]. In was reported that poly(TMC) has a very low modulus and tensile strength. Its poor mechanical properties discouraged any practical

application, other than as a building block in copolymers and blends. Poly(TMC) has been used as a softening unit in stiff and brittle polymers like lactide[187-189] or glycolide[190]. Another application has been the use of TMC to tune the degradation profile of polymer systems for the preparation of matrices for controlled drug release. These included copolymers of TMC with glycolide[191], D,L-lactide (DLLA)[192], CL[185] and blends of TMC and adipic anhydride[193]. As will be shown by our work, very high molecular weight poly(TMC) displays much better physical properties.

It is the aim of this thesis to evaluate the potential use of (co)polymers of TMC with DLLA or CL as degradable elastomers for soft tissue engineering applications. By copolymerisation of TMC with either DLLA or CL we expect to modulate the rates of polymer degradation as well as to modify the material physical properties to suit the requirements for the preparation of scaffolds for cardiac muscle engineering and nerve regeneration. To our knowledge the use of such polymers for the preparation of scaffolds for tissue engineering has never been reported. In view of the previously defined requirements for a synthetic polymer to be applied in soft tissue engineering the use of (co)polymers based on TMC can have important advantages over the polymer systems described in the previous section, namely:

1. TMC, DLLA and CL monomers (and polymers) are FDA (Food and Drugs Administration) approved and already in use in the clinic.
2. The introduction of a carbonate linkage into the polyester backbone can reduce the concentration of acid degradation products resulting from polymer hydrolysis[183,185]. Such acid products can have a detrimental effect on the cells seeded into the scaffold and on the host tissue as well[148,194,195].
3. TMC-DLLA and TMC-CL copolymers are amorphous or have reduced crystallinity. Crystalline debris formed during degradation may cause an undesired late inflammatory response negatively influencing the tissue regeneration process[196]. Therefore, minimal crystallinity is desired.
4. TMC based (co)polymers do not require extensive purification processes. PHAs contain residual proteins, which may induce immune reactions, and high levels of endotoxin, a potent pyrogen[175].

Different examples of catalyst systems used in the copolymerization of the selected monomers can be found in literature[183,187,197-201]. The synthesis of TMC-DLLA and TMC-CL statistical (co)polymers will be performed through ring-opening

polymerization in the melt, using stannous octoate as a catalyst. Stannous octoate was selected as it is highly efficient and commonly used in the preparation of polymers for biomedical applications[202]. Furthermore, this catalyst system allows the preparation of very high molecular weight copolymers[185,188].

The physical properties of a polymer are directly dependent on its molecular weight. By preparing high molecular weight polymers one can obtain materials with good mechanical performance, even after processing methods that can induce chain scission like melt processing[203,204] or sterilization by gamma irradiation[205]. The control of the initial molecular weight of a degradable polymer is also a powerful way to control the time before the onset of mechanical properties and mass loss, as well as the total time for complete polymer resorption[206].

REFERENCES

[1]   Langer R, Vacanti JP. Tissue Engineering. *Science* 1993; 260: 920-926.

[2]   Vacanti JP, Vacanti CA, "The history and scope of tissue engineering" In: Lanza RP, Langer R, Vacanti J. *Principles of tissue engineering*, San Diego, CA: Academic Press; 2000. p 3-7.

[3]   Tranquillo RT, Girton TS, Bromberek BA, Triebes TG, Mooradian DL. Magnetically orientated tissue-equivalent tubes: Application to a circumferentially orientated media-equivalent. *Biomaterials* 1996; 17: 349-357.

[4]   Shapiro L, Cohen S. Novel alginate sponges for cell culture and transplantation. *Biomaterials* 1997; 18: 583-590.

[5]   Butler CE, Orgill DP, Yannas IV, Compton CC. Effect of keratinocyte seeding of collagen-glycosaminoglycan membranes on the regeneration of skin in a porcine model. *Plast Reconstr Surg* 1998; 101: 1572-1579.

[6]   Hadlock TA, Sundback CA, Hunter DA, Vacanti JP, Cheney ML. A new artificial nerve graft containing rolled Schwann cell monolayers. *Microsurgery* 2001; 21: 96-101.

[7]   Mosahebi A, Simon M, Wiberg M, Terenghi G. A novel use of alginate hydrogel as Schwann cell matrix. *Tissue Eng* 2001; 7: 525-534.

[8]   Hubbell JA. Biomaterials in tissue engineering. *Bio-Technol* 1995; 13: 565-576.

[9]   Seal BL, Otero TC, Panitch A. Polymeric biomaterials for tissue and organ regeneration. *Mater Sci Eng R-Rep* 2001; 34: 147-230.

[10]   Meek MF, Robinson PH, Stokroos I, Blaauw EH, Kors G, den Dunnen WFA. Electronmicroscopical evaluation of short-term nerve regeneration through a thin-

walled biodegradable poly(DLLA-ε-CL) nerve guide filled with modified denatured muscle tissue. *Biomaterials* 2001; 22: 1177-1185.

[11] Klompmaker J, Jansen HWB, Veth RPH, Nielsen HKL, Degroot JH, Pennings AJ, Kuijer R. Meniscal repair by fibrocartilage - an experimental-study in the dog. *J Orthop Res* 1992; 10: 359-370.

[12] Valentini RF, "Nerve guidance channels" In: Bronzino JD. *The Biomedical Engineering Handbook*, Boca Raton, FL: CRC Press; 1995. p 1985-1996.

[13] Sikavitsas VI, Bancroft GN, Mikos AG. Formation of three-dimensional cell/polymer constructs for bone tissue engineering in a spinner flask and a rotating wall vessel bioreactor. *J Biomed Mater Res* 2002; 62: 136-148.

[14] Niklason LE, Gao J, Abbott WM, Hirschi KK, Houser S, Marini R, Langer R. Functional arteries grown *in vitro*. *Science* 1999; 284: 489-493.

[15] van Dorp AGM, Verhoeven MCH, Koerten HK, van Blitterswijk CA, Ponec M. Bilayered biodegradable poly(ethylene glycol)/poly(butylene terephthalate) copolymer (polyactive^{TM}) as substrate for human fibroblasts and keratinocytes. *J Biomed Mater Res* 1999; 47: 292-300.

[16] Caplan AI, Bruder SP. Mesenchymal stem cells: building blocks for molecular medicine in the 21st century. *Trends Mol Med* 2001; 7: 259-264.

[17] Bianco P, Robey PG. Stem cells in tissue engineering. *Nature* 2001; 414: 118-121.

[18] Stock UA, Vacanti JP. Tissue engineering: current state and prospects. *Annu Rev Med* 2001; 52: 443-451.

[19] Solchaga LA, Gao JZ, Dennis JE, Awadallah A, Lundberg M, Caplan AI, Goldberg VM. Treatment of osteochondral defects with autologous bone marrow in a hyaluronan-based delivery vehicle. *Tissue Eng* 2002; 8: 333-347.

[20] Mendes SC, Sleijster M, van den Muysenberg A, de Bruijn JD, van Blitterswijk CA. A cultured living bone equivalent enhances bone formation when compared to a cell seeding approach. *J Mater Sci-Mater Med* 2002; 13: 575-581.

[21] Mooney DJ, Sano K, Kaufmann PM, Majahod K, Schloo B, Vacanti JP, Langer R. Long-term engraftment of hepatocytes transplanted on biodegradable polymer sponges. *J Biomed Mater Res* 1997; 37: 413-420.

[22] Choi RS, Vacanti JP. Preliminary studies of tissue-engineered intestine using isolated epithelial organoid units on tubular synthetic biodegradable scaffolds. *Transplant Proc* 1997; 29: 848-851.

[23] Kim SS, Kaihara S, Benvenuto MS, Choi RS, Kim BS, Mooney DJ, Taylor GA, Vacanti JP. Regenerative signals for intestinal epithelial organoid units transplanted on biodegradable polymer scaffolds for tissue engineering of small intestine. *Transplantation* 1999; 67: 227-233.

[24] Compton CC, Butler CE, Yannas IV, Warland G, Orgill DP. Organized skin structure is regenerated *in vivo* from collagen-GAG matrices seeded with autologous keratinocytes. *J Invest Dermatol* 1998; 110: 908-916.

[25] Ishaug-Riley SL, Okun LE, Prado G, Applegate MA, Ratcliffe A. Human articular chondrocyte adhesion and proliferation on synthetic biodegradable polymer films. *Biomaterials* 1999; 20: 2245-2256.

[26] Vunjak-Novakovic G, Obradovic B, Martin I, Freed LE. Bioreactor studies of native and tissue engineered cartilage. *Biorheology* 2002; 39: 259-268.

[27] Mackinnon SE, Dellon AL. A study of nerve regeneration across synthetic (Maxon) and biologic (collagen) nerve conduits for nerve gaps up to 5 cm in the primate. *J Reconstr Microsurg* 1990; 6: 117-121.

[28] Guénard V, Kleitman N, Morrissey TK, Bunge RP, Aebischer P. Syngeneic Schwann cells derived from adult nerves seeded in semipermeable guidance channels enhance peripheral nerve regeneration. *J Neurosci* 1992; 12: 3310-3320.

[29] Evans GRD, Brandt K, Widmer MS, Lu L, Meszlenyi RK, Gupta PK, Mikos AG, Hodges J, Williams J, Gurlek A, Nabawi A, Lohman R, Patrick CW. *In vivo* evaluation of poly(L-lactic acid) porous conduits for peripheral nerve regeneration. *Biomaterials* 1999; 20: 1109-1115.

[30] Leor J, Aboulafia-Etzion S, Dar A, Shapiro L, Barbash IM, Battler A, Granot Y, Cohen S. Bioengineered cardiac grafts. A new approach to repair the infarcted myocardium? *Circulation* 2000; 102: III56-61.

[31] Evans GR. Peripheral nerve injury: a review and approach to tissue engineered constructs. *Anat Rec* 2001; 263: 396-404.

[32] Sunderland S, *Nerve and nerve injuries*. New York, NY: Churchill-Livingstone; 1978.

[33] Seckel BR, Chiu TH, Nyilas E, Sidman RL. Nerve regeneration through synthetic biodegradable nerve guides: regulation by the target organ. *Plast Recon Surg* 1984; 74: 173-181.

[34] Strasberg SR, Mackinnon SE, Genden EM, Bain JR, Purcell CM, Hunter DA, Hay JB. Long-segment nerve allograft regeneration in the sheep model: experimental study and review of the literature. *J Reconstr Microsurg* 1996; 12: 529-537.

[35] Mackinnon SE, Hudson AR, Bain JR, Falk RE, Hunter DA. The peripheral nerve allograft: an assessment of regeneration in the immunosuppressed host. *Plast Recon Surg* 1987; 79: 436-444.

[36] Bryan DJ, Eby PL, Costas PD, Wang K-K, Chakalis DP, Seckel BR. Living artificial organs. *Surg Forum* 1992; 43: 651-652.

[37] Wang K-K, Costas PD, Jones DS, Miller RA, Seckel BR. Sleeve insertion and collagen coating improve nerve regeneration through vein conduits. *J Reconstr Microsurg* 1993; 9: 39-48.

[38] Wang K-K, Costas PD, Bryan DJ, Eby PL, Seckel BR. Inside-out vein graft repair compared with nerve grafting for nerve regeneration in rats. *Microsurgery* 1995; 16: 65-70.

[39] Risitano G, Cavallaro G, Merrino T, Coppolino S, Ruggeri F. Clinical results and thoughts on sensory nerve repair by autologous vein graft in emergency hand reconstruction. *Chir Main* 2002; 21: 194-197.

[40] Glasby MA, Gschmeissner SE, Huang CL-H, de Souza BA. Degenerated muscle grafts used for peripheral nerve repair in primates. *J Hand Surg* 1986; 11B: 347-351.

[41] Brunelli GA, Battiston B, Vigasio A, Brunelli G, Marocolo D. Bridging nerve defects with combined skeletal muscle and vein conduits. *Microsurgery* 1993; 14: 247-251.

[42] Chen L-E, Seaber AV, Urbaniak JR, Murrel GAC. Denaturated muscle as a nerve conduit: a functional, morphological, and electrophysiologic evaluation. *J Reconstr Microsurg* 1994; 10: 137-144.

[43] Thomeer RTWM, Malessy MJA. Surgical repair of brachial-plexus injury. *Clin Neurol Neurosurg* 1993; 95: S65-S72.

[44] Suematsu N. Tubulation for peripheral nerve gap: its history and possibility. *Microsurgery* 1989; 10: 71-74.

[45] Fine EG, Valentini RF, Aebischer P, "Nerve regeneration" In: Lanza RP, Langer R, Vacanti J. *Principles of tissue engineering*, San Diego, CA: Academic Press; 2000. p 785-798.

[46] Favaro G, Bortolami MC, Cereser S, Dona M, Pastorello A, Callegaro L, Fiori M. Peripheral nerve regeneration through a novel bioresorbable nerve guide. *ASAIO Trans* 1990; 36: M291-M294.

[47] Archibald SJ, Shefner J, Krarup C, Madison RD. Monkey median nerve repaired by nerve graft or collagen nerve guide tube. *J Neurosci* 1995; 15: 4109-4123.

[48] Ceballos D, Navarro X, Dubey N, Wendelschafer-Crabb G, Kennedy WR, Tranquillo RT. Magnetically aligned collagen gel filling a collagen nerve guide improves peripheral nerve regeneration. *Exp Neurol* 1999; 158: 290-300.

[49] Lundborg G, Dahlin LB, Danielsen N, Gelberman RH, Longo FM, Powell HC, Varon S. Nerve regeneration in silicone chambers: influence of gap length and of distal stump components. *Exp Neurol* 1982; 76: 361-375.

[50] Lundborg G, Longo FM, Varon S. Nerve regeneration model and trophic factors *in vivo*. *Brain Res* 1982; 232: 157-161.

[51] Dahlin LB, Lundborg G. Use of tubes in peripheral nerve repair. *Neurosurg Clin N Am* 2001; 12: 341-352.

[52] Williams LR, Powell HC, Lundborg G, Varon S. Competence of nerve tissue as distal insert promoting nerve regeneration in a silicone chamber. *Brain Res* 1984; 293: 201-211.

[53] Williams LR, Varon S. Modification of fibrin matrix formation in situ enhances nerve regeneration in silicone chambers. *J Comp Neurol* 1985; 231: 209-220.

[54] Madison RD, Da Silva CF, Dikkes P. Entubulation repair with protein additives increases the maximum nerve gap distance successfully bridged with tubular prostheses. *Brain Res* 1988; 447: 325-334.

[55] Woolley AL, Hollowell JP, Rich KM. Fibronectin-laminin combination enhances peripheral nerve regeneration across long gaps. *Otolaryngol Head Neck Surg* 1990; 103: 509-518.

[56] Fujimoto E, Mizoguchi A, Hanada K, Yajima M, Ide C. Basic fibroblast growth factor promotes extension of regenerating axons of peripheral nerve. *In vivo* experiments using a Schwann cell basal lamina tube model. *J Neurocytol* 1997; 26: 511-528.

[57] Santos X, Rodrigo J, Hontanilla B, Bilbao G. Regeneration of the motor component of the rat sciatic nerve with local administration of neurotrophic growth factor in silicone chambers. *J Reconstr Microsurg* 1999; 15: 207-213.

[58] Lundborg G, Rosen B, Dahlin L, Danielsen N, Holmberg J. Tubular *versus* conventional repair of median and ulnar nerves in the human forearm: early results from a prospective, randomized, clinical study. *J Hand Surg [Am]* 1997; 22: 99-106.

[59] Merle M, Dellon AL, Campbell JN, Chang PS. Complications from silicon-polymer intubulation of nerves. *Microsurgery* 1989; 10: 130-133.

[60] Madison R, Sidman RL, Nyilas E, Chiu T-H, Greatorex D. Nontoxic nerve guide tubes support neovascular growth in transected rat optic nerve. *Exp Neurol* 1984; 86: 448-461.

[61] Kiyotani T, Teramachi M, Takimoto Y, Nakamura T, Shimizu Y, Endo K. Nerve regeneration across a 25-mm gap bridged by a polyglycolic acid-collagen tube: a histological and electrophysiological evaluation of regenerated nerves. *Brain Res* 1996; 740: 66-74.

[62] Mackinnon SE, Dellon AL. Clinical nerve reconstruction with a bioabsorbable polyglycolic acid tube. *Plast Reconstr Surg* 1990; 85: 419-424.

[63] Luciano RM, Zavaglia CAD, Duek EAD. Preparation of bioabsorbable nerve guide tubes. *Artif Organs* 2000; 24: 206-208.

[64] Evans GRD, Brandt K, Niederbichler AD, Chauvin P, Hermann S, Bogle M, Otta L, Wang B, Patrick CW. Clinical long-term *in vivo* evaluation of poly(L-lactic acid) porous conduits for peripheral nerve regeneration. *J Biomater Sci-Polym Ed* 2000; 11: 869-878.

[65] Hadlock T, Elisseeff J, Langer R, Vacanti J, Cheney M. A tissue-engineered conduit for peripheral nerve repair. *Arch Otolaryngol Head Neck Surg* 1998; 124: 1081-1086.

[66] Gautier SE, Oudega M, Fragoso M, Chapon P, Plant GW, Bunge MB, Parel JM. Poly(alpha-hydroxyacids) for application in the spinal cord: resorbability and biocompatibility with adult rat Schwann cells and spinal cord. *J Biomed Mater Res* 1998; 42: 642-654.

[67] Evans GRD, Brandt K, Widmer M, Gürlek A, Savel T, Gupta P, Lohman R, Williams J, Hodges J, Nabawi A, Patrick C, Mikos AG, "Tissue engineered conduits: the use of biodegradable poly-DL-lactic-co-glycolic acid (PLGA) scaffolds in peripheral nerve regeneration" In: Stark GE, Horch R, Tanczos E. *Biological matrices and tissue reconstruction*, Berlin: Spinger; 1998. p 225-235.

[68] den Dunnen WFA, Schakenraad JM, Zondervan GJ, Pennings AJ, van der Lei B, Robinson PH. A new PLLA/PCL copolymer for nerve regeneration. *J Mater Sci: Mater Med* 1993; 4: 521-525.

[69] den Dunnen WFA, Stokroos I, Blaauw EH, Holwerda A, Pennings AJ, Robinson PH, Schakenraad JM. Light-microscopic and electron-microscopic evaluation of short term nerve regeneration using a biodegradable poly(DL-lactide-ε−caprolactone) nerve guide. *J Biomed Mater Res* 1996; 31: 105-115.

[70] Aldini NN, Fini M, Rocca M, Giavaresi G, Giardino R. Guided regeneration with resorbable conduits in experimental peripheral nerve injuries. *Int Orthop* 2000; 24: 121-125.

[71] Perego G, Cella GD, Aldini NN, Rocca M, Giardino R. Preparation of a new nerve guide from a poly(L-Lactide-co-6-caprolactone). *Biomaterials* 1994; 15: 189-193.

[72] Rosen JM, Padilla JA, Nguyen KD, Siedman J, Pham HN. Artificial nerve graft using glycolide trimethylene carbonate as a nerve conduit filled with collagen compared to sutured autograft in a rat model. *J Rehabil Res Dev* 1992; 29: 1-12.

[73] Fabre T, Schappacher M, Bareille R, Dupuy B, Soum A, Bertrand-Barat J, Baquey C. Study of a (trimethylenecarbonate-co-ε-caprolactone) polymer - Part 2: *in vitro* cytocompatibility analysis and *in vivo* ED1 cell response of a new nerve guide. *Biomaterials* 2001; 22: 2951-2958.

[74] Langone F, Lora S, Veronese FM, Caliceti P, Parnigotto PP, Valenti F, Palma G. Peripheral nerve repair using a poly(organo)phosphazene tubular prosthesis. *Biomaterials* 1995; 16: 347-353.

[75] Hoppen HJ, Leenslag JW, Pennings AJ, van der Lei B, Robinson PH. Two-ply biodegradable nerve guide: basic aspects of design, construction and biological performance. *Biomaterials* 1990; 11: 286-290.

[76] Soldani G, Varelli G, Minnocci A, Dario P. Manufacturing and microscopical characterisation of polyurethane nerve guidance channel featuring a highly smooth internal surface. *Biomaterials* 1998; 19: 1919-1924.

[77] Bora FW, Jr., Bednar JM, Osterman AL, Brown MJ, Sumner AJ. Prosthetic nerve grafts: a resorbable tube as an alternative to autogenous nerve grafting. *J Hand Surg [Am]* 1987; 12: 685-692.

[78] Wang S, Wan ACA, Xu X, Gao S, Mao H-Q, Leong KW, Yu H. A new nerve guide conduit material composed of a biodegradable poly(phosphoester). *Biomaterials* 2001; 22: 1157-1169.

[79] Young RC, Wiberg M, Terenghi G. Poly-3-hydroxybutyrate (PHB): a resorbable conduit for long-gap repair in peripheral nerves. *Br J Plast Surg* 2002; 55: 235-240.

[80] Rodriguez FJ, Gomez N, Perego G, Navarro X. Highly permeable polylactide-caprolactone nerve guides enhance peripheral nerve regeneration through long gaps. *Biomaterials* 1999; 20: 1489-1500.

[81] Henry EW, Chiu TH, Nyilas E, Brushart TM, Dikkes P, Sidman RL. Nerve regeneration through biodegradable polyester tubes. *Exp Neurol* 1985; 90: 652-676.

[82] den Dunnen WFA, van der Lei B, Robinson PH, Holwerda A, Pennings AJ, Schakenraad JM. Biological performance of a degradable poly(DL-lactide-ε–caprolactone) nerve guide: Influence of tube dimensions. *J Biomed Mater Res* 1995; 29: 757-766.

[83] Buti M, Verdu E, Labrador RO, Vilches JJ, Fores J, Navarro X. Influence of physical parameters of nerve chambers on peripheral nerve regeneration and reinnervation. *Exp Neurol* 1996; 137: 26-33.

[84] Levi AD, Sonntag VK, Dickman C, Mather J, Li RH, Cordoba SC, Bichard B, Berens M. The role of cultured Schwann cell grafts in the repair of gaps within the peripheral nervous system of primates. *Exp Neurol* 1997; 143: 25-36.

[85] Aebischer P, Guenard V, Winn SR, Valentini RF, Galletti PM. Blind-ended semipermeable guidance channels support peripheral- nerve regeneration in the absence of a distal nerve stump. *Brain Res* 1988; 454: 179-187.

[86] Aebischer P, Guenard V, Brace S. Peripheral-nerve regeneration through blind-ended semipermeable guidance channels - effect of the molecular-weight cutoff. *J Neurosci* 1989; 9: 3590-3595.

[87] Aebischer P, Valentini RF, Winn SR, Kunz S, Sasken H, Galletti PM. Regeneration of transected sciatic nerves through semi-permeable nerve guidance channels. Effects of extracellular matrix protein additives. *ASAIO Trans* 1986; 32: 474-477.

[88] Kim DH, Connolly SE, Zhao S, Beuerman RW, Voorhies RM, Kline DG. Comparison of macropore, semipermeable, and nonpermeable collagen conduits in nerve repair. *J Reconstr Microsurg* 1993; 9: 415-420.

[89] Hudson TW, Evans GR, Schmidt CE. Engineering strategies for peripheral nerve repair. *Clin Plast Surg* 1999; 26: 617-628, ix.

[90] Robinson PH, van der Lei B, Hoppen HJ, Leenslang JW, Pennings AJ, Nieuwenhuis P. Nerve regeneration through a two-ply biodegradable nerve guide in the rat and the Influence of ACTH4-9 nerve growth factor. *Microsurgery* 1991; 12: 412-419.

[91] Sakiyama-Elbert SE, Hubbell JA. Controlled release of nerve growth factor from a heparin- containing fibrin-based cell ingrowth matrix. *J Control Release* 2000; 69: 149-158.

[92] Hadlock T, Sundback C, Hunter D, Cheney M, Vacanti JP. A polymer foam conduit seeded with Schwann cells promotes guided peripheral nerve regeneration. *Tissue Eng* 2000; 6: 119-127.

[93] Arai T, Lundborg G, Dahlin LB. Bioartificial nerve graft for bridging extended nerve defects in rat sciatic nerve based on resorbable guiding filaments. *Scand J Plast Reconstr Surg Hand Surg* 2000; 34: 101-108.

[94] Aebischer P, Valentini RF, Dario P, Domenici C, Galletti PM. Piezoelectric guidance channels enhance regeneration in the mouse sciatic nerve after axotomy. *Brain Res* 1987; 436: 165-168.

[95] Schmidt CE, Shastri VR, Vacanti JP, Langer R. Stimulation of neurite outgrowth using an electrically conducting polymer. *Proc Natl Acad Sci USA* 1997; 94: 8948-8953.

[96] Ceballos D, Valero-Cabre A, Valderrama E, Schuttler M, Stieglitz T, Navarro X. Morphologic and functional evaluation of peripheral nerve fibers regenerated through polyimide sieve electrodes over long-term implantation. *J Biomed Mater Res* 2002; 60: 517-528.

[97] Hinrichs W. "Porous polymer structures for tissue engineering" Ph.D. Thesis. University of Twente, Enschede, The Netherlands. 1992.

[98] Rosen JM, Padilla JA, Nguyen KD, Padilla MA, Sabelman EE, Pham HN. Artificial nerve graft using collagen as an extracellular matrix for nerve repair compared with sutured autograft in a rat model. *Ann Plast Surg* 1990; 25: 375-387.

[99] Terenghi G. Peripheral nerve injury and regeneration. *Histol Histopathol* 1995; 10: 709-718.

[100] Son Y-J, Thompson WJ. Schwann cell processes guide regeneration of peripheral axons. *Neuron* 1995; 14: 125-132.

[101] Fu SY, Gordon T. The cellular and molecular basis of peripheral nerve regeneration. *Mol Neurobiol* 1997; 14: 67-116.

[102] Frostick SP, Yin Q, Kemp GJ. Schwann cells, neurotrophic factors, and peripheral nerve regeneration. *Microsurgery* 1998; 18: 397-405.

[103] Terenghi G, Calder JS, Birch R, Hall SM. A morphological study of Schwann cells and axonal regeneration in chronically transected human peripheral nerves. *J Hand Surg [Br]* 1998; 23: 583-587.

[104] Torigoe K, Tanaka H-F, Takahashi A, Awaya A, Hashimoto K. Basic behavior of migratory Schwann cells in peripheral nerve regeneration. *Exp Neurol* 1996; 137: 301-308.

[105] Bryan DJ, Holway AH, Wang KK, Silva AE, Trantolo DJ, Wise D, Summerhayes IC. Influence of glial growth factor and Schwann cells in a bioresorbable guidance channel on peripheral nerve regeneration. *Tissue Eng* 2000; 6: 129-138.

[106] Evans GRD, Brandt K, Katz S, Chauvin P, Otto L, Bogle M, Wang B, Meszlenyi RK, Lu L, Mikos AG. Bioactive poly(L-lactic acid) conduits seeded with Schwann cells for peripheral nerve regeneration. *Biomaterials* 2002; 23: 841-848.

[107] Keeley R, Atagi T, Sabelman E, Padilla J, Kadlcik P, Agras J, Eng L, Wiedman T-W, Nguyen K, Sudekum A, Rosen J. Synthetic nerve graft containing collagen and synthetic Schwann cells improves functional, electrophysiological, and histological parameters of peripheral nerve regeneration. *Restor Neurol Neurosci* 1993; 5: 353-366.

[108] Kim DH, Connolly SE, Kline DG, Voorhies RM, Smith A, Powell M, Yoes T, Daniloff JK. Labeled Schwann cell transplants *versus* sural nerve grafts in nerve repair. *J Neurosurg* 1994; 80: 254-260.

[109] Bryan DJ, Wang RR, Chakalis-Haley DP. Effect of Schwann cells in the enhancement of pheripheral-nerve regeneration. *J Recon Microsurg* 1996; 12: 439-446.

[110] Ansellin AD, Fink T, Davey DF. Peripheral nerve regeneration through nerve guides seeded with adult Schwann cells. *Neuropathol Appl Neurobiol* 1997; 23: 387-398.

[111] Rodriguez FJ, Verdu E, Ceballos D, Navarro X. Nerve guides seeded with autologous Schwann cells improve nerve regeneration. *Exp Neurol* 2000; 161: 571-584.

[112] Morrissey TK, Kleitman N, Bunge RP. Isolation and functional characterization of Schwann cells derived from adult peripheral nerve. *J Neurosci* 1991; 11: 2433-2442.

[113] Holtzer CAJ, Feirabend HKP, Marani E, Thomeer RTWM. Ultrastructural and quantitative motoneuronal changes after ventral root avulsion favor early surgical repair. *Arch Physiol Biochem* 2000; 108: 293-309.

[114] Gage FH, Kawaja MD, Fisher LJ. Genetically modified cells - applications for intracerebral grafting. *Trends Neurosci* 1991; 14: 328-333.

[115] Patrick CW, Zheng B, Schmidt M, Herman S, Chauvin P, Fan Z, Stark B, Evans GRD. Dermal fibroblasts genetically engineered to release nerve growth factor. *Ann Plast Surg* 2001; 47: 660-665.

[116] Patrick CW, Zheng B, Wu XM, Gurtner G, Barlow M, Koutz C, Chang D, Schmidt M, Evans GRD. Muristerone A - induced nerve growth factor release from genetically engineered human dermal fibroblasts for peripheral nerve tissue engineering. *Tissue Eng* 2001; 7: 303-311.

[117] Dezawa M, Takahashi I, Esaki M, Takano M, Sawada H. Sciatic nerve regeneration in rats induced by transplantation of *in vitro* differentiated bone-marrow stromal cells. *Eur J Neurosci* 2001; 14: 1771-1776.

[118] Bailey SB, Eichler ME, Villadiego A, Rich KM. The influence of fibronectin and laminin during Schwann cell migration and peripheral nerve regeneration through silicon chambers. *J Neurocytol* 1993; 22: 176-184.

[119] Wells MR, Kraus K, Batter DK, Blunt DG, Weremowitz J, Lynch SE, Antoniades HN, Hansson H-A. Gel matrix vehicles for growth factor application in nerve gap injuries repaired with tubes: a comparison of Biomatrix, collagen, and methylcellulose. *Exp Neurol* 1997; 146: 395-402.

[120] Chen YS, Hsieh CL, Tsai CC, Chen TH, Cheng WC, Hu CL, Yao CH. Peripheral nerve regeneration using silicone rubber chambers filled with collagen, laminin and fibronectin. *Biomaterials* 2000; 21: 1541-1547.

[121] Valentini RF, Aebischer P, Winn SR, Galletti PM. Collagen- and laminin-containing gels impede peripheral nerve regeneration through semipermeable nerve guidance channels. *Exp Neurobiol* 1987; 98: 350-356.

[122] Borkenhagen M, Clemence JF, Sigrist H, Aebischer P. Three-dimensional extracellular matrix engineering in the nervous system. *J Biomed Mater Res* 1998; 40: 392-400.

[123] American-Heart-Association, *2002 Heart and stroke statistical update*. Dallas, TX: American Heart Association; 2001.

[124] Sherwood L, *Human physiology: from cells to systems*. Belmont, CA: Wadsworth Publishing Company; 1997.

[125] Grounds MD, White JD, Rosenthal N, Bogoyevitch MA. The role of stem cells in skeletal and cardiac muscle repair. *J Histochem Cytochem* 2002; 50: 589-610.

[126] Sun Y, Weber KT. Infarct scar: a dynamic tissue. *Cardiovasc Res* 2000; 46: 250-256.

[127] Yang Q, Khoury MJ, Mannino D. Trends and patterns of mortality associated with birth defects and genetic diseases in the United States, 1979-1992: an analysis of multiple-cause mortality data. *Genet Epidemiol* 1997; 14: 493-505.

[128] Hoffman JIE, Kaplan S. The incidence of congenital heart disease. *J Am Coll Cardiol* 2002; 39: 1890-1900.

[129] Rosenthal N, Tsao L. Helping the heart to heal with stem cells. *Nat Med* 2001; 7: 412-413.

[130] El Oakley RM, Ooi OC, Bongso A, Yacoub MH. Myocyte transplantation for myocardial repair: a few good cells can mend a broken heart. *Ann Thorac Surg* 2001; 71: 1724-1733.

[131] Pennington DG, Smedira NG, Samuels LE, Acker MA, Curtis JJ, Pagani FD. Mechanical circulatory support for acute heart failure. *Ann Thorac Surg* 2001; 71: S56-59.

[132] Hagege A, Menasche P. Cellular cardiomyoplasty: a new hope in heart failure? *Heart* 2000; 84: 465-466.

[133] Park SE, Cmolik BL, Lazzara RR, Trumble DR, Magovern JA. Right latissimus dorsi cardiomyoplasty augments left ventricular systolic performance (Update). *Ann Thorac Surg* 2001; 71: 2077-2078.

[134] Kessler PD, Byrne BJ. Myoblast cell grafting into heart muscle: cellular biology and potential applications. *Annu Rev Physiol* 1999; 61: 219-242.

[135] Akins RE, Boyce RA, Madonna ML, Schroedl NA, Gonda SR, McLaughlin TA, Hartzell CR. Cardiac organogenesis *in vitro*: reestablishment of three-dimensional tissue architecture by dissociated neonatal rat ventricular cells. *Tissue Eng* 1999; 5: 103-118.

[136] Sakai T, Li RK, Weisel RD, Mickle DA, Kim EJ, Tomita S, Jia ZQ, Yau TM. Autologous heart cell transplantation improves cardiac function after myocardial injury. *Ann Thorac Surg* 1999; 68: 2074-2080.

[137] Vilquin JT, Menasche P, Robert I, Ternaux B, Hagege A, Scorsin M, Benbunan M, Schwartz K, Marolleau JP. Clinical report of autologous muscle cell transplantation for treatment of ischemic heart failure. *Blood* 2000; 96: 1828.

[138] Pouzet B, Vilquin JT, Hagege AA, Scorsin M, Messas E, Fiszman M, Schwartz K, Menasche P. Factors affecting functional outcome after autologous skeletal myoblast transplantation. *Ann Thorac Surg* 2001; 71: 844-850.

[139] Tomita S, Li RK, Jia ZQ, Mickle DAG, Weisel RD, Sakai T, Kim EJ, Yokomuro H, Watarida S, Sakakibara Y, Yau TM. Autotransplanted smooth muscle cells can survive in the scar and improve function of damaged heart. *Circulation* 1999; 100: 3504.

[140] Wang JS, Shum-Tim D, Galipeau J, Chedrawy E, Eliopoulos N, Chiu RC. Marrow stromal cells for cellular cardiomyoplasty: feasibility and potential clinical advantages. *J Thorac Cardiovasc Surg* 2000; 120: 999-1005.

[141] Orlic D, Kajstura J, Chimenti S, Jakoniuk I, Anderson SM, Li B, Pickel J, McKay R, Nadal-Ginard B, Bodine DM, Leri A, Anversa P. Bone marrow cells regenerate infarcted myocardium. *Nature* 2001; 410: 701-705.

[142] Li RK, Jia ZQ, Weisel RD, Mickle DAG, Choi A, Yau TM. Survival and function of bioengineered cardiac grafts. *Circulation* 1999; 100: 63-69.

[143] Eschenhagen T, Fink C, Remmers U, Scholz H, Wattchow J, Weil J, Zimmermann W, Dohmen HH, Schafer H, Bishopric N, Wakatsuki T, Elson EL. Three-dimensional reconstitution of embryonic cardiomyocytes in a collagen matrix: a new heart muscle model system. *FASEB J* 1997; 11: 683-694.

[144] Sakai T, Li RK, Weisel RD, Mickle DA, Kim ET, Jia ZQ, Yau TM. The fate of a tissue-engineered cardiac graft in the right ventricular outflow tract of the rat. *J Thorac Cardiovasc Surg* 2001; 121: 932-942.

[145] van Luyn MJA, Tio RA, Gallego y van Seijen XJ, Plantinga JA, de Leij LFMH, de Jongste MJL, van Wachem PB. Cardiac tissue engineering: Characteristics of in unison contracting two- and three-dimensional neonatal rat ventricle cell (co)-cultures. *Biomaterials* (in press).

[146] Carrier RL, Papadaki M, Rupnick M, Schoen FJ, Bursac N, Langer R, Freed LE, Vunjak-Novakovic G. Cardiac tissue engineering: cell seeding, cultivation parameters, and tissue construct characterization. *Biotechnol Bioeng* 1999; 64: 580-589.

[147] Papadaki M, Bursac N, Langer R, Merok J, Vunjak-Novakovic G, Freed LE. Tissue engineering of functional cardiac muscle: molecular, structural, and electrophysiological studies. *Am J Physiol Heart Circ Physiol* 2001; 280: H168-178.

[148] Folliguet TA, Rucker-Martin C, Pavoine C, Deroubaix E, Henaff M, Mercadier JJ, Hatem SN. Adult cardiac myocytes survive and remain excitable during long-term culture on synthetic supports. *J Thorac Cardiovasc Surg* 2001; 121: 510-519.

[149] Klug MG, Soonpaa MH, Koh GY, Field LJ. Genetically selected cardiomyocytes from differentiating embronic stem cells form stable intracardiac grafts. *J Clin Invest* 1996; 98: 216-224.

[150] Reyes M, Dudek A, Jahagirdar B, Koodie L, Marker PH, Verfaillie CM. Origin of endothelial progenitors in human postnatal bone marrow. *J Clin Invest* 2002; 109: 337-346.

[151] Bouhadir KH, Mooney DJ. Promoting angiogenesis in engineered tissues. *J Drug Target* 2001; 9: 397-406.

[152] Reinlib L, Field L. Cell transplantation as future therapy for cardiovascular disease? A workshop of the National Heart, Lung, and Blood Institute. *Circulation* 2000; 101: E182-E187.

[153] Marler JJ, Upton J, Langer R, Vacanti JP. Transplantation of cells in matrices for tissue regeneration. *Adv Drug Deliv Rev* 1998; 33: 165-182.

[154] McMillin CR. Elastomers for biomedical applications. *Rubber Chem Technol* 1994; 67: 417-446.

[155] Yoda R. Elastomers for biomedical applications. *J Biomater Sci-Polym Ed* 1998; 9: 561-626.

[156] Groot JHd, Nijenhuis AJ, Bruin P, Pennings AJ, Veth RPH, Klompmaker J, Jansen HWB. Use of porous biodegradable polymer implants in meniscus reconstruction. 1) Preparation of porous biodegradable polyurethanes for the reconstruction of meniscus lesions. *Colloid Polym Sci* 1990; 268: 1073-1081.

[157] Storey RF, Hickey TP. Degradable polyurethane networks based on D, L-lactide, glycolide, ε-caprolactone, and trimethylene carbonate homopolyster and copolyester triols. *Polymer* 1994; 35: 830-838.

[158] Storey RF, Wiggins JS, Puckett AD. Hydrolyzable poly(ester-urethane) networks from L-lysine diisocyanate and D,L-lactide ε-caprolactone homopolyester and copolyester triols. *J Polym Sci Pol Chem* 1994; 32: 2345-2363.

[159] Bogdanov B, Toncheva V, Schacht E. Synthesis and characterization of poly(ester-urethanes). *Macromol Symp* 2000; 152: 117-126.

[160] Guan J, Sacks MS, Beckman EJ, Wagner WR. Synthesis, characterization, and cytocompatibility of elastomeric, biodegradable poly(ester-urethane)ureas based on poly(caprolactone) and putrescine. *J Biomed Mater Res* 2002; 61: 493-503.

[161] Skarja GA, Woodhouse KA. Synthesis and characterization of degradable polyurethane elastomers containing and amino acid-based chain extender. *J Biomater Sci Polym Ed* 1998; 9: 271–295.

[162] Dahiyat BI, Hostin E, Posadas EM, Leong KW. Synthesis and characterization of putrescine-based poly(phosphoester-urethanes). *J Biomater Sci Polym Ed* 1993; 4: 529-543.

[163] Grijpma DW, Zondervan GJ, Pennings AJ. High molecular weight copolymers of L-lactide and ε-caprolactone as biodegradable elastomeric implant materials. *Polym Bull* 1991; 25: 327-333.

[164] den Dunnen WFA, Robinson PH, Van Wessel R, Pennings AJ, van Leeuwen MBM, Schakenraad JM. Long-term evaluation of degradation and foreign-body reaction of subcutaneously implanted poly(DL-lactide-ε–caprolactone). *J Biomed Mater Res* 1997; 36: 337-346.

[165] den Dunnen WF, Meek MF, Grijpma DW, Robinson PH, Schakenraad JM. *In vivo* and *in vitro* degradation of poly[50/50 (85/15 L/D)LA/ε-CL], and the implications for the use in nerve reconstruction. *J Biomed Mater Res* 2000; 51: 575-585.

[166] Wagener KB, Jonhson DA. Segmented thermoplastic copolyesters. US 4262114, Akzona Inc., Asheville, NC (1981).

[167] Wagener KB. Biocompatible copolymers. US 4350806, Akzona Inc., Asheville, NC (1982).

[168] Deschamps AA, Grijpma DW, Feijen J. Poly(ethylene oxide)/poly(butylene terephthalate) segmented block copolymers: the effect of copolymer composition on physical properties and degradation behavior. *Polymer* 2001; 42: 9335-9345.

[169] Deschamps AA, van Apeldoorn AA, Hayen H, de Bruijn JD, Karst U, Grijpma DW, Feijen J. *In vivo* and *in vitro* degradation of poly(ether ester) block copolymers based on poly(ethylene glycol) and poly(butylene terephthalate). *(submitted to Biomaterials, 2002)*

[170] van Blitterswijk CA, van der Brink J, Leenders H, Bakker D. The effect of PEO ratio on degradation, calcification and bone bonding of PEO/PBT copolymer (Polyactive). *Cells Mat* 1993; 3: 23-36.

[171] Papadaki M, Mahmood T, Gupta P, Claase MB, Grijpma DW, Riesle J, van Blitterswijk CA, Langer R. The different behaviors of skeletal muscle cells and chondrocytes on PEGT/PBT block copolymers are related to the surface properties of the substrate. *J Biomed Mater Res* 2001; 54: 47-58.

[172] Bezemer JM, Feijen J, Dijkstra PJ. Poly(ether ester amide) and poly(ether ester urethane) copolymers. EP1230290, ISOTIS, The Netherlands (2001).

[173] Deschamps AA, van Apeldoorn AA, de Bruijn JD, Grijpma DW, Feijen J. Poly(ether ester amide)s for tissue engineering. *(submitted to Biomaterials, 2002)*

[174] Deschamps AA, Grijpma DW, Feijen J. Phase separation and physical properties of PEO-containing poly(ether ester amide)s. *J Biomater Sci Polym Ed (*in press*)*.

[175] Williams SF, Martin DP, Horowitz DM, Peoples OP. PHA applications: addressing the price performance issue. I. Tissue engineering. *Int J Biol Macromol* 1999; 25: 111-121.

[176] Conway BR, Eyles JE, Alpar HO. A comparative study on the immune responses to antigens in PLA and PHB microspheres. *J Control Release* 1997; 49: 1-9.

[177] Sodian R, Hoerstrup SP, Sperling JS, Daebritz S, Martin DP, Moran AM, Kim BS, Schoen FJ, Vacanti JP, Mayer JE. Early *in vivo* experience with tissue-engineered trileaflet heart valves. *Circulation* 2000; 102: 22-29.

[178] Crommen J, Vandorpe J, Schacht E. Degradable polyphosphazenes for biomedical applications. *J Control Release* 1993; 24: 167-180.

[179] Lemmouchi Y, Schacht E, Dejardin S. Biodegradable poly[(amino acid ester)phosphazenes] for biomedical applications. *J Bioact Compat Polym* 1998; 13: 4-18.

[180] Laurencin CT, Norman ME, Elgendy HM, el-Amin SF, Allcock HR, Pucher SR, Ambrosio AA. Use of polyphosphazenes for skeletal tissue regeneration. *J Biomed Mater Res* 1993; 27: 963-973.

[181] Laurencin CT, ElAmin SF, Ibim SE, Willoughby DA, Attawia M, Allcock HR, Ambrosio AA. A highly porous 3-dimensional polyphosphazene polymer matrix for skeletal tissue regeneration. *J Biomed Mater Res* 1996; 30: 133-138.

[182] Wang Y, Ameer GA, Sheppard BJ, Langer R. A tough biodegradable elastomer. *Nat Biotechnol* 2002; 20: 602-606.

[183] Zhu KJ, Hendren RW, Jensen K, Pitt CG. Synthesis, properties, and biodegradation of poly(1,3-trimethylene carbonate). *Macromolecules* 1991; 24: 1736-1740.

[184] Carothers WH, van Natta FJ. Studies on polymerization and ring formation. III. Glycol esters of carbonic acid. *J Am Chem Soc* 1930; 52: 314-326.

[185] Albertsson A-C, Eklund M. Influence of molecular structure on the degradation mechanism of degradable polymers: *in vitro* degradation of poly(trimethylene carbonate), poly(trimethylene carbonate-co-caprolactone), and poly(adipic anhydride). *J Appl Polym Sci* 1995; 57: 87-103.

[186] Engelberg I, Kohn J. Physico-mechanical properties of degradable polymers used in medical applications: a comparative study. *Biomaterials* 1991; 12: 292-304.

[187] Buchholz B. Analysis and characterization of resorbable DL-lactide-trimethylene carbonate copolyesters. *J Mater Sci: Mater Med* 1993; 4: 381-388.

[188] Grijpma DW, van Hofslot RDA, Super H, Nijenhuis AJ, Pennings AJ. Rubber toughening of poly(lactide) by blending and block copolymerization. *Polym Eng Sci* 1994; 34: 1674-1684.

[189] Ruckenstein E, Yuan Y. Molten ring-open copolymerization of L-lactide and cyclic trimethylene carbonate. *J Appl Polym Sci* 1998; 69: 1429-1434.

[190] Katz AR, Mukherjee DP, Kaganov AL, Gordon S. A new synthetic monofilament absorbable suture made from polytrimethylene carbonate. *Surg Gynecol Obstet* 1985; 161: 213-222.

[191] Jie C, Zhu KJ, Shilin Y. Preparation, characterization and biodegradable characteristics of poly(1,3-trimethylene carbonate-co-glycolide). *Polym Int* 1996; 41: 369-375.

[192] Jie C, Zhu KJ. Preparation, characterization and biodegradable characteristics of poly(D,L-lactide-co-1,3-trimethylene carbonate). *Polym Int* 1997; 42: 373-379.

[193] Edlund U, Albertsson AC. Copolymerization and polymer blending of trimethylene carbonate and adipic anhydride for tailored drug delivery. *J Appl Polym Sci* 1999; 72: 227-239.

[194] Ambrosio AMA, Allcock HR, Katti DS, Laurencin CT. Degradable polyphosphazene/poly(α-hydroxyester) blends: degradation studies. *Biomaterials* 2002; 23: 1667-1672.

[195] Kohn DH, Sarmadi M, Helman JI, Krebsbach PH. Effects of pH on human bone marrow stromal cells *in vitro*: implications for tissue engineering of bone. *J Biomed Mater Res* 2002; 60: 292-299.

[196] Bos RRM, Rozema FR, Boering G, Nijenhuis AJ, Pennings AJ, Verwey AB, Nieuwenhuis P, Jansen HWB. Degradation of and tissue reaction to biodegradable poly(L-lactide) for use as internal fixation of fractures: a study in rats. *Biomaterials* 1991; 12: 32-36.

[197] Albertsson A-C, Sjoling M. Homopolymerization of 1,3-dioxan-2-one to high molecular weight poly(trimethylene carbonate). *J Mater Sci - Pure Appl Chem* 1992; A29: 43-54.

[198] Albertsson A-C, Eklund M. Synthesis of copolymers of 1,3-dioxa-2-one and oxepan-2-one using coordination catalysts. *J Polym Sci, Part A: Polym Chem* 1994; 32: 265-279.

[199] Deng F, Henderson L, Gross RA. Ring-opening polymerization of ϵ-caprolactone and trimethylene carbonate catalyzed by lipase Novozym 435. *Polym Prep* 1998; 39: 144-145.

[200] Huang Q, Shen Z, Zhang Y, Shen Y, Shen L, Yuan H. Ring-opening copolymerization of trimethylene carbonate and D,L-lactide by rare earth chloride. *Polym J* 1998; 30: 168-170.

[201] Schappacher M, Fabre T, Mingotaud AF, Soum A. Study of a (trimethylenecarbonate-co-ε-caprolactone) polymer - Part 1: preparation of a new nerve guide through controlled random copolymerization using rare earth catalysts. *Biomaterials* 2001; 22: 2849-2855.

[202] Pitt CG, "Poly-ε-caprolactone and its copolymers" In: Chasin M, Langer R. *Biodegradable polymers as drug delivery systems*, New York, NY: Marcel Dekker; 1990. p 71-120.

[203] von Oepen R, Michaeli W. Injection moulding of biodegradable implants. *Clin Mater* 1992; 10: 21-28.

[204] Gogolewski S, Jovanovic M, Perren SM, Dillon JG, Hughes MK. The effect of melt-processing on the degradation of selected polyhydroxyacids - polylactides, polyhydroxybutyrate, and polyhydroxybutyrate-co-valerates. *Polym Degrad Stabil* 1993; 40: 313-322.

[205] Birkinshaw C, Buggy M, Henn GG, Jones E. Irradiation of poly-D,L-lactide. *Polym Degrad Stabil* 1992; 38: 249-253.

[206] Pitt CG, Chasalow FI, Hibionada DM, Klimas DM, Schindler A. Aliphatic polyesters. I. The degradation of poly(ε-caprolactone) *in vivo*. *J Appl Polym Sci* 1981; 26: 3779-3787.

PART II

POLYMER SYNTHESIS AND CHARACTERIZATION

Ser·en·dip·i·ty [from its possession by the heroes of the Persian fairy tale *The Three Princes of Serendip*]: the faculty or phenomenon of finding valuable things not sought for.
In *Merriam Webster's Dictionary*

"Chance favors the prepared mind."
Louis Pasteur (1822-1892)

CHAPTER 3

Copolymers of trimethylene carbonate and ε-caprolactone for porous nerve guides: synthesis and properties*

A.P. PÊGO, A.A. POOT, D.W. GRIJPMA and J. FEIJEN

Institute for Biomedical Technology (BMTI) and Department of Polymer Chemistry and Biomaterials, Faculty of Chemical Technology, University of Twente, P.O. Box 217, 7500 AE Enschede, The Netherlands

ABSTRACT

Copolymers of trimethylene carbonate (TMC) and ε-caprolactone (CL) were synthesized and characterized with the aim of assessing their potential in the development of a flexible and slowly degrading artificial nerve guide for the bridging of large nerve defects.

The effect of the monomer ratio on the physical properties of the polymers and its influence on the processability of the materials was investigated. Under the applied polymerization conditions (130°C, 3 days using stannous octoate as a catalyst) high molecular weight polymers ($\overline{M}_n$ above 93,000) were obtained. All copolymers had glass transition temperatures below room temperature. At TMC contents higher than 25 mol% no crystallinity was detected. A decrease in crystallinity resulted in the loss of strength and decrease in toughness, as well as in an increased polymer wettability. Amorphous poly(TMC), however, showed excellent ultimate mechanical properties due to strain-induced crystallization (Tm=36°C). Low crystallinity copolymers could be processed into dimensionally stable porous structures by means of immersion precipitation and by combination of this technique with the use of porosifying agents. Porous membranes of poly(TMC) could be prepared when blended with small amounts of high molecular weight poly(ethylene oxide).

Poly(TMC) and poly(TMC-CL) copolymers with high ε-caprolactone content possess good physical properties and are processable into porous structures. These materials are most suitable for the preparation of porous artificial nerve guides.

INTRODUCTION

When the extent of nerve damage prohibits the direct approximation of the two nerve stumps in peripheral nerve repair, autologous nerve grafting is considered the surgical treatment of choice[1]. Artificial nerve guides, where a tube bridges the nerve gap, offer a promising alternative, preventing the sacrifice of a donor nerve and possible neuroma formation at the donor site. Furthermore, the use of synthetic nerve guides reduces operation time and prevents the mismatch between the damaged nerve and the graft.

The use of both degradable and non-degradable artificial nerve guides has been extensively investigated *in vivo*. Using nerve guides based on the biodurable silicone, the nerve recovery was jeopardized due to a late foreign body response and chronic nerve compression[2]. Collagen[3], poly(glycolic acid) (poly(GA))[4] and copolymers of lactide (LA) and ε-caprolactone (CL)[5] are among the *in vivo* degradable materials used as alternatives to autologous nerve grafts. However, the correction of large nerve defects with functional recovery using a degradable graft still remains a challenge. Possible causes for the difficulties encountered include the use of polymers with too high degradation rates, a too high degree of swelling or unsuitable mechanical properties. Insufficient permeability of the device to body fluids and lack of nerve growth factors in the regeneration environment may also have a negative influence on the regeneration process[6].

In the clinical situation, where frequently large nerve defects have to be corrected, it would be preferable to use a slowly degrading material, which does not swell extensively during degradation. The material must be non-cytotoxic and the foreign body reaction should be minor without extensive formation of fibrous scar tissue. A late inflammatory response, as observed with the use of slowly degrading highly crystalline poly(L-lactide)[7], should also be prevented. Furthermore, the applied nerve guide should be flexible, but relatively strong, and easy to handle in microsurgery. In order to bridge large nerve defects in clinically relevant situations it is anticipated that a period of up to a year is required for the nerve to regenerate and maturate. During this period the device should keep its form and not fragment in order to avoid the formation of scar tissue that could jeopardize the regeneration process.

Aliphatic polyesters and copolyesters are among the most commonly used degradable materials for the preparation of clinical devices[8]. Polymers of GA and D,L-lactide (DLLA) have the disadvantage of not only being stiff and brittle

materials but also of possessing a relatively high rate of degradation. In addition, high degrees of swelling are also observed at late stages of degradation[9,10]. In view of the desired properties of the graft, high molecular weight copolymers of trimethylene carbonate (TMC) and CL are suitable candidates for the design of these materials, as both homopolymers undergo slow degradation *in vivo* to non-toxic products[11,12].

High molecular weight poly(trimethylene carbonate) (poly(TMC)) is an amorphous, rubbery polymer at room temperature with a glass transition temperature of approximately -15°C[13]. The *in vitro* hydrolytic degradation is reported to be very slow[14]. No decrease in the molecular weight of poly(TMC) samples after six months of subcutaneous implantation in rats was observed. Another *in vivo* study with poly(TMC) of lower starting molecular weight revealed higher degradation rates in comparison with the *in vitro* hydrolysis, suggesting the contribution of an enzymatic process to the polymer degradation[13].

The incorporation of other monomer units into the poly(TMC) chain proved to be a successful method of modulating the rate of polymer degradation as well as modifying its physical properties[11,14,15]. Poly-ε-caprolactone (poly(CL)) is a tough semi-crystalline polymer with a low glass transition temperature (approximately -60°C)[12]. Poly(CL) is degraded very slowly and is most suitable for long patency applications, having been extensively studied for long-term delivery systems such as Capronor, a 1-year contraceptive[16]. The synthesis of TMC and CL copolymers has been previously described[17]. However, the copolymer characterization in terms of mechanical properties and wettability was not reported.

The degree of permeability of the nerve guide was observed to be of influence on nerve regeneration. Several studies showed that nerve regeneration and reinnervation were considerably improved in semipermeable tubes when compared to impermeable ones[18,19]. By being porous the guide will allow the exchange of fluids between the regeneration environment and the surrounding tissue avoiding the building up of pressure due to fluid retention[6].

To enhance the rate of nerve regeneration the porous tube can be seeded with Schwann cells. These cells play a vital role in the regeneration process, producing extracellular matrix proteins and a range of neurotropic and neurotrophic factors essential for neuron growth[20]. Supplementing nerve guides with Schwann cells is a viable strategy which has already shown positive results[21-23]. The Schwann cells can be seeded directly on the inner surface of the graft or after coating of the graft

surface with an adhesive protein[24]. Alternatively the nerve guide can be filled with Schwann cells in a supporting matrix based on extracellular matrix proteins.

Polymers based on TMC and CL, covering a broad range of compositions, were synthesized and characterized to assess their potential in the preparation of porous nerve guides. Initial experiments on the processing of these amorphous or low crystallinity polymers into porous structures are also reported.

MATERIALS AND METHODS

Materials

Polymer grade trimethylene carbonate (TMC) (1,3-dioxan-2-one) was obtained from Boehringer Ingelheim, Germany. ε-Caprolactone (CL) (2-oxepanone) (Acros Organics, Belgium) was purified by drying over CaH_2 and distillation under reduced argon atmosphere. Stannous octoate ($SnOct_2$) (stannous 2-ethylhexanoate) was used as received from Sigma, USA. Sodium chloride (NaCl), used as porosifying agent in the preparation of porous structures, was crushed and fractionated by means of sieving, using standard test sieves with a mesh size of 63 and 38 μm. Fractions with particles smaller than 38 μm and 38-63 μm were used to prepare porous structures. Solvents were of analytical grade.

Polymer Synthesis

In an argon atmosphere, a mixture of monomers was charged into freshly silanized (Serva, Boehringer Ingelheim Bioproducts Partnership, Germany) and dried glass ampoules and $2x10^{-4}$ mol of stannous octoate per mol of monomer was added as a solution in sodium dried pentane. The pentane was removed afterwards by evacuation. The ampoules were purged three times with dry argon and heat-sealed under vacuum. The ampoules were conditioned in an oil bath pre-heated at the polymerization temperature and vigorously shaken in order to obtain a homogeneous mixture of the monomers and the catalyst. All homo- and copolymerizations were carried out for a period of 3 days at 130°C±2°C. After the reaction time the ampoules were quenched to room temperature and the polymers were discharged. For purification the obtained polymers were dissolved in chloroform (2-5 wt/vol% solutions), the resulting solutions were filtered through a sintered glass filter and precipitated into a ten-fold volume of methanol. The

precipitated polymers were collected, washed with fresh methanol and dried under reduced pressure at room temperature until constant weight.

Analysis and Characterization

The synthesized polymers were characterized with respect to the monomer conversion and chemical composition by nuclear magnetic resonance (NMR) spectroscopy. 300 MHz ^{1}H-NMR (Varian Inova 300 MHz) spectra were recorded using polymer solutions in CDCl$_3$ (Sigma, USA). For selected polymers 100 MHz ^{13}C-NMR (Varian Unity 400 WB) spectra were recorded using polymer solutions in CDCl$_3$. For the carbon spectra the number of transients was 5000 with a relaxation time of 10 s.

Molecular weights, molecular weight distributions and intrinsic viscosities of the purified polymers were determined by gel permeation chromatography (GPC) using a Waters Model 510 pump, a HP Ti-Series 1050 autosampler, a Waters Model 410 Differential Refractometer and a Viscotek H502 Viscometer Detector with 10^5- 10^4- 10^3- 500 Å Waters Ultra-Styragel columns placed in series. Chloroform was used as eluent at a flow rate of 1.5 ml/min. Narrow polystyrene standards were used for calibration. Sample concentrations of approximately 0.5 wt/vol% and injection volumes of 30 µl were used. All determinations were performed at 25°C.

The thermal properties of the synthesized materials were evaluated by differential scanning calorimetry (DSC). Samples (5-15 mg) placed in aluminum pans were analyzed with a Perkin Elmer DSC-7 at a heating rate of 10°C/min. All samples were heated to 40°C above their melting temperature (when present) or glass transition temperature. The samples were then quenched rapidly (300°C/min) until 40°C below their glass transition temperature and after 5 min a second scan was recorded. Unless mentioned otherwise, the data presented were collected during the second heating scan. The glass transition temperature was taken as the midpoint of the heat capacity change, the onset and the peak melting temperature were determined from the melting endotherm. Indium and gallium were used as standards for temperature calibration.

Mechanical Properties

Tensile testing was performed on compression molded and on solvent cast films. In the former case purified samples of the prepared polymers were compression molded in a 600 µm thick mould at 140°C. In the latter case, films (40-130 µm thick) were prepared by casting polymer solutions in chloroform (3-10 wt/vol%)

onto glass plates. All test specimens had dimensions in accordance to ASTM standard D882-91 specifications. Tensile tests in three-fold were carried out at room temperature on a Zwick Z020 universal tensile testing machine operated at a crosshead speed of 50 mm/min and a grip-to-grip separation of 50 mm. The specimen deformation was derived from the grip-to-grip separation, therefore the presented values of the Young's modulus give only an indication of the stiffness of the different polymers.

Wettability

Static contact angles of ultra-pure water (MilliQ Plus – Millipore, USA) on the polymer surface and water uptake in phosphate buffered saline (PBS, pH 7.4, NPBI, The Netherlands) were used to evaluate the wettability of TMC and CL copolymers. Initial static contact angles were measured on films spin-coated onto glass slips with a contact angle measuring instrument (Krüss, Germany) equipped with a video measuring system. The measurements were performed at room temperature on profiles of sessile drops and readings were taken within the first 10-15 s. Angles were measured on five different regions of each polymer surface and the results were averaged.

The water uptake was defined as the weight gain of the polymer specimen after conditioning, according to equation 1:

$$\text{water uptake} = \frac{w - w_o}{w_o} \times 100 \quad (\text{wt\%}) \tag{1}$$

where w_o is the initial specimen weight and w the weight of the specimen after conditioning.

Compression molded specimens ($100 \times 50 \times 0.6 \ \text{mm}^3$) were placed in PBS at 37°C and the sample weight was evaluated for a period of 30 days. After 24 hours of conditioning in PBS wet samples were subjected to tensile testing.

Preparation of Porous Structures

In order to investigate the adequacy of phase separation techniques to prepare porous polymer films, a preliminary study was performed with selected copolymer compositions. The explored methods included immersion precipitation and the combination of this technique with porosifying agents. The polymers used were poly(CL), poly(TMC-CL) 10:90 mol% and poly(TMC).

Polymer films were prepared by casting a chloroform solution (4-10 wt/vol%) onto glass plates with a casting knife. The cast membranes were placed in a coagulation

bath (ethanol:water or isopropanol:water 8:1) for 4 hours and subsequently dried under vacuum at room temperature until constant weight. When immersion precipitation was combined with the use of porosifying agents, sodium chloride particles of a particular size were added to polymer solutions to obtain salt suspensions, which were cast as previously described. After phase separation the membranes were placed in a shaking water bath for a few days to leach the salt (the water was regularly refreshed). Thereafter the membranes were dried under vacuum at room temperature until constant weight.

Films were also prepared using blends of poly(TMC) and poly(ethylene oxide) (PEO, $\overline{M}w$ =8x10^6, Aldrich-Chemie, Germany) containing 2, 5 and 10 wt% of PEO per weight of poly(TMC).

To obtain cross sections for morphological analysis, the samples were immersed in ethanol and fractured in liquid nitrogen. Cross sections and surfaces of the samples were coated with a gold-platinum layer using a Polaron E5600 sputter-coater and examined with a Hitachi S800 field emission scanning electron microscope (SEM) operating at 6 kV.

RESULTS AND DISCUSSION

In order to design a suitable polymer system for the preparation of a nerve guides to be used in the reconstruction of large nerve defects several constraints are imposed. Namely, slow degradation *in vivo*, low degree of swelling (even at later stages of degradation) and no or low crystallinity. Furthermore, the device should be flexible and tough to allow the handling in microsurgery. Therefore, the present application requires a material with narrowly defined characteristics in terms of thermal properties, mechanical performance, wettability and degradation behavior. Copolymerization has been widely used to reach the desired characteristics in the final polymer. We prepared a series of copolymers based on TMC and CL. Both poly(TMC) and poly(CL) present a slow degradation behavior, are hydrophobic and have glass transition temperatures below room temperature. By preparing a series of TMC-CL copolymers we investigated the window of compositions that would allow the processing of the polymer into a porous nerve guide with the desired properties.

Polymer Synthesis

The synthesis of statistical copolymers composed of TMC and CL was accomplished through ring-opening polymerization in the melt, using stannous octoate as a catalyst (Figure 1). Different examples of catalyst systems used for the copolymerization of these monomers can be found in literature[17,25]. Stannous octoate was selected as it is highly efficient and commonly used in the preparation of polymers for biomedical applications[12].
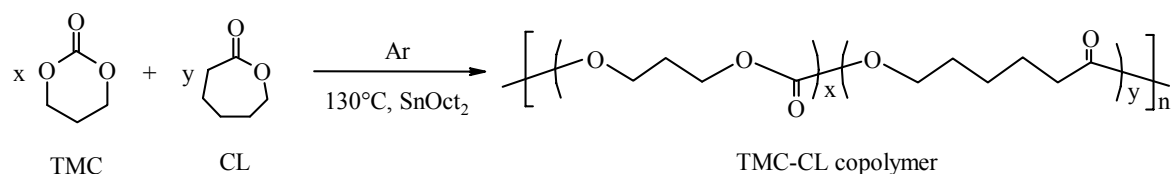
Figure 1. Synthesis of statistical poly(trimethylene carbonate-co-ε-caprolactone).

Table 1. Copolymerization of TMC and CL with stannous octoate as a catalyst at 130°C.

TMC/CL charged (mol ratio)	TMC conversion (%)	CL conversion (%)	Polymer composition[a] TMC/CL (mol ratio)
100/0	99.5	-	100/0
88/12	99.6	100	87/13
80/20	99.6	99.4	77/23
75/25	99.8	100	75/25
75/25	99.0	99.7	72/28
47/53	99.0	100	47/53
25/75	100	100	25/75
14/86	100	100	14/86
9/91	99.6	100	10/90
0/100	-	100	0/100

[a] As determined by ^{1}H-NMR.

The homopolymers and a series of copolymers ranging from 10 to 87 mol% of TMC were prepared. Under the applied conditions the monomer conversion was almost complete and the obtained compositions are in accordance with the ratio of monomers charged (see Table 1). The residual monomer content and the copolymer composition were determined by ^{1}H-NMR analysis of the crude polymerization products, as the α-methylene resonances of monomeric (t, 4H, δ=4.44 ppm) and polymeric TMC (m, 4H, δ=4.18-4.26 ppm) as well as the α-methylene resonances

of monomeric (m, 2H, δ=2.52-2.67 ppm) and polymeric (m, 2H, δ=2.23-2.40 ppm) CL are separated.

Table 2. Molecular weights of TMC-CL copolymers determined by GPC.

Polymer composition TMC /CL (mol ratio)	$\overline{M}w$ x10^{-5}	$\overline{M}n$ x10^{-5}	PDI	$[\eta]^{a}$ (dl·g^{-1})
100/0	5.52	2.90	1.90	4.90
87/13	2.82	1.31	2.14	2.98
77/23	2.46	1.15	2.14	2.83
75/25	2.32	1.09	2.13	2.73
72/28	3.48	1.61	2.17	3.76
47/53	2.07	0.93	2.22	2.79
25/75	1.83	1.02	1.79	2.68
14/86	2.09	1.00	2.09	2.92
10/90	1.84	0.93	1.98	2.63
0/100	3.02	1.34	2.26	3.93

[a] In chloroform, at 25°C.

In Table 2 the values of the weight and number average molecular weight ($\overline{M}w$ and $\overline{M}n$, respectively), polydispersity index (PDI) and intrinsic viscosity of the prepared polymers are given. Under the applied polymerization conditions high molecular weight polymers were obtained. This is an important feature in order to obtain materials that present good mechanical performance during a long period of implantation. The starting molecular weight influences the total time of degradation of a device. Independently of the degradation mechanism of the polymer, the onset of loss of mechanical properties and mass is delayed with increasing initial molecular weight of the material[26]. Taking in consideration the peripheral nerve regeneration rates over clinical relevant distances in humans it is anticipated that the nerve guide should maintain its form and adequate mechanical properties for a period of up to a year. Therefore, the initial molecular weight of the polymer should be high.

The polydispersity values of all (co)polymers are approximately equal to two. This value has been reported before for lactone ring-opening polymerizations where transesterification reactions had occurred[17,27,28].

Thermal Properties

The thermal properties of the TMC copolymers can be varied to a large extent by adjusting the quantity of comonomer used (Figure 2). All TMC and CL copolymers showed a glass transition temperature (Tg) below 0°C, ranging from -60°C for poly(CL) to -13°C for poly(TMC). For random copolymers, Fox derived the following equation that allows the estimation of the glass transition temperature of a copolymer based on the glass transition temperatures of the respective homopolymers[29]:

$$\frac{1}{Tg} = \frac{w1}{Tg_1} + \frac{w2}{Tg_2} \tag{2}$$

Here w_1 and w_2 refer to the weight fraction of the two comonomers and Tg_1 and Tg_2 refer to the glass transition temperatures of the two corresponding homopolymers.
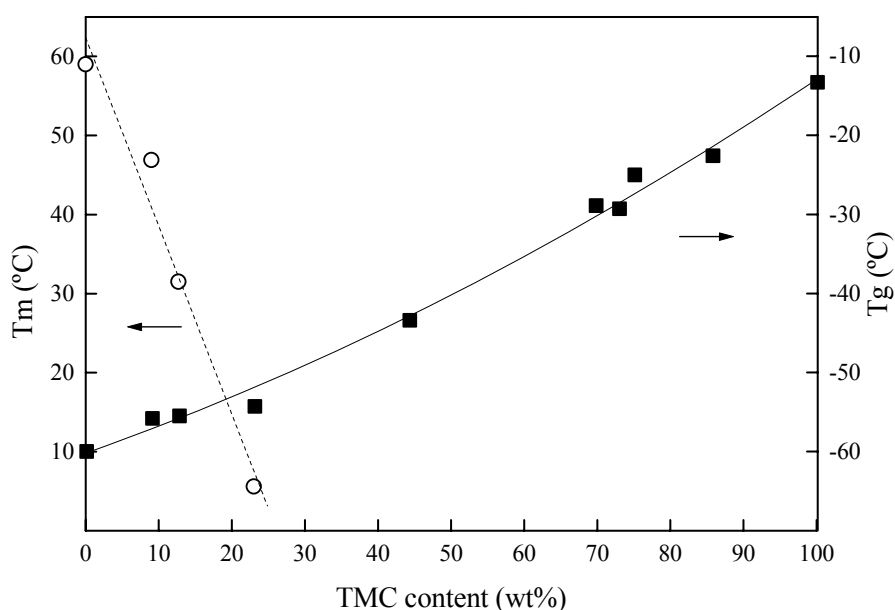
Figure 2. Thermal properties of TMC-CL copolymers as a function of the TMC content. (■) Experimental glass transition temperature (Tg); (—) Fox equation; (○) peak melting temperature (Tm).

The agreement of the experimental results with the model (see Figure 2) indicates that for the range of compositions a single amorphous phase is retained. At CL contents above 70% (wt%) all copolymers were semi-crystalline. A decrease in CL content results in the lowering of melting temperature and a decrease in the heat of

fusion. The heat of fusion can be related to the mass fraction of crystallinity (w_c) by the expression:

$$w_c = \frac{\Delta H}{\Delta H°} \tag{3}$$

The heat of fusion ($\Delta H°$) of 100% crystalline poly(CL) is reported to be 139.4 J/g[30]. This value was used to estimate the crystallinity of the prepared poly(CL) and semi-crystalline copolymers (see Table 3).

Table 3. Degree of crystallinity of TMC-CL copolymers estimated from DSC measurements.

Polymer composition TMC/CL (mol ratio)	$\overline{L}_{CL}$ [a]	Tm (onset) (°C)	Tm (peak) (°C)	ΔH (J/g)	w_c (%)
47/53	1.6	-	-	-	-
25/75	2.6	1.1	5.7	2.2	1.6
14/86	4.3	23.9	31.5	40.2	28.8
10/90	8.4	40.2	49.9	49.9	35.8
0/100	-	52.8	59.0	52.7	37.8

[a] $\overline{L}_{CL}$ - average sequence length of the oxy-ε-caproyl units.

In order to determine the minimum CL average sequence length capable of crystallizing, sequence analysis was performed on selected polymers. In the ^{1}H-NMR spectra of the copolymers it was observed that in particular the ε-methylene resonances of polymeric CL (m, 2H, δ=4.07-4.18 ppm) were sensitive to sequence effects. It was not possible to determine the average monomer sequence lengths as the peak of α-methylene resonances of polymeric TMC overlaps with the multiplet corresponding to ε-methylene resonances of polymeric CL. Therefore, a more detailed analysis was done by means of ^{13}C-NMR spectroscopy, an often used tool for sequence length determination[31]. The ^{13}C-NMR spectra of TMC-CL copolymers obtained were similar to a previously published one[32]. Especially the carbonyl carbon signals were most sensitive to sequence effects. The peaks corresponding to oxy-ε-caproyl (-CO-(CH$_2$)$_5$-O-) were assigned at the dyad level. The average sequence length of the oxy-ε-caproyl units ($\overline{L}_{CL}$) can be calculated from the relative intensities of the CL-CL and CL-TMC signals:

$$\overline{L}_{CL} = \frac{I(CL-CL)}{I(CL-TMC)} + 1 \tag{4}$$

The CL average sequence lengths found for the selected copolymers are presented in Table 3. From the obtained results, one can observe that a CL average sequence length above 2.6 led to crystallization of the polymer. For copolymers consisting of A units which crystallize and B units which do not, with both units occurring at random sequence along the chain, Flory derived the following expression for the melting point depression[33]:

$$\frac{1}{Tm} - \frac{1}{Tm°} = \left(\frac{R}{\Delta H°} \right) \times \left(\frac{2}{\bar{x}n} \right) \tag{5}$$

In Equation 5 Tm is the melting temperature of the polymer, Tm° is the equilibrium melting temperature of the defect-free polymer crystal, R is the gas constant, $\Delta H°$ is the heat of fusion per crystallizable unit and $\bar{x}n$ the number average degree of polymerization of the crystallizable unit. In a study of the thermodynamics of fusion of poly(CL), Crescenzi et al.[30] reported values of $\Delta H°$ (139.4 J/g) and Tm° (63.4°C) for 100% crystalline poly(CL). Based on these values, the expected melting point depressions for the poly(TMC-CL) copolymers were compared to the observed onset melting point depressions. Equating the CL average sequence length to $\bar{x}n$, a plot of the reciprocal of the polymer onset melting temperature versus the reciprocal of the CL average sequence length should give a straight line. From Figure 3, the observed melting depressions are higher than predicted, especially at lower CL average sequence lengths. This can be explained by an alternating distribution of non-crystallizable sequences along the polymer chain[33]. The short CL average sequence length found for poly(TMC-CL) 47:53 (mol%) ($\bar{L}$CL equals 1.6) corresponds to a TMC average sequence length of 1.4. A truly random CL and TMC incorporation would yield average monomer sequence lengths equal to 2, while an alternating incorporation of the monomers would result in average monomer sequence lengths of 1. This observation by ^{13}C-NMR, indicates a copolymer with a distribution of monomers intermediate between random and alternating. Albertsson et al.[17] found that the product of the reactivity ratios of these monomers is smaller than 1, in agreement with our results. Although ^{13}C-NMR analysis revealed the absence of long comonomer segments for poly(TMC-CL) 47:53 mol%, in copolymers with higher CL contents longer CL sequences are formed which are capable of crystallizing.
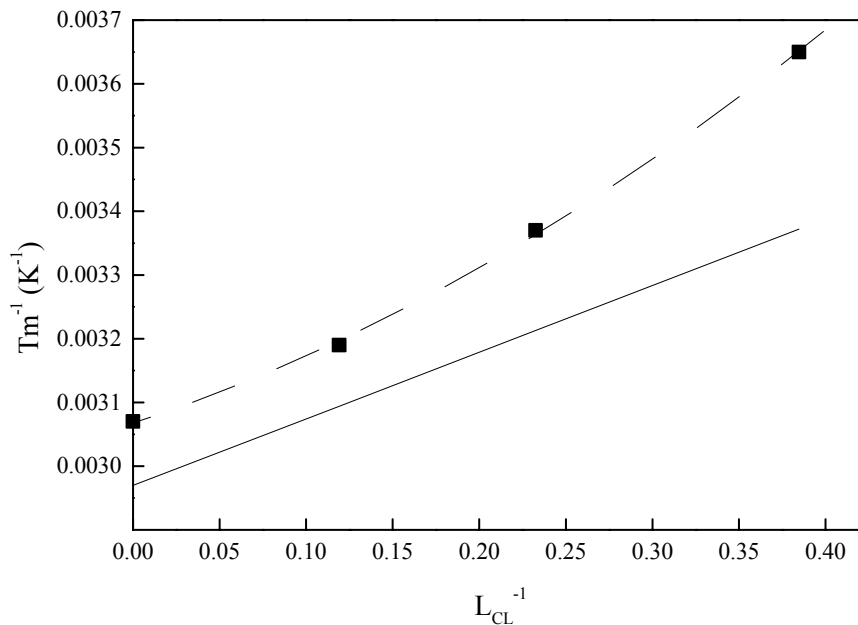
Figure 3. The reciprocal of the melting temperature as a function of the reciprocal of the CL average sequence length. (■) Experimental onset melting temperature (Tm); (—) theoretical melting point depression (using Tm°=63.8°C and ΔH°=139.4 J/g[30]).

In polymers crystallinity is known to play an important role in determining both permeability and biodegradation, as the crystalline phase is inaccessible to water and other permeants. An increase in crystallinity reduces the permeability by both reducing the solute solubility and increasing the tortuosity of the diffusional pathway. The rate of biodegradation (chain scissioning) is reduced by a decrease in accessible hydrolysable bonds. For the use of these polymers in nerve guides, one should consider the fact that crystalline debris formed during degradation may cause an undesired late inflammatory response negatively influencing the regeneration process and the recovery of nerve function. Therefore, minimal crystallinity is desired.

Mechanical Properties
Although implanted nerve guides will not be subjected to severe load bearing conditions they will be susceptible to some stresses during the surgical procedure (handling and suturing) and during the implantation time (movement of the patient). The device should be tough, flexible and should bend without kinking.

The mechanical properties of the prepared TMC-CL copolymers are listed in Table 4. Typical stress-strain curves are presented in Figure 4. It was not possible to solvent cast the polymer with 47 mol% of TMC into a thin film. The obtained film was very tacky and impossible to detach from the glass plate without folding and self-adhering. To assure that the results were not affected by the possible presence of remaining solvent, tensile testing was also performed with compression molded samples. The results are presented in Table 5 and show that no major differences were observed between the mechanical behavior of samples prepared by compression molding and by solvent casting. The yield strength as well as the Young's modulus decrease with increasing TMC content. These effects can be explained by a decrease of the average sequence length of CL on copolymerization and, as a consequence, the loss of crystallinity of the copolymers. As the Tg values for all the polymers are below room temperature, flexibility is observed for the whole range of polymers. The copolymers with a TMC content between 25 and 75% (mol%) are weak, having very low strengths (tensile strength below 1 MPa) and deform irreversibly at very low stresses.

Table 4. Mechanical properties of TMC-CL copolymers (solvent cast films 40-130 μm thick).

TMC content (mol%)	Young's modulus (MPa)	σ_{yield} (MPa)	ε_{yield} (%)	σ_{break} (MPa)	ε_{break} (%)	σ_{max} (MPa)
100	6.8	2.6	139	24	820	24
87	5.1	1.3	106	0.6	617	1.3
77	3.9	0.9	94	0.8	103	0.9
75	3.8	0.8	75	0.7	90	0.8
72	4.7	1.2	94	1.1	115	1.2
47[a]	-	-	-	-	-	-
25	4.6	0.4	50	0.1	236	0.4
14	123	5.3	13	46	1008	46
10	252	11	11	40	906	40
0	400	15	16	43	723	43

[a] Not determined, as no suitable solvent cast films were obtained.
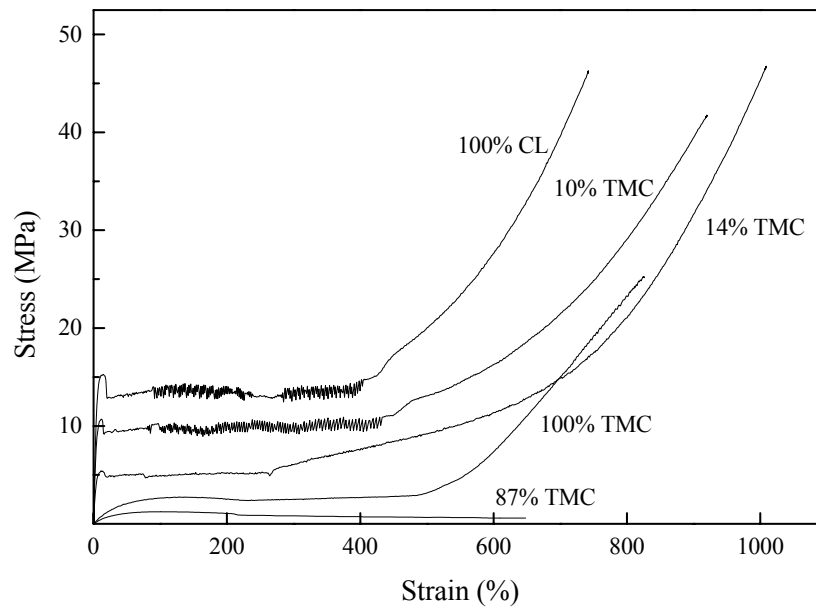
Figure 4. Stress-strain curves of TMC-CL copolymers (solvent cast films).

Table 5. Mechanical properties of TMC-CL copolymers (compression molded films 600 μm thick).

TMC content (mol%)	Young's modulus (MPa)	σ_{yield} (Mpa)	ε_{yield} (%)	σ_{break} (MPa)	ε_{break} (%)	σ_{max} (MPa)
100	6.3	2.3	128	12	831	12
82	5.4	1.6	115	1	1765	1.6
49	3.2	0.6	80	0.5	186	0.6
31	3.1	0.4	66	0.03	1875	0.4
10	141	6.7	16	23	910	23
0	318	14	12	32	754	32

Remarkably, for the TMC homopolymer a large upturn in the stress-strain behavior was observed at high elongations. The high value for the stress at break is due to strain-induced crystallization. After the tensile test, the initially amorphous poly(TMC) specimens now showed a melting endotherm with a melting temperature (Tm) of 36°C (ΔH=25.4 J/g), confirming strain-induced crystallization of the polymer (see Figure 5). Elastomers formed of chains of high structural regularity may crystallize upon deformation. Elongation of such elastomeric networks reduces the entropy of its chains and only a small additional reduction is

required for crystallization. This self-reinforcement, also observed for natural rubber, is the origin of the excellent ultimate mechanical properties, tensile strength and maximum extensibility of this strain-crystallizable physical network[34]. The high molecular weight value of the poly(TMC) synthesized ($\overline{M}_w$ =552,000 and $\overline{M}_n$ =290,000) may be of influence on the stress-strain induced crystallization behavior observed. This effect for poly(TMC) has not been previously reported[15].
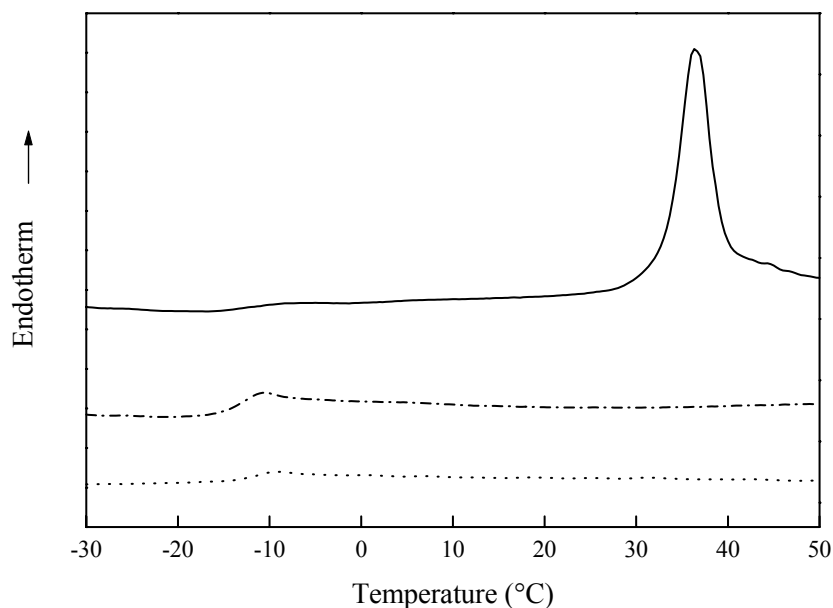
Figure 5. DSC thermograms of poly(TMC) specimen (solvent cast film) before and after tensile testing. First scan before tensile testing (····), first scan after tensile testing (—) and second scan after tensile testing (·–·–·).

Wettability

The wettability of a polymer has important consequences for the bulk properties and degradation behavior of the material, as well as for the interactions of cells with the polymer surface.

The initial static contact angles of the polymers under study, a measure of the polymer surface hydrophilicity, are presented in Figure 6. Although the values do not differ largely along the series, the static contact angle decreases slightly with the increase of TMC content, reaching a plateau at the poly(TMC-CL) 47:53 mol%. The values for the static contact angles are high, indicating relatively hydrophobic polymer surfaces. The water uptake of the poly(TMC-CL) copolymers in PBS at 37°C was followed for a period up to a month (Figure 6). A very low water uptake

was observed. After 24 hours the water absorption had reached equilibrium and after one month no significant changes were observed in the water content of the samples. A decrease in crystallinity by copolymerization resulted in an increased water uptake that reached a maximum of 1.3% for poly(TMC-CL) 31:69 mol% and remained constant for higher TMC contents. The higher water absorption of the polymers with higher TMC content can be explained not only by the relatively higher hydrophilicity of these polymers, but also due to the absence of crystallinity. Despite the described differences in water uptake and static contact angles along the series, all copolymers can be regarded as hydrophobic.
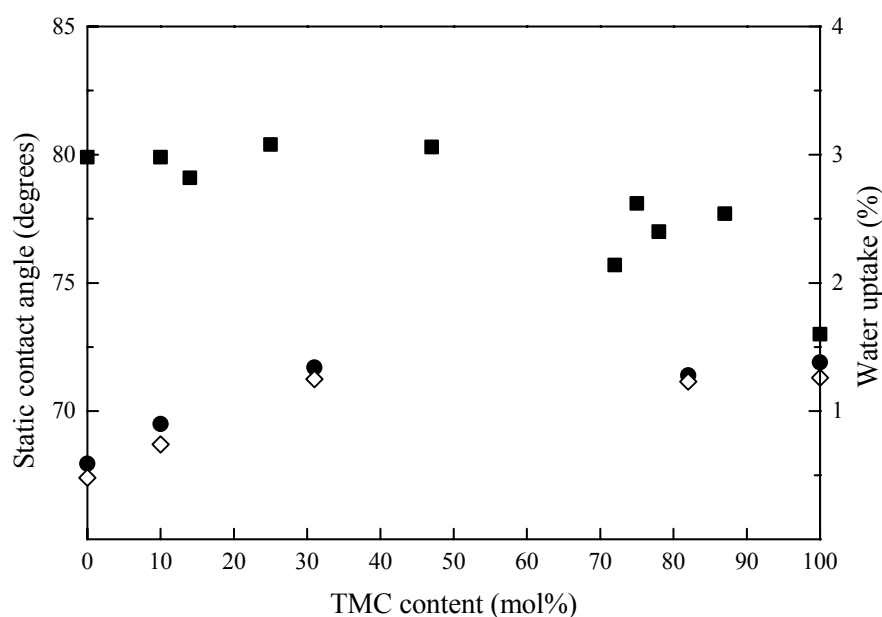
Figure 6. Wettability of TMC-CL copolymers. Static contact angle (■) and water uptake of compression molded samples after 1 day (●) and after 30 days (◇).

Tensile tests were performed on polymer samples after water uptake in order to assess the effect of this parameter on the mechanical properties (Table 6). For the homopolymers no significant deterioration of the mechanical properties was observed when comparing these results with the ones obtained in the dry state (Table 5). For the copolymers a decrease in the Young's modulus and maximum stress were recorded, what can be associated to a limited plasticizing effect of water. Although the water uptake was small after one month of incubation, the monitoring of the final nerve graft should be performed for even longer periods of time.

Table 6. Mechanical properties of TMC-CL copolymers after water uptake in PBS, at 37°C (compression molded films 600 μm thick).

TMC content (mol%)	Water uptake (%)	Young's modulus (MPa)	σ_{max} (MPa)
100	1.4	6.3	19
82	1.3	4.5	1.3
31	1.3	2.2	0.3
10	0.9	94	4.5
0	0.6	292	31

The growth of Schwann cells on the nerve guide surface will depend on their attachment and proliferation on the polymer substrate. In order to have a first insight in the behavior of Schwann cells seeded on these polymer surfaces, cell attachment and proliferation was investigated in a preliminary study. The results indicate that human Schwann cells attach and proliferate on the (co)polymer surfaces. Current work is aimed at the effect of polymer composition, physical properties and surface texture on the cell growth. Also the effect on cell adhesion of coating the polymer surfaces with extracellular matrix proteins is under investigation.

Preparation of Porous Structures

To our knowledge the preparation of rubbery porous structures based on polymers that are not cross-linked by chemical or physical means has not been reported. From the range of synthesized materials poly(CL) (37.8% of crystallinity), poly(TMC-CL) 10:90 mol% (35.8% crystallinity) and poly(TMC) (amorphous, rubbery polymer) were chosen in order to assess their applicability for the preparation of porous nerve guides. Phase inversion, as well as the combination of phase inversion with porosifying agents, are readily used methods to obtain porous films[35]. Here, we explored immersion precipitation and the combination of this technique with salt leaching.

Porous films based on the two semi-crystalline polymers using the mentioned methods were prepared. Stable symmetric structures, with interconnected pores were obtained (see Figure 7.A for an example). When phase separation was induced by immersion precipitation the obtained pore size of the membranes ranged from 2 μm to 7 μm and 2 μm to 27 μm for poly(CL) and poly(TMC-CL) 10:90 mol%, respectively. The formation of these pores can be ascribed to the demixing processes occurring during the exchange of solvent by non-solvent. Membranes

prepared from suspensions containing salt particles of 38-63 μm and smaller than 38 μm showed macropores comparable in size to the salt particles. This indicates that these pores were mainly formed during the entrapment of the salt particles in the polymer matrix and their subsequent removal. Pore formation due to demixing processes also contributed to the interconnection between macropores. In these membranes a few pores of up to 167 μm were observed which could be attributed to the presence of salt agglomerates.
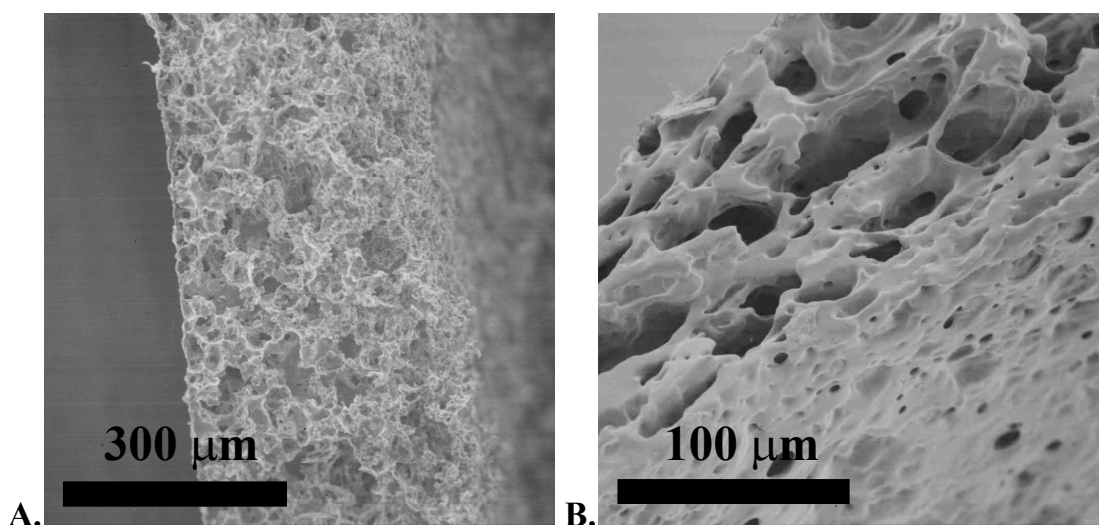
Figure 7. SEM pictures of cross-sections of poly(TMC-CL) 10:90 mol% and poly(TMC) membranes prepared by immersion precipitation. A) Poly(TMC-CL) 10:90 mol% membrane prepared by immersion precipitation using NaCl as porosifying agent, particle size smaller than 38 μm; B) poly(TMC) membrane prepared with a small amount of PEO.

For poly(TMC) membranes a different behavior was observed. Initially, upon phase separation, these membranes presented pores, but these pores collapsed during the salt leaching or the drying steps. Furthermore, during the preparation process the poly(TMC) membranes shrank up to 63% of their initial dimensions. The absence of physical cross-links (crystallinity) that could stabilize the structure and the low Tg, allowed the relaxation of the polymer chains in time, resulting in the collapse of the pores. Even the use of very high molecular weight polymer could not overcome this effect. It was found that the addition of high molecular weight PEO had a stabilizing effect on the porous poly(TMC) structures. By blending poly(TMC) with PEO (2-10 wt% of the amount of poly(TMC)), the preparation of open structures with interconnected pores could be realized (Figure 7.B). Pores up to 20 μm were formed due to demixing processes. Composition determinations based on NMR

analysis showed that the PEO content of the obtained porous membranes was smaller than the PEO content of the starting solutions. This can be explained by the partial leaching out of PEO from the polymer matrix during the presence of the membranes in the coagulation bath.

In view of the present results one can conclude that when using immersion precipitation techniques to prepare suitable porous structures from these copolymers without additives some crystallinity is required. The existence of physical interactions between the polymer chains is essential to the stabilization of the final porous structures. Presently, melt processing in combination with salt leaching is being investigated as an alternative technique for the processability of these copolymers.

CONCLUSIONS

Statistical copolymers of TMC and CL were synthesized, analyzed and characterized with reference to the parent polymers, poly(TMC) and poly(CL). The possibility of tailoring the physical properties of TMC copolymers has been demonstrated.

The obtained results showed that the thermal and mechanical properties of the polymers are strongly determined by the molar composition. The (co)polymers ranged from semi-crystalline tough rubbery materials (copolymers with low TMC content) to amorphous, highly elastic rubbers (copolymers with high TMC content). All materials presented a hydrophobic character, although copolymers with higher TMC content showed higher water uptake and lower static contact angles. Copolymers with intermediate compositions presented less favorable mechanical properties for application in nerve guides due to their very low tensile strengths (<1MPa).

Poly(TMC) and poly(TMC-CL) copolymers with high CL content possess good physical properties and are processable into porous structures. These materials are most suitable for the preparation of porous artificial nerve guides.

ACKNOWLEDGMENTS

REFERENCES

[1]   Suematsu N. Tubulation for peripheral nerve gap: its history and possibility. *Microsurgery* 1989; 10: 71-74.

[2]   Merle M, Dellon AL, Campbell JN, Chang PS. Complications from silicon-polymer intubulation of nerves. *Microsurgery* 1989; 10: 130-133.

[3]   Mackinnon SE, Dellon AL. A study of nerve regeneration across synthetic (Maxon) and biologic (collagen) nerve conduits for nerve gaps up to 5 cm in the primate. *J Reconstr Microsurg* 1990; 6: 117-121.

[4]   Kiyotani T, Teramachi M, Takimoto Y, Nakamura T, Shimizu Y, Endo K. Nerve regeneration across a 25-mm gap bridged by a polyglycolic acid-collagen tube: a histological and electrophysiological evaluation of regenerated nerves. *Brain Res* 1996; 740: 66-74.

[5]   den Dunnen WFA, van der Lei B, Robinson PH, Holwerda A, Pennings AJ, Schakenraad JM. Biological performance of a degradable poly(DL-lactide-ε– caprolactone) nerve guide: Influence of tube dimensions. *J Biomed Mater Res* 1995; 29: 757-766.

[6]   den Dunnen WF, Meek MF, Grijpma DW, Robinson PH, Schakenraad JM. *In vivo* and *in vitro* degradation of poly[50/50 (85/15 L/D)LA/ε-CL], and the implications for the use in nerve reconstruction. *J Biomed Mater Res* 2000; 51: 575-585.

[7]   Bos RRM, Rozema FR, Boering G, Nijenhuis AJ, Pennings AJ, Verwey AB, Nieuwenhuis P, Jansen HWB. Degradation of and tissue reaction to biodegradable poly(L-lactide) for use as internal fixation of fractures: a study in rats. *Biomaterials* 1991; 12: 32-36.

[8]   Kohn J, Langer R, "Bioresorbable and Bioerodible Materials" In: Ratner BD, Hoffman AS, Schoen FJ, Lemons JE. *Biomaterials Science: An introduction to Materials in Medicine*, San Diego: Academic Press; 1996. p 64-73.

[9]   Vert M, Li SM, Spenlehauer G, Guerin P. Bioresorbability and biocompatibility of aliphatic polyesters. *J Mater Sci: Mater in Med* 1992; 3: 432-446.

[10] Lu L, Garcia CA, Mikos AG. *In vitro* degradation of thin poly(DL-lactic-co-glycolic acid) films. *J Biomed Mater Res* 1999; 46: 236-244.

[11] Katz AR, Mukherjee DP, Kaganov AL, Gordon S. A new synthetic monofilament absorbable suture made from polytrimethylene carbonate. *Surg Gynecol Obstet* 1985; 161: 213-222.

[12] Pitt CG, "Poly-ε-caprolactone and its copolymers" In: Chasin M, Langer R. *Biodegradable polymers as drug delivery systems*, New York, NY: Marcel Dekker; 1990. p 71-120.

[13] Zhu KJ, Hendren RW, Jensen K, Pitt CG. Synthesis, properties, and biodegradation of poly(1,3-trimethylene carbonate). *Macromolecules* 1991; 24: 1736-1740.

[14] Albertsson A-C, Eklund M. Influence of molecular structure on the degradation mechanism of degradable polymers: *in vitro* degradation of poly(trimethylene carbonate), poly(trimethylene carbonate-co-caprolactone), and poly(adipic anhydride). *J Appl Polym Sci* 1995; 57: 87-103.

[15] Buchholz B. Analysis and characterization of resorbable DL-lactide-trimethylene carbonate copolyesters. *J Mater Sci: Mater Med* 1993; 4: 381-388.

[16] Pitt CG, Schindler A, "Capronor: A biodegradable delivery system for levonorgestrel" In: Zatuchni GI, Goldsmith A, Shelton JD, Sciarra JJ. *Long-Acting Contraceptive Delivery Systems*, Philadelphia: Harper and Row; 1984. p 48-63.

[17] Albertsson A-C, Eklund M. Synthesis of copolymers of 1,3-dioxa-2-one and oxepan-2-one using coordination catalysts. *J Polym Sci, Part A: Polym Chem* 1994; 32: 265-279.

[18] Kim DH, Connolly SE, Zhao S, Beuerman RW, Voorhies RM, Kline DG. Comparison of macropore, semipermeable, and nonpermeable collagen conduits in nerve repair. *J Reconstr Microsurg* 1993; 9: 415-420.

[19] Rodriguez FJ, Gomez N, Perego G, Navarro X. Highly permeable polylactide-caprolactone nerve guides enhance peripheral nerve regeneration through long gaps. *Biomaterials* 1999; 20: 1489-1500.

[20] Frostick SP, Yin Q, Kemp GJ. Schwann cells, neurotrophic factors, and peripheral nerve regeneration. *Microsurgery* 1998; 18: 397-405.

[21] Ansellin AD, Fink T, Davey DF. Peripheral nerve regeneration through nerve guides seeded with adult Schwann cells. *Neuropathol Appl Neurobiol* 1997; 23: 387-398.

[22] Bryan DJ, Wang RR, Chakalis-Haley DP. Effect of Schwann cells in the enhancement of pheripheral-nerve regeneration. *J Recon Microsurg* 1996; 12: 439-446.

[23] Rodriguez FJ, Verdu E, Ceballos D, Navarro X. Nerve guides seeded with autologous Schwann cells improve nerve regeneration. *Exp Neurol* 2000; 161: 571-584.

[24] Steuer H, Fadale R, Müller E, Müller HW, Planck H, Schlosshauer B. Biohybride nerve guide for regeneration: degradable polylactide fibers coated with rat Schwann cells. *Neurosci Lett* 1999; 277: 165-168.

[25] Shen Y, Shen Z, Zhang Y, Huang Q, Shen L, Yuan H. Random copolymerization of ε-caprolactone and trimethylene carbonate with rare earth catalysts. *J Appl Polym Sci* 1997; 64: 2131-2139.

[26] Pitt CG, Chasalow FI, Hibionada DM, Klimas DM, Schindler A. Aliphatic polyesters. I. The degradation of poly(ε-caprolactone) *in vivo*. *J Appl Polym Sci* 1981; 26: 3779-3787.

[27] van Dijk JAPP, Smit JAM, Kohn FE, Feijen J. Characterization of poly(D,L-lactic acid) by gel permeation chromatography. *J Polym Sci: Polym Chem Ed* 1983; 21: 197-208.

[28] Leenslag JW, Pennings AJ. Synthesis of high-molecular-weight poly(L-lactide) initiated with tin 2-ethylhexanoate. *Makromol Chem* 1987; 188: 1809-1814.

[29] Fox TG. Influence of diluent and copolymer composition on the glass temperature of a polymer system. *Bull Amer Phys Soc* 1956; 2: 123.

[30] Crescenzi V, Manzini G, Calzolari G, Borri C. Thermodynamics of fusion of poly-β-propiolactone and poly-ε-caprolactone. Comparative analysis of the melting of aliphatic polylactone and polyester chains. *Eur Polym J* 1972; 8: 449-463.

[31] Kricheldorf HA, Kreiser I. Polylactones. 13. Transesterification of poly(L-lactide) with poly(glycolide), poly(β-propiolactone), and poly(ε-caprolactone). *J Macromol Sci - Chem* 1987; A24: 1345-1356.

[32] Lemmouchi Y, Schacht E, Kageruka P, De Deken R, Diarra B, Diall O, Geerts S. Biodegradable polyesters for controlled release of trypanocidal drugs: *in vitro* and *in vivo* studies. *Biomaterials* 1998; 19: 1827-1837.

[33] Flory PJ, *Principles of Polymer Chemistry*. Ithaca: Cornell University Press; 1953.

[34] Queslel JP, Mark HF, "Elasticity" In: Kroschwitz JI. *Encyclopedia of polymer science and engineering*, New York: John Wiley & Sons; 1986. p 365-408.

[35] van de Witte P, Dijkstra PJ, van den Berg JWA, Feijen J. Phase separation processes in polymer solutions in relation to membrane formation. *J Membrane Sci* 1996; 117: 1-31.

CHAPTER 4

Influence of catalyst and polymerization conditions on the properties of 1,3-trimethylene carbonate and ε-caprolactone copolymers*

A.P. PÊGO, Z.Y. ZHONG, P.J. DIJKSTRA, D.W. GRIJPMA and J. FEIJEN

Institute for Biomedical Technology (BMTI) and Department of Polymer Chemistry and Biomaterials, Faculty of Chemical Technology, University of Twente, P.O. Box 217, 7500 AE Enschede, The Netherlands

ABSTRACT

The influence of the catalyst/initiator system and polymerization conditions on the microstructure and physical properties of copolymers of equimolar amounts of 1,3-trimethylene carbonate (TMC) and ε-caprolactone (CL) was studied. Statistical copolymers were prepared in the presence of stannous octoate (SnOct$_2$) in the bulk at 80°C (14 and 28 days) and 130°C (1 and 3 days). The copolymerization of TMC and CL initiated by yttrium isopropoxide (Y$_5$(μ-O)(O^{i}Pr)$_{13}$) was done in solution at room temperature (5 min) and in the bulk at 80°C (2 min). Block copolymers, used as reference materials, were also prepared by sequential polymerization of the monomers in solution at room temperature with yttrium isopropoxide.

Both SnOct$_2$ and yttrium isopropoxide yielded polymers with shorter average monomer sequence lengths at higher reaction temperatures. For the polymerizations with SnOct$_2$ a similar effect was observed when the reactions were allowed to proceed for longer periods of time. Independent of the catalyst/initiator system, the statistical copolymers prepared in the bulk at 80°C or 130°C were amorphous, with average monomer sequences lengths shorter than 3. The copolymer prepared in solution at room temperature with yttrium isopropoxide was more blocky, with CL sequences long enough to crystallize ($\overline{L}_{CL}$ =3.93). The former copolymers are highly flexible but show low tensile strengths, in agreement with their amorphous structure and low glass transition temperature. The latter copolymer

is also flexible but much tougher and stiffer, as it is semi-crystalline. Its properties being characteristic of phase separated block copolymers.

INTRODUCTION

Synthetic polymers based on monomers like glycolide, lactide, ε-caprolactone (CL) and 1,3-trimethylene carbonate (TMC) have been studied extensively and several (co)polymers of these series are currently used for the preparation of biodegradable systems and devices for biomedical and pharmaceutical applications. The most important applications include resorbable sutures[1], drug delivery systems[2,3], pins and screws for bone fixation[4] and temporary three-dimensional scaffolds for tissue engineering[5].

The polymerization of the above-mentioned cyclic esters and carbonate can be carried out by cationic, anionic, coordination-insertion or enzymatic ring-opening polymerization mechanisms. Polymerization via a coordination-insertion mechanism has been frequently applied for the preparation of tailor-made polymers[6]. These reactions are very often carried out with metal alkoxides which contain a covalent metal-oxygen bond and have a weak Lewis acid character[7].

Tin (II) 2-ethylhexanoate (SnOct$_2$) is the most often used catalyst/initiator system for the polymerization of lactones[8,9] and TMC[10,11]. SnOct$_2$ is highly efficient and yields almost complete monomer conversions even at high monomer to catalyst ratios. The molecular weight of the prepared polymer can be controlled by addition of pre-determined amounts of hydroxyl-group containing compounds. SnOct$_2$ itself, however, does not contain a reactive alkoxide group. Recent mechanistic studies[9,12-14] have shown that alcohols (ROH) act as coinitiators, in which at least one octoate group is substituted in a rapid equilibrium to form a Sn-alkoxide group. The resulting Sn-alkoxide is the true initiator of the ring-opening polymerization process. In the absence of added coinitiator, the polymerization process is coinitiated by impurities present in the reaction mixture. The preparation of high-molecular weight polymers is only possible when a relatively high purity of the components is assured[9].

Recently, much attention has been drawn to catalyst/initiator systems that are not only highly efficient, but also highly active under mild reaction conditions, with simultaneous good control of molecular weight and molecular weight distributions.

These systems include rare earth alkoxides, like yttrium isopropoxide $(Y_5(\mu\text{-O})(O^iPr)_{13})$[15,16].

We have previously reported on the synthesis and physical properties of statistical poly(ester carbonate)s based on TMC and CL prepared using $SnOct_2$ as a catalyst/initiator system, for the preparation of porous degradable nerve guides[17]. The thermal properties of the polymers, and consequently their mechanical properties, were strongly dependent on the monomer composition. Copolymers of similar monomer compositions prepared with lanthanide isopropoxide showed distinct thermal and mechanical behavior[18]. In order to have an insight in the effect of the catalyst/initiator system and the polymerization conditions on the microstructure and physical properties of TMC and CL based polymers, copolymers with equimolar TMC and CL content were synthesized using the catalyst/initiator systems $SnOct_2$ and yttrium isopropoxide.

MATERIALS AND METHODS

Materials

Polymer grade TMC (1,3-dioxan-2-one) was obtained from Boehringer Ingelheim, Germany. CL (2-oxepanone) (Acros Organics, Belgium) was purified by drying over CaH_2 and distillation under reduced argon pressure. Stannous octoate ($SnOct_2$) (Sigma, USA) and yttrium isopropoxide $(Y_5(\mu\text{-O})(O^iPr)_{13})$ (Strem, The Netherlands) were used without further purification. Solvents were of analytical grade. Prior to use dichloromethane was distilled from CaH_2 and toluene was distilled from sodium.

Polymer Synthesis

(1) Polymerizations with $SnOct_2$

<u>Statistical copolymerizations in the bulk</u> (entries 1-4, Table 1): In an argon atmosphere, an equimolar mixture of TMC and CL (10 g scale) was charged into dried, freshly silanized (Serva, Boehringer Ingelheim Bioproducts Partnership, Germany) glass ampoules and 2×10^{-4} mol of stannous octoate per mol of total monomer was added as a solution in sodium-dried pentane (1.48×10^{-2} M). Subsequently, the pentane was removed afterwards by evacuation. The ampoules were purged three times with dry argon and heat-sealed under vacuum. The ampoules were conditioned in an oil bath pre-heated to the polymerization

temperature and vigorously shaken in order to obtain a homogeneous mixture of monomers and catalyst. After a predetermined time the ampoules were quenched to room temperature and the polymers were discharged. Samples were taken for determination of the monomer conversion by ^{1}H-NMR (nuclear magnetic resonance). For purification, the obtained polymers were dissolved in chloroform, filtered through a sintered glass filter and precipitated into an excess of isopropanol. The precipitated polymers were collected, washed with fresh isopropanol and dried at room temperature (RT) under reduced pressure.

(2) Polymerizations with $Y_5(\mu\text{-O})(O^iPr)_{13}$

Sequential polymerization in solution at RT (entries 5 and 6, Table 2): Reactions were carried out in dried glass ampoules under a dry nitrogen atmosphere in a glove box. $Y_5(\mu\text{-O})(O^iPr)_{13}$ (2.3 ml of a 3.87 mM stock solution in toluene, corresponding to 8.2×10^{-4} mol per total mol of monomer) was added to a vigorously stirred solution of either TMC (10.8 mmol in 7.7 ml CH_2Cl_2) or CL (10.8 mmol in 8.9 ml CH_2Cl_2) in dichloromethane. After 3 min of reaction, an equimolar amount of the second monomer, CL (10.8 mmol in 10.0 ml CH_2Cl_2) or TMC (10.8 mmol in 10.0 ml CH_2Cl_2), respectively, was added. After 2 min, the reaction was terminated by addition of acetic acid. A sample was taken for determination of the monomer conversion by ^{1}H-NMR. The polymer was isolated by precipitation into an excess of methanol and dried at 40°C under reduced pressure.

Statistical copolymerization in solution at RT (entry 7, Table 2): The reaction was carried out in a dried glass ampoule under a dry nitrogen atmosphere in a glove box. $Y_5(\mu\text{-O})(O^iPr)_{13}$ (2.3 ml of a 3.87 mM stock solution in toluene, corresponding to 4.1×10^{-4} mol per total mol of monomer) was added to a vigorously stirred mixture of TMC (10.8 mmol) and CL (10.8 mmol) in dichloromethane (10.0 ml). The polymerization was allowed to proceed for 5 min and then terminated by the addition of acetic acid. A sample was taken for determination of the monomer conversion by ^{1}H-NMR. The polymer was isolated by precipitation into an excess of methanol and dried at 40°C under reduced pressure.

(c) Statistical copolymerization in the bulk at 80°C (entry 8, Table 2): Under a dry nitrogen atmosphere in a glove box a mixture of TMC (32.5 mmol) and CL (32.5 mmol) was charged to a dried glass ampoule equipped with a magnetic stirrer. The vessel was closed with a stopper, transferred and connected to a nitrogen Schlenk line, and placed in an oil bath thermostated at 80°C. A solution of

$Y_5(\mu\text{-}O)(O^iPr)_{13}$ in toluene (0.8 ml; concentration of stock solution 0.034 M, corresponding to 4.1×10^{-4} mol per total mol of monomer) was added by injection into the vigorously stirred mixture of monomers. The reaction was allowed to continue for 2 min at 80°C and then stopped by rapid cooling in a cold-water bath. The polymer was dissolved in chloroform, precipitated into an excess of ethanol and dried at 40°C under reduced pressure.

Analysis and Characterization

The residual monomer content and the copolymer composition were determined by 300 MHz ¹H-NMR analysis of the crude polymerization products, as the α-methylene resonances of monomeric (t, 4H, δ=4.44 ppm) and polymeric TMC (m, 4H, δ=4.18-4.26 ppm) as well as the α-methylene resonances of monomeric (m, 2H, δ=2.52-2.67 ppm) and polymeric (m, 2H, δ=2.23-2.40 ppm) CL are separated[17]. Average monomer sequence lengths were determined by 75 MHz ¹³C-NMR. All spectra were recorded using a Varian Inova 300 MHz (USA) using solutions of polymer in $CDCl_3$ (Sigma, USA).

Weight average ($\overline{M}w$) and number average ($\overline{M}n$) molecular weights, polydispersities ($\overline{M}w/\overline{M}n$) and intrinsic viscosities ([η]) were determined by gel permeation chromatography (GPC) using a Waters Model 510 pump (USA), a HP Ti-Series 1050 autosampler (USA), a Waters Model 410 Differential Refractometer and a Viscotek H502 Viscometer Detector (USA) with Waters Styragel HR5-HR4-HR2-HR1 or HR4-HR2-HR0.5 columns placed in series. Chloroform was used as eluent at a flow rate of 1.5 ml/min. Narrow polystyrene standards were used for calibration. Sample concentrations of approximately 0.5 wt/vol% and injection volumes of 30 μl were used. All determinations were performed at 25°C.

The thermal properties of the purified polymers were evaluated by differential scanning calorimetry (DSC). Samples (5-15 mg) placed in aluminum pans were analyzed with a Perkin Elmer Pyris1 (USA) at a heating rate of 10°C/min. All samples were heated to 40°C above their melting temperature (when present) or glass transition temperature. The samples were then quenched rapidly (300°C/min) to 40°C below their glass transition temperature and after 5 min a second scan was recorded. The glass transition temperature (Tg) was taken as the midpoint of the heat capacity change and the peak melting temperature (Tm) was determined from the melting endotherm. The crystallinity (w_c) of the semi-crystalline TMC-CL copolymers was determined assuming proportionality to the experimental heat of

fusion (ΔH) according to the expression: $w_c = \Delta H / \Delta H°$, where $\Delta H°$ is the heat of fusion of 100% crystalline poly(CL) reported to be 139.4 J/g[19]. Cyclohexane, indium, gallium and tin were used as standards for temperature calibration.

Tensile testing was performed on compression-molded films. Rectangular films (100x5 mm^2) of the purified polymers were compression-molded (laboratory press Fontijne THB008, The Netherlands) to 600 μm thickness at 100°C. The films were cooled to room temperature under pressure. Tensile tests in three-fold were carried out at room temperature on a Zwick Z020 (Germany) universal tensile testing machine operated without extensometers at a crosshead speed of 50 mm/min, and an initial grip-to-grip separation of 50 mm. Under these conditions the determined Young's moduli give only an indication of the stiffness of the different polymers.

RESULTS AND DISCUSSION

Polymer Synthesis

The results of the ring-opening copolymerizations of TMC and CL in the melt with SnOct$_2$ are given in Table 1.

Table 1. Ring-opening copolymerization of TMC and CL in the bulk with SnOct$_2$[a].

No	TMC:CL monomer (mol%)	T (°C)	t (d)	TMC conv. (%)	CL conv. (%)	TMC:CL polymer (mol%)	$\overline{M}_n$ (x10^5)	$\overline{M}_w/\overline{M}_n$	[η] dl/g
1	51:49	130	1	99.5	100	53:47	2.8	1.9	5.1
2	50:50	130	3	99.3	100	49:51	2.2	1.9	4.3
3	50:50	80	14	99.6	100	50:50	3.1	1.7	5.3
4	48:52	80	28	99.9	100	49:51	2.4	1.9	4.7

[a] $2x10^{-4}$ mol of SnOct$_2$ per mol of monomer.

Under the applied polymerization conditions the conversion of the CL monomer was complete and the conversion of the TMC monomer was above 99%. The obtained copolymer compositions are in good agreement with the ratio of monomers charged. The $\overline{M}_n$ of all the prepared polymers was high (>200,000). The highest molecular weight was obtained after 14 days of polymerization at 80°C. Furthermore, at each of the selected polymerization temperatures, $\overline{M}_n$ decreased with longer polymerization times. Similar observations have been previously

reported and may be related to thermal degradation that can occur at higher polymerization temperatures and prolonged polymerization periods[10,20,21]. The $\overline{M}w/\overline{M}n$ values of all copolymers are 1.9, with the exception of entry no. 3 ($\overline{M}w/\overline{M}n$ =1.7). Such values have been reported previously for lactone ring-opening polymerizations catalyzed by $SnOct_2$ where transesterification reactions had occurred[22]. The increase in $\overline{M}w/\overline{M}n$ with polymerization time for the copolymers prepared at 80°C is in agreement with the possible occurrence of bimolecular transesterification reactions of which the extent increases with reaction time[9,22].

The results of the sequential and statistical TMC and CL copolymerizations in the presence of yttrium isopropoxide are presented in Table 2.

Table 2. Ring-opening copolymerization of TMC and CL by $Y_5(\mu\text{-O})(O^iPr)_{13}{}^a$.

No	TMC:CL monomer (mol%)	T	t (min)	TMC conv. (%)	CL conv. (%)	TMC:CL polymer (mol%)	$\overline{M}n$ (10^4) Theor.^{f}	$\overline{M}n$ (10^4) GPC	$\overline{M}w/\overline{M}n$ GPC	[η] dl/g GPC
5	50:50	RT	3+2^b	98.1	100	47:53	2.0	5.3	1.3	1.1
6	50:50	RT	3+2^c	98.7	86.1	57:43	1.9	2.6	3.7	1.5
7	50:50	RT	5^d	99.2	99.5	46:54	2.0	4.1	2.6	1.7
8	50:50	80°C	2^e	100	100	50:50	2.0	2.6	3.1	1.2

^{a} 4.1x10^{-4} mol of $Y_5(\mu\text{-O})(O^iPr)_{13}$ per mol of monomer.

^{b} Sequential polymerization in CH_2Cl_2, polymerization of CL followed by TMC.

^{c} Sequential polymerization in CH_2Cl_2, polymerization of TMC followed by CL.

^{d} Polymerization in CH_2Cl_2.

^{e} Polymerization in the bulk.

^{f} Defined as[23]: $\overline{M}n_{\text{Theor}}=((102\text{x}0.5+114\text{x}0.5)\text{x}([TMC]\text{xTMC}_{conv}+[CL]\text{xCL}_{conv})/[I]))/2.6$.

Yttrium isopropoxide initiator/catalyst systems are most often used to prepare block copolymers[23-25]. In the present study block copolymers of TMC and CL were prepared by the sequential polymerization of TMC and CL in the presence of yttrium isopropoxide and used as a reference.

All polymerizations proceeded very fast and the $\overline{M}n$ of the obtained copolymers is significantly lower than the $\overline{M}n$ of the copolymers prepared with $SnOct_2$ (Table 1). This can be anticipated, as the monomer to initiator ratio was higher in the polymerizations with $SnOct_2$. In the polymerizations performed with yttrium isopropoxide more initiating species were added per mol of monomer. Furthermore, as in the polymerizations with $SnOct_2$ no coinitiator was added, the initiating

species are formed in situ as the result of the reaction of 'hydroxyl' containing impurities and $SnOct_2$. Therefore, the final concentration of initiator is only dependent on the number of these impurities present in the reaction mixture capable of reacting with $SnOct_2$.

The sequential copolymerizations of TMC and CL initiated by yttrium isopropoxide were performed in solution (dichloromethane) at room temperature.

With CL as the first monomer (entry 5, Table 2) the conversion of CL was complete. In the second polymerization step the TMC conversion was very high (>98%). The resulting copolymer had a relatively high molecular weight and a relatively narrow molecular weight distribution. The $\overline{M}n$ of the obtained polymer is higher than expected from the monomer to initiator ratio charged. Yttrium isopropoxide is a cluster compound with 2.6 (13/5) possible active alkoxide groups[26]. It appears from the results that not all potentially active groups of the yttrium isopropoxide added to the reaction mixture were available for initiation of the polymerization[18,23,27].

When the sequential polymerization of the monomers was done in reverse order (TMC was the first monomer to be polymerized; entry 6, Table 2) the conversion of CL was not complete, resulting in a polymer enriched in TMC. From GPC analysis it was noticed that the copolymer prepared exhibited a broad bimodal molecular weight distribution ($\overline{M}w/\overline{M}n$ =3.7). This bimodal molecular weight distribution observed can be explained by a relatively slow ring-opening of CL by the living poly(TMC) end (the cross-over step) in comparison to the CL polymerization by living CL growing ends. The obtained molecular weight was once again slightly higher than expected.

The statistical copolymerization of TMC and CL with yttrium isopropoxide in solution at room temperature (entry 7, Table 2) resulted in polymers with monomodal molecular weight distributions, but with relatively high $\overline{M}w/\overline{M}n$. As polymers resulting from the homopolymerization of TMC[28] or CL[29] initiated by lanthanide derivatives are reported to have low polydispersities, differences in monomer reactivity may explain this broadening of the molecular weight distribution. The copolymerization of mixtures of these monomers with lanthanide isopropoxide at room temperature has been previously reported[18]. A better control of the $\overline{M}w/\overline{M}n$ values observed in that study ($\overline{M}w/\overline{M}n$ =1.6) may be explained by the higher reactivity of the lanthanide initiator compared to yttrium isopropoxide[28]. This results in a decrease of the effect of the monomer reactivity

in the determination of the polymer chain growth rate. When the polymerization of mixtures of TMC and CL was performed in the bulk at 80°C (entry 8, Table 2) the reaction was extremely fast resulting in solidification of the mixture immediately after addition of the catalyst. The conversion of the monomers was complete within the reaction time of 2 min. The $\overline{M}n$ determined by GPC was close to the expected value. These polymerization conditions may have led to an increase in the number of available catalyst sites involved in the initiation of the polymerization. However, the molecular weight distribution becomes broader ($\overline{M}w/\overline{M}n$ of 2.6 in solution at room temperature vs. 3.1 in the bulk at 80°C). The polymerization in bulk at 80°C is so fast that a homogeneous mixture of reactants in the melt is difficult to achieve (locally) before the reaction has progressed to a considerable extent what can lead to a broadening of the molecular weight distribution. Furthermore, under these conditions (bulk polymerization at higher temperature) the difference between the rate of the initiation and propagation steps decreases, what may also result in an increase in polydispersity.

Average Monomer Sequence Length

The effect of the polymerization conditions on the monomer distribution in the polymer chain of different lactone-based copolymers prepared in the presence of SnOct$_2$ is well documented[30,31]. Two major factors play a role in determining the average monomer sequence length in these systems: the reactivity ratios of the monomers that are dependent on the polymerization temperature, and the occurrence of transesterification reactions, of which the extent is known to increase with the increase in reaction time and temperature. A similar effect can be expected for polymerizations performed in the presence of lanthanide alkoxide initiators [29,32], although such studies have not yet been reported.

In order to determine to which extent the polymerization conditions (time and temperature) affect the microstructure of TMC and CL based copolymers synthesized in the presence of SnOct$_2$ or yttrium isopropoxide, the average monomer sequence lengths in the different synthesized copolymers were determined. Sequence determination was performed by ^{13}C-NMR analysis, as carbonyl carbon atoms are particularly sensitive to sequence effects.

Figure 1 shows the enlargement of the spectra in the carbonyl region for selected polymers prepared in the presence of yttrium isopropoxide.

A

Chemical Shift

B

Chemical Shift
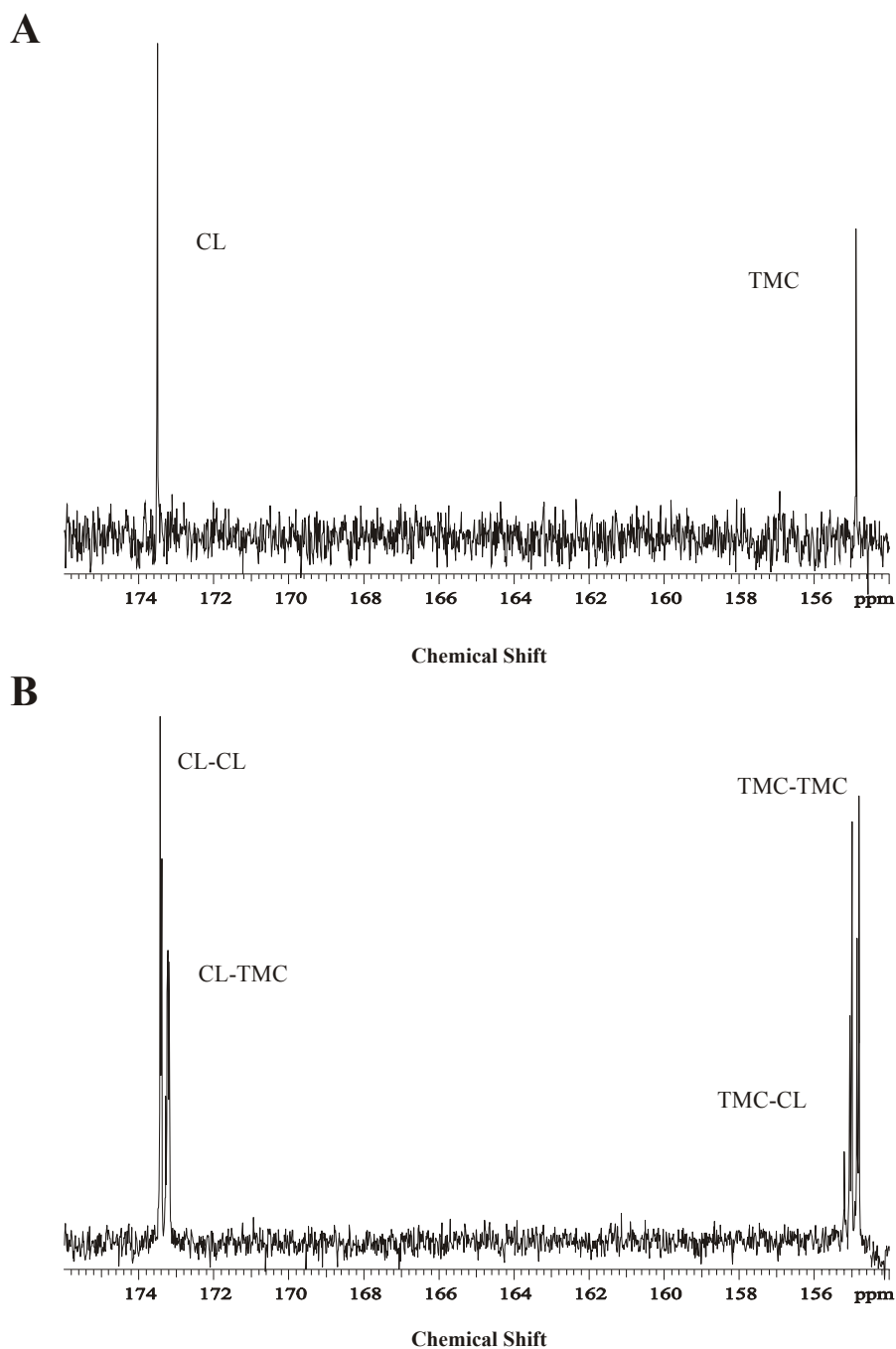
Figure 1. Expanded regions of carbonyl carbon atoms in ^{13}C-NMR (75.5MHz) spectra of (A) CL-TMC block copolymer prepared at RT in solution (entry 5, Table 2) and (B) TMC-CL copolymer prepared at 80°C in the bulk (entry 8, Table 2) in the presence of yttrium isopropoxide.

The different peaks were assigned at a dyad level, according to previously published results[10,17,33]. The average sequence length of the CL sequences ($\overline{L}_{CL}$) and TMC sequences ($\overline{L}_{TMC}$) can be calculated from the relative intensities of, respectively, the <u>CL</u>-CL and <u>CL</u>-TMC, and <u>TMC</u>-TMC and <u>TMC</u>-CL signals:

$$\bar{L}_{CL} = \frac{I(\underline{CL} - CL)}{I(\underline{CL} - TMC)} + 1 \qquad (1)$$

$$\bar{L}_{TMC} = \frac{I(\underline{TMC} - TMC)}{I(\underline{TMC} - CL)} + 1 \qquad (2)$$

The TMC and CL average sequence lengths are presented in Table 3. $\bar{L}_{TMC}$ and $\bar{L}_{CL}$ determined by ^{13}C-NMR are much influenced by the polymerization conditions.

Table 3. Average sequence lengths of TMC units ($\bar{L}_{TMC}$) and CL units ($\bar{L}_{CL}$) of TMC-CL copolymers based on ^{13}C-NMR analysis.

No	Polymerization conditions	$\bar{L}_{TMC}$	$\bar{L}_{CL}$
1	SnOct$_2$, in the bulk, 130°C for 1 day	2.45	2.52
2	SnOct$_2$, in the bulk, 130°C for 3 days	1.76	1.44
3	SnOct$_2$, in the bulk, 80°C for 14 days	3.32	2.84
4	SnOct$_2$, in the bulk, 80°C for 28 days	3.02	2.78
5	Y$_5$(μ-O)(O^{i}Pr)$_{13}$, in solution, sequential, RT for 5 min	∞^a	∞^a
6	Y$_5$(μ-O)(O^{i}Pr)$_{13}$, in solution, sequential, RT for 5 min	∞^a	∞^a
7	Y$_5$(μ-O)(O^{i}Pr)$_{13}$, in solution, RT for 5 min	3.78	3.93
8	Y$_5$(μ-O)(O^{i}Pr)$_{13}$, in the bulk, 80°C for 2 min	2.02	1.95

[a] No dyad splitting was observed (block copolymers)

Considering the polymerizations in the presence of SnOct$_2$ (entries 1-4) one can observe a decrease of $\bar{L}_{TMC}$ and $\bar{L}_{CL}$ with extension of the reaction time at both reaction temperatures. This can be attributed to the occurrence of transesterification reactions. The decrease was more significant at 130°C, showing that transesterification plays a more important role at higher polymerization temperatures. The average monomer sequence lengths are also shorter for copolymers synthesized at 130°C, indicating the formation of a more random copolymer. This can be attributed not only to the occurrence of transesterification but also to reduced differences in monomer reactivity at higher temperatures.

In the case of the sequential copolymerizations catalyzed by yttrium isopropoxide, ^{13}C-NMR analysis confirmed the block structure of both copolymers, as no splitting of the TMC or CL carbonyl peaks was observed (see Figure 1A for an example). This also points to negligible incidence of transesterification reactions induced by

this catalyst system at room temperature, in a similar manner to what was observed in the polymerization of other monomers[23,32].

In contrast, the copolymers resulting from the statistical copolymerization of TMC and CL in the presence of yttrium isopropoxide, both at room temperature and at 80°C, are more random (see Figure 1B for an example). As observed for the polymerizations with SnOct$_2$, the average monomer sequence lengths also decrease with increasing reaction temperature. This may be attributed to a change in the difference between monomer reactivity ratios with temperature. However, transesterification reactions should not be ruled out, although in the present study the effect of extending the reaction time was not investigated for the yttrium isopropoxide initiator system.

In the comparison of the results obtained with both initiator/catalyst systems at the same polymerization temperature (80°C) it is worth noticing that the statistical copolymer prepared with yttrium isopropoxide shows much shorter average monomer sequence lengths. These copolymers are more random than copolymers prepared with SnOct$_2$ even after long polymerization times of 28 days.

Thermal properties

The thermal properties of the synthesized copolymers are presented in Table 4. As may be expected, copolymers varying in average sequence length show quite distinct thermal behavior.

Table 4. Thermal properties (second scan) of purified TMC and CL copolymers synthesized with SnOct$_2$ and yttrium isopropoxide (see Table 1 and 2 for details).

No	Tg (°C)	Tm (°C)	ΔH (J/g)	w_c (%)
1	-49	-	-	-
2	-50	-	-	-
3	-50	-	-	-
4	-51	-	-	-
5	-67; -20	55	39	28
6	-67; -19	54	28	20
7	-63; -34	48	26	19
8	-51	-	-	-

In the present study, block copolymers were only prepared in the presence of yttrium isopropoxide. As can be anticipated, the thermal properties of the block copolymers reflect the thermal properties of the parent homopolymers. The CL-TMC (entry 5) and the TMC-CL (entry 6) block copolymers showed two distinct glass transition temperatures: the first from the CL block (at -65°C) and the second from the TMC block (at -20°C)[34]. Melting endotherms corresponding to the fusion of CL crystals were also observed. A slight depression of Tm of the CL block (normally of 60°C[34]) arises from the presence of a TMC block. The lower crystallinity of the TMC-CL block copolymer may be explained by the lower content of CL present in this copolymer.

The thermal behavior of the statistical TMC and CL copolymers differed from that of the block copolymers. The statistical copolymer prepared at room temperature with yttrium isopropoxide (entry 7) still showed two glass transition temperatures, corresponding to two amorphous phases, one richer in TMC the other richer in CL. A melting endotherm with a peak Tm of 48°C (ΔH=26 J/g) was also observed, corresponding to fusion of shorter crystallizable CL sequences. These results point to a blocky structure of the polymer, with CL sequences that are long enough to crystallize ($\overline{L}_{CL}$=3.93). All other polymers resulting from polymerization of mixtures of TMC and CL in the presence of SnOct$_2$ (entries 1-4) or yttrium isopropoxide at 80°C (entry 8) have a $\overline{L}_{CL}$<3 and are amorphous polymers with a Tg around -50°C.

Mechanical Properties

The mechanical properties of compression molded specimens of the prepared TMC and CL copolymers are listed in Table 5.

The determined $\overline{M}_n$ and $\overline{M}_w/\overline{M}_n$ values of the compression molded specimens are also given, indicating the thermal processing did not have a significant effect on the polymer molecular weights. Independent of their microstructure, none of the polymers suffered thermal degradation under the applied processing conditions.

As for the thermal properties, 50:50 mol% copolymers of TMC and CL with different average monomer sequence lengths also show very different mechanical behavior.

The mechanical properties of the CL-TMC block copolymer (entry 5) were the most similar to the ones of the CL homopolymer[17], although the copolymer showed a lower Young's modulus due to the presence of the TMC block (210 MPa vs.

300 MPa for poly(CL)). The TMC-CL block copolymer (entry 6) resulting from the sequential polymerization of TMC and CL with yttrium isopropoxide has a lower Young's modulus than the previously described CL-TMC copolymer. This can be explained by the slightly higher TMC mol content present in the copolymer and a possible plasticizing effect of TMC homopolymer chains that may have resulted from unreacted living TMC prepolymer. The ultimate mechanical properties (maximum tensile strength and strain at break) of this copolymer are also lower than those of the equivalent block copolymer prepared from the sequential polymerization of CL followed by TMC. This may be attributed to the lower $\overline{M}_n$ of the former TMC-CL block copolymer (0.2×10^{-5} vs. 0.5×10^{-5}).

Table 5. Mechanical properties of TMC and CL copolymer compression molded films.

No	$\overline{M}_n \times 10^{-5}$	$\overline{M}_w/\overline{M}_n$	E (MPa)	σ_{yield} (MPa)	ε_{yield} (%)	σ_{break} (MPa)	ε_{break} (%)	σ_{max} (MPa)
1	2.7	1.8	4	1	90	0.4^a	1880^a	1
2	2.2	2.0	4	1	90	0.4	270	1
3	3.1	1.7	4	1	100	7	1070	7
4	2.4	1.9	4	1	75	1^a	1870^a	1
5	0.5	1.3	210	8	10	27	960	27
6	0.2	3.9	100	5	30	11	650	11
7	0.5	2.4	45	3	50	14	1030	15
8	0.3	3.0	0.3	0.02	20	$-^b$	$-^b$	0.02
Poly(TMC)^c	3.2	1.8	6	2	130	12	830	12
Poly(CL)^c	1.8	1.9	320	14	12	32	750	32

E – Young's modulus, σ – stress; ε – strain.

^{a} The samples did not break but reached the limit of displacement of the tensile testing apparatus.

^{b} Specimens draw with negligible force.

^{c} Data from references[17,34]; polymerization in the bulk at 130°C for 3 days with SnOct$_2$.

Due to its blocky structure the statistical TMC-CL copolymer prepared at room temperature with yttrium isopropoxide (entry 7) showed a behavior intermediate between the previously described block copolymers and the amorphous copolymers – higher flexibility with relatively high tensile strength. These properties compare favorably with the ones reported previously for the TMC-CL statistical copolymers prepared under similar conditions with lanthanum isopropoxide[18].

All the other copolymers (entries 1-4 and 8) had a low Young's modulus due to their low Tg and amorphous nature. Furthermore, these specimens deformed irreversibly at very low stresses. However, differences in the average monomer sequence length of these polymers still had an effect on the tensile strengths and elongations at brake. The amorphous copolymer with the highest $\overline{L}_{CL}$ (entry 3) showed the best mechanical performance. For this polymer a large upturn in the stress-strain behavior was observed at high elongations. Probably the CL sequences were still long enough to allow a certain degree of organization upon straining of the specimen, resulting in an improvement of the ultimate mechanical properties of the material (tensile strength=7 MPa). The copolymers with the shortest monomer average sequence lengths (entries 1, 2, 4 and 8) are very weak with very low strengths (tensile strength $\leq$ 1 MPa).

CONCLUSIONS

The polymerization conditions (catalyst system, temperature and time) have a pronounced effect on the microstructure of statistical 50:50 mol% TMC and CL copolymers.

In the presence of $SnOct_2$, high molecular weight, amorphous copolymers were prepared. The average monomer sequence lengths were shorter in copolymers prepared at higher temperatures and decreased with reaction time. In the presence of yttrium isopropoxide at room temperature a more blocky and semi-crystalline copolymer resulted from the reaction of TMC and CL mixtures. However, when the reaction was carried out in the bulk at 80°C the average monomer sequence lengths were significantly reduced and an amorphous polymer was obtained. At room temperature the final molecular weight of the polymer was higher than expected considering the monomer to initiator ratio, as not all catalyst sites of the yttrium isopropoxide system were active. In both cases $\overline{M}_w/\overline{M}_n$ was higher than for the polymers obtained from the polymerization with $SnOct_2$ (>2.6 vs. <1.9).

As a result of the differences in microstructure of the copolymer chains, the mechanical behavior of the synthesized copolymers was also greatly influenced by the polymerization conditions. As the Tg values for all the polymers are below room temperature, flexibility is observed for all materials. Statistical copolymers with an average CL sequence length smaller than 3 are amorphous showing low

tensile strength and deforming irreversibly at low stresses. Of the statistical copolymers prepared, the TMC-CL copolymer synthesized in solution at room temperature with yttrium isopropoxide shows the highest average CL sequence length ($\overline{L}_{CL}$ =3.93). With CL sequences long enough to crystallize, this polymer is flexible but much tougher and stiffer, with mechanical properties closer to the ones characteristic for phase separated block copolymers.

ACKNOWLEDGMENTS

REFERENCES

[1] Katz AR, Mukherjee DP, Kaganov AL, Gordon S. A new synthetic monofilament absorbable suture made from polytrimethylene carbonate. *Surg Gynecol Obstet* 1985; 161: 213-222.

[2] Jain RA. The manufacturing techniques of various drug loaded biodegradable poly(lactide-co-glycolide) (PLGA) devices. *Biomaterials* 2000; 21: 2475-2490.

[3] Kumar N, Ravikumar MN, Domb AJ. Biodegradable block copolymers. *Adv Drug Deliv Rev* 2001; 53: 23-44.

[4] Edwards RC, Kiely KD, Eppley BL. The fate of resorbable poly-L-lactic/polyglycolic acid (LactoSorb) bone fixation devices in orthognathic surgery. *J Oral Maxillofac Surg* 2001; 59: 19-25.

[5] Seal BL, Otero TC, Panitch A. Polymeric biomaterials for tissue and organ regeneration. *Mater Sci Eng R-Rep* 2001; 34: 147-230.

[6] Lofgren A, Albertsson A-C, Dubois P, Jerome R. Recent advances in ring-opening polymerization of lactones and related compounds. *J Macromol Sci-Rev Macromol Chem Phys* 1995; C35: 379-418.

[7] Kricheldorf HR. Syntheses and application of polylactides. *Chemosphere* 2001; 43: 49-54.

[8] Nijenhuis AJ, Grijpma DW, Pennings AJ. Lewis acid catalyzed polymerization of L-lactide - Kinetics and mechanism of the bulk-polymerization. *Macromolecules* 1992; 25: 6419-6424.

[9] Kowalski A, Duda A, Penczek S. Kinetics and mechanism of cyclic esters polymerization initiated with tin(II) octoate. 1. Polymerization of ε-caprolactone. *Macromol Rapid Commun* 1998; 19: 567-572.

[10] Albertsson A-C, Eklund M. Synthesis of copolymers of 1,3-dioxa-2-one and oxepan-2-one using coordination catalysts. *J Polym Sci, Part A: Polym Chem* 1994; 32: 265-279.

[11] Kricheldorf HR, Stricker A. Polymers of carbonic acid, 28 - SnOct(2)-initiated polymerizations of trimethylene carbonate (TMC, 1,3-dioxanone-2). *Macromol Chem Phys* 2000; 201: 2557-2565.

[12] Kowalski A, Duda A, Penczek S. Kinetics and mechanism of cyclic esters polymerization initiated with tin(II) octoate. 3. Polymerization of L,L-dilactide. *Macromolecules* 2000; 33: 7359-7370.

[13] Kricheldorf HR, Kreiser-Saunders I, Stricker A. Polylactones 48. SnOct$_2$-initiated polymerizations of lactide: A mechanistic study. *Macromolecules* 2000; 33: 702-709.

[14] Storey RF, Sherman JW. Kinetics and mechanism of the stannous octoate-catalyzed bulk polymerization of ε-caprolactone. *Macromolecules* 2002; 35: 1504-1512.

[15] McLain SJ, Drysdale NE. Yttrium and rare earth compounds catalyzed lactone polymerization. U.S. Patent 5,028,667, E.I. Du Pont de Nemours and Company (1991).

[16] Stevels WM, Dijkstra PJ, Feijen J. New initiators for the ring-opening polymerization of cyclic esters. *Trends Polym Sci* 1997; 5: 300-305.

[17] Pêgo AP, Poot AA, Grijpma DW, Feijen J. Copolymers of trimethylene carbonate and ε-caprolactone for porous nerve guides: synthesis and properties. *J Biomater Sci Polym Ed* 2001; 12: 35-53. Chapter 3 of this thesis.

[18] Schappacher M, Fabre T, Mingotaud AF, Soum A. Study of a (trimethylenecarbonate-co-ε-caprolactone) polymer - Part 1: preparation of a new nerve guide through controlled random copolymerization using rare earth catalysts. *Biomaterials* 2001; 22: 2849-2855.

[19] Crescenzi V, Manzini G, Calzolari G, Borri C. Thermodynamics of fusion of poly-β-propiolactone and poly-ε-caprolactone. Comparative analysis of the melting of aliphatic polylactone and polyester chains. *Eur Polym J* 1972; 8: 449-463.

[20] Hyon S-H, Jamshidi K, Ikada Y. Biocompatible poly-L-lactide fibers. *Polym Prepr* 1983; 24: 6-7.

[21] Leenslag JW, Pennings AJ. Synthesis of high-molecular-weight poly(L-lactide) initiated with tin 2-ethylhexanoate. *Makromol Chem* 1987; 188: 1809-1814.

[22] Schindler A, Hibionada YM, Pitt CG. Aliphatic Polyesters. III. Molecular weight and molecular weight distribution in alcohol-initiated polymerizations of ε-caprolactone. *J Polym Sci Polym Chem Ed* 1982; 20: 319-326.

[23] Stevels WM, Ankone MJK, Dijkstra PJ, Feijen J. Well defined block copolymers of ε-caprolactone and L- lactide using $Y_5(\mu\text{-O})(O^iPr)_{13}$ as an initiator. *Macromol Chem Phys* 1995; 196: 1153-1161.

[24] Stevels WM, Ankone MJK, Dijkstra PJ, Feijen J. Stereocomplex formation in ABA triblock copolymers of poly(lactide)(A) and poly(ethylene-glycol)(B). *Macromol Chem Phys* 1995; 196: 3687-3694.

[25] Stevels WM, Ankone MJK, Dijkstra PJ, Feijen J. Stereocomplex formation in AB di-block copolymers of poly(ε-caprolactone) (A) and poly(lactide) (B). *Macromol Symp* 1996; 102: 107-113.

[26] Poncelet O, Sartain WJ, Hubertpfalzgraf LG, Folting K, Caulton KG. Chemistry of yttrium triisopropoxide revisited. Characterization and crystal structure of $Y_5(\mu_5\text{-O})(\mu_3\text{-O}^iPr)_4(\mu_2\text{-O}^iPr)_4(O^iPr)_5$. *Inorg Chem* 1989; 28: 263-267.

[27] Thiam M, Spassky N. Polymerization of cyclohexene oxide using yttrium isopropoxide and a bimetallic yttrium-aluminium isopropoxide as initiators. *Macromol Chem Phys* 1999; 200: 2107-2110.

[28] Onfroy V, Schappacher M, Soum A. Controlled ring-opening polymerization of trimethylene carbonate initiated by lanthanide derivatives. International Symposium on Ionic Polymerization. Paris, France (1997), p. 246-249.

[29] McLain SJ, Drysdale NE. Living ring-opening polymerization of ε-caprolactone by yttrium and lanthanide alkoxides. *Polym Prepr* 1992; 33: 174-175.

[30] Grijpma DW, Pennings AJ. Polymerization temperature effects on the properties of L-lactide and ε-caprolactone copolymers. *Polym Bull* 1991; 25: 335-341.

[31] Veld PJA, Ye WP, Klap R, Dijkstra PJ, Feijen J. Copolymerization of ε-caprolactone and morpholine-2,5-dione derivatives. *Macromol Chem Phys* 1992; 193: 1927-1942.

[32] Spassky N, Simic V, Hubert-Pfalzgraf LG, Montaudo MS. Synthesis of aliphatic polyesters by controlled ring-opening polymerization of cyclic esters. Characterization, properties, transesterification reactions. *Macromol Symp* 1999; 144: 257-267.

[33] Lemmouchi Y, Schacht E, Kageruka P, De Deken R, Diarra B, Diall O, Geerts S. Biodegradable polyesters for controlled release of trypanocidal drugs: *in vitro* and *in vivo* studies. *Biomaterials* 1998; 19: 1827-1837.

[34] Pêgo AP, Poot AA, Grijpma DW, Feijen J. *In vitro* degradation of trimethylene carbonate based (co)polymers. *Macromol Chem Phys (accepted for publication)* Chapter 6 of this thesis.

CHAPTER 5

Physical properties of high molecular weight 1,3-trimethylene carbonate and D,L-lactide copolymers*

A.P. PÊGO, A.A. POOT, D.W. GRIJPMA and J. FEIJEN

Institute for Biomedical Technology (BMTI) and Department of Polymer Chemistry and Biomaterials, Faculty of Chemical Technology, University of Twente, P.O. Box 217, 7500 AE Enschede, The Netherlands

ABSTRACT

High molecular weight statistical copolymers of 1,3-trimethylene carbonate (TMC) and D,L-lactide (DLLA) were synthesized and characterized with the aim of assessing their potential in the development of degradable and flexible materials for application in the biomedical field. Under the applied polymerization conditions (130°C, 3 days using stannous octoate as a catalyst) monomer conversion was high or almost complete, and high molecular weight polymers ($\overline{M}_n$ above 170,000) were obtained. Significant improvement of the mechanical performance of these materials was observed in comparison to results previously reported for TMC and DLLA based copolymers of lower molecular weight. For the entire range of compositions the polymers are amorphous with a glass transition temperature ranging between -17°C for poly(TMC) and 53°C for poly(DLLA). The polymers vary from rubbers to stiff materials as the content of TMC decreases. All polymers are hydrophobic with very low equilibrium water absorption (<1.5 wt%). Thermal analyses and tensile tests were performed on polymer samples after water uptake. Due to a plasticizing effect of the water the thermal properties, and consequently the mechanical performance, of the copolymers with higher content of DLLA were the most affected. After water absorption the polymer mechanical behavior can change from glassy to rubbery, as observed for the copolymer with 80 mol% of DLLA. The obtained results suggest that these copolymers are promising candidates as biomaterials in the preparation of degradable medical devices and systems.

INTRODUCTION

Synthetic bioresorbable polymers have found application in different fields of medicine. Already in clinical use are sutures (Vicryl[®]), carriers for controlled drug release (Lupron Depot[®]) and several medical devices such as bone plates and screws (Lactosorb[®]). In the past few years much interest has risen in the use of degradable polymers for the preparation of three-dimensional scaffolds for tissue engineering[1,2]. Studies involving bioresorbable polymers are numerous and deal with the synthesis and characterization of the polymer chemical structure, biocompatibility, degradation behavior and processing of the material into the desired device or system. Despite the extensive advances made in the biomaterial field, the number of polymers available for biomedical applications is still restricted. In particular, most attention has been given to polymers based on poly(lactic acid) (PLA) and poly(glycolic acid) (PGA), as well as their copolymers. This is largely due to their biocompatibility and to their resorbability through natural pathways but also because these polymers are approved by the Food and Drug Administration, provided that they are synthesized by ring-opening polymerization of the corresponding cyclic dimers, using stannous octoate as catalyst[3]. However, these materials, either crystalline or amorphous, are relatively stiff and brittle and can have too high degradation rates for certain applications[4]. For example, in soft tissue engineering applications, a flexible but relatively tough material with tunable degradation properties would be preferable[5,6]. Amorphous polymers with glass transition temperatures below body temperature are expected to exhibit high permeabilities making them very suitable in drug delivery applications[7].

Copolymerization has been widely used to reach the desired material characteristics in the final polymer[8-10]. In the search for elastomeric degradable materials for biomedical applications we have been using poly(1,3-trimethylene carbonate) (poly(TMC)) – an amorphous polymer with a glass transition temperature of approximately -15°C[11,12] – as a starting point in the design of alternative synthetic materials. The incorporation of other monomer units into the poly(TMC) chain proved to be a successful method of modulating the rate of polymer degradation as well as modifying its physical properties[13,14]. We have previously reported on the synthesis and physical properties of poly(ester carbonate)s based on TMC and ε-caprolactone (CL) for the preparation of porous degradable nerve guides[12]. These materials are expected to degrade slowly[15] and are more suitable for long-term

applications where the integrity of the system should be kept for relatively long periods of time. In order to further tune the physical properties and degradation profile of poly(TMC), TMC was copolymerized with D,L-lactide (DLLA). Poly(DLLA) is an amorphous polymer with a glass transition temperature around 54°C[16], which degrades more rapidly than poly(CL)[17]. The copolymerization of TMC with DLLA yields amorphous materials with degradation rates that are expected to be faster than the ones of copolymers based on TMC and CL[14].

The physical properties of a polymer are directly dependent on its molecular weight. By preparing high molecular weight polymers one can obtain materials with good mechanical performance, even after processing methods that can induce chain scission like melt processing[18,19] or sterilization by gamma irradiation[20]. The control of the initial molecular weight of a degradable polymer is also a powerful way to control the time lag before the onset of mechanical properties and mass loss, as well as the total time for complete polymer resorption[21]. The synthesis and characterization of relatively low molecular weight TMC and DLLA based copolymers have been previously described[14,22]. In the present study the effect of copolymerization on the physical properties of TMC and DLLA copolymers of much higher molecular weight was evaluated.

MATERIALS AND METHODS

Materials

Polymer grade 1,3-trimethylene carbonate (TMC) (1,3-dioxan-2-one) and D,L-lactide (DLLA) (racemic mixture of D and L enantiomers of 3,6-dimethyl-dioxan-2,5-dione) were obtained, respectively, from Boehringer Ingelheim, Germany and Purac Biochem, The Netherlands. Stannous octoate (SnOct$_2$) (stannous 2-ethylhexanoate) was used as received from Sigma, USA. Solvents were of analytical grade (Biosolve, The Netherlands).

Polymer Synthesis

In an argon atmosphere, a mixture of monomers was charged into dried freshly silanized (Serva, Boehringer Ingelheim Bioproducts Partnership, Germany) glass ampoules and $2x10^{-4}$ mol of stannous octoate per mol of monomer was added as a solution in sodium-dried pentane. The pentane was removed afterwards by evacuation. The ampoules were purged three times with dry argon and heat-sealed

under vacuum. The ampoules were conditioned in an oil bath pre-heated to the polymerization temperature and vigorously shaken in order to obtain a homogeneous mixture of the monomers and the catalyst. All homo- and copolymerizations were carried out over a period of 3 days at 130°C±2°C. The ampoules were then quenched to room temperature and the polymers were discharged. For purification the obtained polymers were dissolved in chloroform (2-5 wt/vol%), filtered through a sintered glass filter, and subsequently precipitated into a ten-fold volume of isopropanol. The precipitated polymers were washed with fresh isopropanol and dried under reduced pressure at room temperature until constant weight.

Polymer Analysis and Characterization

The synthesized polymers were characterized with regard to the monomer conversion and chemical composition by nuclear magnetic resonance (NMR) spectroscopy. 300 MHz ^{1}H-NMR (Varian Inova 300 MHz, USA) spectra were recorded using polymer solutions in CDCl$_3$ (Sigma, USA).

Molecular weights, molecular weight distributions and intrinsic viscosities of the purified polymers were determined by gel permeation chromatography (GPC) using a Waters Model 510 pump (USA), a HP Ti-Series 1050 autosampler (USA), a Waters Model 410 Differential Refractometer and a Viscotek H502 Viscometer Detector (USA) with 10^5- 10^4- 10^3- 500 Å Waters Ultra-Styragel columns placed in series. Chloroform was used as eluent at a flow rate of 1.5 ml/min. Narrow polystyrene standards were used for calibration. Sample concentrations of approximately 0.5 wt/vol% and injection volumes of 30 μl were used. All determinations were performed at 25°C.

The thermal properties of the synthesized materials were evaluated by differential scanning calorimetry (DSC). Samples (5-15 mg) placed in aluminum pans were analyzed with a Perkin Elmer Pyris1 (USA) at a heating rate of 10°C/min. All samples were heated to 40°C above their glass transition temperature. The samples were then quenched rapidly (300°C/min) until 40°C below their glass transition temperature and after 5 min a second scan was recorded. Unless mentioned otherwise, the data presented were collected during the second heating scan. The glass transition temperature was taken as the midpoint of the heat capacity change. Indium, gallium and tin were used as standards for temperature calibration.

Mechanical Properties

Tensile testing was performed on compression molded films. Purified polymer samples were compression molded in a 600 μm thick mould at 140°C. All test specimens had dimensions in accordance to ASTM D882-91 specifications. Tensile tests in three-fold were carried out at room temperature on a Zwick Z020 (Germany) universal tensile testing machine operated at a crosshead speed of 50 mm/min and a grip-to-grip separation of 50 mm. The specimen deformation was derived from the grip-to-grip separation, therefore the presented values of Young's modulus (calculated from the initial slope of the stress-strain curves) give only an indication of the stiffness of the different polymers.

Wettability and Water Uptake

Static contact angles of ultra-pure water (MilliQ Plus – Millipore, France) and water uptake in phosphate buffered saline (PBS, pH 7.4, NPBI, The Netherlands) were used to evaluate the wettability of the TMC and DLLA based (co)polymers.

Static contact angles of films spin-coated from chloroform solutions (2.1-2.5 wt/vol%) onto glass slips were measured with a Video-based Optical Contact Angle Meter OCA 15 (DataPhysics Instruments GmbH, Germany). The measurements were performed at room temperature on profiles of sessile drops and readings were taken within the first 10-15 s. Angles were measured on at least five different regions of each polymer surface and the results were averaged.

The water uptake was defined as the weight gain of the polymer specimen after conditioning, according to equation 1:

$$\text{water uptake} = \frac{w - w_o}{w_o} \times 100 \quad (wt\%) \tag{1}$$

where w_o is the initial specimen weight and w the weight of the specimen after conditioning. Compression molded specimens ($100 \times 50 \times 0.6$ mm^3) were placed in PBS at 37°C and the sample weight was evaluated for a period of 24 hrs. After this time the wet samples were subjected to thermal analysis and tensile testing.

RESULTS AND DISCUSSION

Polymer Synthesis

Statistical copolymers of TMC and DLLA were synthesized by ring-opening polymerization in the melt using stannous octoate as a catalyst (Figure 1). Different

examples of catalyst systems used for the copolymerization of these monomers can be found in literature[22-24]. Stannous octoate was selected, as it is highly efficient and frequently used in the preparation of polymers for biomedical applications[25].
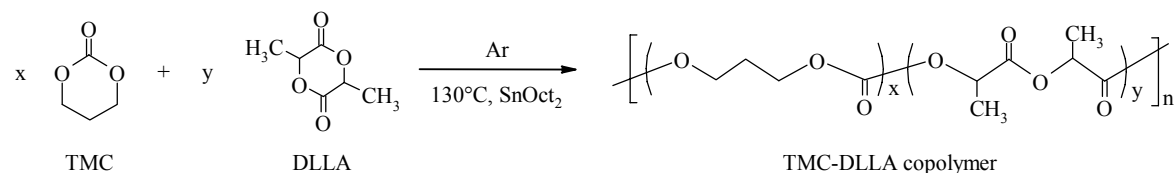

Figure 1. Synthesis of statistical poly(1,3-trimethylene carbonate-co-D,L-lactide).

A series of copolymers with a TMC content ranging from 20 to 79 mol% and the corresponding homopolymers were prepared (Table 1).

Table 1. Copolymerization of TMC and DLLA with stannous octoate as a catalyst at 130°C.

TMC/DLLA charged (mol ratio)	TMC conversion (%)	DLLA conversion (%)	Polymer composition[a] TMC/DLLA (mol ratio)
100/0	99.5	-	100/0
85/15	99.7	99.6	79/21
75/25	99.3	99.0	72/28
50/50	97.8	98.3	50/50
30/70	98.4	96.5	34/66
22/78	93.6	98.0	20/80
0/100	-	97.4	0/100

[a] As determined by ^{1}H-NMR.

The copolymer composition and monomer conversion could be determined by ^{1}H-NMR spectroscopy of the crude polymerization products, since the α-methylene resonances of monomeric (t, 4H, δ=4.44 ppm) and polymeric TMC (m, 4H, δ=4.18-4.26 ppm) as well as the methyl resonances of monomeric (d, 6H, 1.65 and 1.67 ppm) and polymeric (m, 2H, δ=1.39-1.63 ppm) DLLA are separated. Under the applied polymerization conditions the monomer conversion was high or almost complete. In some cases the obtained compositions differ slightly from the ratio of monomers charged. This may be explained by a small loss of monomer that sublimated during the purging and evacuation of the ampoules. In addition to the doublet corresponding to the DLLA monomer, another doublet (1.69 and 1.71 ppm)

was identified downfield in the spectrum of the polymers with high content of DLLA. By comparison with values found in literature[22,26], these peaks were assigned to methyl protons belonging to traces of mesolactide monomer. ^{1}H-NMR analysis of the crude polymerization products also allowed the determination of the monomer distribution in the copolymers as the methine portion of the spectrum is sensitive to sequence effects. The NMR signal of D,L-lactyl units (-CO-C$\underline{H}$(CH$_3$)-O-) next to other D,L-lactyl units at $\delta > 5.08$ ppm can be distinguished from the signal of D,L-lactyl units next to TMC units (-CO-O-(CH$_2$)$_3$-O-) at $\delta < 5.08$, allowing the calculation of the average sequence length of lactyl units ($\overline{L}_{LA}$) from the relative intensity of these signals:

$$\overline{L}_{LA} = \frac{I_{(\underline{LA} - LA)}}{I_{(\underline{LA} - TMC)}} + 1 \qquad (2)$$

Table 2 shows the average sequence length of the lactyl units determined this way, as well as the average sequence length of the TMC units ($\overline{L}_{TMC}$). The latter was determined from the average lactyl sequence length and the monomer ratio in the polymer. Previous reports confirm the correctness of this method by showing that the sequence lengths determined by ^{1}H-NMR are in accordance with those determined by integration of the carbonyl signals obtained by ^{13}C-NMR analysis[27].

Table 2. Average sequence lengths of lactyl units ($\overline{L}_{LA}$) and TMC units ($\overline{L}_{TMC}$) of TMC and DLLA copolymers based on ^{1}H-NMR analysis.

Polymer composition TMC/DLLA (mol ratio)	$\overline{L}_{LA}$	$\overline{L}_{TMC}$
79/21	1.35	2.54
72/28	1.65	2.12
50/50	2.67	1.34
34/66	4.08	1.05
20/80	7.70	0.96

For the copolymer containing 50:50 mol% of TMC and DLLA the average sequence lengths are 2.67 and 1.34 for the lactyl and TMC repeating units, respectively. A truly random monomer incorporation would yield average monomer sequence lengths equal to 4 for the lactyl units and 2 for the TMC units. An alternating incorporation of the monomers would result in average monomer sequence lengths of 2 for the lactyl units and 1 for the TMC units. The obtained values indicate a monomer distribution between random and alternating. This

observation is in accordance with previous reports in which the product of the reactivity ratios of these monomers was found to be smaller than 1[14]. Furthermore, these results show that copolymers with a TMC/DLLA mole ratio of 79/21 and 72/28 have single lactyl units connected to TMC on both sides, as the average lactyl sequence length is smaller than 2. The occurrence of TMC-lactyl-TMC sequences can only be explained by the occurrence of transesterification reactions, as the ring-opening polymerization of DLLA monomer could never yield such triad. This last observation is supported by the detection by ^{1}H-NMR analysis of mesolactide in the crude polymer. As no mesolactide contamination was detected in the DLLA monomer used in the polymerizations, such structure can result from the transesterification of the racemic monomer or be a consequence of depolymerization.

Table 3. Molecular weights and intrinsic viscosity of TMC and DLLA (co)polymers determined by GPC.

Polymer composition TMC/DLLA (mol%)	$\overline{M}_w \times 10^{-5}$	$\overline{M}_n \times 10^{-5}$	PDI	$[\eta]$ (dl/g)
100	5.59	3.37	1.66	4.49
79	3.58	1.72	2.08	2.59
72	3.65	1.75	2.08	2.63
50	6.44	2.75	2.34	2.91
34	5.80	2.60	2.23	3.11
20	7.18	4.49	1.60	3.40
0	8.79	3.78	2.32	4.15

In Table 3 the values of the weight and number average molecular weight ($\overline{M}_w$ and $\overline{M}_n$, respectively), polydispersity index (PDI) and intrinsic viscosity ($[\eta]$) of the prepared polymers are given. Under the applied polymerization conditions high molecular weight polymers were obtained. In previous work molecular weights for these (co)polymers include: $[\eta]$ values between 0.9-1.7 dl/g[22] and $\overline{M}_n$ in the range of 20,000 or lower[14]. The polydispersity values of all (co)polymers are approximately equal to two. This value has been reported before for lactone ring-opening polymerizations where transesterification reactions had occurred[28,29].

Thermal Properties

The thermal properties of the TMC copolymers can be varied to a large extent by adjusting the quantity of comonomer used.

In the DSC scans no evidence of crystallinity was found. As the crystalline phase is poorly accessible to water and other permeants, an increase in crystallinity reduces the polymer permeability and the rate of biodegradation by chain scission due to a decrease in accessible hydrolysable bonds. Concerning the use of these polymers for biomedical applications, one should further consider the fact that crystalline debris formed during degradation may cause an undesired late inflammatory response, negatively influencing tissue growth and normal function[30]. Therefore, little or no crystallinity is desired.

Almost for all polymers it was possible to observe an endotherm superimposed on the change of heat capacity at the glass transition temperature (Tg) in the first DSC scan. This endotherm is due to enthalpy relaxation, a phenomenon dependent on the thermal history of the samples[16]. In order to investigate the effect of monomer composition on the thermal properties of the polymers, the glass transition temperature was determined from the second heating scan. An increase in DLLA content resulted in an increase in Tg, with values ranging from 53°C for poly(DLLA) to -17°C for poly(TMC) (Figure 2). At DLLA contents above 60 wt% all copolymers were in the glassy state at room temperature.

The Fox equation allows the estimation of the glass transition temperature of a copolymer based on the glass transition temperatures of the respective homopolymers[31]:

$$\frac{1}{Tg} = \frac{w1}{Tg1} + \frac{w2}{Tg2} \tag{3}$$

where w_1 and w_2 refer to the weight fraction of the two comonomers and Tg_1 and Tg_2 refer to the glass transition temperatures of the two corresponding homopolymers. The close fit of the experimental values with the Fox equation (Figure 2) indicates that for all compositions a single amorphous phase exists.
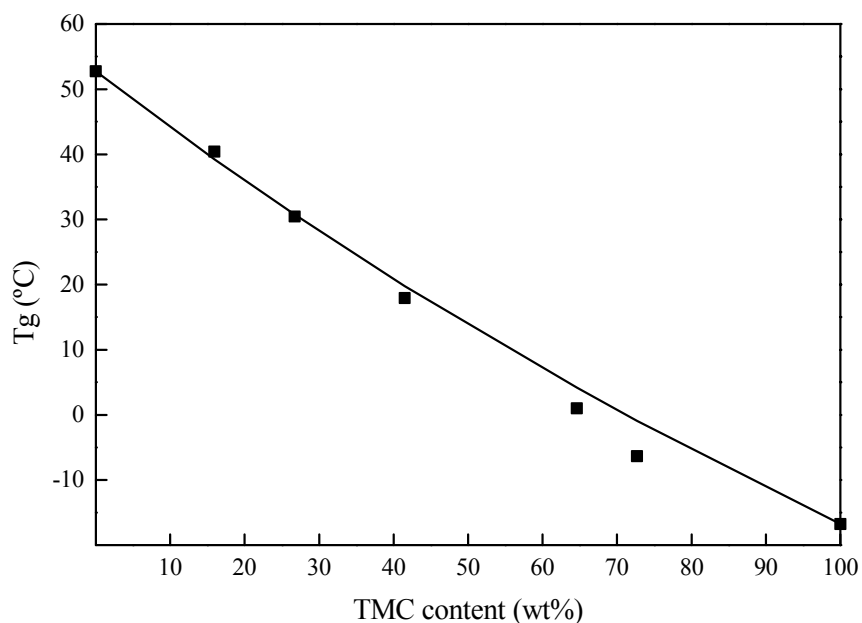
Figure 2. Thermal properties of TMC and DLLA (co)polymers as a function of the TMC content: (■) Experimental glass transition temperature (Tg); (—) Fox equation.

Mechanical Properties

Considering the thermal properties of the synthesized TMC and DLLA (co)polymers one can expect a great effect of the polymer composition on the mechanical behavior of these materials.

Initially, specimens for tensile testing were obtained from films prepared by casting chloroform solutions of these polymers. However, for the polymers containing high contents of DLLA, the last traces of solvent were extremely difficult to remove from the films, requiring a series of time consuming extraction and drying steps. Even in small amounts, the presence of solvent in the films has a strong influence on the specimen mechanical properties due to the lowering of the polymer Tg, as a consequence of a plasticizing effect of the solvent[32,33]. To ensure that the results were not affected by the possible presence of remaining solvent, tensile testing was performed on compression molded samples. Typical stress-strain curves are presented in Figure 3.
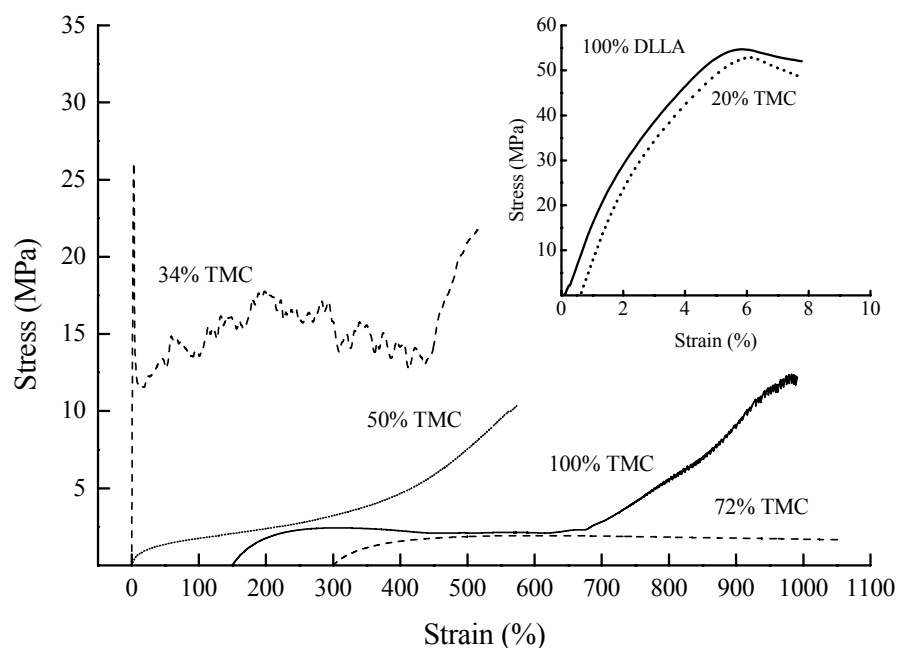
Figure 3. Stress-strain curves of TMC and DLLA (co)polymers (curves are offset for clarity).

The mechanical properties of the prepared TMC-DLLA copolymers are listed in Table 4. The $\overline{M}_n$ and $[\eta]$ of the compression molded samples are also given. One can observe that especially for poly(DLLA) and the TMC-DLLA copolymer with 20 mol% of TMC heat processing resulted in extensive chain scission. This observation illustrates the previously mentioned need for high molecular weight polymers, to ensure good mechanical performance after heat processing.

The high modulus and strength, and the small elongations at break observed for the copolymer with 20 mol% of TMC and the DLLA homopolymer reflect the stiffness and relatively brittle character of these polymers in the glassy state at room temperature. The copolymer with 34 mol% of TMC is stiff but more ductile than the (co)polymers with lower TMC content, despite the fact that its Tg is above room temperature. The copolymer with 50 mol% of TMC (Tg=18°C) shows highly flexible behavior but is still reasonably strong as its Tg is only slightly below room temperature. The copolymers with higher TMC content are highly flexible but rather weak, having low strength (tensile strength below 2 MPa) and deforming irreversibly at very low stresses. As previously reported[12], not only a high elongation at break but also a large upturn at high elongations in the stress-strain behavior of the TMC homopolymer were observed. The high value for the stress at

break (corresponding also to the maximum stress) was found to be the result of strain-induced crystallization. This significantly improves the mechanical performance of this material at room temperature.

In comparison with the previously reported values for the TMC and DLLA based copolymers of lower molecular weight[22], a significant improvement of mechanical performance of these polymers was observed. Strain-induced crystallization of poly(TMC) was also shown to be dependent on the molecular weight of the specimens (see Chapter 8).

Table 4. Mechanical properties of TMC and DLLA (co)polymer compression molded films.

TMC content (mol%)	$\overline{M_n} \times 10^{-5}$	$[\eta]$ (dl/g)	Young's Modulus (MPa)	σ_{yield} (MPa)	ε_{yield} (%)	σ_{break} (MPa)	ε_{break} (%)	σ_{max} (MPa)
100	3.24	4.34	6	2	130	12	830	12
79	1.71	2.63	5	2	160	2	270	2
72	1.76	2.66	5	2	300	2	730	2
50	2.56	3.24	16	1	54	10	570	10
34	2.58	3.25	1500	28	3	24	480	28
20	2.85	3.50	1900	51	5	46	7	51
0	2.91	3.85	1900	53	6	52	6	53

Wettability and Water Uptake

The water uptake of a polymer can have important consequences for its thermal and mechanical properties. When designing a biodegradable material for use in the preparation of implantable biomedical devices and systems, the impact of the material's hydrophilicity extends further to other polymer properties. Protein-polymer interactions are particularly dependent on the hydrophilicity of the polymer surface[34] and directly affect the biocompatibility of the polymer and cell-material interactions[35]. Hydrophilicity will also influence the degradation rate of the material[36].

The static contact angles of the TMC and DLLA (co)polymers, which are a measure of the polymer surface hydrophilicity, are presented in Figure 4. Although the values do not differ largely, the static contact angle decreases slightly with the increase of either monomer content, reaching a maximum for the copolymers with 50 to 60 mol% of TMC. The values for the static contact angles of these polymers

are high, indicating relatively hydrophobic surfaces[34,37]. The water uptake of the TMC and DLLA (co)polymers in PBS at 37°C was followed for a period of one day. After 24 hrs the water absorption had reached equilibrium and for all materials a very low (<1.5 wt%) water uptake was observed (Figure 4). Despite the small differences one can observe that the water uptake slightly increases with TMC content. This can be explained by a decrease in Tg that increases polymer chain mobility and free volume, increasing water accessibility. Regardless of the described differences in water uptake and static contact angles, all (co)polymers can be considered hydrophobic.

The low water uptake observed for these materials is in accordance with the high values of the contact angle, which are characteristic of hydrophobic materials. Much lower static contact angles have been previously reported for TMC-DLLA based copolymers[14]. Copolymers with TMC contents ranging from 40 to 80 mol% respectively possessed, water static contact angles between approximately 15 and 50 degrees. These values seem inconsistent with the water uptake values (<5 wt%) reported in the same study.
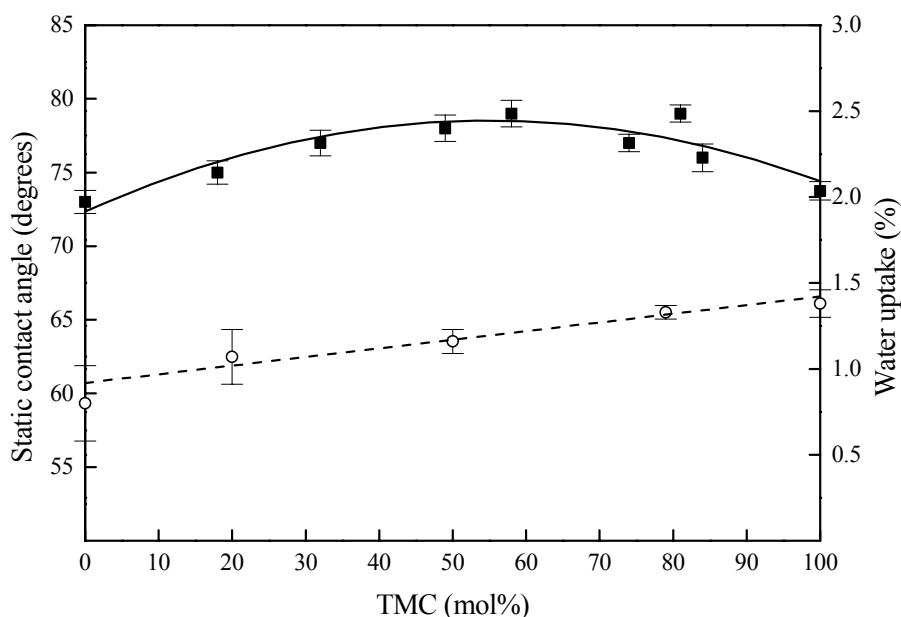

Figure 4. Wettability of TMC and DLLA (co)polymers. Static contact angle (■) and water uptake of compression molded samples after 1 day (○).

Thermal analyses and tensile tests were performed on polymer samples after water uptake in order to assess the effect of this parameter on the polymer thermal and

mechanical properties (Table 5). After water uptake the thermal properties of the copolymers with higher DLLA contents were the most affected (see Table 4 for comparison). Related to this plasticizing effect of water a decrease in the Young's modulus and maximum stress were recorded for all samples with the exception of poly(TMC). In particular the behavior of the copolymer containing 20 mol% of TMC is worth noticing. At room temperature this material is in the glassy state (Tg=40°C) allowing easy processing and handling. After water uptake, Tg decreases to below body temperature and the material will show rubbery behavior under physiologic conditions.

Table 5. Mechanical properties of TMC and DLLA (co)polymers after water uptake (in PBS, at 37°C).

TMC content (mol%)	Water uptake (%)	Tg^a (°C)	Young's modulus (MPa)	σ_{max} (MPa)
100	1.11	-19	6	18
79	1.32	-9	4	1
50	1.04	11	13	11
20	0.77	33	1100	38
0	0.69	46	1400	50

^{a} First heating scan (DSC).

CONCLUSIONS

High molecular weight statistical copolymers of TMC and DLLA were synthesized, characterized and compared with the parent polymers - poly(TMC) and poly(DLLA). The obtained results show that the thermal and mechanical properties of the polymers are strongly dependent on the composition. Furthermore, significant improvement of the mechanical performance of these materials was observed in comparison to results previously reported for TMC and DLLA based copolymers of lower molecular weight. All TMC and DLLA based (co)polymers are amorphous with Tg values varying between -17°C for poly(TMC) and 53°C for poly(DLLA). Therefore, the obtained materials vary from rubbers to stiff materials as the content of TMC decreases.

All materials are hydrophobic (water uptake <1.5%), although copolymers with higher TMC contents showed a slightly higher water uptake. The thermal

properties, and consequently the mechanical performance, of the copolymers with higher content of DLLA were the most affected when evaluated in the wet state. After water absorption the mechanical behavior of the polymer can change from glassy to rubbery, as observed for the copolymer with 20 mol% of TMC.

The properties of the TMC and DLLA copolymers suggest their suitability as materials for resorbable biomedical devices. Copolymers with a high content of DLLA show good mechanical performance for application in the preparation of non-load bearing implants such as in soft tissue engineering. The highly elastic poly(TMC) and copolymers with high content of TMC seem more suitable for application as coatings or drug delivery systems.

ACKNOWLEDGMENTS

REFERENCES

[1]   Marler JJ, Upton J, Langer R, Vacanti JP. Transplantation of cells in matrices for tissue regeneration. *Adv Drug Deliv Rev* 1998; 33: 165-182.

[2]   Seal BL, Otero TC, Panitch A. Polymeric biomaterials for tissue and organ regeneration. *Mater Sci Eng R-Rep* 2001; 34: 147-230.

[3]   Vert M, Schwach G, Engel R, Coudane J. Something new in the field of PLA/GA bioresorbable polymers? *J Control Release* 1998; 53: 85-92.

[4]   Folliguet TA, Rucker-Martin C, Pavoine C, Deroubaix E, Henaff M, Mercadier JJ, Hatem SN. Adult cardiac myocytes survive and remain excitable during long-term culture on synthetic supports. *J Thorac Cardiovasc Surg* 2001; 121: 510-519.

[5]   Niklason LE, Gao J, Abbott WM, Hirschi KK, Houser S, Marini R, Langer R. Functional arteries grown *in vitro*. *Science* 1999; 284: 489-493.

[6]   Stock UA, Vacanti JP. Tissue engineering: current state and prospects. *Annu Rev Med* 2001; 52: 443-451.

[7]   Pitt CG, "Poly-ε-caprolactone and its copolymers" In: Chasin M, Langer R. *Biodegradable polymers as drug delivery systems*, New York, NY: Marcel Dekker; 1990. p 71-120.

[8]   Gilding DK, Reed AM. Biodegradable polymers for use in surgery-polyglycolic/poly(lactic acid) homo- and copolymers:1. *Polymer* 1979; 20: 1459-1464.

[9]   Reed AM, Gilding DK. Biodegradable polymers for use in surgery - poly(glycolic)/poly(lactic acid) homo and copolymers: 2. *In vitro* degradation. *Polymer* 1981; 22: 494-498.

[10]   Schakenraad JM, Nieuwenhuis P, Molenaar I, Helder J, Dijkstra PJ, Feijen J. *In vivo* and *in vitro* degradation of glycine/DL-lactic acid copolymers. *J Biomed Mater Res* 1989; 23: 1271-1288.

[11]   Zhu KJ, Hendren RW, Jensen K, Pitt CG. Synthesis, properties, and biodegradation of poly(1,3-trimethylene carbonate). *Macromolecules* 1991; 24: 1736-1740.

[12]   Pêgo AP, Poot AA, Grijpma DW, Feijen J. Copolymers of trimethylene carbonate and ε-caprolactone for porous nerve guides: synthesis and properties. *J Biomater Sci Polym Ed* 2001; 12: 35-53. Chapter 3 of this thesis.

[13]   Katz AR, Mukherjee DP, Kaganov AL, Gordon S. A new synthetic monofilament absorbable suture made from polytrimethylene carbonate. *Surg Gynecol Obstet* 1985; 161: 213-222.

[14]   Jie C, Zhu KJ. Preparation, characterization and biodegradable characteristics of poly(D,L-lactide-co-1,3-trimethylene carbonate). *Polym Int* 1997; 42: 373-379.

[15]   Albertsson A-C, Eklund M. Influence of molecular structure on the degradation mechanism of degradable polymers: *in vitro* degradation of poly(trimethylene carbonate), poly(trimethylene carbonate-co-caprolactone), and poly(adipic anhydride). *J Appl Polym Sci* 1995; 57: 87-103.

[16]   Joziasse CAP, Veenstra H, Grijpma DW, Pennings AJ. On the chain stiffness of poly(lactide)s. *Macromol Chem Phys* 1996; 197: 2219-2229.

[17]   Pitt CG, Gratzl MM, Kimmel GL, Surles J, Schindler A. Aliphatic polyesters II. The degradation of poly(DL-lactide), poly (ε-caprolactone), and their copolymers *in vivo*. *Biomaterials* 1981; 2: 215-220.

[18]   von Oepen R, Michaeli W. Injection moulding of biodegradable implants. *Clin Mater* 1992; 10: 21-28.

[19]   Gogolewski S, Jovanovic M, Perren SM, Dillon JG, Hughes MK. The effect of melt-processing on the degradation of selected polyhydroxyacids - polylactides, polyhydroxybutyrate, and polyhydroxybutyrate-co-valerates. *Polym Degrad Stabil* 1993; 40: 313-322.

[20]   Birkinshaw C, Buggy M, Henn GG, Jones E. Irradiation of poly-D,L-lactide. *Polym Degrad Stabil* 1992; 38: 249-253.

[21]   Pitt CG, Chasalow FI, Hibionada DM, Klimas DM, Schindler A. Aliphatic polyesters. I. The degradation of poly(ε-caprolactone) *in vivo*. *J Appl Polym Sci* 1981; 26: 3779-3787.

[22] Buchholz B. Analysis and characterization of resorbable DL-lactide-trimethylene carbonate copolyesters. *J Mater Sci: Mater Med* 1993; 4: 381-388.

[23] Huang Q, Shen Z, Zhang Y, Shen Y, Shen L, Yuan H. Ring-opening copolymerization of trimethylene carbonate and D,L-lactide by rare earth chloride. *Polym J* 1998; 30: 168-170.

[24] Matsumura S, Tsukada K, Toshima K. Novel lipase-catalyzed ring-opening copolymerization of lactide and trimethylene carbonate forming poly(ester carbonate)s. *Int J Biol Macromol* 1999; 25: 161-167.

[25] Kricheldorf HR, Kreiser-Saunders I, Boettcher C. Polylactones: 31. Sn(II)octoate-initiated polymerization of L-lactide: a mechanistic study. *Polymer* 1995; 36: 1253-1259.

[26] Chisholm MH, Eilerts NW, Huffman JC, Iyer SS, Pacold M, Phomphrai K. Molecular design of single-site metal alkoxide catalyst precursors for ring-opening polymerization reactions leading to polyoxygenates. 1. Polylactide formation by achiral and chiral magnesium and zinc alkoxides, (eta(3)-L)MOR, where L = trispyrazolyl- and trisindazolylborate ligands. *J Am Chem Soc* 2000; 122: 11845-11854.

[27] Grijpma DW, Pennings AJ. (Co)polymers of L-lactide.1. Synthesis, thermal properties and hydrolytic degradation. *Macromol Chem Phys* 1994; 195: 1633-1647.

[28] Leenslag JW, Pennings AJ. Synthesis of high-molecular-weight poly(L-lactide) initiated with tin 2-ethylhexanoate. *Makromol Chem* 1987; 188: 1809-1814.

[29] van Dijk JAPP, Smit JAM, Kohn FE, Feijen J. Characterization of poly(D,L-lactic acid) by gel permeation chromatography. *J Polym Sci: Polym Chem Ed* 1983; 21: 197-208.

[30] Bos RRM, Rozema FR, Boering G, Nijenhuis AJ, Pennings AJ, Verwey AB, Nieuwenhuis P, Jansen HWB. Degradation of and tissue reaction to biodegradable poly(L-lactide) for use as internal fixation of fractures: a study in rats. *Biomaterials* 1991; 12: 32-36.

[31] Fox TG. Influence of diluent and copolymer composition on the glass temperature of a polymer system. *Bull Amer Phys Soc* 1956; 2: 123.

[32] Triolo PM. "The release of bovine serum albumin from biodegradable poly(L-lactic acid) matrices" Ph.D. Thesis. University of Utah, Salt Lake City. 1987.

[33] Mauduit J, Perouse E, Vert M. Hydrolytic degradation of films prepared from blends of high and low molecular weight poly(DL-lactic acid)s. *J Biomed Mater Res* 1996; 30: 201-207.

[34] van Wachem PB, Beugeling T, Feijen J, Bantjes A, Detmers JP, van Aken WG. Interaction of cultured human endothelial cells with polymeric surfaces of different wettabilities. *Biomaterials* 1985; 6: 403-408.

[35] Hubbell JA. Biomaterials in tissue engineering. *Bio-Technol* 1995; 13: 565-576.

[36] Li SM, Garreau H, Vert M. Structure-property relationships in the case of the degradation of massive poly(α-hydroxy acids) in aqueous-media. Part 2. Degradation of lactide-glycolide copolymers - PLA37.5GA25 and PLA75GA25. *J Mater Sci: Mater Med* 1990; 1: 131-139.

[37] Ishaug-Riley SL, Okun LE, Prado G, Applegate MA, Ratcliffe A. Human articular chondrocyte adhesion and proliferation on synthetic biodegradable polymer films. *Biomaterials* 1999; 20: 2245-2256.

CHAPTER 6

In vitro degradation of trimethylene carbonate based (co)polymers*

A.P. PÊGO, A.A. POOT, D.W. GRIJPMA and J. FEIJEN
Institute for Biomedical Technology (BMTI) and Department of Polymer Chemistry and Biomaterials, Faculty of Chemical Technology, University of Twente, P.O. Box 217, 7500 AE Enschede, The Netherlands

ABSTRACT

Trimethylene carbonate (TMC) was copolymerized with D,L-lactide (DLLA) or with ε-caprolactone (CL) and the degradation of melt-pressed solid copolymer films in phosphate buffered saline at pH 7.4 and 37°C was followed for a period of over two years. The parent homopolymers were used as reference materials. The degradation profile of TMC-DLLA and TMC-CL based copolymers was similar, being best described by autocatalyzed bulk hydrolysis, preferentially of ester bonds. The hydrolysis rates varied by 2 orders of magnitude, depending on polymer composition and physical characteristics at the degradation conditions.

TMC-DLLA copolymers degraded faster than the parent homopolymers. The copolymers lost their tensile strength in less than 5 months, after which mass loss occurred. Copolymers with 50 or 80 mol% of TMC underwent total degradation in 11 months.

For TMC-CL copolymers a slow and gradual decrease in molecular weight and deterioration of the mechanical performance was observed. These copolymers maintained suitable mechanical properties for 17 months or longer. Chain scission in the semi-crystalline copolymers resulted in an increase in crystallinity. In comparison to the CL homopolymer, the introduction of a small amount of TMC (10 mol%) significantly reduced the increase in crystallinity during degradation.

Poly(TMC) specimens were dimensionally stable and showed a negligible decrease in molecular weight. A 60% decrease in the initial tensile strength of the polymer samples was observed after two years.

INTRODUCTION

Biodegradable synthetic polymers have found application in different areas of medicine. Particularly in surgery (sutures, bone plates and screws) and as carriers for controlled drug release, several degradable polymers have already reached the market and are presently in clinical use. More recently, much interest has been paid to the use of degradable polymers as temporary three-dimensional scaffolds in tissue engineering[1,2].

In general, degradable polymers for the preparation of biomedical devices should be biocompatible and degrade to non-toxic products. Depending on their final application they should comply with specific requirements in terms of mechanical performance, processing possibilities, degradation behavior, etc. In soft tissue engineering applications, flexible but relatively tough materials that degrade in accordance with the rate of tissue regeneration are required[3,4].

Copolymerization has been frequently used to tune the properties of polymers[5-8]. High molecular weight poly(trimethylene carbonate) (poly(TMC)) - an amorphous, rubbery polymer at room temperature[9] – shows good mechanical performance, combining high flexibility with high tensile strength[10]. The *in vitro* hydrolytic degradation of poly(TMC) at 37°C or 60°C is reported to be very slow and independent of initial molecular weight and ionic strength of the conditioning medium[11]. The mechanism of *in vivo* degradation is still a matter of discussion. In one study no decrease of the molecular weight of poly(TMC) samples ($\overline{M}_n$ =75,100) after six months of subcutaneous implantation in rats was observed[11]. Another study with poly(TMC) of relatively low molecular weight ($\overline{M}_n$ =19,100) revealed higher degradation rates in comparison with the *in vitro* hydrolysis, suggesting a contribution of enzymatic activity[9]. Previous studies showed that the rate of hydrolysis of TMC based copolymers increased with increasing ester content[11-14], as ester linkages in solid polymer specimens were found to be more susceptible to hydrolysis than carbonate linkages[9,11]. TMC-CL copolymers are expected to degrade slowly[11], making them suitable for long-term applications where the integrity of the system should be kept for relatively long periods of time. TMC-DLLA copolymers are expected to degrade faster than TMC-CL based copolymers[14].

In order to obtain polymers with different physical properties and degradation profiles, high molecular weight copolymers of trimethylene carbonate (TMC) with either ε-caprolactone (CL) or D,L-lactide (DLLA) were prepared. We have

previously reported on the physical properties of these poly(ester carbonate)s for use in soft tissue engineering[10,15]. In this study the effect of copolymer composition on the *in vitro* hydrolytic degradation of these materials was investigated.

Water uptake, molecular weight, weight loss, composition and the thermal and mechanical properties of the different copolymers were evaluated as a function of degradation time. The parent homopolymers were used as reference materials.

The *in vivo* biocompatibility and degradation of the TMC homopolymer and of selected TMC-DLLA and TMC-CL copolymers are subjects of a separate paper[16] (see Chapter 7).

MATERIALS AND METHODS

Materials

Polymer grade 1,3-trimethylene carbonate (TMC) was obtained from Boehringer Ingelheim, Germany. ε-Caprolactone (CL) (Acros Organics, Belgium) was purified by drying over CaH_2 (Acros Organics, Belgium) and distillation under reduced argon atmosphere. Polymer grade D,L-lactide (DLLA) (Purac Biochem, The Netherlands) was used without further purification. Stannous octoate ($SnOct_2$) (stannous 2-ethylhexanoate) was used as received from Sigma, USA. Solvents were of analytical grade (Biosolve, The Netherlands).

Polymer Synthesis

TMC-CL[10] and TMC-DLLA[15] based (co)polymers were synthesized as previously described. Briefly, the polymerizations were conducted by ring-opening polymerization in evacuated and sealed glass ampoules using $SnOct_2$ as catalyst. All homo- and copolymerizations were carried out for a period of 3 days at 130°C±2°C. The obtained polymers were purified by dissolution in chloroform and subsequent precipitation into a ten-fold volume of isopropanol. The precipitated polymers were collected, washed with fresh isopropanol and dried under reduced pressure at room temperature until constant weight.

Preparation of Polymer Samples

Rectangular films (100x5 mm^2) of the different polymers were melt-pressed (Fontijne laboratory press THB008, The Netherlands) to 600 μm thickness at

140°C. The films were cooled to room temperature under pressure. The molar composition, molecular weight and thermal properties of the polymers were evaluated after processing and compiled in Table 1 (see following paragraphs for experimental details).

Table 1. Characterization of the TMC (co)polymers used.

Polymer	TMC (mol%)	$\overline{M}_n \times 10^{-5}$	PDI	$[\eta]$ (dl/g)	T_g^a (°C)	T_m^a (°C)	w_c^a (%)
Poly(TMC)	100	3.2	1.8	4.3	-17	-	-
Poly(TMC-DLLA)	79	1.7	2.0	2.6	-7	-	-
	50	2.6	2.2	3.2	17	-	-
	20	2.9	2.1	3.5	43	-	-
Poly(DLLA)	0	2.9	2.5	3.6	52	-	-
Poly(TMC-CL)	82	2.5	1.9	4.3	-27	-	-
	31	2.0	1.9	4.2	-55	-	-
	10	1.5	1.8	3.3	-62	42	33
Poly(CL)	0	1.8	1.9	4.0	-66	60	48

[a] First heating scan (DSC).

In Vitro Hydrolysis

For each (co)polymer, 20-22 films were used to follow the *in vitro* degradation as a function of time. Each film was weighed, placed in an individual test tube and incubated at 37°C in phosphate buffered saline (PBS, pH 7.4, NPBI, The Netherlands) containing 0.02 wt/vol% of NaN_3 (Sigma, USA) to prevent bacterial growth. PBS was changed once a month at the initial stages of degradation and every two weeks after the onset of mass loss. At each analysis point duplicate samples were withdrawn and, after blotting, weighed and measured. The mechanical properties of the wet samples were measured at room temperature. After drying under vacuum at room temperature, the dry weight of the samples was determined. Subsequently, the molar composition, molecular weight and thermal properties of the specimens were determined.

The water uptake was calculated according to the following relationship:

$$\text{water uptake (wut)} = \frac{\text{Ww} - \text{Wr}}{\text{Wr}} \times 100 \qquad (\text{wt\%}) \qquad (1)$$

where w_w represents the weight of the wet sample after blotting and w_r represents the weight of the sample after drying.

Mass loss was calculated using the following expression:

$$\text{mass loss} = \frac{W_o - W_r}{W_o} \times 100 \qquad (\text{wt\%}) \tag{2}$$

where w_o corresponds to the initial weight of the polymer sample.

Nuclear Magnetic Resonance (NMR) Spectroscopy

A Varian Inova 300 MHz spectrometer was used for molar composition analysis. ^{1}H-NMR spectra were recorded at 300 MHz using polymer solutions in $CDCl_3$ (Sigma, USA).

Gel Permeation Chromatography (GPC)

Weight and number average molecular weight ($\overline{M}w$ and $\overline{M}n$, respectively), polydispersity index (PDI) and intrinsic viscosity ($[\eta]$) were determined by gel permeation chromatography (GPC) using a Waters Model 510 pump (USA), a HP Ti-Series 1050 autosampler (USA), a Waters Model 410 Differential Refractometer and a Viscotek H502 Viscometer Detector (USA) with Waters Styragel HR5-HR4-HR2-HR1 columns placed in series. At later stages of sample degradation Waters Styragel HR4-HR2-HR0.5 columns placed in series were used instead. Chloroform was used as eluent at a flow rate of 1.5 ml/min. Narrow polystyrene standards were used for calibration. Sample concentrations of approximately 0.5 wt/vol% and injection volumes of 30 µl were used. All determinations were performed at 25°C.

Differential Scanning Calorimetry (DSC)

The thermal properties of the processed and degraded samples were evaluated by DSC. Samples (5-15 mg) placed in aluminum pans were analyzed with a Perkin Elmer Pyris1 (USA) at a heating rate of 10°C/min. All samples were heated to 40°C above their melting temperature (when present) or glass transition temperature. The samples were then quenched rapidly (300°C/min) until 40°C below their glass transition temperature and after 5 min a second scan was recorded. The glass transition temperature (Tg) was taken as the midpoint of the heat capacity change and the peak melting temperature (Tm) was determined from the melting endotherm. The crystallinity (w_c) of the semicrystalline TMC-CL (co)polymers was determined assuming proportionality to the experimental heat of fusion (ΔH) according to the expression: $w_c = \Delta H / \Delta H°$, where $\Delta H°$ is the heat of fusion of 100%

crystalline poly(CL) reported to be 139.4 J/g[17]. Cyclohexane, indium, gallium and tin were used as standards for temperature calibration.

Mechanical Properties

Unless mentioned otherwise, tensile tests were carried out in two-fold at room temperature on a Zwick Z020 (Germany) universal tensile testing machine operated at a crosshead speed of 50 mm/min and a grip-to-grip separation of 50 mm. The specimen deformation was derived from the grip-to-grip separation. The Young's modulus (E) was calculated from the initial slope of the stress-strain curves.

RESULTS AND DISCUSSION

TMC-DLLA (Co)polymers

TMC-DLLA (co)polymers are hydrophobic[15] and the initial water uptake of the DLLA based copolymers was low (below 2%). However, water uptake did result in a decrease of the Tg, with direct consequences for the mechanical properties of the polymers. All materials had lower Young's modulus after water uptake (see Table 2). In particular the behavior of the copolymer containing 20 mol% of TMC is worth noticing. At room temperature this material is in the glassy state allowing easy processing and handling. After water uptake, Tg decreases to below the conditioning temperature of 37°C and the material now shows rubbery behavior.

Table 2. Physical properties[a] of TMC-DLLA (co)polymer films in the dry and wet state[b].

TMC content (mol%)	Dry State					Wet State					
	Tg^c (°C)	E (MPa)	σ_{yield} (MPa)	σ_{max} (MPa)	ε_{break} (%)	wut (%)	Tg^c (°C)	E (MPa)	σ_{yield} (MPa)	σ_{max} (MPa)	ε_{break} (%)
100	-17	6	2	12	830	1.4	-19	6	2	18	920
79	-7	5	2	2	270	1.6	-9	4	1	1	170
50	17	16	1	10	570	1.6	11	13	1	11	900
20	43	1900	51	51	7	1.2	33	1100	38	38	7
0	52	1900	53	53	6	1.1	46	1400	50	50	4

[a] Tensile tests carried out in three-fold. σ_{yield} – Stress at yield; σ_{max} – Maximum tensile strength; ε_{break} – Strain at break.
[b] Equilibrium water uptake (wut) in PBS, at 37°C for 24 hours.
[c] First heating scan (DSC).

During incubation at 37°C the specimen lengths of polymers containing high amounts of TMC had decreased and their thickness had increased. Poly(TMC) specimens displayed a small reduction in length (less than 10%) during the degradation time of 99 weeks. The copolymers with 79 and 50 mol% of TMC shrunk much more. The maximum observed sample length reductions were 30% and 25%, respectively. These observations are the result of chain relaxation facilitated by an increase in chain mobility at 37°C, combined with a plasticizing effect of water. Poly(DLLA) and poly(TMC-DLLA) (20:80 mol%) specimens did not show any dimensional change.

Figure 1 shows the variation of $\overline{M}n$ of the (co)polymers as a function of immersion time in PBS. For all samples and at all stages of the degradation monomodal molecular weight distributions were observed. After more than 2 years in PBS, poly(TMC) did not show a significant decrease in $\overline{M}n$, which is in accordance with previous findings[11]. In contrast, for the DLLA homopolymer ($\overline{M}n^0$=291,000) a continuous reduction was observed, in which $\overline{M}n$ decreased to 0.5% of its initial value in 99 weeks.
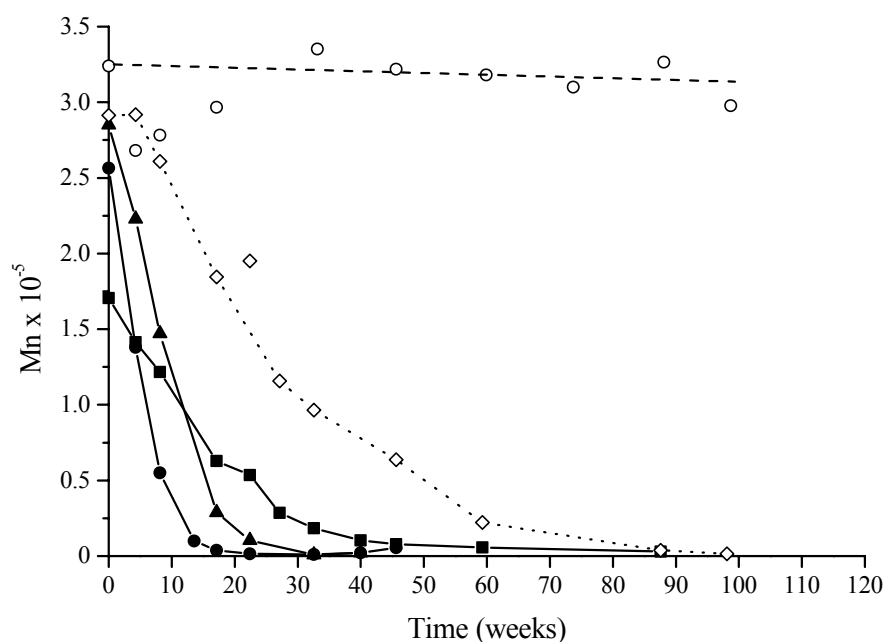

Figure 1. Molecular weight ($\overline{M}n$) as a function of degradation time for TMC and DLLA (co)polymers. (○) 100% TMC; (■) 79% TMC; (●) 50% TMC; (▲) 20% TMC and (◇) 100% DLLA.

Even though the Tg of the polyester is higher, poly(DLLA) degraded much faster than poly(TMC). Apparently, the ester bonds are more susceptible to hydrolysis than the carbonate bonds, as was also observed previously[11]. The copolymers degraded at higher rates than both homopolymers. The ester bond content is an important rate determining factor. It should be noticed however, that the access of water to the more labile ester bonds is facilitated in the copolymers by the reduction of Tg to values below the incubation temperature of 37°C (see Table 2) increasing the hydrolysis rates of the copolymers in comparison to poly(DLLA).

The initial mechanical properties of the wet polymer specimens vary with composition. With decreasing Tg, the polymers range from stiff and glassy materials to highly elastic rubbers (Table 2). In Figure 2 the maximum tensile strength (σ_{max}) is shown as a function of degradation time. The rates of decrease in σ_{max} could be related to the rates of decrease in $\overline{M}n$.
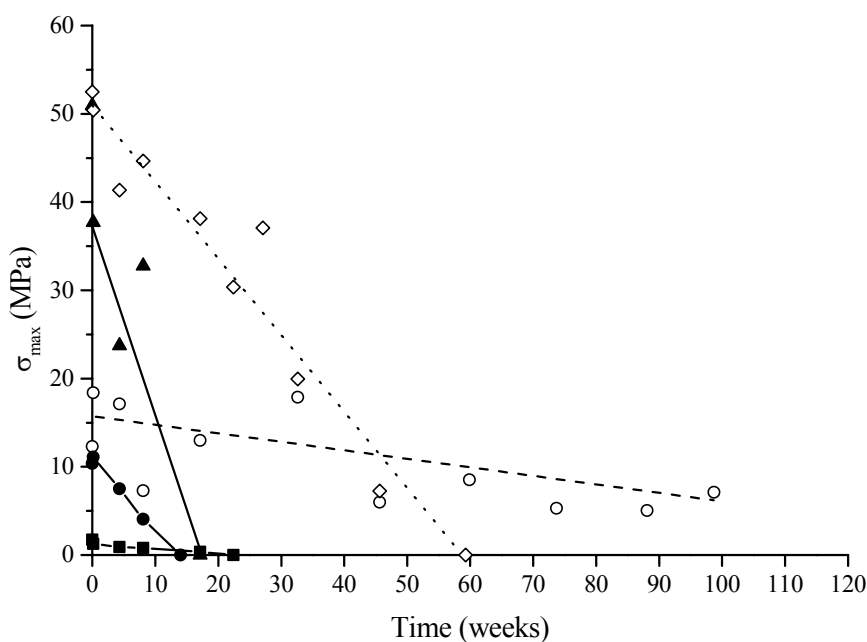

Figure 2. Maximum tensile strength (σ_{max}) as a function of degradation time for TMC and DLLA (co)polymers. (○) 100% TMC; (■) 79% TMC; (●) 50% TMC; (▲) 20% TMC and (◇) 100% DLLA.

Poly(TMC-DLLA) (50:50 mol%) is the fastest degrading polymer, specimens had broken up into pieces after 3 months. Poly(TMC-DLLA) (20:80 mol%) specimens were still intact at 4 months, although they broke brittle when handled. The rubbery poly(TMC-DLLA) (79:21 mol%) had lost its tensile strength in 5 months. For

poly(DLLA) a steady decrease in the mechanical properties was observed. Samples lost their mechanical strength after 60 weeks of incubation under hydrolytic conditions, breaking brittle when handled. In the case of poly(TMC) only a decrease in σ_{max} of approximately 60% was observed.

Figure 3 shows σ_{max} as a function of the $\overline{M}n$ of partially degraded TMC-DLLA copolymers and poly(DLLA). The maximum tensile strength decreases with the decrease in polymer molecular weight. An $\overline{M}n$ of approximately 25,000 seems to be a limiting value below which the mechanical properties are lost. The changes in molecular weight of poly(TMC) were too small to correlate σ_{max} with $\overline{M}n$.
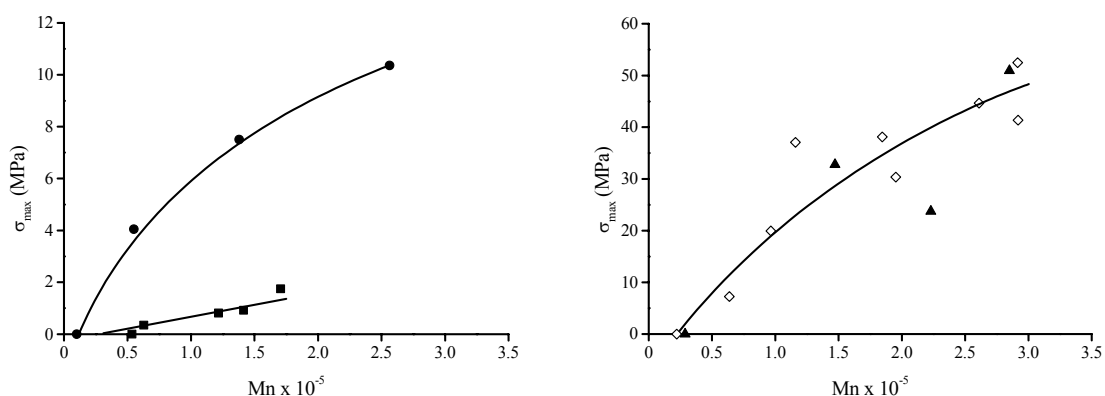

Figure 3. Maximum tensile strength (σ_{max}) as a function of molecular weight ($\overline{M}n$) of TMC and DLLA (co)polymers during degradation (■) 79% TMC; (●) 50% TMC; (▲) 20% TMC and (◇) 100% DLLA.

During the initial stages of degradation, limited water uptake without mass loss was observed for all the polymers (Figure 4 and 5, respectively). The loss of mechanical strength, which results from the decrease in $\overline{M}n$, preceded the onset of substantial water uptake. Following the increase in water uptake a rapid loss in mass occurred. The time required for total polymer resorption was again determined by the copolymer composition. Copolymers with 50 and 20 mol% of TMC underwent total mass loss in less than 11 months. In contrast, the total degradation of poly(DLLA) took nearly 2 years. For poly(TMC-DLLA) (79:21 mol%) total resorption was not observed during the evaluation period.

The rapid decrease in remaining mass, which occurred after loss of mechanical properties, resulted in a narrowing of the molecular weight distribution of the samples from an initial value of approximately 2 to values approaching 1. At advanced stages of hydrolysis, the low-molecular weight degradation products can

diffuse into the surrounding medium. At this point $\overline{M}n$ had reached values smaller than approximately 20,000 (determined from Figure 1 and 5).

The mol% of TMC in the copolymers was found to increase after the onset of mass loss (Table 3). This can be due to preferential chain cleavage at the ester bonds and differences in solubility of the formed fragments.

Table 3. Change in TMC content of TMC-DLLA copolymers during hydrolytic degradation.

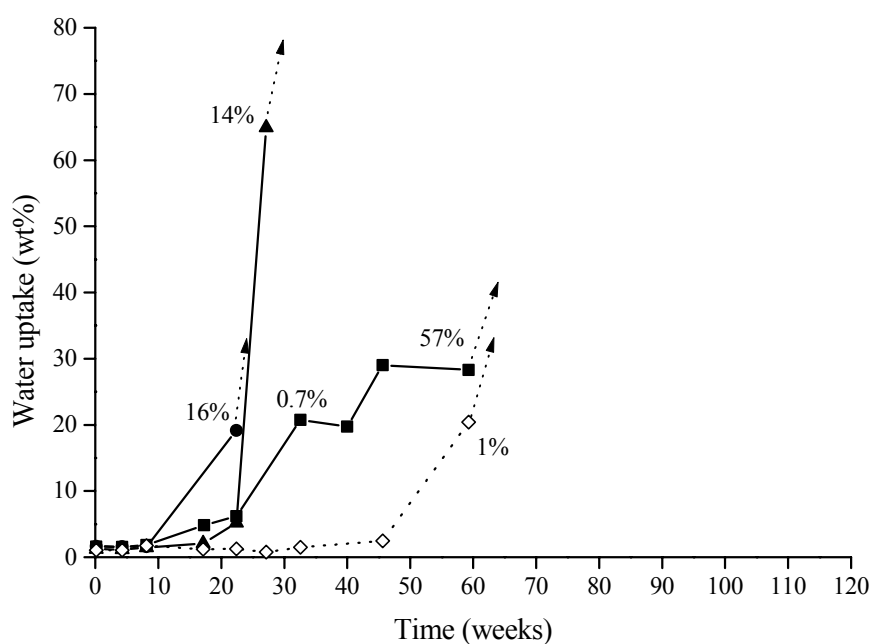|	Degradation time (weeks)											
	0	4	8	14	17	22	33	40	46	55	59	88
TMC	79	83	83	nd	84	84	85	84	84	nd	85	88
content	50	49	49	49	49	50	63	76	74	78	-	-
(mol%)	20	20	20	nd	21	20	28	53	44	-	-	-

nd - Not determined.

Figure 4. Water uptake as a function of degradation time for TMC and DLLA (co)polymers. Mass loss at the corresponding time point is indicated in the figure. (■) 79% TMC; (●) 50% TMC; (▲) 20% TMC and (◇) 100% DLLA.

At late stages of degradation it was not possible to accurately weigh the degraded specimens in the wet state. After the initial water uptake no further uptake was detected for poly(TMC) during the time span of this study.

Comonomer composition, water content and molecular weight affect the thermal properties of polymers. The observed molecular weight decrease due to hydrolytic degradation led to an increase in water uptake and, upon mass loss, to changes in the molar composition of the copolymers. These changes resulted in a decrease in Tg for all polymers. The thermal properties of the (co)polymers did not significantly change until $\overline{Mn}$ had reached values below 10,000.
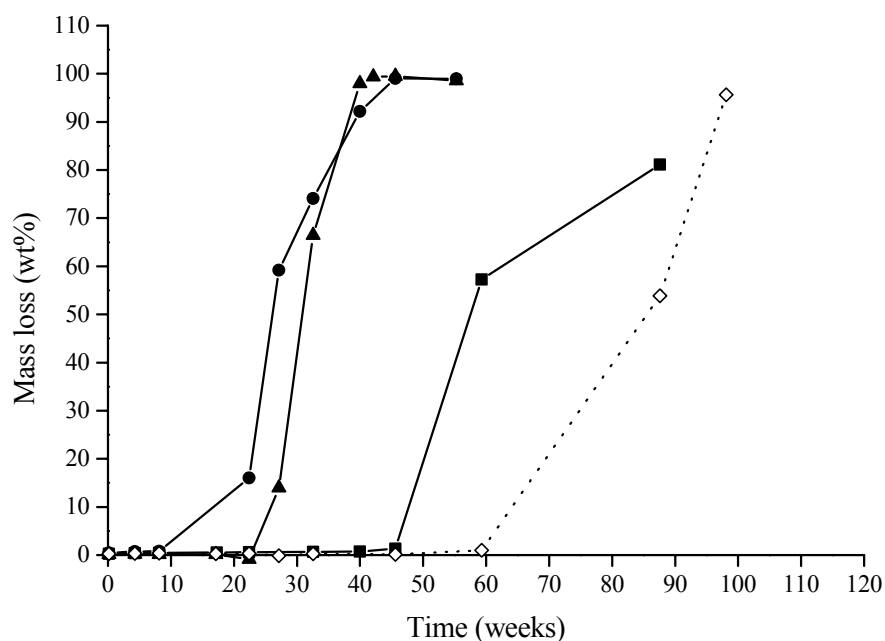

Figure 5. Mass loss as a function of degradation time for TMC and DLLA (co)polymers. (■) 79% TMC; (●) 50% TMC; (▲) 20% TMC and (◇) 100% DLLA. No mass loss was observed for poly(TMC) during the time span of this study.

TMC-CL (Co)polymers

Initially, poly(CL) and poly(TMC-CL) (10:90 mol%) were white and opaque, while the other CL based copolymers and poly(TMC) were transparent. This is in agreement with the crystalline structure of the former polymers and the amorphous nature of the latter (Table 1). The observed water absorption of all polymers was low (below 2%) in accordance with previous reports[10]. For the semi-crystalline specimens no changes in visual appearance or dimensions were observed in this two-year degradation study. From the first day on, the amorphous polymers became translucent. With the exception of poly(TMC), the sample dimensions changed significantly in time. In 2 years, specimens with 82 mol% TMC decreased 20% in

length. The thickness of the specimens increased and the samples became more undulated and twisted. Specimens of poly(TMC-CL) (31:69 mol%) gradually became shapeless polymer masses after 18 weeks. This can be explained by a relaxation effect due to increased chain mobility at 37°C in combination with a plasticizing effect of water.

The degradation of TMC-CL based copolymers was much slower than that of TMC-DLLA based copolymers. Figure 6 shows $\overline{M}n$ as a function of degradation time for the TMC-CL copolymers. For all samples and at all evaluation times a monomodal molecular weight distribution was observed (ranging from 1.4-2.4). For CL based copolymers the hydrolysis rates increased with CL (ester) content. In this case an increase in chain mobility due to water uptake had no significant effect on the hydrolysis rates, as all these polymers have a very low Tg.

During the time of the study, no significant changes in water uptake or mass were observed for the TMC-CL copolymers with 31 and 82 mol% of TMC. For poly(CL) and poly(TMC-CL) (10:90 mol%) the first signs of mass loss (0.4%) were detected at 2 years, with an increase in TMC content in the copolymer from 10 to 13 mol%.
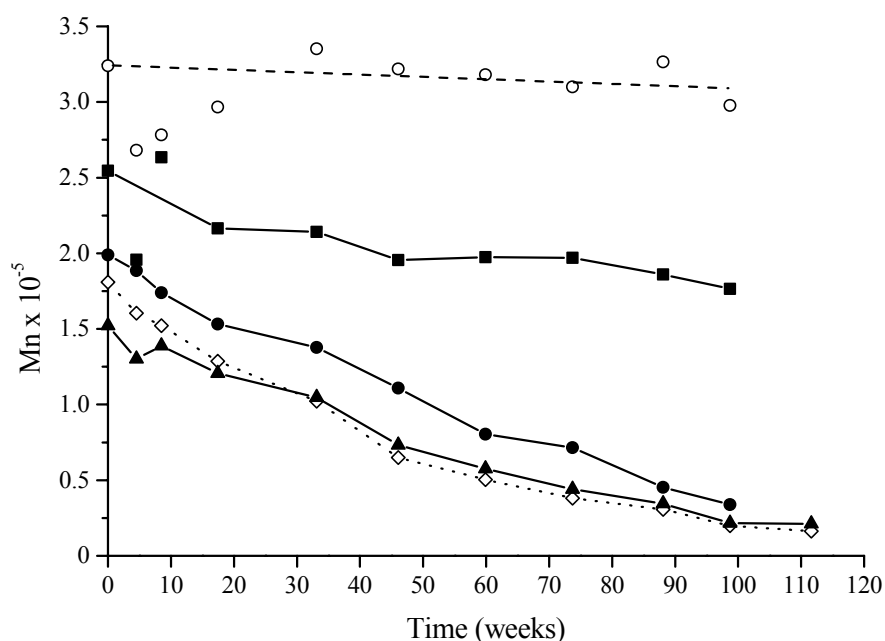

Figure 6. Molecular weight ($\overline{M}n$) as a function of degradation time for TMC and CL (co)polymers. (○) 100% TMC; (■) 82% TMC; (●) 31% TMC; (▲) 10% TMC and (◇) 100% CL.

The mechanical properties of the TMC-CL copolymers in the wet state were not significantly different from those in the dry state[10]. In time σ_{max} decreased with the reduction in $\overline{M}n$ (Figure 7). Poly(TMC-CL) (82:18 mol%), like poly(TMC), showed the smallest decrease in σ_{max}. The copolymer with 31 mol% of TMC showed a low σ_{max} from the start. At evaluation points later than 18 weeks it was not possible to perform tensile tests, as the specimens had lost their original shape. For the semi-crystalline polymers, poly(TMC-CL) (10:90 mol%) and poly(CL), the tensile strength was constant during the first 50 weeks of degradation. During the second year a linear decrease of σ_{max} was observed. The onset of the decline of σ_{max} at 50 weeks coincided with the point in time that $\overline{M}n$ of both polymers had reached values below 75,000 (Figure 8). At the end of the study (111 weeks) the samples were very frail and broke brittle when tested. An $\overline{M}n$ of 25,000 seems to be a limiting value below which the tensile strength is negligible.
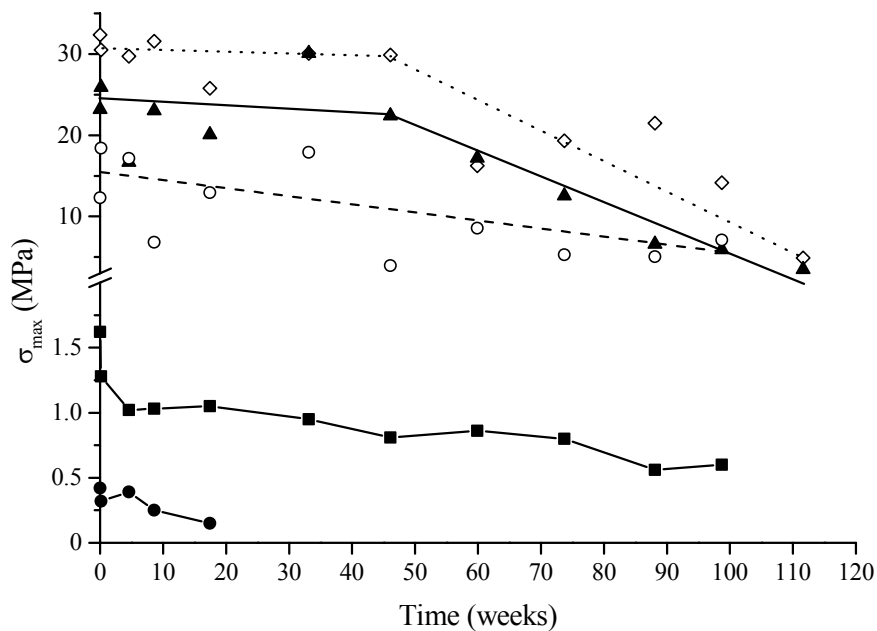

Figure 7. Maximum tensile strength (σ_{max}) as a function of degradation time for TMC and CL (co)polymers. (○) 100% TMC; (■) 82% TMC; (●) 31% TMC; (▲) 10% TMC and (◇) 100% CL.
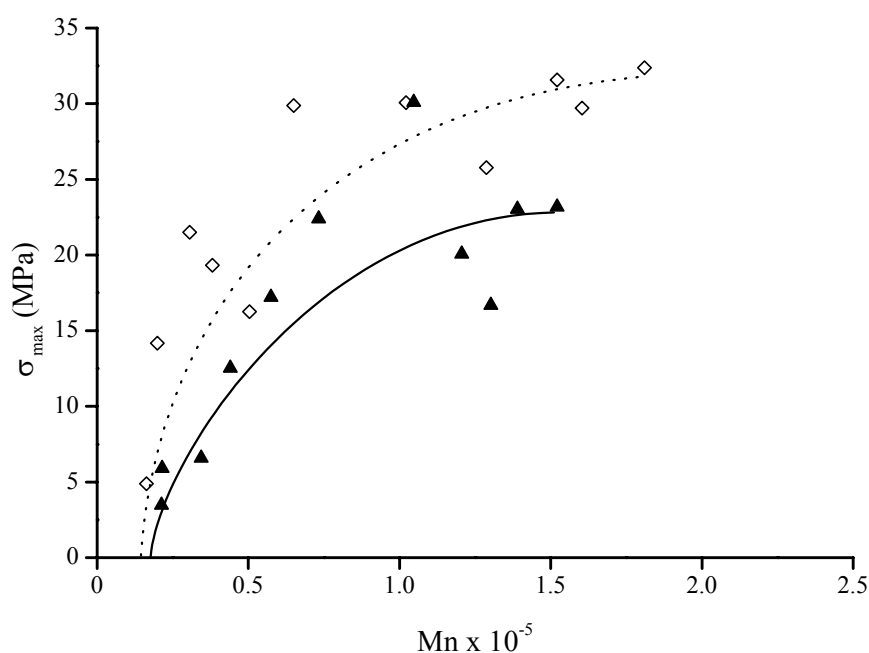
Figure 8. Maximum tensile strength (σ_{max}) as a function of molecular weight ($\overline{M}n$) of TMC and CL (co)polymers during degradation. (▲) 10% TMC and (◇) 100% CL.

For the semi-crystalline copolymers the decrease in molecular weight was accompanied by a steady rise in Young's modulus. As can be seen in Figure 9, this increase in Young's modulus is associated with an increase in the crystalline content of these polymers. The increase in the heat of fusion of poly(TMC-CL) (10:90 mol%) and poly(CL), is the result of annealing at 37°C which is enhanced in the wet state, and crystallization of conformationally hindered chain segments made possible by chain cleavage in the amorphous phase.

Concerning the use of these polymers in medical implants, one should realize that crystalline debris formed during degradation may cause an undesired late inflammatory response[18]. Therefore, a polymer with little or no crystallinity is preferred. During hydrolysis a 44% increase in crystalline content was observed for poly(TMC-CL) (10:90 mol%) compared to a 60% increase observed for poly(CL). These results show that by introducing a small amount of TMC in the poly(CL) chain one can significantly limit the increase in crystallinity during degradation.

The thermal properties of the amorphous copolymers did not significantly change during the 2 years of the study.
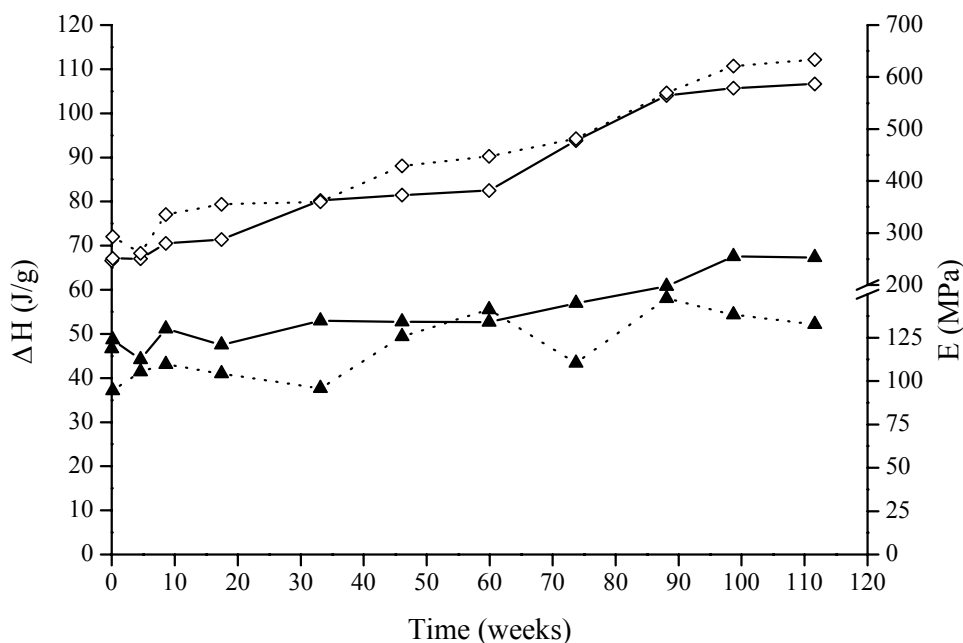
Figure 9. Heat of fusion (ΔH) (—), recorded by DSC at the first heating scan, and Young's modulus (E) (·····) as a function of degradation time for TMC and CL (co)polymers. (▲) 10% TMC and (◇) 100% CL.

Degradation Rates of TMC-DLLA and TMC-CL Based (Co)polymers

Both TMC-DLLA and TMC-CL (co)polymers showed a decrease of molecular weight with no mass loss in the first stages of the degradation process. This is consistent with hydrolytic degradation by chain scission in the bulk of the material. Chain scission occurs both at ester and at carbonate groups, although preferentially at the ester bonds. Upon degradation, all films exhibited monomodal molecular weight distributions indicating homogeneous degradation.

The *in vitro* hydrolytic degradation of poly(CL), poly(DLLA) and related aliphatic polyesters involves the generation of carboxylic end groups that are able to catalyze the reaction[19,20]. Based on a first-order kinetic model, Pitt and co-workers[19] related the rate of chain scission of an aliphatic polyester autocatalyzed by the generated carboxylic acid end groups to the decrease of $\overline{M}_n$ in time:

$$ln(\overline{M}_n) = ln(\overline{M}_n^0) - kt \tag{3}$$

where, $\overline{M}_n^0$ is the average number molecular weight at the start of the hydrolysis, *k* is the rate constant and t is the degradation time.

If the hydrolysis is not autocatalytic, chain cleavage will follow the rate law[21]:

117

$$\frac{1}{\overline{Mn}} = \frac{1}{\overline{Mn}^0} + k't \tag{4}$$

In the derivation of these equations it is assumed that the extent of chain cleavage is small and that no significant mass loss had occurred.

For poly(TMC) and poly(TMC-CL) (82:18 mol%) it is not possible to see a clear trend in the decrease in $\overline{Mn}$ as these polymers showed very limited degradation in the 2 years of the study. Both models fit the experimental results with no significant difference. For the other polymers a linear relationship was only found between $\ln(\overline{Mn})$ and degradation time (Figure 10 and 11).

Figure 10. Plot of $\ln(\overline{Mn})$ as a function of degradation time for TMC and DLLA (co)polymers. (○) 100% TMC; (■) 79% TMC; (●) 50% TMC; (▲) 20% TMC and (◇) 100% DLLA.

In Table 4 the hydrolysis rates determined from linear fitting of the data in the plots of $\ln(\overline{Mn})$ versus time are presented. The data points at later stages of degradation of the TMC-DLLA copolymers and poly(DLLA), where extensive mass loss had occurred, were excluded in the determination of the hydrolysis rates. In general, the hydrolysis rates increased with ester bond content.
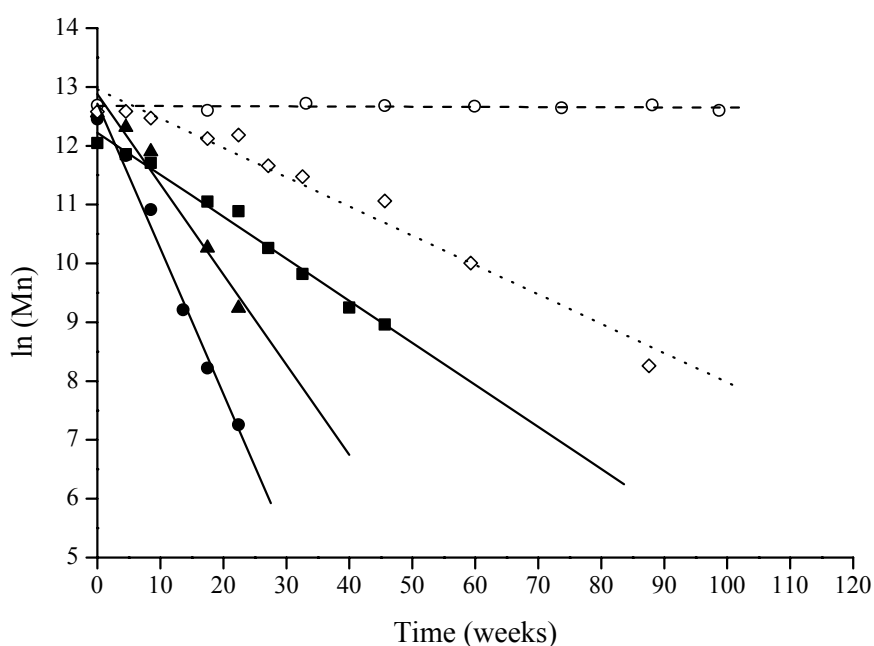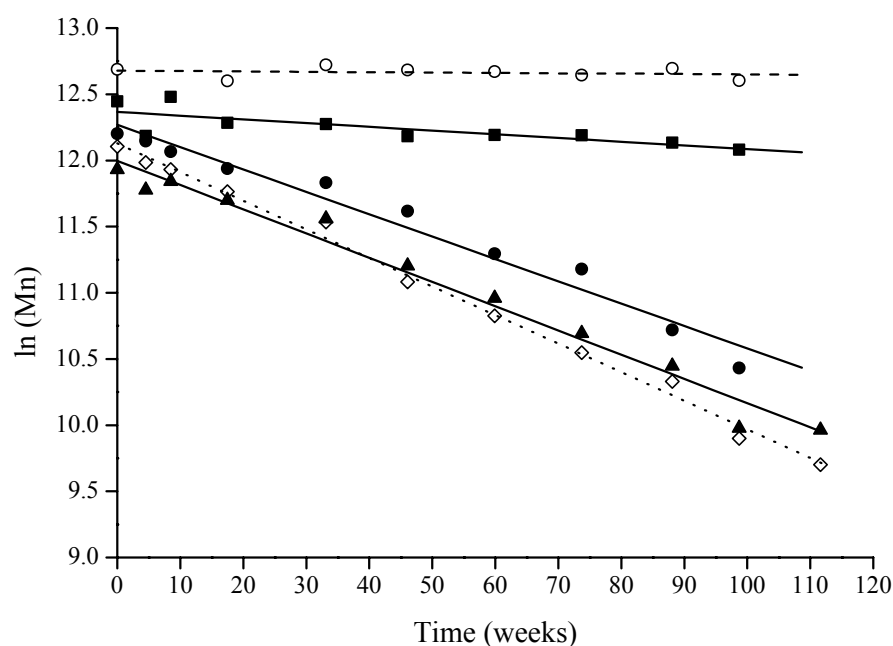
Figure 11. Plot of $\ln(\overline{M}_n)$ as a function of degradation time for TMC and CL (co)polymers. (○) 100% TMC; (■) 82% TMC; (●) 31% TMC; (▲) 10% TMC and (◇) 100% CL.

Table 4. Hydrolytic degradation rates of TMC-DLLA and TMC-CL (co)polymers in PBS at 37°C, determined from Figure 10 and 11.

Polymer	TMC (mol%)	Rate constant ($\times 10^{-2}$ day^{-1})	Correlation coefficient, r
Poly(TMC)	100	0.004[a]	-0.22[b]
Poly(TMC-DLLA)	79	1.0	-0.99
	50	3.6	-0.99
	20	2.1	-0.98
Poly(DLLA)	0	0.71	-0.98
Poly(TMC-CL)	82	0.04	-0.78[b]
	31	0.24	-0.99
	10	0.26	-0.99
Poly(CL)	0	0.31	-0.99

[a] Linear fitting excluding measurements at 4 and 8 weeks of degradation.

[b] These values reflect the low decrease in molecular weight observed for poly(TMC) and poly(TMC-CL) (82:18 mol%).

The rates determined for the reference homopolymers show that the homopolymers degrade in the order: poly(DLLA), poly(CL) and poly(TMC).

The higher rate of hydrolysis of poly(DLLA) compared to poly(CL) may be attributed to the inductive effect of the α-oxygen atom in the lactyl structure[20]. Additionally, the different thermal properties of the polymers may play a role too. On the one hand the reduced chain mobility, free volume and permeability of poly(DLLA), which is in the glassy state, will tend to reduce the hydrolysis of this polymer. While on the other hand, the crystallinity of poly(CL) will result in decreased accessibility of the ester groups. Pitt and co-workers[21] found the value of the rate constant for the autocatalytic degradation of poly(CL) melt-pressed films *in vitro* to be 0.18×10^{-2} day^{-1}, what is close to the result found in the present study. In previous work we have reported on the hydrolysis of solvent cast poly(DLLA) films at pH 7.4[8]. The rate constant for the autocatalytic degradation of high molecular weight poly(DLLA) ($\overline{M}$n 142,000 relative to polystyrene) was determined to be 5×10^{-2} day^{-1}, which is higher than the value determined in this study (0.71×10^{-2} day^{-1}). In contrast with the heterogeneous degradation of the solvent cast films, we now observed homogeneous degradation of poly(DLLA), what might explain the lower hydrolysis rate[22,23].

The negligible decrease in molecular weight of solid specimens of high molecular weight poly(TMC) observed in this study is in line with previous findings[11]. This implies that under these degradation conditions the polymeric ester linkages are much more susceptible to hydrolysis than polymeric carbonate linkages. As opposed to the auto-catalyzed hydrolysis of poly(DLLA) and poly(CL), generation of catalytic acid end groups is not expected to occur in poly(TMC).

Copolymers of TMC and DLLA degraded much faster than poly(DLLA). This can be attributed to the low Tg of the copolymers in the wet state (below the conditioning temperature of 37°C), which increases chain mobility and enhances cleavage of the ester linkages. In his hydrolytic degradation study of TMC-DLLA based copolymers at 80°C, Buchholz[12] did not observe a faster degradation of the copolymers when compared to the DLLA homopolymer. This is due to the fact that for all polymers the conditioning temperature was higher than the glass transition temperature.

TMC-CL copolymers degraded slower than poly(CL). The increase in hydrolysis rates with increased ester content, as follows from Table 4, is apparently not influenced by crystalline content.

The mass loss rates of TMC based copolymers were also dependent on the copolymer compositions. In the present study complete polymer resorption was only observed for poly(DLLA) and TMC-DLLA copolymers. For these (co)polymers mass loss occurred when $\overline{M}n$ had decreased to a critical value of about 20,000. The limiting value of $\overline{M}n$ seems to be lower for the TMC-CL copolymers. Poly(CL) and the copolymer with 10 mol% of TMC reached an $\overline{M}n$ below 20,000 after 2 years and no significant mass loss was detected. These critical values of $\overline{M}n$ are in accordance with the ones found for the *in vivo* degradation of poly(CL) and poly(DLLA)[19,20].

CONCLUSIONS

Under hydrolytic conditions poly(TMC) degrades very slowly. In the two years of this study poly(TMC) showed a negligible change in molecular weight and only a small decrease in mechanical properties. Copolymerization of TMC with DLLA or CL allowed tuning of the degradation of these biomaterials within a very wide time range.

Copolymers of TMC-DLLA are amorphous polymers that can undergo complete degradation *in vitro*. Poly(DLLA) was resorbed in 2 years, while copolymers with 20 and 50 mol% of TMC were resorbed in less than a year. In contrast (semi-crystalline) TMC-CL copolymers degraded much slower. These materials maintained suitable mechanical properties for more than 1 year and in the time scope of this study no mass loss was observed for any of the TMC-CL (co)polymers.

The degradation mechanism of these TMC based copolymers was qualitatively similar. The *in vitro* degradation of these copolymers is best described by the preferential hydrolysis of ester bonds throughout the bulk, autocatalyzed by the generated acidic end groups. As the molecular weight decreases, the mechanical properties of the polymers deteriorate. A $\overline{M}n$ of 25,000 seems to be a limiting value below which the tensile properties are lost. Mass loss occurs at a later stage of degradation, when degraded polymer chains are able to leach out into the degradation medium. For the TMC-DLLA (co)polymers, this was observed when $\overline{M}n$ had reached a value of 20,000.

ACKNOWLEDGMENTS

REFERENCES

[1]   Marler JJ, Upton J, Langer R, Vacanti JP. Transplantation of cells in matrices for tissue regeneration. *Adv Drug Deliv Rev* 1998; 33: 165-182.

[2]   Seal BL, Otero TC, Panitch A. Polymeric biomaterials for tissue and organ regeneration. *Mater Sci Eng R-Rep* 2001; 34: 147-230.

[3]   Niklason LE, Gao J, Abbott WM, Hirschi KK, Houser S, Marini R, Langer R. Functional arteries grown *in vitro*. *Science* 1999; 284: 489-493.

[4]   den Dunnen WF, Meek MF, Grijpma DW, Robinson PH, Schakenraad JM. *In vivo* and *in vitro* degradation of poly[50/50 (85/15 L/D)LA/ε-CL], and the implications for the use in nerve reconstruction. *J Biomed Mater Res* 2000; 51: 575-585.

[5]   Gilding DK, Reed AM. Biodegradable polymers for use in surgery-polyglycolic/poly(lactic acid) homo- and copolymers:1. *Polymer* 1979; 20: 1459-1464.

[6]   Reed AM, Gilding DK. Biodegradable polymers for use in surgery - poly(glycolic)/poly(lactic acid) homo and copolymers: 2. *In vitro* degradation. *Polymer* 1981; 22: 494-498.

[7]   Katz AR, Mukherjee DP, Kaganov AL, Gordon S. A new synthetic monofilament absorbable suture made from polytrimethylene carbonate. *Surg Gynecol Obstet* 1985; 161: 213-222.

[8]   Helder J, Dijkstra PJ, Feijen J. *In vitro* degradation of glycine/DL-lactic acid copolymers. *J Biomed Mater Res* 1990; 24: 1005-1020.

[9]   Zhu KJ, Hendren RW, Jensen K, Pitt CG. Synthesis, properties, and biodegradation of poly(1,3-trimethylene carbonate). *Macromolecules* 1991; 24: 1736-1740.

[10]   Pêgo AP, Poot AA, Grijpma DW, Feijen J. Copolymers of trimethylene carbonate and ε-caprolactone for porous nerve guides: synthesis and properties. *J Biomater Sci Polym Ed* 2001; 12: 35-53. Chapter 3 of this thesis.

[11]   Albertsson A-C, Eklund M. Influence of molecular structure on the degradation mechanism of degradable polymers: *in vitro* degradation of poly(trimethylene carbonate), poly(trimethylene carbonate-co-caprolactone), and poly(adipic anhydride). *J Appl Polym Sci* 1995; 57: 87-103.

[12] Buchholz B. Analysis and characterization of resorbable DL-lactide-trimethylene carbonate copolyesters. *J Mater Sci: Mater Med* 1993; 4: 381-388.

[13] Jie C, Zhu KJ, Shilin Y. Preparation, characterization and biodegradable characteristics of poly(1,3-trimethylene carbonate-co-glycolide). *Polym Int* 1996; 41: 369-375.

[14] Jie C, Zhu KJ. Preparation, characterization and biodegradable characteristics of poly(D,L-lactide-co-1,3-trimethylene carbonate). *Polym Int* 1997; 42: 373-379.

[15] Pêgo AP, Poot AA, Grijpma DW, Feijen J. Physical properties of high molecular weight 1,3-trimethylene carbonate and D,L-lactide copolymers. *(submitted to J Mater Sci: Mater Med, 2002)* Chapter 5 of this thesis.

[16] Pêgo AP, van Luyn MJA, Brouwer LA, van Wachem PB, Poot AA, Grijpma DW, Feijen J. *In vivo* behavior of poly(1,3-trimethylene carbonate) and copolymers of 1,3-trimethylene carbonate with D,L-lactide or ε-caprolactone. Degradation and tissue response. *(submitted to J Biomed Mater Res, 2002)* Chapter 7 of this thesis.

[17] Crescenzi V, Manzini G, Calzolari G, Borri C. Thermodynamics of fusion of poly-β-propiolactone and poly-ε-caprolactone. Comparative analysis of the melting of aliphatic polylactone and polyester chains. *Eur Polym J* 1972; 8: 449-463.

[18] Bos RRM, Rozema FR, Boering G, Nijenhuis AJ, Pennings AJ, Verwey AB, Nieuwenhuis P, Jansen HWB. Degradation of and tissue reaction to biodegradable poly(L-lactide) for use as internal fixation of fractures: a study in rats. *Biomaterials* 1991; 12: 32-36.

[19] Pitt CG, Chasalow FI, Hibionada DM, Klimas DM, Schindler A. Aliphatic polyesters. I. The degradation of poly(ε-caprolactone) *in vivo*. *J Appl Polym Sci* 1981; 26: 3779-3787.

[20] Pitt CG, Gratzl MM, Kimmel GL, Surles J, Schindler A. Aliphatic polyesters II. The degradation of poly(DL-lactide), poly (ε-caprolactone), and their copolymers *in vivo*. *Biomaterials* 1981; 2: 215-220.

[21] Pitt CG, Gu Z. Modification of the rates of chain cleavage of poly(ε-caprolactone) and related polyesters in the solid state. *J Control Release* 1987; 4: 283-292.

[22] Li SM, Garreau H, Vert M. Structure property relationships in the case of the degradation of massive aliphatic poly-(α-hydroxy acids) in aqueous media. 1. Poly(DL-lactic acid). *J Mater Sci: Mater Med* 1990; 1: 123-130.

[23] Grizzi I, Garreau H, Li S, Vert M. Hydrolytic degradation of devices based on poly(DL-lactic acid) size-dependence. *Biomaterials* 1995; 16: 305-311.

CHAPTER 7

In vivo behavior of poly(1,3-trimethylene carbonate) and copolymers of 1,3-trimethylene carbonate with D,L-lactide or ε-caprolactone. Degradation and tissue response*

A.P. PÊGO[1], M.J.A. VAN LUYN[2], L.A. BROUWER[2], P.B. VAN WACHEM[2], A.A. POOT[1], D.W. GRIJPMA[1] and J. FEIJEN[1]

[1] *Institute for Biomedical Technology (BMTI) and Department of Polymer Chemistry and Biomaterials, Faculty of Chemical Technology, University of Twente, P.O. Box 217, 7500 AE Enschede, The Netherlands*
[2] *Department of Pathology & Lab. Medicine, Medical Biology, Tissue Engineering, Faculty of Medical Sciences, University of Groningen, Hanzeplein 1 - Entrance 25, 9713 GZ Groningen, The Netherlands*

ABSTRACT

In order to evaluate the *in vivo* degradation and the tissue response evoked by poly(1,3-trimethylene carbonate) (poly(TMC)) and copolymers of TMC with either 52 mol% D,L-lactide (DLLA) or 89 mol% ε-caprolactone (CL), melt-pressed films of these polymers were subcutaneously implanted in rats for periods up to one year.

In contrast to the previously reported very slow degradation in phosphate buffered saline at 37°C, poly(TMC) degraded rapidly *in vivo*. Only a few polymer particles could be detected extracellularly in the tissue after 3 weeks of implantation and histological evaluation showed that the polymer disks resorbed totally in less than a year. A fast linear decrease in thickness and mass, without a change in molecular weight was found (except at the late stage of degradation where a bimodal molecular weight distribution was observed). The degradation of poly(TMC) induced a mild tissue reaction associated with the infiltration of macrophages and formation of giant cells. As early as 5 days after implantation, these cells were involved in the phagocytosis of particles of the degrading implant. It is concluded that *in vivo*, poly(TMC) is degraded via surface erosion involving enzymatic processes.

The *in vivo* degradation of the copolymers was similar to that observed *in vitro*, taking place via autocatalyzed bulk hydrolysis, preferentially of ester bonds. Poly(TMC-DLLA) (48:52 mol%) degraded 20 times faster than poly(TMC-CL) (11:89 mol%). The molecular weight decreased from the start of the implantation. Mass loss occurred at a later stage of degradation, and in this study was only significant for the TMC-DLLA copolymer, which underwent 96% mass loss in one year. The copolymers were well tolerated by the tissue upon subcutaneous implantation. After the initial acute sterile inflammatory reaction, due to the implantation procedure, foreign body reactions followed that led to encapsulation of the materials. For the TMC-DLLA copolymer a secondary foreign body reaction was observed from 26 weeks on (when extensive mass loss occurred) that could be associated with the clearance of the polymer degradation products.

The results presented in this study demonstrate that poly(TMC) and both TMC copolymers are biodegradable and biocompatible materials, making these polymers attractive for the preparation of short- and long-term degradable devices for soft tissue engineering.

INTRODUCTION

The concept of tissue engineering involves a carrier-scaffold that provides an architecture on which seeded cells can organize and develop into a desired tissue *in vitro* and/or *in vivo*. The biological, chemical and physical properties of the scaffolding material should allow the proper development of such tissue. In soft tissue engineering the use of a flexible material is preferred. The selected material should also be relatively tough and should degrade and resorb at a rate in accordance with the cell and tissue growth.

We have previously reported on the use of poly(1,3-trimethylene carbonate) (poly(TMC)) for the preparation of scaffolds for the engineering of soft tissues, like heart muscle and the preparation of nerve conduits for guided nerve regeneration[1]. High molecular weight poly(TMC) is an amorphous elastomer which shows good mechanical performance, combining high flexibility with high tensile strength[2]. Under hydrolytic conditions (in phosphate buffered saline (PBS) at pH 7.4 and 37°C) poly(TMC) degrades very slowly[3].

The incorporation of other monomer units into the poly(TMC) chain proved to be a successful method of modifying its physical properties and modulating the rate of polymer degradation.

High molecular weight copolymers of TMC and D,L-lactide (DLLA) with 20 and 50 mol% of TMC are amorphous, relatively strong elastomers under physiological

conditions[4]. In a previous study we have shown that these copolymers can maintain suitable mechanical properties up to 3 months of *in vitro* degradation and are resorbed in less than a year[3]. Therefore, these copolymers are promising candidates for the preparation of scaffolds for heart tissue engineering. In the tissue engineering approach to cardiomyoplasty, we hypothesize that the material strength needs to be retained for a relatively short period of time and that the scaffold should be resorbed soon after loss of mechanical performance inducing minimal tissue response.

For the preparation of nerve guides for the bridging of nerve gaps over clinically relevant distances, we are aiming at a more slowly degrading scaffold. The graft should keep its integrity and mechanical properties during the 3 to 6 month period of nerve regeneration and maturation. Copolymers of TMC and ε-caprolactone (CL) degrade slower than TMC-DLLA copolymers. TMC-CL copolymers with high CL content are semi-crystalline, very flexible and tough materials that can maintain suitable mechanical properties for more than 1 year when incubated in PBS at pH 7.4 and 37°C[2,3]. Therefore, these polymers are interesting candidates for the preparation of slowly degrading nerve guides.

Independent of composition, both TMC-DLLA and TMC-CL (co)polymers degrade *in vitro* by bulk hydrolysis, preferentially of ester bonds.

While the *in vivo* degradation of poly(DLLA) and poly(CL) is well documented[5-8], the degradation of poly(TMC) is still in discussion. In one study no decrease of the molecular weight or mass loss of poly(TMC) samples ($\overline{M}_n$ =75,100) was observed after six months of subcutaneous implantation in rats[9]. Another study with poly(TMC) of relatively low molecular weight ($\overline{M}_n$ =19,100) revealed higher degradation rates in comparison with the *in vitro* hydrolysis, suggesting surface degradation with the contribution of enzymatic activity[10]. Neither study provides details on changes in implant dimensions in time or a histological evaluation of the degradation process. The *in vivo* degradation of TMC based copolymers with DLLA or CL has also not yet been investigated thoroughly.

The aim of this study was to assess the *in vivo* biodegradation and tissue response evoked by a TMC-DLLA and a TMC-CL based copolymer as well as that of poly(TMC). Poly(TMC-DLLA) (48:52 mol%) and poly(TMC-CL) (11:89 mol%) were selected as promising candidates for the development of flexible heart constructs and artificial nerve guides, respectively. Polymer disks were implanted in subcutaneous pockets at the back of rats and the tissue reaction at the site of implantation, the implant dimensions as well as mass loss, molecular weight,

composition and thermal properties of the polymers were monitored and evaluated as a function of implantation time.

MATERIALS AND METHODS

Materials

Polymer grade 1,3-trimethylene carbonate (TMC) was obtained from Boehringer Ingelheim, Germany. ε-Caprolactone (CL) (Acros Organics, Belgium) was purified by drying over CaH_2 (Acros Organics, Belgium) and distillation under reduced argon pressure. Polymer grade D,L-lactide (DLLA) (Purac Biochem, The Netherlands) was used without further purification. Stannous octoate ($SnOct_2$) (stannous 2-ethylhexanoate) was used as received from Sigma, USA. Solvents were of analytical grade (Biosolve, The Netherlands).

Polymer Synthesis

Poly(TMC), poly(TMC-DLLA) with 48 mol% of TMC and poly(TMC-CL) with 11 mol% of TMC were synthesized as previously described[2,4]. Briefly, the polymerizations were conducted by ring-opening polymerization in evacuated and sealed glass ampoules using $SnOct_2$ as catalyst. All polymerizations were carried out for a period of 3 days at 130°C±2°C. The obtained polymers were purified by dissolution in chloroform and subsequent precipitation into a ten-fold volume of isopropanol. The precipitated polymers were recovered, washed with fresh isopropanol and dried under reduced pressure at room temperature until constant weight.

Preparation of Polymer Disks

The polymers were melt-pressed (Fontijne laboratory press THB008, The Netherlands) at 140°C to 600 μm thickness. The films were cooled to room temperature under pressure. Circular specimens with a diameter of 1 cm were punched out of the films and stored at -20°C until further use.

The molar composition, molecular weights and thermal properties of the polymers were evaluated after processing and are compiled in Table 1 (see following paragraphs for experimental details).

Table 1. Characterization of the TMC (co)polymers used.

Polymer	$\overline{M}n \times 10^{-5}$	PDI[a]	$[\eta]^b$ (dl/g)	Tg^c (°C)	Tm^c (°C)	$w_c{}^c$ (%)
Poly(TMC-DLLA) (48:52 mol%)	2.32	2.33	3.38	17	-	-
Poly(TMC-CL) (11:89 mol%)	1.54	2.06	4.02	-65	43	33
Poly(TMC)	3.16	2.13	4.28	-17	-	-

[a] PDI – Polydispersity index.

[b] In $CHCl_3$, at 25°C.

[c] First heating scan (DSC).

Implantations

Animal experiments were carried out according to the National Institute of Health (NIH) guidelines for care and use of laboratory animals (NIH publication # 85-23 rev. 1985). Male Wistar rats of approximately 3 months of age (weighing 300-350 g) were anesthetized with a mixture of halothane, N_2O and O_2. After shaving and disinfection, subcutaneous pockets were made to the right and left of three 1 cm midline incisions on the back of the rat. A single sterilized disk was placed in each pocket. Samples were sterilized by incubation in 70 vol% ethanol solution for 15 min followed by two rinsing steps of 5 min in sterile water. Care was taken to implant completely flat specimens. Per evaluation time point, 6 disks of each polymer were randomly implanted in 4 rats. After surgery, the animals were housed in a temperature- and humidity-controlled room with 12 hrs light/dark cycles and they had access to water and standard rat food *ad libitum*.

At 2, 5 and 10 days, 3 wks, 3, 6 and 12 months after implantation, rats were anesthetized and the implants with surrounding tissue were excised, after which the rats were sacrificed. Of each polymer three disks were further processed for histology and 3 disks for chemical and physical characterization.

Histological Examination

The explants were immediately fixed in 2 vol% glutaraldehyde in PBS (0.1 M, pH 7.4) for at least 24 hrs at 4°C. After rinsing in distilled water and dehydration in graded alcohols (50, 70, 96 and 100 vol%), explants were cut in halves and each part was embedded in glycol methacrylate (GMA) (Kulzer Histo-Technik, Heraeus Kulzer, Germany) for light microscopic evaluations. GMA-sections (2 μm) were routinely stained with toluidine blue. The tissue response was independently rated by 3 persons according to the following scoring system: - = no infiltration,

sp to +++ = sporadic to relatively high infiltration of polymorphonuclear cells, macrophages, multinucleated giant cells and/or lymphocytes. The sections were also examined for the presence of fibrin, exudate, the induction of vascularization and the formation of a fibrous capsule around the polymer sample.

Evaluation of Polymer Degradation

The explants were immediately immersed in PBS containing 1 wt/vol% of penicillin/streptomycin (Gibco BRL, Life Technologies, Germany) and kept at 4°C until further evaluation. After the specimens were freed from the surrounding tissue and capsule (when present), the specimens were rinsed in PBS. Subsequently the samples were blotted, weighed and their dimensions monitored. After drying under vacuum at room temperature, the weight of the dry samples was determined.

The water uptake was defined as follows:

$$\text{water uptake (wut)} = \frac{W_w - W_r}{W_r} \times 100 \qquad (\text{wt}\%) \qquad (1)$$

where w_w represents the weight of the wet sample after blotting and w_r represents the remaining weight of the sample after drying.

Mass loss was expressed as:

$$\text{mass loss} = \frac{W_o - W_r}{W_o} \times 100 \qquad (\text{wt}\%) \qquad (2)$$

where w_o corresponds to the initial weight of the polymer sample.

Subsequently, the molar composition, molecular weight and thermal properties of the specimens were determined.

Nuclear Magnetic Resonance (NMR) Spectroscopy

A Varian Inova 300 MHz spectrometer (USA) was used for molar composition analysis. ^{1}H-NMR spectra were recorded at 300 MHz using polymer solutions in $CDCl_3$ (Sigma, USA).

Gel Permeation Chromatography (GPC)

Weight and number average molecular weight ($\overline{M}_w$ and $\overline{M}_n$, respectively), polydispersity index (PDI) and intrinsic viscosity ([η]) were determined by GPC using a Waters Model 510 pump (USA), a HP Ti-Series 1050 autosampler (USA), a Waters Model 410 Differential Refractometer and a Viscotek H502 Viscometer Detector (USA) with Waters Styragel HR5-HR4-HR2-HR1 columns placed in series. At later stages of sample degradation, Waters Styragel HR4-HR2-HR0.5

columns placed in series were used instead. Chloroform was used as eluent at a flow rate of 1.5 ml/min. Narrow polystyrene standards were used for calibration. Sample concentrations of approximately 0.5 wt/vol% and injection volumes of 30 μl were used. All determinations were performed at 25°C.

Differential Scanning Calorimetry (DSC)

The thermal properties of the processed and degraded samples were evaluated by DSC. Samples (5-15 mg) placed in aluminum pans were analyzed with a Perkin Elmer Pyris1 (USA) at a heating rate of 10°C/min. All samples were heated to 40°C above their melting temperature (when present) or glass transition temperature. The samples were then quenched rapidly (300°C/min) until 40°C below their glass transition temperature and after 5 min a second scan was recorded. The glass transition temperature (Tg) was taken as the midpoint of the heat capacity change and the peak melting temperature (Tm) was determined from the melting endotherm. The crystallinity (w_c) of the semicrystalline TMC-CL (co)polymers was determined assuming proportionality to the experimental heat of fusion (ΔH) according to the expression: $w_c=\Delta H/\Delta H°$, where $\Delta H°$ is the heat of fusion of 100% crystalline poly(CL) reported to be 139.4 J/g[11]. Cyclohexane, indium, gallium and tin were used as standards for temperature calibration.

Scanning Electron Microscopy (SEM)

The surface structure of the polymer disks was observed at selected time points using a LEO1550 Gemini field emission scanning electron microscope (LEO, Germany) operating at 1 kV.

RESULTS

Macroscopic Observations

The aspect of the polymers before implantation and upon explantation can be seen in Figure 1. Initially, the amorphous poly(TMC-DLLA) (48:52 mol%) and poly(TMC) were transparent, and poly(TMC-CL) (11:89 mol%) was opaque. This is in agreement with the amorphous nature of the former polymers and the semi-crystalline structure of the latter (Table 1). The initial water absorption of all polymers was below 2 wt%, in accordance with previous reports[3].
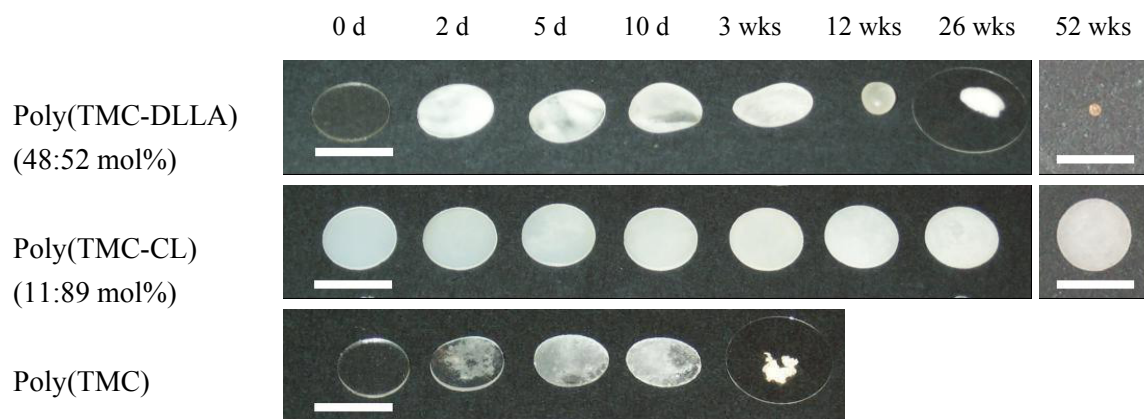
Figure 1. Polymer specimens after retrieval (bar = 1 cm).

As a result of water uptake poly(TMC-DLLA) (48:52 mol%) samples became opaque after implantation. In time the specimens shrunk. The samples that were recovered as from 12 weeks were significantly smaller and shapeless polymer masses compared to earlier time points (Figure 1).

For the poly(TMC-CL) (11:89 mol%) specimens no changes in visual appearance (Figure 1) or dimensions (Figure 2) were observed during this one-year degradation study.
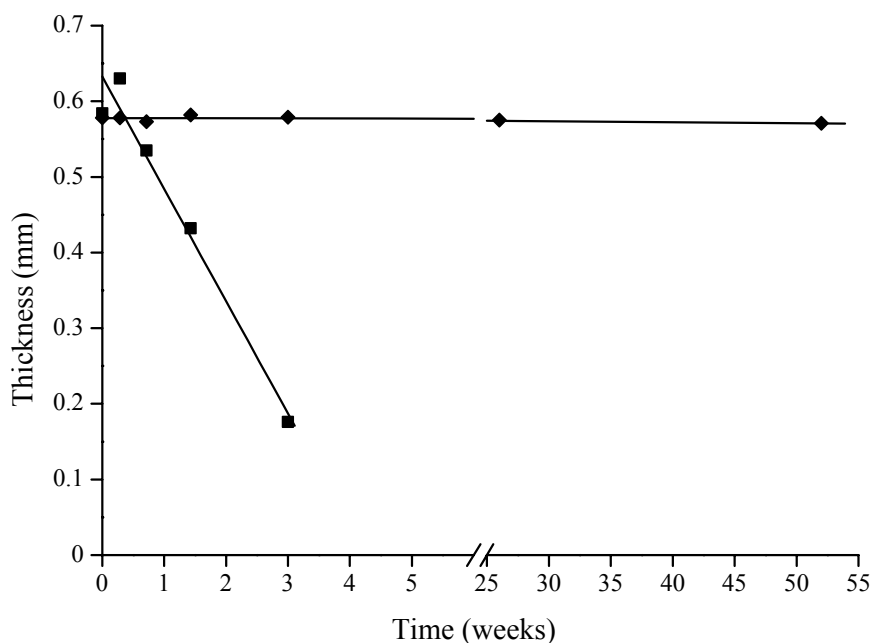

Figure 2. Thickness of the (■) poly(TMC) and (♦) poly(TMC-CL) (11:89 mol%) specimens after retrieval as a function of implantation time.

All retrieved poly(TMC) specimens were round with a diameter of approximately 1 cm, but the implant thickness decreased linearly during the implantation period (see Figure 2 for a comparison with poly(TMC-CL) (11:89 mol%)) and the surface of the specimens became increasingly pitted. Surprisingly, at 3 wks only one out of the three specimens implanted for physical and chemical properties analysis could be macroscopically detected and retrieved. Its initial shape was still intact, but the specimen was very thin and covered with firmly adhering tissue. This made retrieval of the sample very difficult and it was not possible to recover it in one piece (Figure 1, 3 wks). When the sample was freed from the surrounding tissue, small pores could be observed at the specimen's surface. At later time points no poly(TMC) samples could be detected macroscopically, but polymer remnants were observed in the tissue after microscopical analysis up to 6 months of implantation (see next paragraph for more details).

Tissue Response

Table 2 gives an overview of the nature and extent of the observed tissue reactions after implantation of the different polymers.

At day 2 all polymer implants (Figure 3) were surrounded by a discontinuous fibrin layer containing macrophages and fibroblasts. In the case of poly(TMC) the macrophages were concentrated at the tissue-implant interface while for the copolymers these cells were more evenly distributed in the surrounding tissue. Some granulocytes (PMN) and lymphocytes were seen as well (<1% of the total number of cells). In all cases vascularization was observed, which was more extensive in the case of the copolymers.

Five days after the implantation, less fibrin was present in the surroundings of all implants but from this time point on, the tissue reaction towards the copolymers and the TMC homopolymer was different. Therefore, from 5 days after implantation onwards the events concerning the TMC homopolymer will be described separately. For both poly(TMC-DLLA) (48:52 mol%) and poly(TMC-CL) (11:89 mol%) implants at day 5 the tissue reaction was mainly dominated by encapsulation. However, some macrophages were present and sprouting of blood vessels could still be observed. PMN were no longer present and lymphocytes were only sporadically seen.

Table 2. Tissue reactions to TMC based (co)polymers disks.

	Time	Fibrin	Lympho-cytes	PMN	Macro-phages	Giant cells	Vascula-rization	Phago-cytosis
Poly(TMC-DLLA)	2 d	+	±	sp	+	-	+++	no
(48:52 mol%)	5 d	±	sp	-	+	-	+	no
	10 d	-	sp	-	+±	+	+±	no
	3 wks	-	±	-	+	+±	+++	no
	12 wks	-	sp	-	sp	-	+	yes
	26 wks	-	sp	-	++	+	++	yes
	52 wks	-	+	-	++	+±	+++	yes
Poly(TMC-CL)	2 d	+	±	sp	+	-	+++	no
(11:89 mol%)	5 d	±	sp	sp	+±	-	++	no
	10 d	-	-	-	+	±	+	no
	3 wks	-	-	-	±	+	+±	no
	12 wks	-	-	-	sp	sp	+±	no
	26 wks	-	-	-	sp	-	+±	no
	52 wks	-	sp	-	sp	-	+	no
Poly(TMC)	2 d	+	±	±	+±	-	++	no
	5 d	sp	±	-	+++	+	+++	yes
	10 d	-	sp	-	+	+±	++	yes
	3 wks	-	±	-	++	++	++	yes
	12 wks	-	±	-	++	+	+±	yes
	26 wks	-	sp	-	+	++	+±	yes
	52 wks[a]	-	sp	-	-	-	±	no

PMN – Polymorph nuclear cells (granulocytes).

-: not present; sp to +++: sporadic to high infiltration.

[a] No polymer remnants were observed at the site of implantation.

At 10 days (Figure 4A and 5A) a capsule was formed, with the highest numbers of macrophages and fibroblasts observed with poly(TMC-DLLA) (48:52 mol%). Giant cells were formed at the interface of both copolymer implants. Some lymphocytes (<1% of the total number of cells) were only seen in the tissue surrounding the DLLA containing copolymer implants.

At 3 and 12 wks (Figure 4B and 5B) a quiet capsule was present around the copolymer implants. The capsules mainly consisted of 10 to 15 layers of cells aligned parallel to the implant. At 3 months giant cells were not present anymore

and macrophages could only be observed sporadically. When compared to the previous time points, the presence of blood vessels had diminished.
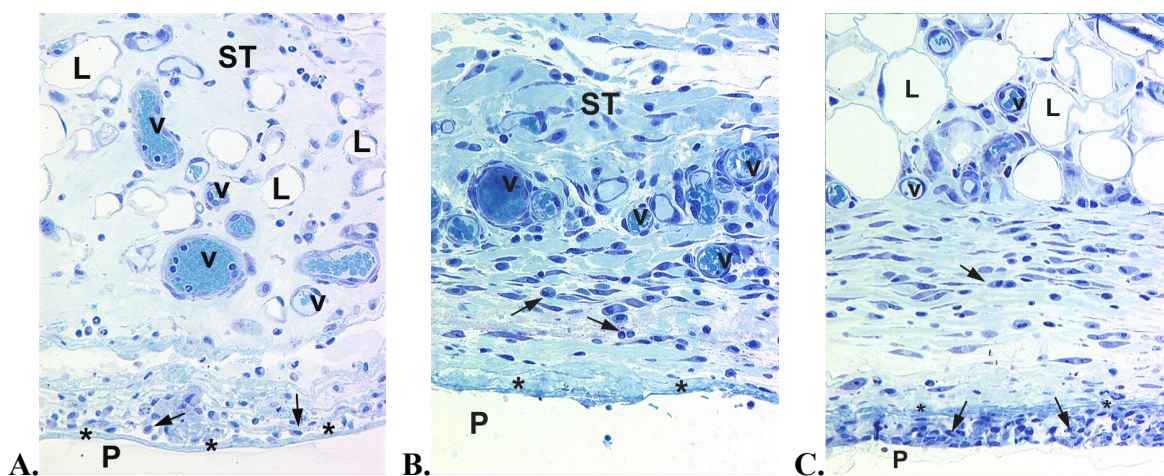

Figure 3. Light micrographs (200x) of (A) poly(TMC-DLLA) (48:52 mol%); (B) poly(TMC-CL) (11:89 mol%) and (C) poly(TMC) at day 2 of implantation. (P) Polymer, (ST) surrounding tissue, (L) lipid tissue, (v) blood vessel, (∗) fibrin and (arrow) macrophage.

After longer implantation periods, the tissue reaction towards poly(TMC-CL) (11:89 mol%) implants did not change (Figure 5C). The tissue surrounding the CL containing implants was very quiet. Vascularization was low and macrophages and lymphocytes were only sporadically detected. The capsules consisted of approximately 10 cell layers. Maturation of the extracellular matrix (ECM) of the capsule increased in time.

In contrast, after 26 wks, at the implantation site of the DLLA based copolymers many cells had infiltrated the capsule (Figure 4C). Vascularization had increased and macrophages with phagocytosed (small) polymer particles were observed at the tissue-implant interface (Figure 4D). Lymphocytes were seen only sporadically. At 52 wks of implantation the copolymer was disintegrated (Figure 4E). Larger and smaller remnants were surrounded by a fibrous capsule. Giant cells were surrounding polymer particles and in between phagocytosis of small polymer particles was observed. At this time point some lymphocytes as well as some plasma cells were present in the tissue surrounding the polymer remnants (Figure 4F).

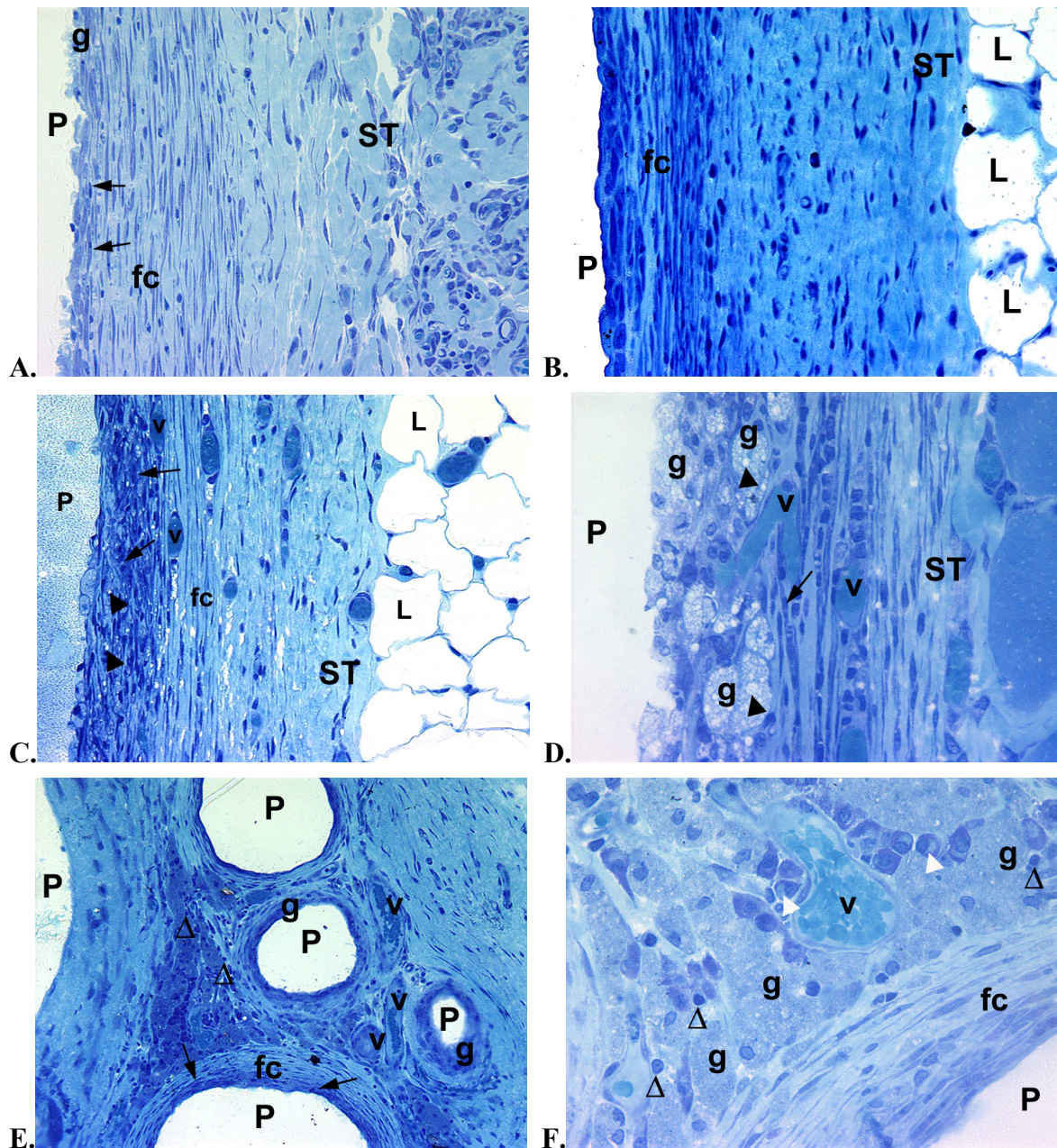**Figure 4.** Light micrographs of poly(TMC-DLLA) (48:52 mol%) at (A) 10 days (200x); (B) 12 wks (200x); (C and D) 26 wks (200x and 400x detail) and (E and F) 52 wks (100x and 400x detail) of implantation. (P) Polymer, (ST) surrounding tissue, (fc) fibrous capsule, (g) giant cell, (arrow) macrophage, (L) lipid tissue, (v) blood vessel, (arrow head) phagocytosis, (Δ) lymphocytes and (white arrow head) plasma cells.
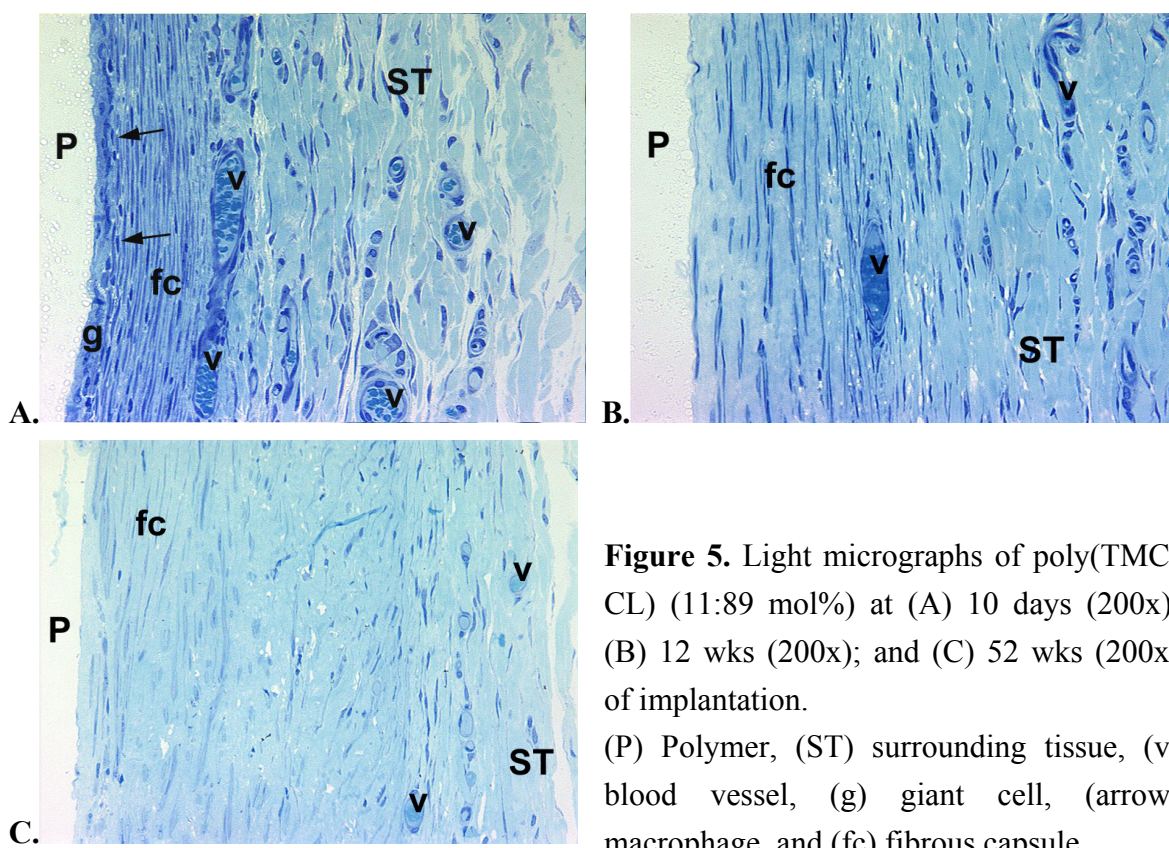
Figure 5. Light micrographs of poly(TMC-CL) (11:89 mol%) at (A) 10 days (200x); (B) 12 wks (200x); and (C) 52 wks (200x) of implantation.
(P) Polymer, (ST) surrounding tissue, (v) blood vessel, (g) giant cell, (arrow) macrophage, and (fc) fibrous capsule.

At day 5 after the implantation of poly(TMC) a layer of macrophages and some fibroblasts surrounded the implants (Figure 6A) in a comparable way as with the copolymers. However, at the tissue-implant interface giant cells could already be observed as well as the first signs of polymer phagocytosis. The tissue surrounding the poly(TMC) specimens was also very active including newly formed blood vessels and infiltrating macrophages arriving at the implant site. No granulocytes were present and only few lymphocytes (<1% of the total number of cells) were detected.

At day 10 a monolayer of (mature) giant cells was observed at the tissue-implant interface. The following layers of cells consisted of more elongated macrophages (with engulfed polymer particles) and fibroblasts aligned parallel to the polymer. Vascularization remained relatively high (Table 2). Within 3 wks, extensive phagocytosis had occurred (Figure 6C) and the implants had become much thinner.

At 12 wks most of the polymer had been phagocytosed (Figure 6D) and only a small area of inflammatory cells could be observed at the site of implantation. At 26 wks, in only one of the retrieved explants, few polymer remnants engulfed by macrophages and giant cells were found (Figure 6E and 6F). In the surrounding tissue small blood vessels were observed. At 3, 12 and 26 wks of implantation some

lymphocytes were observed in the surrounding tissue. After 1 year no evidence of the presence of the polymer was found.
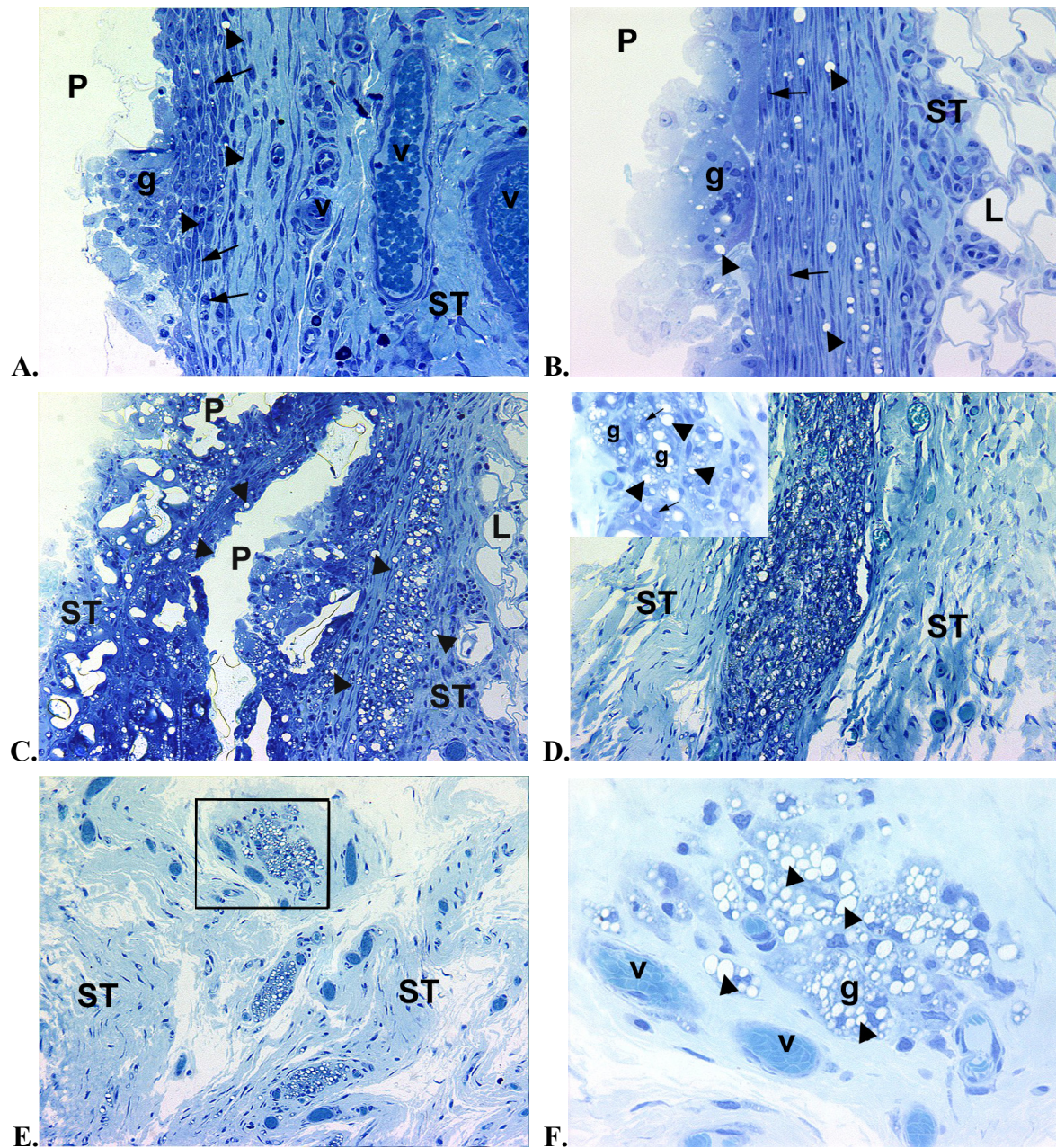

Figure 6. Light micrographs of poly(TMC) at (A) 5 days (200x); (B) 10 days (200x); (C) 3 wks (100x); (D) 12 wks (100x and 400x detail) and (E and F) 26 wks (100x and 400x detail) of implantation. (P) Polymer, (ST) surrounding tissue, (L) lipid tissue, (g) giant cell, (arrow) macrophage, (v) blood vessel, and (arrow head) phagocytosis.

Changes in Molecular Weight and Mass

Table 3 shows the molecular weights of the TMC based (co)polymers at different periods of subcutaneous implantation.

Table 3. Molecular weight of TMC based (co)polymers as a function of implantation time.

Polymer	$[\eta]^a$ (dl/g)	$\overline{M}w \times 10^{-5}$	$\overline{M}n \times 10^{-5}$	PDI
Poly(TMC-DLLA) (48:52 mol%)				
Compression-molded disks	3.38	5.39	2.32	2.33
2 days	3.01	5.72	2.60	2.21
5 days	3.11	5.02	2.12	2.37
10 days	3.17	4.26	1.88	2.27
3 wks	2.42	3.39	1.66	2.07
12 wks	0.41	0.35	0.17	2.13
26 wks	0.09	0.04	0.03	1.47
52 wks	-	0.07^b	0.05^b	1.42
Poly(TMC-CL) (11:89 mol%)				
Compression-molded disks	4.02	3.18	1.54	2.06
2 days	3.82	3.08	1.52	2.04
5 days	3.68	2.91	1.43	2.04
10 days	3.84	3.13	1.49	2.11
3 wks	3.78	3.16	1.52	2.07
12 wks	3.56	2.68	1.33	2.02
26 wks	3.39	2.37	1.13	2.14
52 wks	2.56	1.90	0.95	2.01
Poly(TMC)				
Compression-molded disks	4.28	6.73	3.16	2.13
2 days	4.19	5.67	2.58	2.20
5 days	4.06	5.48	2.46	2.23
10 days	4.14	5.84	2.52	2.32
3 wks	-	6.44^b	0.43^b	nd

^{a} In CHCl$_3$, at 25°C.

^{b} Relative to poly(styrene).

nd – Not determined because the molecular weight distribution was bimodal.

Both copolymers showed a continuous decrease in molecular weight. In 52 wks the $\overline{M}n$ of poly(TMC-CL) decreased to less than half of its initial value. For the TMC-DLLA copolymer the decrease in $\overline{M}n$ was faster and at 26 wks the $\overline{M}n$ had already decreased to 1% of its initial value. For poly(TMC-DLLA) (48:52 mol%) at 52 wks

it was not possible to determine the absolute molecular weight of the remaining polymer as only a very small amount of polymer could be recovered (mass loss > 96%) and it could not be totally freed from the fibrous capsule. For all samples and at all stages of degradation monomodal molecular weight distributions were observed.

The molecular weight of the poly(TMC) implants did not show a significant decrease up to 3 wks, the last evaluation point where it was possible to recover a specimen for evaluation. At this point it was not possible to determine the absolute molecular weight of the sample for similar reasons as previously described for the TMC-DLLA copolymer. For this sample the molecular weight showed a bimodal distribution with the main polymer fraction having an $\overline{M}n$ of 540,000 and a smaller polymer fraction showing an $\overline{M}n$ of 8,400 (both values relative to poly(styrene)).

In Figures 7 to 9 the number average molecular weight ($\overline{M}n$) and mass loss determined for each polymer are presented as a function of implantation time.
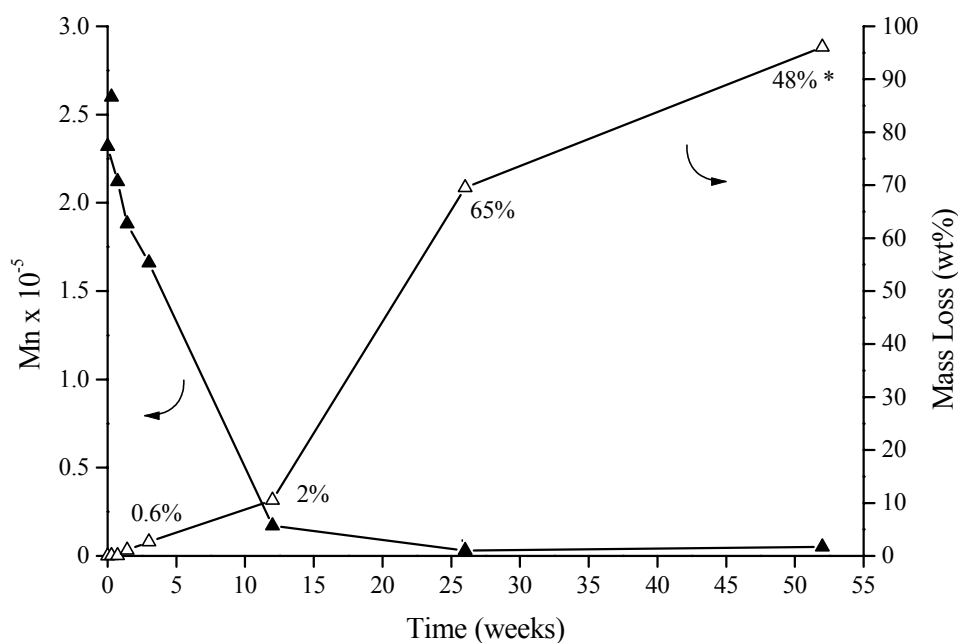

Figure 7. Molecular weight ($\overline{M}n$) and mass loss as a function of implantation time for poly(TMC-DLLA) (48:52 mol%). Water uptake (wt%) is indicated at the corresponding time point. (∗) At this time point the accurate determination of the specimen weight was not possible.

The $\overline{M}n$ of the poly(TMC-DLLA) (48:52 mol%) implants decreased from the start of the implantation time (Figure 7). During the initial stages of the degradation,

limited mass loss was observed. But at implantation periods later than 12 wks a rapid decrease in remaining mass occurred. At this point $\overline{M}n$ had reached values of approximately 20,000. The material resorption was nearly complete at 1 year. After substantial mass loss, the polydispersity index decreased from initial values above 2 to values of around 1.4 (Table 3).
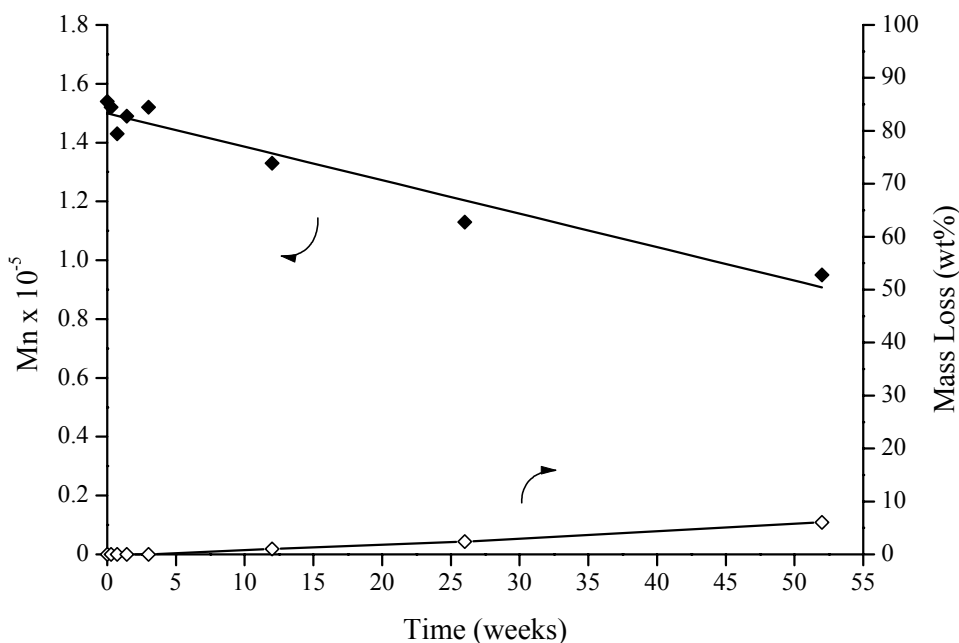

Figure 8. Molecular weight ($\overline{M}n$) and mass loss as a function of implantation time for poly(TMC-CL) (11:89 mol%). After the initial water uptake (<2 wt%) no further significant water uptake was detected.

For poly(TMC-CL) (11:89 mol%) a linear and continuous reduction of the $\overline{M}n$ was observed in time but at a much lower rate (Figure 8). At 1 year the mass loss was less than 7%.

In contrast to the degradation profile of the copolymers, the molecular weight of the poly(TMC) implants did not significantly change during resorption (Table 3 and Figure 9). However, mass loss was already detected at 2 days of implantation. In time, mass loss increased linearly and after 3 wks it was nearly complete.
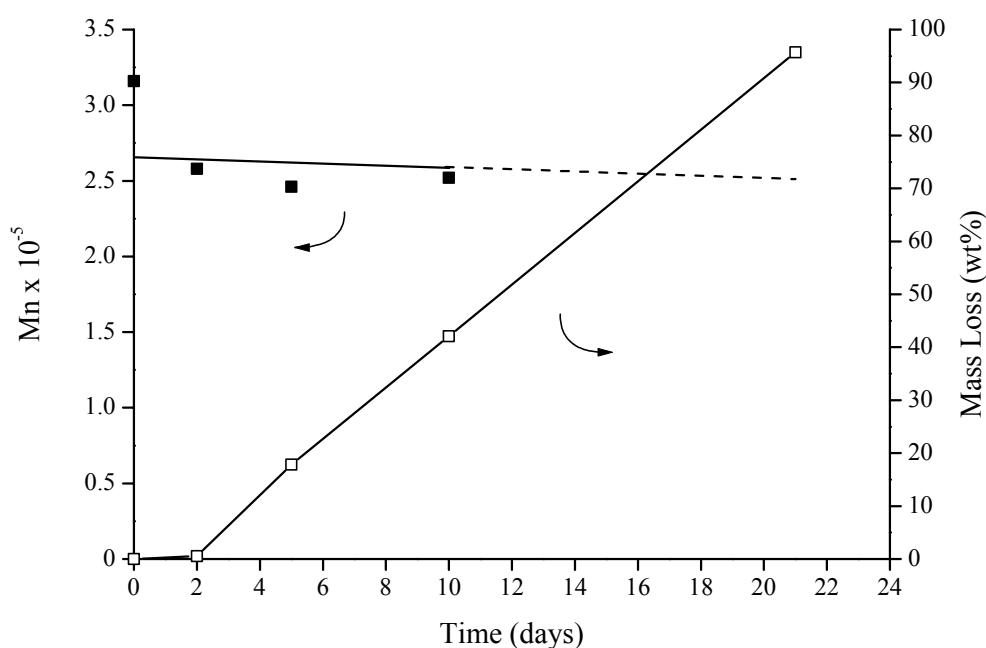
Figure 9. Molecular weight ($\overline{M}n$) and mass loss as a function of implantation time for poly(TMC). After the initial water uptake (<2 wt%) no further water uptake was detected.

As previously mentioned, the TMC based (co)polymers investigated are hydrophobic. After the initial water uptake no further uptake was detected for poly(TMC-CL) (11:89 mol%) and poly(TMC) implants during the implantation period. For poly(TMC-DLLA) (48:52 mol%) limited water uptake occurred at the initial degradation stages. The first indication of an increase in the water uptake of the samples was detected at 3 months (Figure 7). This coincided with the total loss of the initial sample shape and steep increase of mass loss.

Molecular Composition
The TMC content of the TMC-DLLA copolymer was found to increase after mass loss had started (Table 4).

Table 4. Change in TMC content for poly(TMC-DLLA) (48:52 mol%) during *in vivo* degradation.

	Degradation time							
	0	2 d	5 d	10 d	3 wks	12 wks	26 wks	52 wks
TMC content (mol%)	48	48	48	48	48	49	56	53

For the CL containing copolymer no changes in the molecular composition were observed during the implantation time.

Thermal Properties

For the semi-crystalline poly(TMC-CL) (11:89 mol%) the decrease in molecular weight was accompanied by an increase in crystallinity. The increase in the heat of fusion (Figure 10) is the result of annealing at rat body temperature, a process that is enhanced in the wet state, and of crystallization of hindered chain segments made possible by chain cleavage in the amorphous phase.
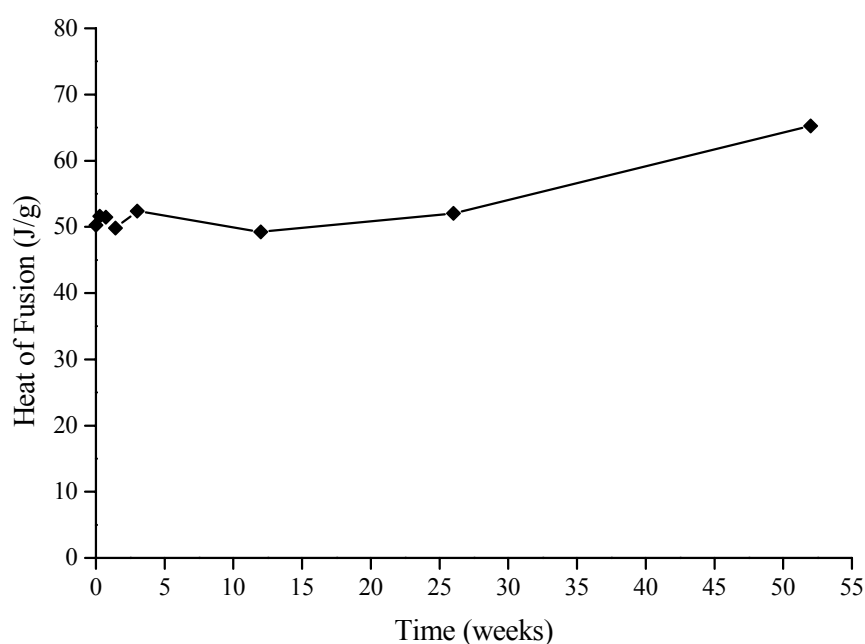

Figure 10. Heat of fusion (ΔH), recorded by DSC in the first heating scan, as a function of implantation time for poly(TMC-CL) (11:89 mol%).

In the case of poly(TMC-DLLA) (48:52 mol%) the thermal properties were only evaluated until 12 wks of implantation. At later evaluation points there was not enough material available for DSC analysis. Up to 3 wks, the thermal properties of the DLLA based TMC copolymer remained unchanged. During the 3rd to 12th wk of implantation, the Tg (second scan) of the samples had decreased from 20 to 15°C. This change can be explained by the decrease of the polymer molecular weight, as no significant change in composition had occurred during that period.

The thermal properties of poly(TMC) did not significantly alter during implantation (data not shown).

DISCUSSION

We have previously reported on the degradation of poly(TMC) and TMC copolymers with DLLA or CL in PBS (pH 7.4) at 37°C[3]. During the two-year period of that study, poly(TMC) showed a negligible decrease in molecular weight with a small deterioration of mechanical performance and no mass loss. From the start the copolymers showed a decrease in molecular weight. The *in vitro* degradation could therefore be described by preferential hydrolysis of ester bonds throughout the bulk, autocatalyzed by the generated acidic end groups. The rate of chain cleavage was lower for TMC-CL copolymers than for TMC-DLLA copolymers. Consistent with polymer degradation in the bulk, the mechanical properties of the polymers deteriorated as the molecular weight decreased. Mass loss occurred only at advanced stages of degradation. The TMC-DLLA copolymer with 48 mol% of TMC resorbed completely within one year. In contrast TMC-CL copolymers degraded much slower. These materials retained suitable mechanical properties for more than 1 year and up to 2 years no mass loss was observed.

The *in vivo* degradation of poly(TMC-DLLA) (48:52 mol%) and poly(TMC-CL) (11:89 mol%) followed a similar trend to that observed *in vitro*. The molecular weight of both copolymer specimens decreased from the early stages of implantation.

Up to 12 wks the $\overline{M}_n$ of the specimens containing DLLA decreased from 230,000 to less than 20,000. The samples retrieved at 12 wks were shapeless polymer masses. At this time point water uptake and mass loss were detected. These observations fit in the sequence of events described for the degradation of this copolymer *in vitro*. As $\overline{M}_n$ reaches values below approximately 25,000, the mechanical properties of the polymer are lost[3]. The decrease in mechanical strength together with the high mobility of the polymer due to its low Tg, may have contributed to the loss of the initial shape of the specimens. *In vitro* the loss of mechanical strength preceded the onset of substantial water uptake and the onset of mass loss. Mass loss started, both *in vitro* and *in vivo*, when $\overline{M}_n$ had reached a value of approximately 20,000. The rapid decrease in remaining mass resulted in a decrease in the polydispersity index from an initial value of 2.3 to approximately 1.4 (Table 3). At advanced stages of hydrolysis, the low-molecular weight degradation products can diffuse into the surrounding medium. The mol% of TMC in the copolymer increased after the onset of mass loss. This can be due to

preferential chain cleavage at the ester bonds and differences in solubility of the formed chain fragments.

The TMC-CL copolymer with 11 mol% of TMC degraded much slower. Despite the decrease in molecular weight observed in the 1-year implantation period, $\overline{M}_n$ was still above 90,000. One can expect that after this time the implants still possess suitable mechanical properties.

Both copolymers showed good tissue tolerance after subcutaneous implantation. The tissue reaction upon implantation resembled a sterile inflammatory reaction followed by a normal foreign body reaction, as commonly seen after implantation of other biodegradable polymers[8,12,13]. The tissue response was characterized by the presence of foreign body giant cells and granulation tissue, which consisted of macrophages, fibroblasts and newly formed blood vessels. Lymphocytes were only occasionally observed. As a result of the foreign body response, encapsulation of the implants was observed.

Up to one year, the degradation of poly(TMC-CL) (11:89 mol%) was accompanied by the formation of a mature capsule. In a similar manner as observed *in vitro*[3], the crystallinity of the TMC-CL copolymer increased in time. After 1 year of implantation a 30% increase was detected (Figure 10). It was found for poly(L-lactide) that stable particles of high crystallinity formed upon degradation, which seems to be related with a subcutaneous swelling seen in patients 3 years post-operatively[14,15]. Although this has not been reported for poly(CL) implants, changes in crystallinity should be investigated for longer periods of implantation.

For poly(TMC-DLLA) (48:52 mol%) the capsule remained quiet during the first 3 months of implantation. At later stages, between 12 and 26 wks, a second inflammatory reaction was triggered that coincided with the onset of mechanical strength deterioration and mass loss. This rather mild secondary inflammatory reaction (Table 2) could be related to the clearance of the polymer residues resulting from the polymer degradation.

As seen *in vitro,* the kinetics of chain scission *in vivo* is indicative of an autocatalytic process by the generated acidic end groups (Figure 11). The hydrolysis rates *in vivo*, determined according to an autocatalytic kinetic model[5] were respectively, 2.6×10^{-2} d^{-1} and 0.13×10^{-2} d^{-1} for the TMC-DLLA and TMC-CL copolymers. The rates of hydrolysis *in vivo* were lower than the *in vitro* rates (3.6×10^{-2} d^{-1} and 0.26×10^{-2} d^{-1} for poly(TMC-DLLA) (50:50 mol%) and poly(TMC-CL) (10:90 mol%), respectively). These observations suggest that enzymatic degradation did not play an important role in the early stages of the degradation

process of the copolymers. Nevertheless, at later stages of degradation enzymatic activity might still be involved[16,17]. In the present study we have shown evidence of TMC-DLLA copolymer engulfment at advanced stages of degradation. When polymer fragments are small enough to be endocytosed by phagocytic cells, the polymer can be further degraded by intracellular enzymatic processes[18].
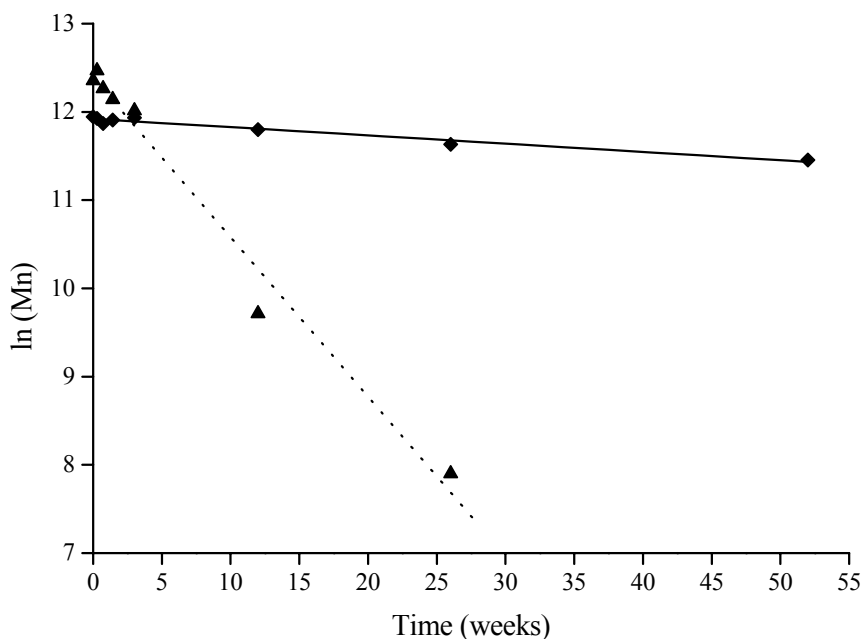

Figure 11. Plot of ln($\overline{M}_n$) as a function of degradation time for poly(TMC-DLLA) (48:52 mol%) (▲) and poly(TMC-CL) (11:89 mol%) (♦). Note: The last data point for the TMC-DLLA copolymer, where extensive mass loss had occurred, was excluded in the determination of the hydrolysis rates.

In contrast to the very slow hydrolytic degradation of poly(TMC) *in vitro*, this polymer was totally resorbed within a year of implantation. Poly(TMC) implants showed a large decrease in mass from the start without a change in molecular weight (Figure 9). Furthermore, after 3 wks of implantation the molecular weight distribution of the polymer was bimodal, what may be explained by differences in molecular weight between the surface and the bulk of the specimens[10]. These can only be detected when the surface to bulk ratio had significantly increased. Such observations in combination with the decrease of the specimen thickness (Figure 2) and the extensive phagocytosis occurring at the implant surface (Figure 6), indicate a surface erosion process. Considering the short time it took for the complete resorption of the polymer *in vivo* and that after a 2-year period *in vitro* no

significant decrease of molecular weight was observed, it seems likely that enzymatic activity has played a significant role. Other factors such as differences in pH or ionic strength can however be of influence and their contribution to the process should not be ruled out.

In Figure 12 one can compare the aspect of the surface of poly(TMC-CL) (11:89 mol%) disks before and after 6 months of implantation with the surface of poly(TMC) specimens before and after only 10 days of implantation. The surface of the CL based copolymer, which degrades by bulk hydrolysis, remained nearly unchanged after 26 wks of implantation. As early as at 10 days of degradation the TMC homopolymer showed clear signs of pitting.
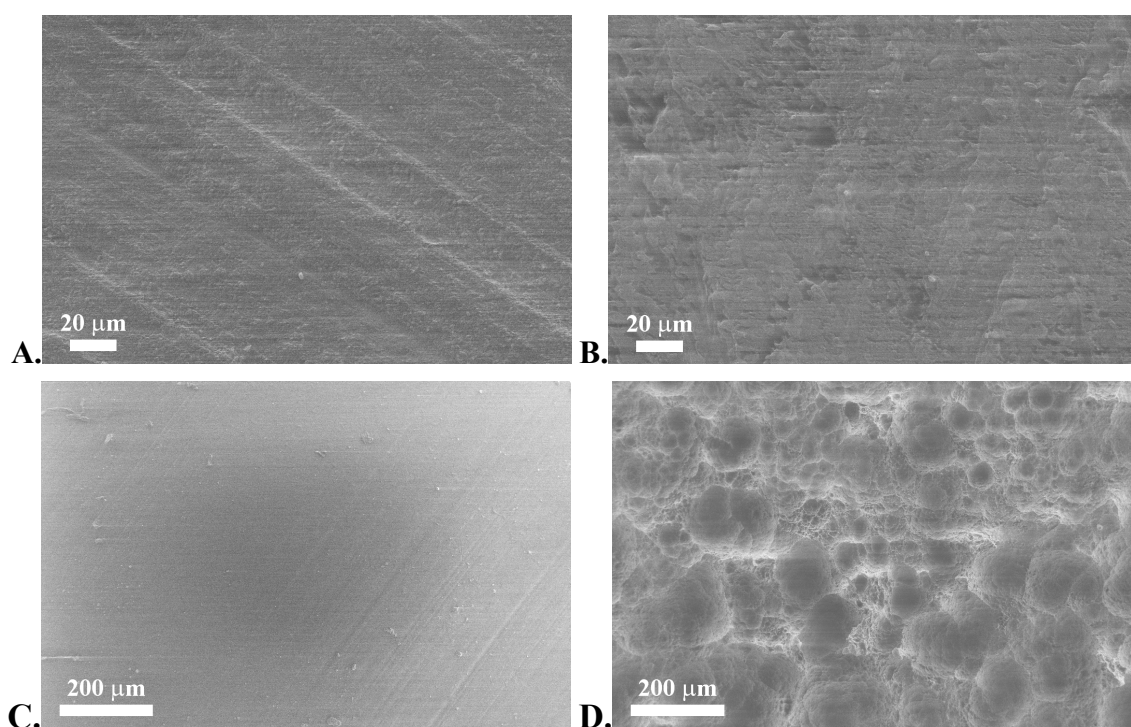
Figure 12. SEM pictures of the surface of the poly(TMC-CL) (11:89 mol%) specimens before (A) and after 26 wks (B) of implantation, and poly(TMC) specimens before (C) and after 10 days (D) of implantation. Note: The electron microscope employed enables the measurement at very low voltage (1 kV) so coating of the surfaces with a conductive layer was not necessary.

Although enzymatic contribution to the *in vivo* degradation of poly(TMC) has previously been suggested[10], this is the first report where clear evidence of surface erosion of the polymer involving enzymatic processes is presented. The rate of degradation was also significantly higher than the one previously reported[10] although polymer of much higher initial molecular weight was used in the present

study. After 3 wks we have measured a 95 wt% mass loss, while in the previous study only 21 wt% of mass loss was seen after 26 weeks.

Examples of synthetic polymers that undergo surface erosion *in vivo* via chemical hydrolysis can be found in literature[19-21]. There are few reports on the enzymatic surface erosion of synthetic polymers *in vivo*[22-24]. Possible factors involved in the susceptibility of a polymer to enzymatic attack are segmental mobility of the polymer chains and the specificity of the active site of the enzyme towards a certain chemical structure[10,24]. The incorporation of other monomer units in the poly(TMC) chain may inhibit the interaction between the enzyme's active site and the labile linkage, explaining the absence of an enzymatic contribution to the degradation of the copolymers.

In general poly(TMC) induced a mild tissue reaction when subcutaneously implanted. The foreign body reaction resembled a sterile chronic inflammatory reaction, mainly characterized by the presence of macrophages, giant cells and vascularization during the entire period necessary for the polymer resorption. One year after implantation the polymer had been completely resorbed and tissue at the site of implantation had regenerated.

CONCLUSIONS

To our knowledge this is the first time that surface erosion of poly(TMC) involving enzymatic processes is clearly demonstrated. High molecular weight poly(TMC) specimens were extensively degraded after 3 wks of subcutaneous implantation in the back of rats and, as confirmed by histology, were totally resorbed within less than a year. Upon implantation, an acute sterile inflammatory reaction was observed followed by a mild macrophage-mediated foreign body reaction that lasted during the resorption period of the polymer.

Contrary to poly(TMC), the degradation of poly(TMC-DLLA) (48:52 mol%) and poly(TMC-CL) (11:89 mol%) showed the same pattern *in vitro* and *in vivo*, what indicates that enzymatic activity does not have a significant role in the initial stages of the *in vivo* degradation of these copolymers. Degradation takes place throughout the bulk via hydrolysis, preferentially of ester bonds, autocatalyzed by the generated acidic end groups. Tissue reaction against the copolymers started with an acute sterile inflammatory reaction caused by the trauma of implantation, followed by a foreign body reaction that led to the polymer encapsulation.

At advanced degradation stages mass loss occurred. In this study this was only observed for the TMC-DLLA copolymer. When extensive mass loss started, a relatively mild second foreign body reaction, related to clearance of the polymer fragments, was triggered. The TMC-DLLA copolymer was almost completely resorbed in one year.

These results show that both copolymers are well tolerated upon subcutaneous implantation in rats. Their degradation profiles as well as their flexibility make these materials promising polymers for several soft tissue engineering applications. The TMC-CL copolymer degrading slowly is suitable for preparation of nerve guides that should keep their shape and mechanical performance for periods of up to a year. The TMC-DLLA copolymer degrades faster and can be totally resorbed in approximately one year, fitting the requirements for the preparation of scaffolds for heart tissue engineering.

ACKNOWLEDGMENTS

REFERENCES

[1]   Pêgo AP, Poot AA, Grijpma DW, Feijen J. Biodegradable elastomeric scaffolds for soft tissue engineering. *J Control Release* (in press).

[2]   Pêgo AP, Poot AA, Grijpma DW, Feijen J. Copolymers of trimethylene carbonate and ε-caprolactone for porous nerve guides: synthesis and properties. *J Biomater Sci Polym Ed* 2001; 12: 35-53. Chapter 3 of this thesis.

[3]   Pêgo AP, Poot AA, Grijpma DW, Feijen J. *In vitro* degradation of trimethylene carbonate based (co)polymers. *Macromol Chem Phys (accepted for publication)* Chapter 6 of this thesis.

[4]   Pêgo AP, Poot AA, Grijpma DW, Feijen J. Physical properties of high molecular weight 1,3-trimethylene carbonate and D,L-lactide copolymers. *(submitted to J Mater Sci: Mater Med, 2002)* Chapter 5 of this thesis.

[5]   Pitt CG, Chasalow FI, Hibionada DM, Klimas DM, Schindler A. Aliphatic polyesters. I. The degradation of poly(ε-caprolactone) *in vivo*. *J Appl Polym Sci* 1981; 26: 3779-3787.

[6]   Pitt CG, Gratzl MM, Kimmel GL, Surles J, Schindler A. Aliphatic polyesters II. The degradation of poly(DL-lactide), poly (ε-caprolactone), and their copolymers *in vivo*. *Biomaterials* 1981; 2: 215-220.

[7]   Leenslag JW, Pennings AJ, Bos RR, Rozema FR, Boering G. Resorbable materials of poly(L-lactide). VII. *In vivo* and *in vitro* degradation. *Biomaterials* 1987; 8: 311-314.

[8]   Schakenraad JM, Nieuwenhuis P, Molenaar I, Helder J, Dijkstra PJ, Feijen J. *In vivo* and *in vitro* degradation of glycine/DL-lactic acid copolymers. *J Biomed Mater Res* 1989; 23: 1271-1288.

[9]   Albertsson A-C, Eklund M. Influence of molecular structure on the degradation mechanism of degradable polymers: *in vitro* degradation of poly(trimethylene carbonate), poly(trimethylene carbonate-co-caprolactone), and poly(adipic anhydride). *J Appl Polym Sci* 1995; 57: 87-103.

[10]   Zhu KJ, Hendren RW, Jensen K, Pitt CG. Synthesis, properties, and biodegradation of poly(1,3-trimethylene carbonate). *Macromolecules* 1991; 24: 1736-1740.

[11]   Crescenzi V, Manzini G, Calzolari G, Borri C. Thermodynamics of fusion of poly-β-propiolactone and poly-ε-caprolactone. Comparative analysis of the melting of aliphatic polylactone and polyester chains. *Eur Polym J* 1972; 8: 449-463.

[12]   Kopecek J, Ulbrich K. Biodegradation of biomedical polymers. *Prog Polym Sci* 1983; 9: 1-58.

[13]   Bos RRM, Rozema FR, Boering G, Nijenhuis AJ, Pennings AJ, Verwey AB, Nieuwenhuis P, Jansen HWB. Degradation of and tissue reaction to biodegradable poly(L-lactide) for use as internal fixation of fractures: a study in rats. *Biomaterials* 1991; 12: 32-36.

[14]   Bergsma EJ, Rozema FR, Bos RR, de Bruijn WC. Foreign body reactions to resorbable poly(L-lactide) bone plates and screws used for the fixation of unstable zygomatic fractures. *J Oral Maxillofac Surg* 1993; 51: 666-670.

[15]   Bergsma JE, de Bruijn WC, Rozema FR, Bos RR, Boering G. Late degradation tissue response to poly(L-lactide) bone plates and screws. *Biomaterials* 1995; 16: 25-31.

[16]   Salthouse TN, Matlaga BF. Polyglactin 910 suture absorption and the role of cellular enzymes. *Surg Gynecol Obstet* 1976; 142: 544-550.

[17]   Woodward SC, Brewer PS, Moatamed F, Schindler A, Pitt CG. The intracellular degradation of poly(ε-caprolactone). *J Biomed Mater Res* 1985; 19: 437-444.

[18] Vert M, Li SM, Spenlehauer G, Guerin P. Bioresorbability and biocompatibility of aliphatic polyesters. *J Mater Sci: Mater in Med* 1992; 3: 432-446.

[19] Holland SJ, Jolly AM, Yasin M, Tighe BJ. Polymers for biodegradable medical devices. II. Hydroxybutyrate-hydroxyvalerate copolymers: hydrolytic degradation studies. *Biomaterials* 1987; 8: 289-295.

[20] Heller J. Development of poly(ortho esters): a historical overview. *Biomaterials* 1990; 11: 659-665.

[21] Tamada J, Langer R. The development of polyanhydrides for drug delivery applications. *J Biomater Sci Polym Ed* 1992; 3: 315-353.

[22] Gumargalieva KZ, Moiseev YV, Daurova TT, Voronkova OS, Rozanova IB. Polycaproamide degradation in rabbits and in several model media. *Biomaterials* 1980; 1: 214-216.

[23] Kawaguchi T, Nakano M, Juni K, Inoue S, Yoshida Y. Examination of biodegradability of poly(ethylene carbonate) and poly(propylene carbonate) in the peritoneal cavity in rats. *Chem Pharm Bull* 1983; 31: 1400-1403.

[24] Pitt CG, Hendren RW, Schindler A, Woodward SC. The enzymatic surface erosion of aliphatic polyesters. *J Control Release* 1984; 3-14.

Extraordinary properties of very high molecular weight poly(1,3-trimethylene carbonate)*

A.P. PÊGO, D.W. GRIJPMA and J. FEIJEN

Institute for Biomedical Technology (BMTI) and Department of Polymer Chemistry and Biomaterials, Faculty of Chemical Technology, University of Twente, P.O. Box 217, 7500 AE Enschede, The Netherlands

ABSTRACT

Poly(1,3-trimethylene carbonate), poly(TMC), has often been regarded as a rubbery polymer that can not be applied in the biomedical field due to its poor dimensional stability, tackiness and inadequate mechanical properties. In this study we show that high molecular weight, amorphous poly(TMC) is very flexible, tough and has excellent ultimate mechanical properties due to strain-induced crystallization. A number average molecular weight ($\overline{M}_n$) of 100,000 was determined to be a critical value below which the polymer has negligible mechanical properties and poor dimensional stability. This corresponds to a molecular weight that is forty times higher than the molecular weight between entanglements. The dependency of the mechanical properties levels off at $\overline{M}_n$ values above 200,000. This very high molecular weight poly(TMC) shows good recovery after mechanical deformation, considering that the only resistance to chain flow is due to chain entanglement.

Poly(TMC) cross-linked upon gamma-irradiation, resulting in the formation of an insoluble network. The degree of cross-linking increases with the radiation dose. The final mechanical properties of the high molecular weight poly(TMC) rubbers improve upon irradiation. Especially, the creep resistance increased, while the Young's modulus and tensile strength were not significantly affected.

These biodegradable cross-linked rubbers may find wide application in soft tissue engineering where tough and elastomeric scaffolds are desirable.

INTRODUCTION

The need for biodegradable elastomeric polymers for the preparation of medical implants and porous scaffolds to be used for tissue engineering has been documented in literature in recent years[1-3]. The traditionally used glycolide and lactide based (co)polymers are not well suited for the preparation of soft tissue implants. These materials are rigid as their glass transition temperature (Tg) is above body temperature[4].

For soft tissue engineering, the matrices and scaffolds on which seeded cells organize and develop into a desired tissue *in vitro* and/or *in vivo* would ideally be made of biodegradable polymers of which the properties resemble those of the extracellular matrix (ECM). Elastomeric porous structures, which adjust to the dynamics of the surrounding and developing tissue and provide adequate micro-stresses to the cells as well as ensure mechanical stability and structural integrity to the developing tissue, are therefore desirable.

Biodegradable elastomeric materials that have previously been investigated include copolymers of lactide (LA) and ε-caprolactone (CL)[5], poly-4-hydroxybutyrate[6] and poly(glycerol-sebacate) networks[3]. Homopolymeric 1,3-trimethylene carbonate (TMC), an elastomeric aliphatic polycarbonate, has long been known[7] and its suitability for the preparation of biomedical implants has been previously evaluated[8]. Poly(TMC) used in those studies had a very low modulus and low tensile strength. These poor mechanical properties discouraged any practical application, other than the use of TMC as a softening unit in copolymers or poly(TMC) blends with high modulus polymers[1,9,10]. Furthermore, TMC based copolymers and poly(TMC) blends were used as matrices for controlled drug release[11-13].

We recently reported[14] that very high molecular weight amorphous poly(TMC) ($\overline{M}_n$ =290,000 and $\overline{M}_w$ =552,000), is very flexible and tough with excellent ultimate mechanical properties due to strain-induced crystallization (Tm=36°C). This self-reinforcement, also observed for natural rubber, is the origin of the high tensile strength and maximal extensibility of this strain-crystallizable physical network[15]. In addition, high molecular weight poly(TMC) was found to be totally

resorbed after 3 weeks of subcutaneous implantation in rats. The degradation and resorption of the polymer induced only a mild tissue reaction[16].

In this paper, the influence of the molecular weight of poly(TMC) on its mechanical properties is addressed. The stress-strain behavior in cyclic loading and the creep behavior of high molecular weight poly(TMC) were determined to get insight in the performance of this polymer in a dynamic environment. Finally, in view of the possible use of implants based on poly(TMC) in the clinic, the possibility to sterilize the scaffolds by means of a standard sterilization method was studied. Poly(TMC) films were sterilized by gamma-radiation and analyzed for changes in physical and mechanical properties.

MATERIALS AND METHODS

Materials

Polymer grade 1,3-trimethylene carbonate (TMC) was obtained from Boehringer Ingelheim, Germany and used without further purification. Hexanol (Merck, Germany) was distilled from CaH_2 (Acros, Belgium). Stannous octoate ($SnOct_2$) (stannous 2-ethylhexanoate) was used as received from Sigma, USA. Solvents (Biosolve, The Netherlands) were of analytical grade.

Polymer Synthesis

In an argon atmosphere, TMC monomer was charged into freshly silanized (Serva, Boehringer Ingelheim Bioproducts Partnership, Germany) and dried glass ampoules and $2x10^{-4}$ mol of stannous octoate per mol of monomer was added as a solution in sodium dried pentane. The pentane was removed afterwards by evacuation. The ampoules were purged three times with dry argon and heat-sealed under vacuum. Several poly(TMC) batches were prepared (Table 1). For batches 1 and 2, $2x10^{-5}$ mol of hexanol per mol of monomer was added prior to the purging step. In this case purging was performed after cooling of the ampoules with liquid nitrogen to prevent evaporation of the hexanol (initiator). By exposing the monomer to air for different periods of time, the purity of the monomer can be decreased in a more or less controlled manner. In this way very high molecular poly(TMC) of differing molecular weights could be prepared. For batches 3 to 8, the monomer was exposed to air for a period of time up to 120 min. The ampoules were conditioned in an oil bath pre-heated at the polymerization temperature and vigorously shaken in order to

obtain a homogeneous mixture of the monomers and the catalyst. Polymerizations were carried out for a period of 2 hrs (batch 1), 3 hrs (batch 2) or 3 days at 130°C±2°C. After the selected reaction time the ampoules were quenched to room temperature and the polymers were discharged. The polymers were purified by dissolution in chloroform (2-5 wt/vol% solutions), filtration of the solutions through a sintered glass filter and precipitation into a ten-fold volume of methanol. Subsequently the polymers were collected, washed with fresh methanol and dried under reduced pressure at room temperature until constant weight.

Polymer Processing

Compression molding of purified polymers was done on a Fontijne laboratory press THB008 (The Netherlands) in 600 μm thick stainless steel molds. The films were melt-pressed at 140°C and subsequently cooled to 15°C under pressure.

Polymer Characterization

Gel permeation chromatography (GPC). Weight and number average molecular weight ($\overline{M}_w$ and $\overline{M}_n$, respectively), polydispersity index (PDI) and intrinsic viscosity ([η]) were determined by GPC using a Waters Model 510 pump (USA), a HP Ti-Series 1050 autosampler (USA), a Waters Model 410 Differential Refractometer and a Viscotek H502 Viscometer Detector (USA) with Waters Styragel HR5-HR4-HR2-HR1 columns placed in series. Chloroform was used as eluent at a flow rate of 1.5 ml/min. Narrow polystyrene standards were used for calibration. Sample concentrations of approximately 0.5 wt/vol% and injection volumes of 30 μl were used. All determinations were performed at 25°C.

Differential scanning calorimetry (DSC). The thermal properties of the purified samples were evaluated by DSC. Samples (5-15 mg) placed in aluminum pans were analyzed with a Perkin Elmer Pyris1 (USA) at a heating rate of 10°C/min. All samples were heated to 40°C above their glass transition temperature. Subsequently, the samples were quenched rapidly (300°C/min) until 40°C below their glass transition temperature and after 5 min a second scan was recorded. Unless mentioned otherwise, the data presented were collected during the second heating scan. The glass transition temperature (Tg) was taken as the midpoint of the heat capacity change and the peak melting temperature (Tm) was determined from the melting endotherm. Indium, gallium and tin were used as standards for temperature calibration.

Density. The density of poly(TMC) was determined by measuring the dimensions and the mass of melt-pressed polymer films (poly(TMC)$_6$). The density of poly(TMC) is 1.31 g/cm^3.

Mechanical Properties

All mechanical tests were performed in triplicate on compression-molded films with dimensions in accordance to ASTM standard D882-91 specifications (100x5x0.6 mm^3). The mechanical tests were carried out on a Zwick Z020 universal tensile testing machine (Germany) at room temperature (18-20°C).

Tensile testing. Tensile tests were carried out on the tensile testing machine equipped with a 500 N load cell, operated at a crosshead speed of 50 mm/min. The specimen deformation was derived from the grip-to-grip separation, the initial grip-to-grip separation being 50 mm.

Cyclic loading. Cyclic tests were carried out on the tensile testing machine equipped with a 10 N load cell, operated at a crosshead speed of 50 mm/min. The specimen deformation was derived from the grip-to-grip separation, the initial grip-to-grip separation being 50 mm. The films were deformed cyclically (20 cycles) up to 50% strain. The 21st cycle was started after a 1-hour recovery period.

Creep. For the creep experiments the tensile testing machine was equipped with a 10 N load cell. The specimen deformation was derived from the grip-to-grip separation, the starting grip-to-grip separation being 50 mm. The samples were stressed to 0.1, 0.2, 0.4 and 0.6 N/mm^2 and the strain was measured as a function of time during 1 hour.

Wide Angle X-ray Scattering

X-ray diffraction data of compression molded poly(TMC) films were collected on a Philips PW3710 based X'Pert-1 diffractometer (The Netherlands) in Bragg-Brentano geometry, using Cu Kα radiation and a θ compensating divergence slit. Data collection was performed at room temperature, using a low-background spinning specimen holder. The measured diffractograms were converted to fixed slit intensities. The peak positions were extracted using the pattern decomposition program PROFIT. The observed individual lines and clusters of lines were fitted using Pearson VII functions, taking the K$_{\alpha2}$ component into account. The obtained peak positions and relative intensities are, therefore, extracted from the analytical K$_{\alpha1}$ peak profiles. The absolute, relative and integral intensities are based on peak

heights or areas, respectively, using a θ compensating divergence slit, or, when using the back-calculated diffractograms, on a fixed slit width.

Plateau Modulus Determinations in the Melt

The cross-over modulus (Gc, where G'(ω)=G''(ω)) of a poly(TMC) melt was measured by dynamic oscillation using parallel plates on a Universal Dynamic Spectrometer (Physica UDS200, Paar Physica, USA) at 195°C. The frequency sweeps were performed at 1% strain. From this the plateau modulus (Gn^0) can be calculated, using the polydispersity index (PDI) of the polymer post testing, according to the following relationship[17]:

$$\log\left(\frac{Gn^0}{Gc}\right) = 0.38 + \frac{2.63 \times \log(PDI)}{1 + 2.45 \times \log(PDI)} \tag{1}$$

Calculation of the molecular weight between entanglements (Me) proceeds according to equation 2[18]:

$$Me = \frac{\rho RT}{Gn^0} \tag{2}$$

where ρ is the density of the polymer, T is the temperature and R is the gas constant. Samples for dynamic oscillation measurements were punched out (ϕ=26 mm) from compression molded films of purified polymer (poly(TMC)$_7$) with a thickness of 600 μm.

Gamma-Irradiation

Poly(TMC)$_5$ samples (in triplicate) were placed in poly(ethylene)/poly(amide) bags and sealed after evacuation. The samples were exposed to 15, 25 and 40 kGy gamma-irradiation from a ^{60}Co source (Gammaster, Ede, The Netherlands). In another experiment poly(TMC) films (poly(TMC)$_3$) were packed under vacuum, in N$_2$ or in air and were exposed to 25 kGy gamma-irradiation from a ^{60}Co source.

Equilibrium swelling experiments (in triplicate) were performed at room temperature using chloroform. The samples were swollen for one week to reach equilibrium and subsequently the extracted gels were dried under vacuum at room temperature for two weeks until constant weight. The gel and the sol fractions of the irradiated samples were calculated according to equation 3 and 4, respectively:

$$\text{gel fraction} = \frac{md}{mi} \tag{3}$$

$$\text{sol fraction} = 1 - \frac{m_d}{m_i} \qquad (4)$$

where m_d is the mass of the extracted and dried gels and m_i is the mass of the specimens before swelling and extraction. The degree of swelling (q) was calculated from the ratio of the weight of swollen and extracted samples (m_s) and the dried gels (m_d) and the specific densities of solvent (ρ_s) (1.4832 g/cm^3 for chloroform[19]) and poly(TMC) (ρ) using:

$$q = 1 + \rho \times \left(\frac{m_s}{m_d \times \rho_s} - \frac{1}{\rho_s} \right) \qquad (5)$$

RESULTS AND DISCUSSION

Polymer Synthesis and Characterization

Until now in studies dealing with the determination of the mechanical properties of poly(TMC), polymer with a relatively low molecular weight was used ($\overline{M}_n$ <55,000 or [η]<1.7 dl/g in CHCl$_3$ at 25°C)[1,8,20]. Previously, we have seen that strain-induced crystallization occurred upon stretching of poly(TMC) samples of high molecular weight ($\overline{M}_n$=290,000 and $\overline{M}_w$=552,000)[14]. In order to evaluate the effect of the molecular weight on the mechanical properties of poly(TMC) a number of polymers covering a broad range of molecular weights was synthesized by ring-opening polymerization in the melt, using stannous octoate as a catalyst/initiator. An overview of the properties of purified TMC polymers is given in Table 1.

Table 1. Characteristics of the TMC homopolymers after purification.

Sample	$\overline{M}_n$ x10^{-5}	$\overline{M}_w$ x10^{-5}	PDI	[η]^a (dl/g)	Tg (°C)
Poly(TMC)$_1$	0.57	0.92	1.62	1.19	-19
Poly(TMC)$_2$	1.09	1.85	1.70	1.79	-18
Poly(TMC)$_3$	2.72	5.38	1.98	4.51	-19
Poly(TMC)$_4$	3.06	5.30	1.73	4.29	-17
Poly(TMC)$_5$	3.27	4.82	1.47	4.20	-19
Poly(TMC)$_6$	3.33	5.83	1.75	4.52	-17
Poly(TMC)$_7$	3.37	5.59	1.67	4.49	-17
Poly(TMC)$_8$	3.55	6.17	1.74	4.85	-18

^{a} In CHCl$_3$, 25°C.

In polymerizations with $SnOct_2$ the initiating species are formed in situ as the result of the reaction of 'hydroxyl' containing impurities present in the polymerization atmosphere, the monomer, or the $SnOct_2$ catalyst[21]. Poly(TMC) specimens with different molecular weights were obtained by the addition of hexanol to the reaction mixture as a co-initiator (specimens 1 and 2) or by exposing the monomer to air for different time periods prior to polymerization (specimens 3 to 8).

Mark-Houwink coefficients for poly(TMC) in chloroform were determined by plotting $\log[\eta]$ against $\log \overline{M}w$ derived from the GPC measurements. Linear fitting of the data (r=0.994) gave values of $K=2.43 \times 10^{-4}$ and a=0.74, in good agreement with previously reported results[20] for lower molecular weight polymers.

All polymers were amorphous and in the rubbery state at room temperature.

Effect of poly(TMC) Molecular Weight on Stress-Strain Behavior

Transparent films could readily be obtained by compression molding. Films prepared from poly(TMC)$_1$ and poly(TMC)$_2$ were not dimensionally stable and had the tendency to stick together when pressed against each other. Films prepared from the other batches maintained their initial dimensions even when incubated under physiological conditions (in phosphate buffered saline, at 37°C) for long periods of time[22] or when implanted *in vivo*[16], as shown in previous studies.

The mechanical properties of the prepared TMC polymers are listed in Table 2. The $\overline{M}n$ and $[\eta]$ of the polymers after compression molding are also given. Independent of the initial molecular weight, thermal processing of the purified polymers did not result in extensive chain scission.

Table 2. Molecular weights and stress-strain behavior of compression molded poly(TMC) films.

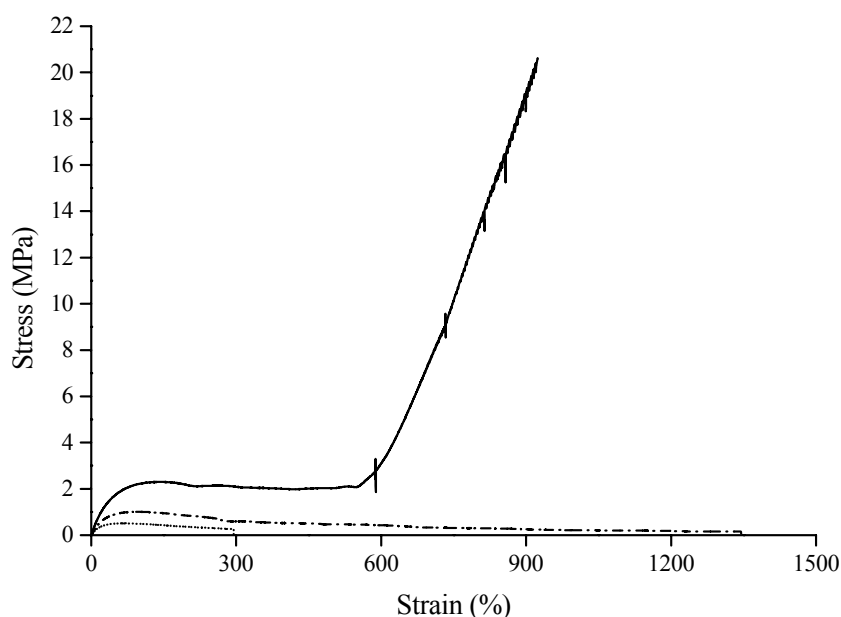| TMC content (mol%)	$\overline{M}n \times 10^{-5}$	$[\eta]$ (dl/g)	Young's Modulus (MPa)	σ_{yield} (MPa)	ε_{yield} (%)	σ_{break} (MPa)	ε_{break} (%)	σ_{max} (MPa)
Poly(TMC)$_1$	0.53	1.16	3.0	0.5	63	0.2	230	0.5
Poly(TMC)$_2$	0.94	1.81	4.7	1.1	98	0.2	1250	1.1
Poly(TMC)$_4$	2.23	4.21	6.6	2.1	120	15	890	16
Poly(TMC)$_6$	2.73	4.59	6.2	2.3	140	16	850	16
Poly(TMC)$_7$	3.37	4.34	6.3	2.3	130	12[a]	830[a]	12[a]
Poly(TMC)$_8$	2.21	4.83	6.8	2.3	150	17	830	17

[a] Specimen slipped from grips.

Figure 1. Stress-strain curves of TMC homopolymers with different molecular weights. (····) Poly(TMC)$_1$, $\overline{M}_n$ =53,000; (·-·-) Poly(TMC)$_2$, $\overline{M}_n$ =94,000 and (—) Poly(TMC)$_6$, $\overline{M}_n$ =273,000.

Typical stress-strain curves are presented in Figure 1. The polymer with the lowest molecular weight ($\overline{M}_n$ =53,000) has the lowest modulus, but also the lowest tensile strength. Poly(TMC)$_2$ has a higher Young's modulus and a very high ultimate tensile strain, but is also very weak, having a tensile strength of approximately 1 MPa and deforming irreversibly at very low stresses. Polymers with a $\overline{M}_n$ above 200,000 have a higher modulus and a higher strain at yield. The Young's modulus, the yield stress and the maximum tensile strength do not change with molecular weight above $\overline{M}_n$ values higher than 200,000 (Figure 2.A, 2.B and 2.C, respectively). An upturn in the stress-strain curve at high elongations was only observed for the very high molecular weight ($\overline{M}_n$ >200,000) polymers. Upon fracture and release of the applied force in the tensile testing experiments, the specimens did not recoil.

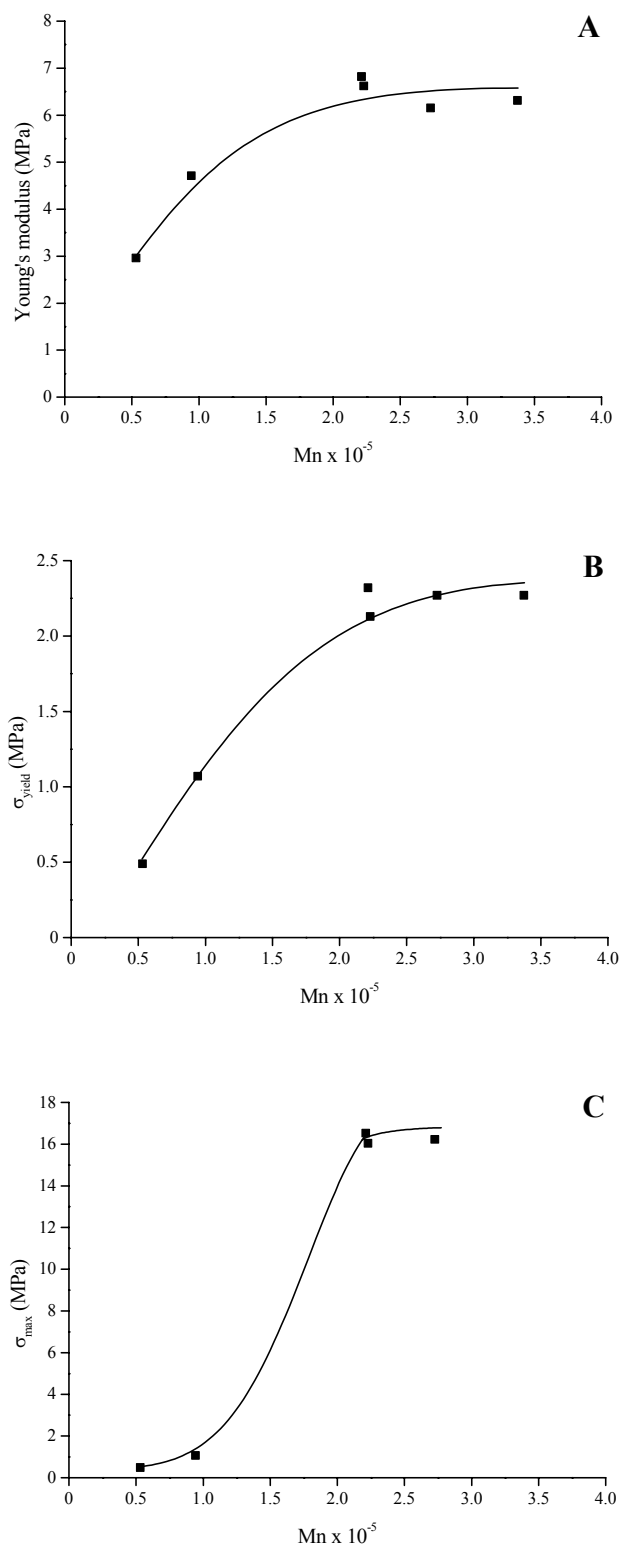**Figure 2.** Young's modulus, stress at yield (σ_{yield}) and maximum tensile strength (σ_{max}) as a function of the number average molecular weight ($\overline{M}n$) of poly(TMC).

The thermal behavior of sections of the drawn specimens was analyzed by DSC. With the exception of poly(TMC)$_1$ samples, which had the lowest $\overline{M}n$, the initially amorphous poly(TMC) specimens now showed a melting endotherm with a peak melting temperature (Tm) that ranged between 30 and 50°C. The DSC scans for one of these samples, before and after tensile testing, are shown in an earlier publication[14]. These findings confirm that the increase in the stress at break found for these polymers results from strain-induced crystallization. In Figure 3 the tensile strength for each polymer is plotted as a function of the heat of fusion of the strained specimens. A higher crystallinity of the polymer resulted in a higher tensile strength.
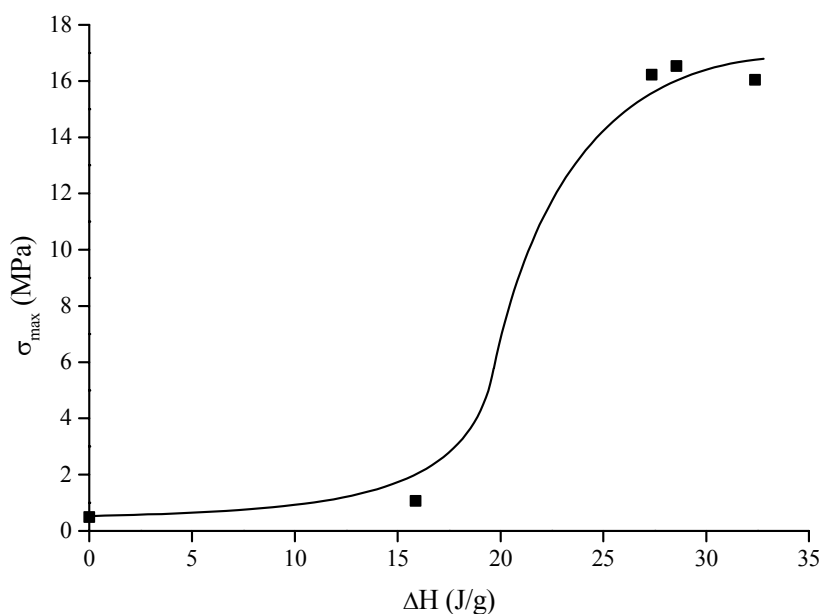

Figure 3. Maximum tensile strength (σ_{max}) of the TMC homopolymers as a function of the heat of fusion (ΔH) of the specimens after tensile testing.

Wide angle x-ray scattering (WAXS) measurements performed on a completely amorphous poly(TMC) film and on the same specimen after crystallization upon stretching, confirmed the results of the thermal analyses. In the amorphous state two broad peaks were detected with maxima at $2\theta = 21.2$ and $41.8°$. After straining to 850%, the level of order of the polymer chains increased, as can be seen from the WAXS pattern shown in Figure 4. The x-ray scan of the sample after tensile testing shows distinct and narrower peaks at 2θ values of 20.2, 21.4, 25.8 and 31.2°.
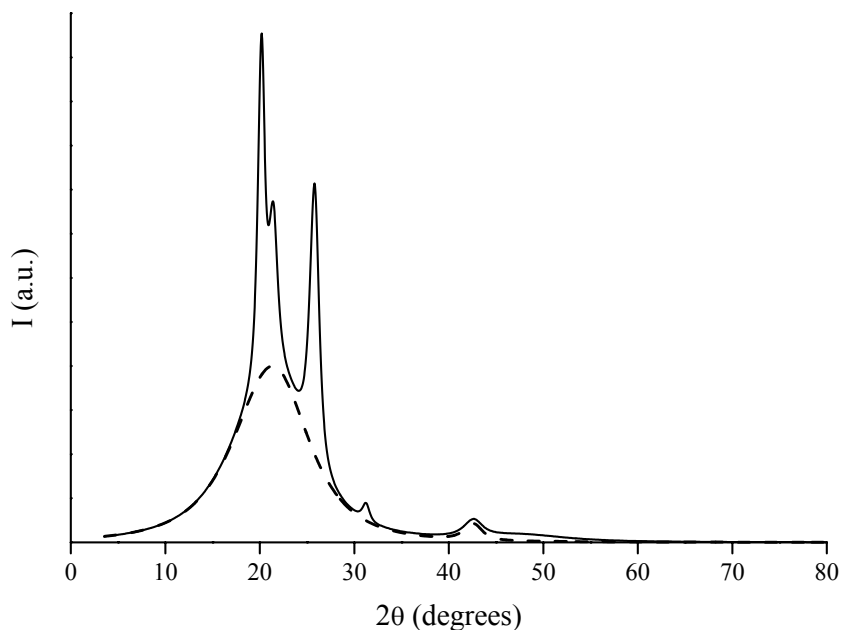
Figure 4. WAXS pattern of a poly(TMC)$_6$ film after tensile testing (solid line). The area under the dotted line corresponds to the scattering intensity of the amorphous fraction (I_a).

The crystallinity (x_c) of the drawn sample was determined by comparison of the area under the peaks corresponding to the scattering intensities of the amorphous (I_a) and crystalline (I_c) fractions, according to the expression[23]:

$$x_c = \frac{I_c}{I_c + I_a} \qquad (6)$$

The contribution of the crystalline fraction to the scattering was determined after deconvolution of the peak signals. For this the WAXS pattern of the amorphous sample was taken into consideration (Figure 4). A degree of crystallinity of 31% was calculated as described above, corresponding to a ΔH of 27 J/g as determined by DSC. Assuming proportionality of the degree of crystallinity and the experimental ΔH, the heat of fusion of 100% poly(TMC) ($\Delta H°$) can then be estimated to be 87 J/g. It should be noticed that this value is only a rough estimation[23] and should be validated by other methods to determine crystallinity such as based on the densities of the crystalline and amorphous polymer[24]. The crystal structure of (oriented) poly(TMC) then needs to be determined from WAXS measurements. This is beyond the scope of this study.

From the dependency of the mechanical properties on molecular weight it can be concluded that for poly(TMC) an $\overline{M}n$ of 100,000 is a characteristic minimum

molecular weight [25] below which the tensile strength is still typical for a low molecular weight material. Above this value the tensile strength increases significantly with increasing molecular weight. For $\overline{M}_n$ values above 200,000 the change in tensile strength as well as in the other measured mechanical properties levels off. Low molecular weight poly(TMC) possesses a high number of chain ends per unit volume which reduce the packing efficiency of the polymer chains preventing crystallization. With an increase in molecular weight, a higher percentage of the structure can be permanently oriented by stretching, resulting in a higher tensile strength[26].
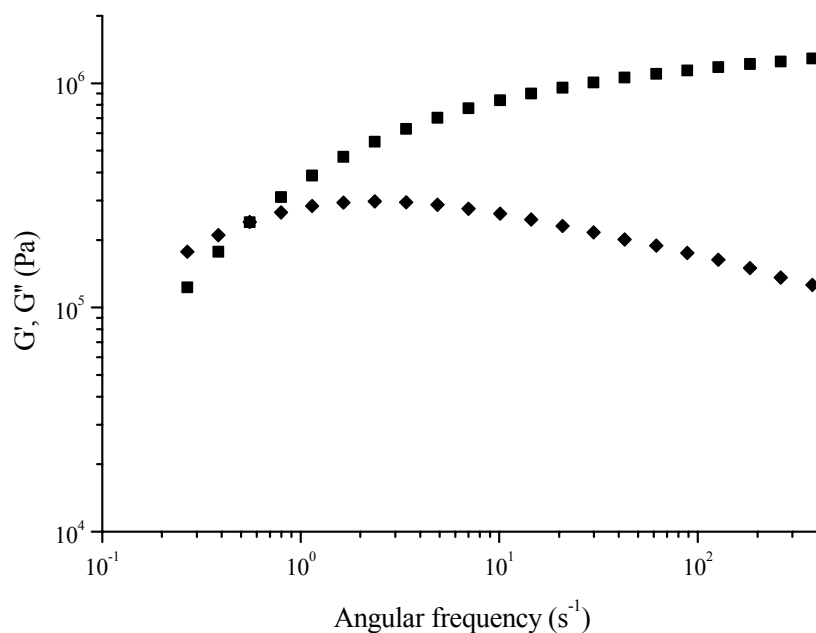

Figure 5. Linear viscoelastic G' (■) and G'' (♦) master curves at 195°C for poly(TMC) (poly(TMC)$_7$ films).

The tensile strength of amorphous polymers is influenced by the density of chain entanglements. Amorphous polymers above the glass transition temperature only have any appreciable strength when their molecular weight is at least 2-4 times higher than the molecular weight between entanglements (Me)[25,27,28]. In the polymer melt, the value of Me is determined by the intrinsic stiffness of the polymer chain. Estimations of the Me in the melt can be obtained from determination of the cross-over modulus of the polymer melt in dynamic oscillation. The cross-over modulus (where G'=G'', see Figure 5) was determined to be 2.4×10^5 Pa.

Considering that the PDI of the poly(TMC) sample after the test was 2.40 ($\overline{M}_n$=2.1x10^5 and [η]=3.8), the plateau modulus (G_n^0) was estimated to be approximately 1.9x10^6 Pa. Using the measured density of 1.31 g/cm^3, for poly(TMC) at 195°C the value for the molecular weight between entanglements (Me) was calculated to be 2700. This shows that in the melt the entanglement density of poly(TMC) is high. Surprisingly, a molecular weight that is at least 40 times higher than this Me is required for the polymer to show appreciable mechanical properties.

Stress-strain Behavior in Cyclic Loading and Creep Behavior of Poly(TMC)

To be of practical use in the preparation of medical implants or scaffolds for tissue engineering that will be used in the body, poly(TMC) must sustain and recover from repeatedly applied stresses and strains.

In order to evaluate the behavior of high molecular weight poly(TMC) under cyclic loading, polymer films were deformed cyclically up to 50% strain. After 20 cycles a 2-hour recovery period was allowed and subsequently a last cycle was recorded. In Figure 6 the typical stress-strain curves recorded for the different loading cycles are presented.

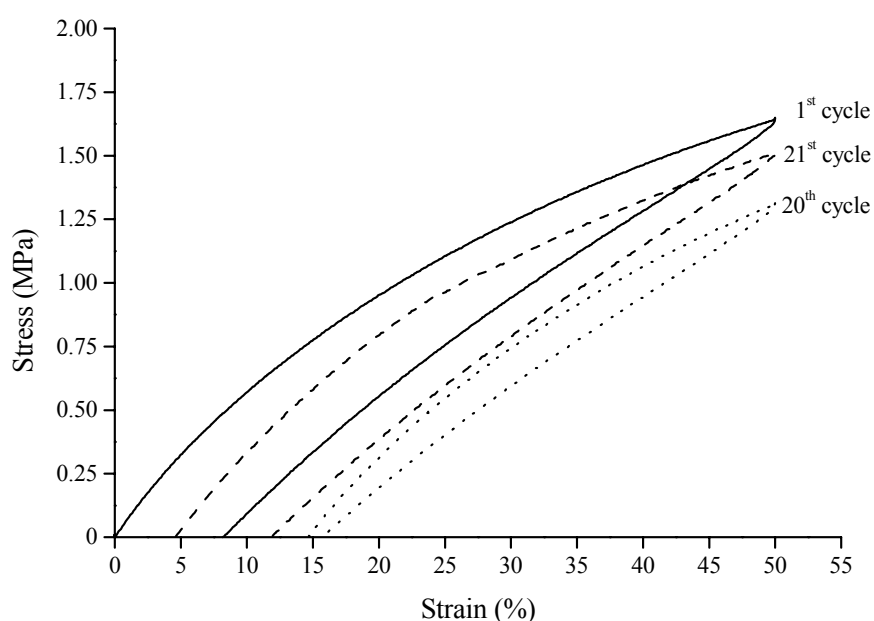

Figure 6. Cyclic tensile test for high molecular weight poly(TMC)$_5$ films.

At the beginning of the 21st cycle the permanent set was determined. This permanent deformation is an important parameter as it can be directly related to the

hysteresis phenomenon[29]. For high molecular weight poly(TMC) a permanent set of 4.6% was found after 2 hrs. For an ideal elastomer, plastic deformation is absent and the permanent set is zero.

The creep behavior of a polymer is another phenomenon resulting from viscous flow. Creep can be defined as a progressive increase in strain over an extended period of time in a polymer subjected to a constant stress.

Creep curves were obtained by applying a constant stress to poly(TMC) films during one hour and monitoring the strain as a function of time. The applied stresses corresponded to 5 to 30% of the yield stress measured by conventional tensile testing. A typical creep curve obtained in this way consisted of an initial elastic response where the elongation of the tensile stress is inversely proportional to the modulus of the material. This was followed by a stage of primary creep, where the creep rate decreases in time and a secondary creep stage, characterized by a constant creep rate. The creep behavior of poly(TMC) films was expressed in terms of the constant creep rate (ASTM standard D2990). The results obtained are summarized in Table 3.

Table 3. Creep behavior of high molecular weight poly(TMC)[a].

Applied stress (MPa)	Creep rate (s^{-1})
0.1 (5%)[a]	1.9 x 10^{-5}
0.2 (10%)	2.4 x 10^{-5}
0.4 (20%)	3.8 x 10^{-5}
0.6 (30%)	12.5 x 10^{-5}

[a] Poly(TMC)$_3$ films.

[b] The values in brackets represent the percentages of the yield stress in tensile tests.

As can be expected the constant creep rate increased with the increase of the applied stress. At 30% of the yield stress the constant deformation rate is substantially higher than at lower stresses. Although poly(TMC) scaffolds to be used in soft tissue engineering will not be subjected to severe load bearing conditions, they will be subjected to some stresses for long periods of time, therefore the creep behavior of the polymer should be taken into account.

Gamma-Irradiation

The possibility of sterilization of a polymer is a sine qua non for its application in the preparation of implantable medical devices. We investigated the possibility of

using ^{60}Co gamma-radiation sterilization, as it is has the advantages of high efficiency, negligible thermal effects and does not involve the use of toxic substances[30]. In order to evaluate the effect of gamma-radiation on the mechanical properties of poly(TMC), high molecular weight polymer films (packed under vacuum) were exposed to different radiation doses, including 25 kGy, the standard radiation dose for the sterilization of medical devices[30].

Unexpectedly[31], after irradiation at average radiation doses of 15, 25 or 40 kGy, the specimens were not soluble anymore in chloroform. Instead a gel was obtained indicating that poly(TMC) had cross-linked upon radiation. Table 4 presents the degree of swelling of the formed gels as well as the gel fraction of irradiated samples.

Table 4. Degree of swelling and gel fraction of poly(TMC) films treated with different gamma-radiation doses.

Radiation dose (kGy)	Degree of swelling, q (%)	Gel fraction (wt%)
15	355	15
25	140	33
40	61	51

Consistent with a decrease in the degree of swelling, the gel fraction of the samples increased with radiation dose, indicating an increase in cross-linking density with radiation dose.

Cross-linking and/or chain scission are known to occur in polymers when these are exposed to high-energy radiation. For most polymers either cross-linking or chain scission prevails[32-34]. In order to investigate the behavior of poly(TMC) the obtained results were analyzed in terms of the Charlesby-Pinner equation[35], which relates the sol fraction (s) of the irradiated samples to the radiation dose (r, expressed in Mrad):

$$s + \sqrt{s} = \frac{G(s)}{2G(x)} + \frac{1}{2.08 \times 10^{-6} \times G(x) \times \overline{M}n \times r} \qquad (7)$$

where, G(s) is the number of main-chain scissions and G(x) the number of cross-links, both produced per 100 eV absorbed energy and $\overline{M}n$ the number average molecular weight of the polymer before treatment. It is assumed that chain-scission and cross-linking occur at random and in proportion to the radiation dose. Equation 7 holds for polymers with random, monomodal molecular weight distributions whether or not main-chain fracture occurs simultaneously with cross-linking. A plot

of $s + \sqrt{s}$ as a function of the reciprocal of the radiation dose is presented in Figure 7.
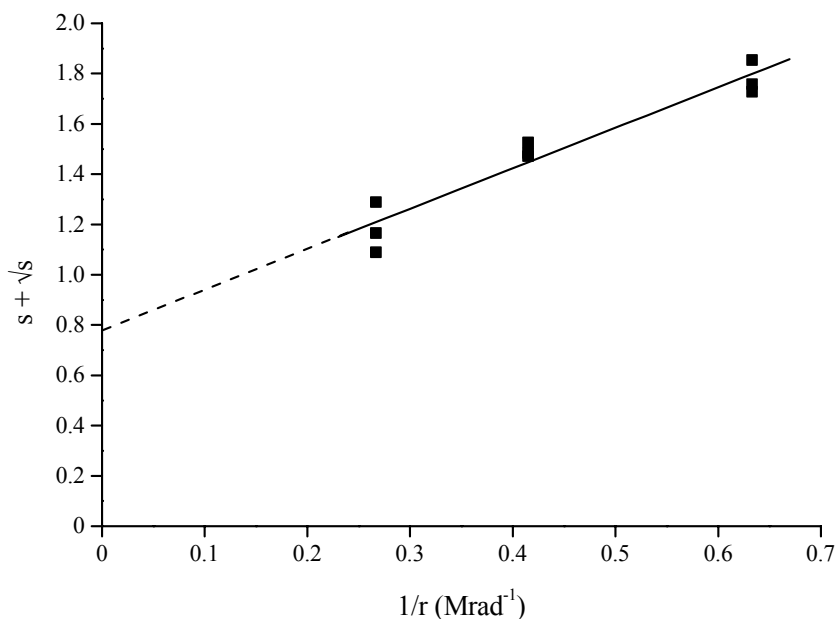

Figure 7. Charlesby-Pinner plot for poly(TMC)$_5$ samples irradiated under vacuum. (1 kGy = 0.1 Mrad)

The network formation for the gamma-irradiated poly(TMC) could be adequately described using the Charlesby-Pinner model. The intercept for the best straight line was 0.78. This value corresponds to the ratio of chain scission to cross-linking per radiation dose. Gel formation can only occur if this ratio is lower than 2[35]. In the absence of air, cross-linking is the main reaction that occurs upon gamma-irradiation of poly(TMC).

Considering the determined ratio of chain scission density to cross-linking density per radiation dose, the maximum obtainable gel fraction $(1-s)_{max}$ can be determined as follows[36]:

$$(1\text{-}s)max = \frac{1}{2} \times \left[1 - \frac{G(s)}{G(x)} + \left(1 + \frac{2G(s)}{G(x)} \right)^{1/2} \right] \quad (8)$$

According to this expression, the maximum attainable gel fraction is 73% for poly(TMC) irradiated in the absence of air.

As previously observed for other polymer systems, the extent of cross-linking of poly(TMC) upon gamma-irradiation is affected by the presence of air[35] (Table 5). Poly(TMC) films were packed in nitrogen, in air and under vacuum and were

irradiated with a 25 kGy standard radiation dose. The gel fraction was significantly lower for air-packed films than for poly(TMC) films packed and sterilized in nitrogen or vacuum. This indicates a lower extent of cross-linking, possibly due to an increase of oxidative chain scission.

Table 5. Degree of swelling and gel fraction of poly(TMC) treated with a 25 kGy radiation dose under vacuum or in the presence of nitrogen or air.

Packed under	Degree of swelling, q (%)	Gel fraction (wt%)
vacuum	84	54
N_2	83	48
Air	107	29

Mechanical Properties of Irradiated Poly(TMC)

It is known that mechanical behavior of polymers can be improved by cross-linking[34,37]. However, as mentioned above, the cross-linking of poly(TMC) upon gamma-irradiation is accompanied by main chain-scissioning, which can lead to a reduction of elasticity modulus, tensile strength and creep resistance.

The tensile properties of high molecular weight poly(TMC) films irradiated in the absence of air with an average dose of 25 kGy are presented in Table 6.

Table 6. Stress-strain behavior of poly(TMC)$_4$ compression molded films before and after gamma irradiation[a] (25 kGy) under vacuum.

Films	Young's Modulus (MPa)	σ_{yield} (MPa)	ε_{yield} (%)	σ_{break} (MPa)	ε_{break} (%)	σ_{max} (MPa)
Untreated	6.6	2.1	120	15	890	16
Gamma-irradiated	5.0	1.5	150	9	1200	9

[a] Non-extracted films.

At the standard sterilization dose of 25 kGy a slight decrease in the Young's modulus and stress at yield was found, compared to the results found for untreated samples (Table 6). In contrast, the strain at break had increased. This can be attributed to a plasticizing effect of lower molecular weight chains formed upon irradiation due to chain scission. Strain-induced crystallization was still observed, but the upturn in the stress-strain curves was found at higher strain values than for the non-irradiated samples (850% versus 500%). After the tensile test, the initially amorphous, irradiated poly(TMC) specimens (Tg=-18°C) now showed a melting

endotherm with a melting temperature (Tm) of 33°C (ΔH=12 J/g), confirming strain-induced crystallization of the polymer network. The lower heat of fusion reflects the lower degree of crystallinity attained by the cross-linked films upon straining which in turn accounts for the lower tensile strength of the samples.

Although the tensile properties of these samples had decreases slightly upon gamma-irradiation, a great improvement was noticed in terms of the hysteresis effect. Tested under similar conditions as the non-treated samples, the irradiated compression-molded films showed better recovery 2 hrs after 20 consecutive deformation cycles (Figure 8) as well as a much higher creep resistance (Table 7).
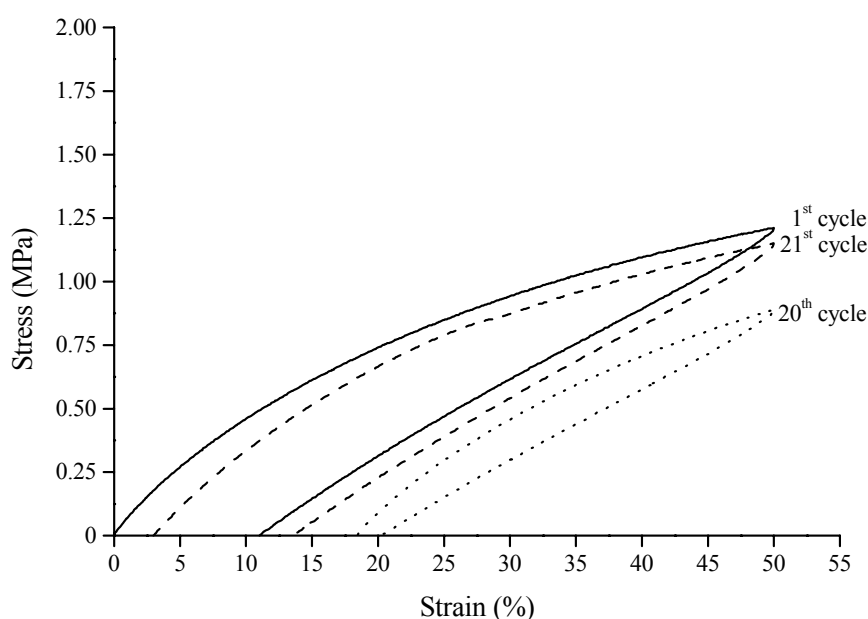

Figure 8. Cyclic tensile test for high molecular weight poly(TMC)$_5$ films after gamma-irradiation treatment (25 kGy). Non-extracted films.

Poly(TMC) films irradiated in vacuum showed a permanent set of 3% after cyclic testing and subsequent recovery. The creep rates of these films decreased approximately two-fold in comparison with the non-irradiated films. The cross-links hinder the movement of polymer chains and reduce the viscous flow. The polymer becomes more elastic. As can be expected, the positive contribution of the covalent cross-links to the resistance of the polymer to creep increases with the extent of cross-linking. Samples irradiated in the presence of air showed higher creep rates than samples irradiated in the absence of air at the same stress applied (Table 7).

Table 7. Creep behavior of high molecular weight poly(TMC)[a] after gamma-irradiation treatment (25 kGy) in the presence or absence of air. Non-extracted films.

Applied stress (MPa)	Creep rate (s^{-1}) (vacuum)	Creep rate (s^{-1}) (air)
0.1 (5%)[b]	0.4×10^{-5}	0.9×10^{-5}
0.2 (10%)	1.2×10^{-5}	1.9×10^{-5}
0.4 (20%)	2.7×10^{-5}	8.8×10^{-5}
0.6 (30%)	6.5×10^{-5}	not determined

[a] Poly(TMC)$_3$ films.

[b] The values in brackets represent the percentages of the yield stress in tensile tests performed on non-treated samples

Presently, we are investigating the possibility of further improving the dimensional recovery of poly(TMC) upon mechanical deformation by irradiating the polymer with higher gamma-radiation doses and the effect of cross-linking upon gamma-irradiation on the *in vivo* degradation behavior of the polymer.

CONCLUSIONS

Very high molecular weight poly(TMC) (with $\overline{M}_n$ above 200,000) shows rubber-like properties despite being totally amorphous and not cross-linked. In comparison to poly(TMC) of lower molecular weight it shows improved handling characteristics (lower tackiness), better dimensional stability and much improved mechanical behavior. Very high molecular weight poly(TMC) is flexible and tough. The high tensile strength of the polymer results from reinforcement of the structure upon strain-induced crystallization. These very high molecular weight rubbers show good recovery after mechanical deformation, considering that the only resistance to viscous flow comes from chain entanglement. A critical molecular weight ($\overline{M}_n$) below which the mechanical performance of the polymer is poor was determined to be 100,000. This is 40 times higher than the molecular weight between entanglements.

Gamma-irradiation of poly(TMC) results in simultaneous cross-linking and chain-scission. The ratio of scission density to cross-linking density per unit radiation dose was found to be 0.78. Upon irradiation of the polymer an insoluble network is formed, with increasing cross-linking density as the radiation dose is increased. The

mechanical properties of very high molecular weight poly(TMC) rubbers improve upon irradiation. The irradiated polymer has significantly higher resistance to creep.

ACKNOWLEDGMENTS

REFERENCES

[1]   Buchholz B. Analysis and characterization of resorbable DL-lactide-trimethylene carbonate copolyesters. *J Mater Sci: Mater Med* 1993; 4: 381-388.

[2]   Stock UA, Vacanti JP. Tissue engineering: current state and prospects. *Annu Rev Med* 2001; 52: 443-451.

[3]   Wang Y, Ameer GA, Sheppard BJ, Langer R. A tough biodegradable elastomer. *Nat Biotechnol* 2002; 20: 602-606.

[4]   Sodergard A, Stolt M. Properties of lactic acid based polymers and their correlation with composition. *Prog Polym Sci* 2002; 27: 1123-1163.

[5]   Grijpma DW, Zondervan GJ, Pennings AJ. High molecular weight copolymers of L-lactide and ε-caprolactone as biodegradable elastomeric implant materials. *Polym Bull* 1991; 25: 327-333.

[6]   Williams SF, Martin DP, Horowitz DM, Peoples OP. PHA applications: addressing the price performance issue. I. Tissue engineering. *Int J Biol Macromol* 1999; 25: 111-121.

[7]   Carothers WH, van Natta FJ. Studies on polymerization and ring formation. III. Glycol esters of carbonic acid. *J Am Chem Soc* 1930; 52: 314-326.

[8]   Engelberg I, Kohn J. Physico-mechanical properties of degradable polymers used in medical applications: a comparative study. *Biomaterials* 1991; 12: 292-304.

[9]   Katz AR, Mukherjee DP, Kaganov AL, Gordon S. A new synthetic monofilament absorbable suture made from polytrimethylene carbonate. *Surg Gynecol Obstet* 1985; 161: 213-222.

[10]   Grijpma DW, van Hofslot RDA, Super H, Nijenhuis AJ, Pennings AJ. Rubber toughening of poly(lactide) by blending and block copolymerization. *Polym Eng Sci* 1994; 34: 1674-1684.

[11] Jie C, Zhu KJ, Shilin Y. Preparation, characterization and biodegradable characteristics of poly(1,3-trimethylene carbonate-co-glycolide). *Polym Int* 1996; 41: 369-375.

[12] Jie C, Zhu KJ. Preparation, characterization and biodegradable characteristics of poly(D,L-lactide-co-1,3-trimethylene carbonate). *Polym Int* 1997; 42: 373-379.

[13] Edlund U, Albertsson AC. Copolymerization and polymer blending of trimethylene carbonate and adipic anhydride for tailored drug delivery. *J Appl Polym Sci* 1999; 72: 227-239.

[14] Pêgo AP, Poot AA, Grijpma DW, Feijen J. Copolymers of trimethylene carbonate and ε-caprolactone for porous nerve guides: synthesis and properties. *J Biomater Sci Polym Ed* 2001; 12: 35-53. Chapter 3 of this thesis.

[15] Queslel JP, Mark HF, "Elasticity" In: Kroschwitz JI. *Encyclopedia of polymer science and engineering*, New York: John Wiley & Sons; 1986. p 365-408.

[16] Pêgo AP, van Luyn MJA, Brouwer LA, van Wachem PB, Poot AA, Grijpma DW, Feijen J. *In vivo* behavior of poly(1,3-trimethylene carbonate) and copolymers of 1,3-trimethylene carbonate with D,L-lactide or ε-caprolactone. Degradation and tissue response. *(submitted to J Biomed Mater Res, 2002)* Chapter 7 of this thesis.

[17] Wu S. Chain structure and entanglement. *J Polym Sci Polym Phys* 1989; 27: 723-741.

[18] Ferry JD, *Viscoelastic properties of polymers*. New York: Wiley; 1970.

[19] *CRC Handbook of Chemistry and Physics*. Lide DR Ed-in-Chief, Boca Raton, FL: CRC Press; 2002.

[20] Zhu KJ, Hendren RW, Jensen K, Pitt CG. Synthesis, properties, and biodegradation of poly(1,3-trimethylene carbonate). *Macromolecules* 1991; 24: 1736-1740.

[21] Kowalski A, Duda A, Penczek S. Kinetics and mechanism of cyclic esters polymerization initiated with tin(II) octoate. 1. Polymerization of ε-caprolactone. *Macromol Rapid Commun* 1998; 19: 567-572.

[22] Pêgo AP, Poot AA, Grijpma DW, Feijen J. *In vitro* degradation of trimethylene carbonate based (co)polymers. *Macromol Chem Phys (accepted for publication)* Chapter 6 of this thesis.

[23] Kavesh S, Schultz JM. Meaning and measurement of crystallinity in polymers: a review. *Polym Eng Sci* 1969; 9: 452-460.

[24] Crescenzi V, Manzini G, Calzolari G, Borri C. Thermodynamics of fusion of poly-β-propiolactone and poly-ε-caprolactone. Comparative analysis of the melting of aliphatic polylactone and polyester chains. *Eur Polym J* 1972; 8: 449-463.

[25] Gent AN, Thomas AG. Effect of molecular weight on the tensile strength of glassy plastics. *J Polym Sci A2* 1972; 10: 571-573.

[26] Flory PJ. Tensile strength in relation to molecular weight of high polymers. *J Am Chem Soc* 1945; 67: 2048-2050.

[27] Turner DT. Tensile strength elevation of brittle polymers by entanglements. *Polymer* 1982; 23: 626-629.

[28] Grijpma DW, Penning JP, Pennings AJ. Chain entanglement, mechanical properties and drawability of poly(lactide). *Colloid Polym Sci* 1994; 272: 1068-1081.

[29] Morbitzer L, Hespe H. Correlation between chemical structure, stress-induced crystallization and deformation behaviour of polyurethane elastomers. *J Appl Polym Sci* 1972; 16: 2697-2708.

[30] Kowalski JB, Morrissey RF, "Sterilization of implants" In: Ratner BD, Hoffman AS, Schoen FJ, Lemons JE. *Biomaterials science. An introduction to materials in medicine*, San Diego, CA: Academic Press; 1996. p 415-420.

[31] Edlund U, Albertsson AC, Singh SK, Fogelberg I, Lundgren BO. Sterilization, storage stability and *in vivo* biocompatibility of poly(trimethylene carbonate)/poly(adipic anhydride) blends. *Biomaterials* 2000; 21: 945-955.

[32] Gilding DK, Reed AM. Biodegradable polymers for use in surgery-polyglycolic/poly(lactic acid) homo- and copolymers:1. *Polymer* 1979; 20: 1459-1464.

[33] Birkinshaw C, Buggy M, Henn GG, Jones E. Irradiation of poly-D,L-lactide. *Polym Degrad Stabil* 1992; 38: 249-253.

[34] Darwis D, Mitomo H, Enjoji T, Yoshii F, Makuuchi K. Heat resistance of radiation crosslinked poly(ε-caprolactone). *J Appl Polym Sci* 1998; 68: 581-588.

[35] Charlesby A, Pinner SH. Analysis of the solubility behaviour of irradiated polyethylene and other polymers. *Proc Roy Soc London* 1959; A249: 367-386.

[36] Inokuti M. Gel formation in polymers resulting from simultaneous crosslinking and scission. *J Chem Phys* 1963; 38: 2999-3005.

[37] Penning JP, Pras HE, Pennings AJ. Influence of chemical cross-linking on the creep-behavior of ultra-high-molecular-weight polyethylene fibers. *Colloid Polym Sci* 1994; 272: 664-676.

PART III

APPLICATIONS: NERVE GRAFTING AND HEART TISSUE ENGINEERING

"For material scientists, the cell is evidently a biomaterial – rich with polymer, surface forces, solvent-solute interactions, liquid-crystalline structures, etc. Yet, the language of the materials scientist is a as foreign to the biological world as French is to Chinese."

Pollack, G.H. The cell as a biomaterial. *J. Mater. Sci. – Mater.* Med. 2002 13:811-821

CHAPTER 9

Adhesion and growth of human Schwann cells on trimethylene carbonate (co)polymers*

A.P. PÊGO[1], C.L.A.M. VLEGGEERT-LANKAMP[2], M. DEENEN[2], E.A.J.F. LAKKE[2], D.W. GRIJPMA[1], A.A. POOT[1], E. MARANI[1,2] and J. FEIJEN[1]

[1] *Institute for Biomedical Technology (BMTI) and Department of Polymer Chemistry and Biomaterials, Faculty of Chemical Technology, University of Twente, P.O. Box 217, 7500 AE Enschede, The Netherlands*
[2] *Neuroregulation Group, Department of Neurosurgery, Leiden University Medical Center (LUMC), P.O. Box 9604, 2300 RC Leiden, The Netherlands*

ABSTRACT

Seeding of artificial nerve grafts with Schwann cells is a promising strategy for bridging large nerve defects. The aim of the present study was to evaluate the adhesion and growth of human Schwann cells (HSCs) on 1,3-trimethylene carbonate (TMC) and ε-caprolactone (CL) copolymers, with the final goal of using these materials in the development of an artificial nerve graft. The adhesion, proliferation and morphology of HSCs on copolymers containing 10 and 82 mol% of TMC and on the parent homopolymers were investigated. HSCs adhered faster and in greater numbers on the copolymer with 82 mol% of TMC and on the TMC homopolymer compared to the other (co)polymers. On all polymer films cell adhesion was lower than on gelatin (positive control). Despite differences in cell adhesion, cells displayed exponential growth on all tested surfaces, with similar growth rates. Cell numbers doubled approximately every three days on all substrates. When the polymer films were coated with fibronectin, no significant differences in cell adhesion and proliferation were observed between coated polymer surfaces and gelatin. The results indicate that all tested materials support the adhesion and proliferation of HSCs and can in principle be used for the preparation of flexible and slowly degrading nerve guides.

INTRODUCTION

Autologous nerve grafts are regarded as the "gold standard" for the repair of large peripheral nerve lesions. Nerve grafts can be placed between nerve fascicles, or more generally, between two severed nerve ends, providing a direct, unbroken path between nerve ends and preventing the ingrowth of scar tissue that might hinder nerve regeneration. However, the current technology is limited by donor tissue availability, secondary deformities and possible mismatch in tissue organization and dimensions. An off-the-shelf artificial graft adaptable to the neurosurgeon's needs would be a welcome alternative in the treatment of nerve defects. The nerve conduit should preferably degrade after axonal regeneration to avoid an eventual late foreign body response and chronic nerve compression that can jeopardize nerve recovery[1].

The use of degradable artificial nerve guides has been extensively investigated *in vivo*[2-7]. But despite the many advances and contributions in the field of nerve tissue engineering the results obtained with degradable nerve guides in the correction of large nerve defects have never reached the levels of nerve function recovery obtained with autologous nerve grafts[8,9]. Considering the graft material, the use of polymers with too high degradation rates, unsuitable mechanical properties, and impermeability of the device to body fluids have been listed as possible causes for graft failure[10]. Furthermore, a limited knowledge of the biochemical components and pathways involved in the nerve regeneration process might have prevented the successful selection of key elements for the regeneration process to be incorporated into the nerve guide.

In the past few years much effort has been put into the identification of the factors involved in axonal regeneration. Outgrowth over clinically relevant distances and functional recovery seems to require additional stimulation by, for instance, contact with Schwann cells (SCs) and/or extracellular matrix (ECM) components. The incorporation of SCs into a nerve guide, with a few exceptions[11], already proved to have a positive effect on the overall regeneration process, increasing peripheral nerve growth, myelination and functional recovery[12-17]. These cells play a vital role in the natural nerve regeneration process, producing ECM proteins and a range of neurotropic and neurotrophic factors essential for neuron growth[18-21].

Recently, we have published on the potential use of 1,3-trimethylene carbonate (TMC) and ε-caprolactone (CL) based (co)polymers in the preparation of porous nerve conduits for bridging nerve gaps[22]. Poly(TMC) and TMC-CL copolymers

with high CL content are very flexible and tough materials, that can be processed into highly porous structures. These materials are biocompatible and their degradation rates can be tuned by adjusting the comonomer content[23,24]. The aim of the present study was to evaluate how variations in the polymer composition affect the adhesion, proliferation and morphology of human Schwann cells (HSCs) on TMC and CL (co)polymer substrates, with the final goal of using these materials in the preparation of artificial nerve grafts seeded with SCs.

Ultimately, the HSCs will be seeded on the inner surface of the graft either directly or after coating of the graft luminal surface with an adhesive protein[25-27]. Alternatively, the nerve guide can be filled with SCs in a supporting adhesive matrix[12-14,17,28]. Therefore, the effect of fibronectin coating of TMC and CL (co)polymers on the behavior of HSCs was also investigated.

MATERIALS AND METHODS

Materials

Unless indicated otherwise, all reagents and biochemicals were purchased from Sigma (USA). Solvents were of analytical grade (Biosolve, The Netherlands).

Polymer Synthesis and Characterization

The synthesis and characterization of the TMC (Boehringer Ingelheim, Germany) and CL (Acros Organics, Belgium) based polymers have been described in a previous study[22]. Briefly, the polymerizations were conducted by ring-opening polymerization in evacuated and sealed glass ampoules using stannous octoate as a catalyst. All homo- and copolymerizations were carried out for a period of 3 days at 130°C. The obtained polymers were purified by dissolution in chloroform and subsequent precipitation into a ten-fold volume of isopropanol. The precipitated polymers were recovered, washed with fresh isopropanol and dried under reduced pressure at room temperature until constant weight. The (co)polymer composition was determined by proton nuclear magnetic resonance (^{1}H-NMR; Varian Inova 300 MHz, USA), the molecular weight by gel permeation chromatography (GPC; Waters, USA) and thermal properties were evaluated by means of differential scanning calorimetry (DSC; Perkin Elmer Pyris 1, USA).

Preparation of Polymer Disks

Films were prepared by casting polymer solutions (4.0-6.5 wt/vol%) in chloroform onto glass plates. After drying the films under reduced pressure at room temperature, disks with a diameter of 17 mm were punched out.

The disks were sterilized by two incubation steps in 70 vol% ethanol solution for 15 min, followed by a rinsing step of 30 min in sterile water. After sterilization, individual disks were gently placed in wells of 24-well tissue culture plates (Costar, USA) and fixed with sterile rubber rings with a 15 mm internal diameter (Eriks, The Netherlands). After drying overnight in a laminar flow chamber the disks were used for cell culture.

In selected experiments, sterilized disks were pre-coated by incubation at room temperature for 45 min with a 50 μg/ml human fibronectin solution (Roche Diagnostics, Germany) in phosphate buffered saline (PBS; pH 7.4, NPBI, The Netherlands).

Characterization of Polymer Films

Static contact angles of ultra-pure water (MilliQ Plus - Millipore, France) on dry and wet polymer films and water uptake in PBS were used to evaluate the wettability of TMC and CL (co)polymers. Contact angle measurements based on the sessile drop (dry films) and captive bubble (wet films) methods were performed at room temperature using a video-based optical contact angle meter OCA 15 (DataPhysics Instruments GmbH, Germany). For the dry polymer surfaces sessile drop contact angles were determined using films spin-coated from chloroform solutions (2 wt/vol%) onto glass slips (Menzel-Gläser, Germany) (readings were taken within the first 10-15 s). Contact angles of five different regions of each polymer film were measured and averaged. Contact angles of wet films were determined using the captive bubble method on 10 mm diameter disks punched out of the cast films, which were conditioned in ultra-pure water for 1 wk. Contact angles of four different disks of each polymer were averaged.

The water uptake was defined as the weight gain of the polymer specimen after conditioning, according to:

$$\text{water uptake} = \frac{w - w_o}{w_o} \times 100 \quad (\text{wt\%}) \tag{1}$$

where w_o is the initial specimen weight and w the weight of the specimen after conditioning.

Compression molded specimens were placed in PBS at 37°C and the weight change of the samples was evaluated until equilibrium was reached (within 24 hrs). Purified polymer samples 600 μm thick were compression molded at 140°C in a 100x50x0.6 mm^3 mould.

The surface structure of the films was evaluated using a S800 Field Emission scanning electron microscope (SEM; Hitachi, Japan) operating at 5 kV. Prior to SEM analysis samples were sputtered with a gold layer (Polaron, UK).

Isolation of Human Schwann Cells

Pieces of sural nerve that remained after nerve transplantation to restore brachial plexus lesions in two patients, were used to establish two HSC cultures (NCN61 and NCN68) by means of a sequential explantation technique[29]. All material was obtained from the Leiden University Medical Center (Department of Neurosurgery) after informed consent from the patients. After careful stripping of the epineurium and connective tissue, the sural nerve was cut into pieces of approximately 1 mm^3. These were placed in gelatin-coated culture flasks (Greiner, The Netherlands) and covered with a thin layer of LAK culture medium consisting of Dulbecco's modified Eagle's medium (DMEM; Bio-Whittaker Europe, Belgium), 10% lymphokine activated killer cells conditioned medium (LAK)[30], 5% fetal calf serum (FCS; Gibco BRL, Life Technologies, Germany), 0.25 μl/ml phytohaema-agglutinin (PHA; Difco Laboratories, USA), 100 IU/ml penicillin (Gist-Brocades, The Netherlands) and 50 μg/ml streptomycin (Gist-Brocades).

Gelatin coatings on the culture flasks were prepared by incubating a 0.5 wt/vol% solution of gelatin (Difco Laboratories) for 45 min at room temperature, followed by 15 min incubation with 0.5 wt/vol% glutaraldehyde (Merck, Germany) solution. The coated flasks were subsequently thoroughly rinsed with distilled water and dried overnight in a laminar flow chamber.

Immunocytochemistry of Human Schwann Cells

In order to differentiate between SCs and fibroblasts, cultures of NCN61 and NCN68 were made on gelatin-coated coverslips (same coating procedure as described above for coating of the culture flasks), fixed with Cryofix® (Merck), rinsed 3 times with PBS and incubated with antibodies appropriately diluted in PBS containing 0.1% bovine serum albumin (BSA) and 1% normal goat serum (NGS; CLB, The Netherlands). To identify Schwann cells, antibodies were added directed against S100 and glial fibrillary associated protein (GFAP; Boehringer Mannheim

Biochemica, Germany) in a dilution of 1:1,000 and 1:500, respectively. For fibroblast identification, a antibodies directed against fibroblasts (S5 clone), Thy 1.1 (Serotec, UK) and smooth muscle actin were used in a dilution of 1:100, 1:10,000 and 1:200 respectively. After overnight incubation at 4°C and 100% humidity, cultures were again rinsed 3 times with PBS and subsequently stained with GAM/FITC (Molecular Probes, The Netherlands) appropriately diluted in PBS containing 0.1% BSA and 1% NGS. After extensive rinsing with PBS, sections were mounted, dehydrated and coverslipped with Fluoromount® (Merck) and viewed with a fluorescence microscope (Olympus, The Netherlands).

SC identity and functionality were further confirmed by testing for myelin production around cortical neurons as described elsewhere[31].

Human Schwann Cell Seeding

HSCs were collected from the gelatin-coated culture flasks, by incubation for approximately 2 min at room temperature with a solution of 0.25% trypsin (Difco Laboratories, USA) and 10 mM ethylenediaminetetraacetic acid (EDTA) in DMEM, followed by the addition of an equal amount of culture medium. A small cell sample was stained with True Blue (Janssen Chimica, Belgium) to evaluate cell viability. The cell number was estimated using a Bürker-Türk chamber and subsequently the cell suspension was centrifuged for 5 min at 1,600 rpm. The cell pellet was washed with LAK culture medium and after a second centrifugation step (5 min, 1,600 rpm) the cells were resuspended in fresh culture medium to a final concentration of 2.8×10^3 cells/ml (the same seeding concentration was used in all studies). The cell suspension (500 µl aliquots) was added to the wells and incubated at 37°C in humidified air/5% CO_2. In proliferation experiments, the medium was refreshed 3 times per wk. Glass slides (Menzel-Gläser) coated with gelatin were used as positive control (same coating procedure as described above for coating of the culture flasks).

Human Schwann Cell Adhesion and Proliferation

At the indicated times, cultures (in triplicate for each surface) were gently rinsed with PBS, fixed with Cryofix® and stained with 0.25 wt/vol% coommassie blue solution in methanol:water:acetic acid (5:5:1). Subsequently, samples were fixed with an 8.8 wt/vol% trichloroacetic acid and 2.6 wt/vol% sulfosalicylic acid solution in a 23:77 vol% methanol:water mixture. Finally, the disks were coverslipped with Gur® (BDH, UK) and examined under the light microscope

(Olympus) at 100× magnification. Cell numbers were determined by counting the cells present on the total area of the disks by direct microscopical observation. Morphology was assessed in terms of the size of the cells, the existence of clusters and the presence of spaces between cells. Also the relative homogeneity and overall morphology of the cells in culture were evaluated. Light micrographs of HSC cultures on the different surfaces were taken at the different evaluation time points (Nikon, Japan).

Statistical Data Analysis

Data are given as mean±standard deviation (SD) and were analyzed using one-way ANOVA, followed by Tukey's least significant differences multiple comparisons test. In the studies of HSC adhesion and proliferation on the polymer surfaces, the comparison between the cell counts on each polymer surface and gelatin at each time point was made by a two-sample *t* test (equal variances not assumed). Differences were considered statistically significant when $p<0.05$. All calculations were performed using SPSS software for Windows (version 10.0) (SPSS, USA).

RESULTS

Polymer Characterization

The characteristics of the TMC and CL (co)polymers used in this study can be found in Table 1. All synthesized materials have high molecular weight and range from amorphous rubbers in case of TMC rich (co)polymers, to semi-crystalline rubbers in case of the CL rich (co)polymers.

Characterization of Polymer Films

In Table 2 the equilibrium water uptake and the sessile drop and captive bubble contact angles of the different polymer films under study are presented. The water uptake is higher for the amorphous polymers. This can be explained by the absence of the denser crystalline domains. The contact angle determined by the sessile drop method (films in the dry state) slightly increased with the TMC content, nevertheless all compositions yielded relatively hydrophobic polymer surfaces. The contact angle was also determined by the captive bubble method since an aqueous environment resembles the conditions in which the films were tested for SC adhesion and proliferation. For all polymer compositions the contact angle on wet

films was lower than the contact angle on dry films. An increase in TMC content had no effect on the contact angle values determined by the captive bubble method. Despite the described differences in water uptake and static contact angle in the dry and wet state between the polymers, all surfaces can be regarded as hydrophobic. Scanning electron microscopic analysis of the films used for SC culture (data not shown) showed that poly(TMC) and 82:18 TMC-CL copolymer films have a very smooth surface. Poly(CL) and 10:90 TMC-CL copolymer film surfaces exhibited the spherulitic morphology characteristic of a semi-crystalline material.

Table 1. Characterization of the synthesized TMC and CL (co)polymers used in the preparation of the polymer disks.

Polymer composition TMC/CL (mol ratio)	$\overline{M}n \times 10^{-5}$	PDI	Tg (°C)	Tm (°C)	$w_c{}^a$ (%)
100/0	3.4	1.7	-17	-	-
82/18	2.8	1.8	-29	-	-
10/90	1.4	1.8	-64	33	32
0/100	1.6	2.0	-68	55	45

$\overline{M}n$: Number average molecular weight; PDI: polydispersity index; Tg: glass transition temperature and Tm: melting temperature.

^{a} The mass fraction of crystallinity (w_c) was determined according to the expression: $w_c = \Delta H / \Delta H°$, where ΔH is the heat of fusion as determined by differential scanning calorimetry and $\Delta H°$ the heat of fusion of 100% crystalline poly(CL) reported to be 139.4 J/g[32].

Table 2. Wettability of the TMC and CL (co)polymer films.

Polymer composition TMC/CL (mol ratio)	Water uptake^a (wt%)	Sessile drop contact angle (°)	Captive bubble contact angle (°)
100/0	1.37±0.15	73±1	57±2
82/18	1.24±0.02	77±1	52±2
10/90	0.83±0.03	80±1	56±2
0/100	0.51±0.05	80±1	62±1

^{a} Equilibrium water uptake, after conditioning in PBS, at 37°C for 24 hrs.

Purification and Characterization of Human Schwann Cell Cultures
Purification by the sequential explantation method resulted in cultures that stained almost exclusively with S100 and GFAP antibodies, and only sporadically with fibroblast, Thy1.1 and smooth muscle actin antibodies, indicating highly purified

(95-98%) HSC cultures. Both cell lines (NCN61 and NCN 68) tested positive for myelin production around cortical neurons (data not shown).

99-100% of the cells that were to be seeded stained with True Blue, indicating high HSC viability.

Human Schwann Cell Adhesion to TMC (Co)polymers

HSC (NCN61) adhesion to TMC-CL copolymers and parent homopolymers was determined at 1, 3, 6 and 24 hrs after seeding (Figure 1).
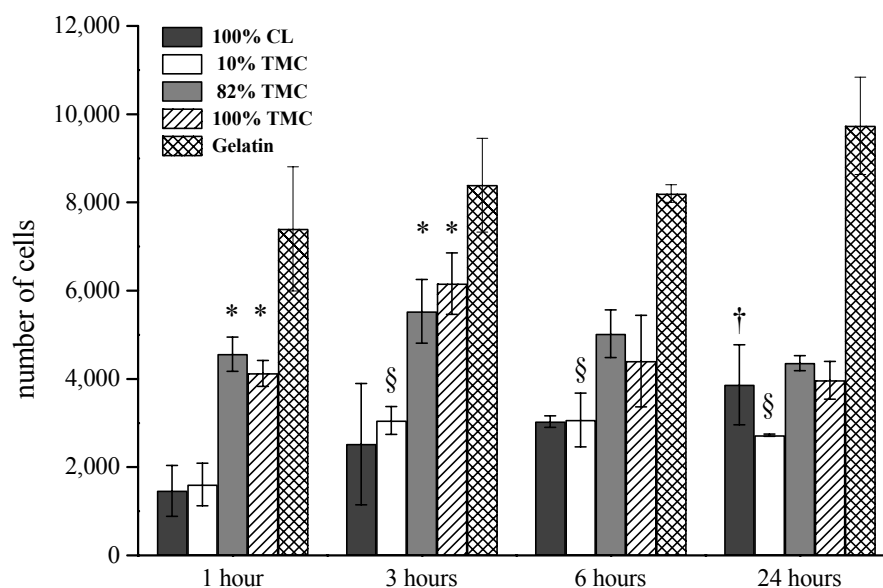

Figure 1. Total number of HSCs (NCN61) adhering to different TMC and CL (co)polymer films and gelatin at different time points. The data represent a mean ± SD of three independent measurements. The four (co)polymer compositions were compared among each other: * = significantly different from poly(CL) and the 10:90 TMC-CL copolymer at the corresponding time point; § = significantly different from the 10:90 TMC-CL copolymer at 1 hr; † = significantly different from poly(CL) at 1 hr.

Of all the polymer surfaces tested, poly(TMC) and 82:18 TMC-CL copolymer films showed the fastest and highest adhesion of SCs. One hour after seeding the number of cells adhering to TMC rich materials was higher compared to materials with lower TMC content. The number of cells that adhered to poly(CL) and the 10:90 TMC-CL copolymer showed an increase over time, reaching a plateau after 3 hrs of culture. In time the number of cells attached to poly(TMC) and the 82:18 TMC-CL copolymer did not change. At all time points, the cell density was generally lower on CL rich polymers than on TMC rich materials. No increase in cell numbers was

observed on gelatin over time. At the different time points cell numbers on the polymer surfaces were significantly lower than those on gelatin (except at 1 hr where there was no statistical difference between the number of cells on the TMC rich (co)polymers and on gelatin).

In order to determine if patient-to-patient variation would have an effect on HSC adhesion to the polymeric surfaces under study, cells derived from another patient (NCN 68) were seeded onto the TMC copolymer films (Figure 2).
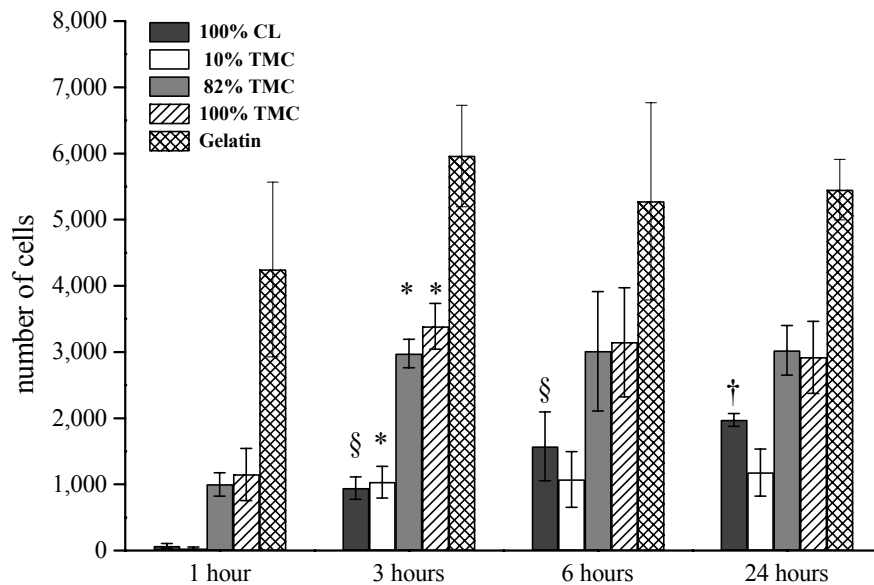

Figure 2. Total number of HSCs (NCN68) adhering to different TMC and CL (co)polymer films and gelatin at different time points. The data represent a mean ± SD of three independent measurements. The four (co)polymer compositions were compared among each other: * = significantly different from corresponding polymer at 1 hr; § = significantly different from poly(CL) at 1 hr; † = significantly different from poly(CL) at 1 and 3 hrs.

Cell adhesion to the five different surfaces showed a similar trend as observed for the NCN61 culture. The number of cells adhering to the TMC rich materials was generally higher compared with the number of cells adhering to materials with lower TMC content. However, cell adhesion to the polymers proceeded slower compared to the NCN61 culture. Cell density increased up to 3 hrs for the TMC containing polymers and up to 6 hrs for poly(CL). Cell numbers on all tested polymer surfaces were significantly lower than those on gelatin at the different time points (except at 6 hr where there was no statistical difference between the number

of cells on the poly(TMC) films and on gelatin). Cell numbers on gelatin also did not change over time, as observed with the NCN61 culture.

Human Schwann Cell Proliferation on TMC (Co)polymers

In a separate study, HSC proliferation (NCN61) on the TMC-CL copolymers and parent homopolymer films was evaluated at 3, 6, 9, and 15 days of culture (Figure 3). All surfaces tested showed significant cell proliferation between 3 and 15 days of culture.
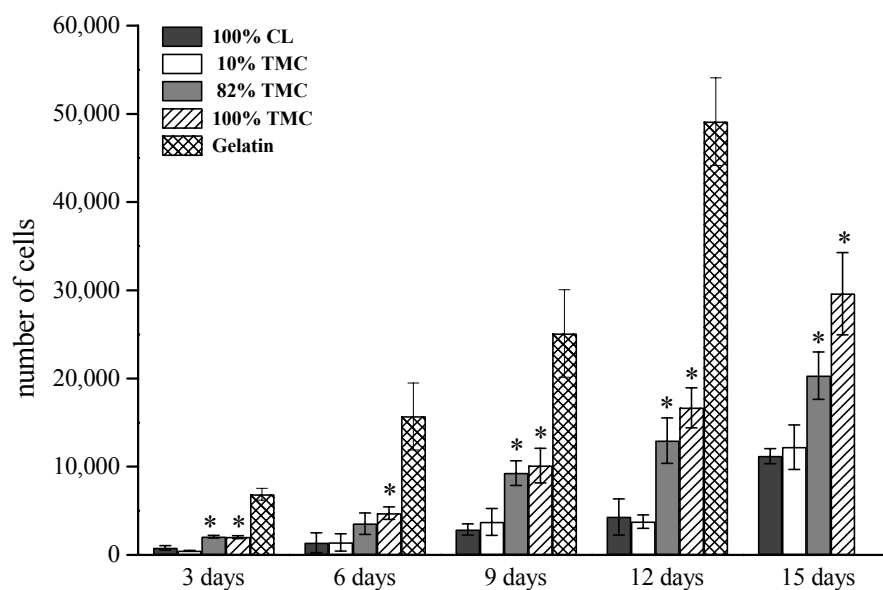

Figure 3. Total number of HSCs (NCN61) on different TMC and CL (co)polymer films and gelatin at different culturing times. At 15 days the cell number on gelatin could not be determined accurately due to the very large number of cells covering the surface. The data represent a mean ± SD of three independent measurements. The four (co)polymer compositions were compared among each other: * = significantly different from poly(CL) and the 10:90 TMC-CL copolymer at the corresponding time point.

In accordance to the observations at shorter culture times, the number of cells on poly(TMC) and the 82:18 TMC-CL copolymer was generally higher than on the polymers with higher CL content. Also in agreement with the higher initial cell adhesion, the total number of cells observed at all time points on gelatin was higher than on the polymeric surfaces.

The natural logarithm of the average cell number on each surface increases linearly as a function of time (Figure 4). Therefore, despite differences in total cell numbers, HSCs displayed exponential cell growth when cultured on all the tested surfaces

during the time scope of this study. From the slopes of the linear fittings, growth rates and doubling times were calculated for the HSCs on the different surfaces (Table 3). There were no major differences between the growth rates and consequently doubling times of the cells cultured on the different polymer surfaces and gelatin. The cells divided approximately every three days.
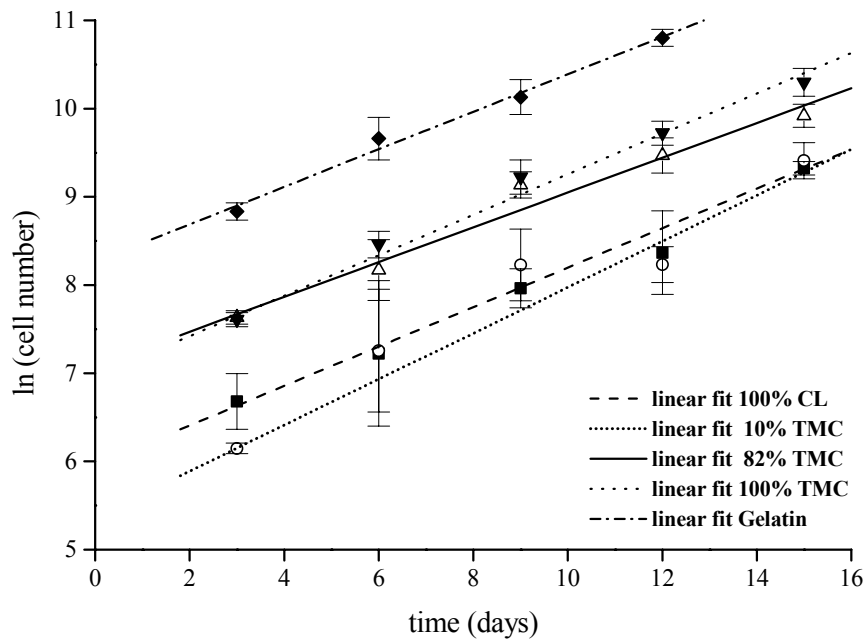

Figure 4. Natural logarithm of the average cell numbers observed on each surface versus time and correspondent linear fittings. The data represent a mean ± SD of three independent measurements. (■) 100% CL; (○) 10% TMC; (△) 82% TMC; (▼) 100% TMC and (♦) gelatin.

Table 3. Growth rates and doubling times ± SD for HSCs (NCN61) cultured on the different TMC and CL (co)polymer films and on gelatin.

Surface	Growth rate (day^{-1})	Correlation coefficient of linear fit (R)	Doubling time (days)
100% CL	0.22±0.01	0.998	3.10±0.08
10:90% TMC-CL	0.26±0.02	0.994	2.66±0.12
82:18% TMC-CL	0.20±0.01	0.992	3.52±0.18
100% TMC	0.23±0.01	0.997	3.02±0.10
Gelatin	0.22±0.01	0.999	3.19±0.07

Human Schwann Cell Morphology on TMC (Co)polymers

Figure 5 shows the appearance of HSCs (NCN61) on different TMC and CL based (co)polymer films and on gelatin at selected evaluation points. The time points 1hr, 24hrs and 9 days of culture, were selected as indicative for the initial adhesion, the post-adhesion state and advanced proliferation stage, respectively.

After 1 hr of culture more than 90% of the SCs present on poly(CL) and 10:90 TMC-CL copolymer films maintained their round shape (14<diameter<60 μm), but small lamellopodial extensions, the first signs of spreading, were present (Figure 5.A1 and 5.B1). On the 82:18 TMC-CL copolymer and poly(TMC) films only approximately 50% of the SCs maintained their round shape (17<diameter<32 μm) while the rest of the cells was flattening, and exhibited lamellopodial extensions (96<length<185 μm) (Figure 5.C1 and 5.D1). In the case of gelatin, all SCs were flattening after 1 hr of culture, and exhibited many lamellopodial extensions (42<length<172 μm) (Figure 5.E1).

At 24 hrs of culture, both spindle-shaped and well-flattened SCs were observed on gelatin (110<length<285 μm) (Figure 5.E2). On all polymeric surfaces SCs formed clusters and were still not totally flattened. On the copolymers with high TMC content cells tended to be more extended (70<length<206 μm) (Figure 5.C2 and 5.D2) than on films with high CL content where the cells were generally smaller (68<length<128 μm) (Figure 5.A2 and 5.B2).

After longer periods of culture, SCs were flattened on all surfaces and demonstrated a typical bi- or tripolar morphology and oval nuclei[33]. However, there were significant differences between the surfaces. On gelatin a confluent packed layer of cells was observed after 9 days (Figure 5.E3). Both spindle-shaped and elongated flattened SCs were observed. After 15 days (data not shown) the number of cells on gelatin continued to increase. The cells were well-aligned and even more densely packed than at 9 days. On TMC rich (co)polymers SCs tended to be slightly elongated or spindle-shaped, and appeared more flattened than at initial culture times (Figure 5.C3 and 5.D3). After 15 days of culture on these polymers the cell layer was nearly confluent, but clusters of cells remained present. On the poly(CL) and the 10:90 TMC-CL copolymer even at later stages of culture the total SC numbers were lower than on the other surfaces tested, as previously mentioned (Figure 5.A3 and 5.B3). After 15 days cultures were still not confluent and clusters of cells remained present. Furthermore, on these surfaces the SCs had smaller dimensions (37<length<201 μm) than SCs cultured on gelatin (91<length<303 μm)

or on the (co)polymers with high TMC content (41<length<289 μm), and were mainly spindle-shaped or with rounded morphology. Some flattened cells were also observed, but with thin and long cell protrusions.

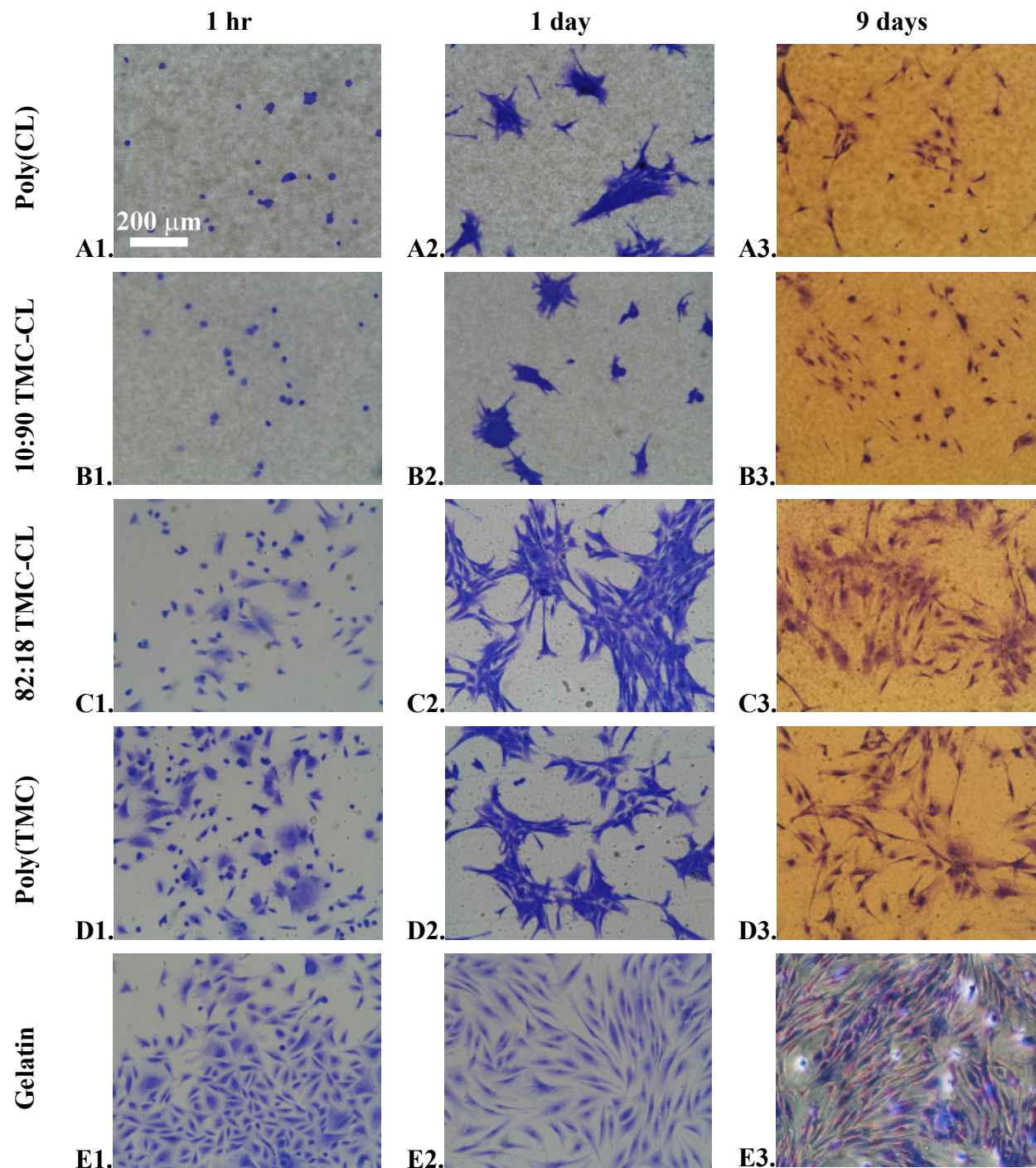|	1 hr	1 day	9 days

Figure 5. Light micrographs of HSCs (NCN61) on different surfaces at different time points (1st column - 1hr, 2nd column - 24 hrs and 3rd column - 9 days). (A1-A3) poly(CL); (B1-B3) 10:90 TMC-CL copolymer; (C1-C3) 82:18 TMC-CL copolymer; (D1-D3) poly(TMC); (E1-E3) gelatin.

Human Schwann Cell Culture on Fibronectin-Coated TMC (Co)polymers

Adhesion and proliferation of HSCs (NCN61) on fibronectin-coated polymer films were evaluated at 1, 6 and 24 hrs and 3 and 9 days of culture, respectively. Gelatin surfaces (not coated with fibronectin) were used as control.

Both for short and long culture times no significant differences were observed between the total cell numbers on the five different surfaces (Figure 6). Between 1 and 24 hrs of culturing, the number of cells adhering to the different surfaces did not significantly increase. In all cases, after the initial adhesion period, HSC numbers showed an exponential increase over time. Using the results obtained at 1, 3 and 9 days of culture, growth rates and doubling times for the HSCs cultured on the fibronectin-coated polymer films and gelatin were calculated (Table 4). There were no major differences between growth rates on the different surfaces; the cells divided approximately every 4 days.
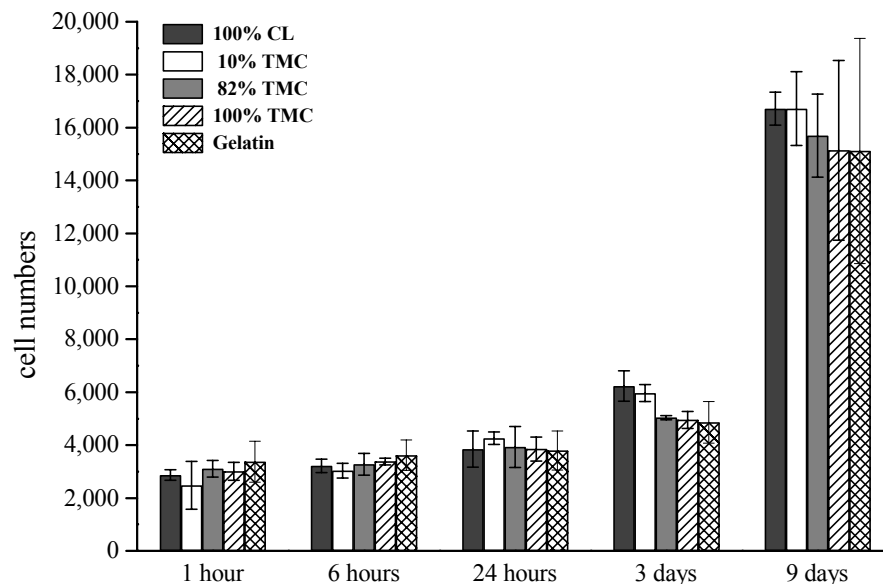
Figure 6. Total number of HSCs (NCN61) on different fibronectin-coated TMC and CL (co)polymer films and gelatin at different culturing times. The data represent a mean ± SD of three independent measurements.

In terms of morphology, the SCs appeared very similar on all surfaces at the different time points. After 1 hr of culture cells were still rather small (52<length<169 μm) but all were flattening. At 24 hrs of culture on all surfaces cells were mainly flattened showing several lamellipodial extensions. However, in

case of copolymers with high CL content the cell extensions were thinner and longer than on the polymeric surfaces based on TMC rich polymers or gelatin.

All cultures were confluent at 9 days with cells showing a more elongated (100<length<279 μm) and packed conformation. At this time it was possible to observe both spindle-shaped and flattened cells in all cultures. Flattened cells on films of poly(CL) or on the 10:90 TMC-CL copolymer had thinner cell extensions appearing more like "ink-splashes" than like a "fried-egg" shape as observed for cell on the other (co)polymer surfaces and on gelatin.

Table 4. Growth rates and doubling times ± SD for HSCs (NCN61) cultured on the different TMC and CL (co)polymer films coated with fibronectin and on gelatin.

Surface	Growth rate (day^{-1})	Correlation coefficient of linear fit (R)	Doubling time (days)
100% CL	0.17±0.01	0.998	4.06±0.16
10:90% TMC-CL	0.17±0.01	0.999	4.05±0.02
82:18% TMC-CL	0.19±0.01	0.998	3.70±0.15
100% TMC	0.17±0.02	0.991	4.09±0.39
Gelatin	0.17±0.02	0.995	3.97±0.29

DISCUSSION

The optimal way to incorporate SCs into an artificial nerve guide still needs to be determined. SCs can be seeded directly on the inner surface of the graft or after coating of the luminal graft surface with an adhesive substrate. Alternatively, the nerve guide can be filled with SCs in a supporting adhesive three-dimensional matrix, e.g. based on ECM proteins. In all cases, a prerequisite in the design of an artificial conduit with cultured SCs to be used in the clinic is the cell adhesion to the selected substrate and subsequent proliferation and functionality. In the present study we evaluated the adhesion and proliferation of pure and viable HSC cultures on fibronectin-coated and non-coated TMC and CL (co)polymer films.

Cell adhesion and proliferation occurred on all tested polymer surfaces. However, for both primary HSC lines tested a faster and higher cell adhesion was observed on films with higher TMC content. Cell attachment on the polymeric surfaces was lower and slower than on gelatin (positive control). The determined number of cells that had attached to the surfaces under study was higher than the estimated number

of seeded cells (except in the study of the proliferation of HSC on non-coated polymeric surfaces). In contrast with the cell number determination by direct observation, the estimation of the cell concentration in the cell suspension to be seeded by means of the Bürker-Türk chamber method can be hampered by the agglomeration of the cells after trypsinisation. Therefore, the observed differences can be explained by an underestimation of the number of cells initially seeded. Despite differences in cell adhesion, exponential cell growth was observed on all polymer films as well as on gelatin. The growth rates were similar on all surfaces with cell numbers doubling approximately every three days. The growth rates previously reported for HSCs cultured in the presence of mitogens vary between 3-4 days[34], similar to the ones observed in our study, to 1-2 wks[35]. Such differences in the growth rates may arise from isolation of the cells from different donors or donor sites and the use of different culture conditions such as cell culture substrate, culture media composition and seeding densities.

When proliferating on the polymer films and on gelatin, cells presented the typical bi- or tripolar morphology[33]. However, on the polymer films cells tended to form clusters, and on the CL rich materials in particular, at all time points the cells were smaller and with fewer lamellipodial extensions.

The results demonstrate that the surface properties of the TMC based polymers have an effect on the initial adhesion and overall morphology of HSCs. In terms of the substrate wettability TMC rich films were found to be slightly less hydrophobic than CL rich films. However, in view of the small differences observed, all polymer surfaces can be considered equally hydrophobic. Therefore, dissimilarities in cell behavior cannot be directly correlated to the surface wettability. With the increase of CL content in the polymer, the ratio of ester/carbonate units increases as well as the number of crystallizable units per polymer chain. CL rich (co)polymer films are semicrystalline, featuring the characteristic spherulite morphology, in contrast to the amorphous and more flexible TMC rich (co)polymers. Chemical composition, polymer morphology (crystallinity) and mechanical characteristics may affect the polymer surface properties. Ultimately this may not only influence the nature and the amount of protein adsorption from serum containing medium onto the polymer film, but can also regulate conformational changes of the adsorbed protein, thus indirectly controlling cell adhesion and protein-mediated cell functions[36]. ECM proteins in the culture medium, like fibronectin, contain RGD amino acid sequences that can be recognized by integrin receptors present in the cell membrane of the SC[37,38]. This interaction causes the SC to attach to the surface and promotes a series

of other events such as cell spreading and cytoskeletal reorganization. The effect of polymer composition on the adsorption of proteins present in the culture medium onto the prepared TMC and CL (co)polymer films is currently being investigated by means of surface plasmon resonance (SPR), an optical technique that allows the investigation of dynamic surface events *in situ* in real time[39].

Although the mechanism mediating HSC behavior on the different polymers is not yet fully understood, the results described so far show that all materials allow SC adhesion and proliferation independently of the donor source, and that HSCs proliferate at comparable growth rates. Therefore, TMC and CL based (co)polymers can in principle be used for the preparation of artificial nerve grafts. If cells are to be seeded directly on the inner surface of the graft, higher cell numbers may be reached in shorter periods by increasing the initial cell seeding densities.

SCs can also be seeded onto the luminal surface of a nerve graft that has been pre-coated with an adhesive substrate. ECM proteins like fibronectin, laminin or collagen stimulate the outgrowth of neurites and improve nerve regeneration over large nerve gaps[40-42]. In this study fibronectin was selected as a coating, since it is known to promote cell-substratum adhesion under a variety of conditions. The adhesion and proliferation of HSCs on different ECM protein coatings, including fibronectin, was evaluated in a separate study[43]. When the TMC and CL based polymer surfaces were coated with fibronectin prior to culture, no significant differences in cell behavior between the polymer surfaces and gelatin were found. HSC adhesion was improved to levels comparable to gelatin and SC morphology was similar as observed on gelatin. Surface modification with fibronectin apparently masks the polymer surface properties and provides optimal HSC adhesion and proliferation. Exponential cell growth was also observed on the fibronectin-coated polymer substrates. The growth rates were similar on all surfaces, with cell numbers now doubling approximately every four days. Since more cells adhere to the polymer surfaces as a result of fibronectin coating, the use of ECM protein-coated nerve guides can reduce the required number of HSCs needed for seeding.

ACKNOWLEDGEMENTS

REFERENCES

[1]   Merle M, Dellon AL, Campbell JN, Chang PS. Complications from silicon-polymer intubulation of nerves. *Microsurgery* 1989; 10: 130-133.

[2]   Madison R, Sidman RL, Nyilas E, Chiu T-H, Greatorex D. Nontoxic nerve guide tubes support neovascular growth in transected rat optic nerve. *Exp Neurol* 1984; 86: 448-461.

[3]   Kiyotani T, Teramachi M, Takimoto Y, Nakamura T, Shimizu Y, Endo K. Nerve regeneration across a 25-mm gap bridged by a polyglycolic acid-collagen tube: a histological and electrophysiological evaluation of regenerated nerves. *Brain Res* 1996; 740: 66-74.

[4]   den Dunnen WFA, van der Lei B, Robinson PH, Holwerda A, Pennings AJ, Schakenraad JM. Biological performance of a degradable poly(DL-lactide-ε–caprolactone) nerve guide: Influence of tube dimensions. *J Biomed Mater Res* 1995; 29: 757-766.

[5]   Langone F, Lora S, Veronese FM, Caliceti P, Parnigotto PP, Valenti F, Palma G. Peripheral nerve repair using a poly(organo)phosphazene tubular prosthesis. *Biomaterials* 1995; 16: 347-353.

[6]   Aldini NN, Perego G, Cella GD, Maltarello MC, Fini M, Rocca M, Giardino R. Effectiveness of a bioabsorbable conduit in the repair of peripheral nerves. *Biomaterials* 1996; 17: 959-962.

[7]   Chamberlain LJ, Yannas IV, Hsu H-P, Spector M. Histological response to a fully degradable collagen device implanted in a gap in the rat sciatic nerve. *Tissue Eng* 1997; 3: 353-362.

[8]   Mackinnon SE, Dellon AL. A study of nerve regeneration across synthetic (Maxon) and biologic (collagen) nerve conduits for nerve gaps up to 5 cm in the primate. *J Reconstr Microsurg* 1990; 6: 117-121.

[9]   Rodriguez FJ, Gomez N, Perego G, Navarro X. Highly permeable polylactide-caprolactone nerve guides enhance peripheral nerve regeneration through long gaps. *Biomaterials* 1999; 20: 1489-1500.

[10]   den Dunnen WF, Meek MF, Grijpma DW, Robinson PH, Schakenraad JM. *In vivo* and *in vitro* degradation of poly[50/50 (85/15 L/D)LA/ε-CL], and the implications for the use in nerve reconstruction. *J Biomed Mater Res* 2000; 51: 575-585.

[11]   Bryan DJ, Holway AH, Wang KK, Silva AE, Trantolo DJ, Wise D, Summerhayes IC. Influence of glial growth factor and Schwann cells in a bioresorbable guidance channel on peripheral nerve regeneration. *Tissue Eng* 2000; 6: 129-138.

[12] Guénard V, Kleitman N, Morrissey TK, Bunge RP, Aebischer P. Syngeneic Schwann cells derived from adult nerves seeded in semipermeable guidance channels enhance peripheral nerve regeneration. *J Neurosci* 1992; 12: 3310-3320.

[13] Keeley R, Atagi T, Sabelman E, Padilla J, Kadlcik P, Agras J, Eng L, Wiedman T-W, Nguyen K, Sudekum A, Rosen J. Synthetic nerve graft containing collagen and synthetic Schwann cells improves functional, electrophysiological, and histological parameters of peripheral nerve regeneration. *Restor Neurol Neurosci* 1993; 5: 353-366.

[14] Kim DH, Connolly SE, Kline DG, Voorhies RM, Smith A, Powell M, Yoes T, Daniloff JK. Labeled Schwann cell transplants *versus* sural nerve grafts in nerve repair. *J Neurosurg* 1994; 80: 254-260.

[15] Bryan DJ, Wang RR, Chakalis-Haley DP. Effect of Schwann cells in the enhancement of pheripheral-nerve regeneration. *J Recon Microsurg* 1996; 12: 439-446.

[16] Ansellin AD, Fink T, Davey DF. Peripheral nerve regeneration through nerve guides seeded with adult Schwann cells. *Neuropathol Appl Neurobiol* 1997; 23: 387-398.

[17] Rodriguez FJ, Verdu E, Ceballos D, Navarro X. Nerve guides seeded with autologous Schwann cells improve nerve regeneration. *Exp Neurol* 2000; 161: 571-584.

[18] Terenghi G. Peripheral nerve injury and regeneration. *Histol Histopathol* 1995; 10: 709-718.

[19] Son Y-J, Thompson WJ. Schwann cell processes guide regeneration of peripheral axons. *Neuron* 1995; 14: 125-132.

[20] Fu SY, Gordon T. The cellular and molecular basis of peripheral nerve regeneration. *Mol Neurobiol* 1997; 14: 67-116.

[21] Frostick SP, Yin Q, Kemp GJ. Schwann cells, neurotrophic factors, and peripheral nerve regeneration. *Microsurgery* 1998; 18: 397-405.

[22] Pêgo AP, Poot AA, Grijpma DW, Feijen J. Copolymers of trimethylene carbonate and ε-caprolactone for porous nerve guides: synthesis and properties. *J Biomater Sci Polym Ed* 2001; 12: 35-53. Chapter 3 of this thesis.

[23] Pêgo AP, Poot AA, Grijpma DW, Feijen J. *In vitro* degradation of trimethylene carbonate based (co)polymers. *Macromol Chem Phys (accepted for publication)* Chapter 6 of this thesis.

[24] Pêgo AP, van Luyn MJA, Brouwer LA, van Wachem PB, Poot AA, Grijpma DW, Feijen J. *In vivo* behavior of poly(1,3-trimethylene carbonate) and copolymers of 1,3-trimethylene carbonate with D,L-lactide or ε-caprolactone. Degradation and tissue response. *(submitted to J Biomed Mater Res, 2002)* Chapter 7 of this thesis.

[25] Steuer H, Fadale R, Müller E, Müller HW, Planck H, Schlosshauer B. Biohybride nerve guide for regeneration: degradable polylactide fibers coated with rat Schwann cells. *Neurosci Lett* 1999; 277: 165-168.

[26] Hadlock T, Sundback C, Hunter D, Cheney M, Vacanti JP. A polymer foam conduit seeded with Schwann cells promotes guided peripheral nerve regeneration. *Tissue Eng* 2000; 6: 119-127.

[27] Hadlock TA, Sundback CA, Hunter DA, Vacanti JP, Cheney ML. A new artificial nerve graft containing rolled Schwann cell monolayers. *Microsurgery* 2001; 21: 96-101.

[28] Mosahebi A, Simon M, Wiberg M, Terenghi G. A novel use of alginate hydrogel as Schwann cell matrix. *Tissue Eng* 2001; 7: 525-534.

[29] Morrissey TK, Kleitman N, Bunge RP. Isolation and functional characterization of Schwann cells derived from adult peripheral nerve. *J Neurosci* 1991; 11: 2433-2442.

[30] Lamers CH, van de Griend RJ, Braakman E, Ronteltap CP, Benard J, Stoter G, Gratama JW, Bolhuis RL. Optimization of culture conditions for activation and large-scale expansion of human T lymphocytes for bispecific antibody-directed cellular immunotherapy. *Int J Cancer* 1992; 51: 973-979.

[31] Marani E. Culturing neurons and Schwann cells - Abstracts XIV National Congress Bulgarian Anatomical Society. *European J Morphol (in press)*.

[32] Crescenzi V, Manzini G, Calzolari G, Borri C. Thermodynamics of fusion of poly-β-propiolactone and poly-ε-caprolactone. Comparative analysis of the melting of aliphatic polylactone and polyester chains. *Eur Polym J* 1972; 8: 449-463.

[33] Levi AD. Characterization of the technique involved in isolating Schwann cells from adult human peripheral nerve. *J Neurosci Methods* 1996; 68: 21-26.

[34] Casella GT, Wieser R, Bunge RP, Margitich IS, Katz J, Olson L, Wood PM. Density dependent regulation of human Schwann cell proliferation. *Glia* 2000; 30: 165-177.

[35] Spierings E, de Boer T, Wieles B, Adams LB, Marani E, Ottenhoff TH. Mycobacterium leprae-Specific, HLA class II-restricted killing of human Schwann cells by CD4(+) Th1 cells: a novel immunopathogenic mechanism of nerve damage in leprosy. *J Immunol* 2001; 166: 5883-5888.

[36] Garcia AJ, Vega MD, Boettiger D. Modulation of cell proliferation and differentiation through substrate-dependent changes in fibronectin conformation. *Mol Biol Cell* 1999; 10: 785-798.

[37] Chernousov MA, Carey DJ. Schwann cell extracellular matrix molecules and their receptors. *Histol Histopath* 2000; 15: 593-601.

[38] Previtali SC, Feltri ML, Archelos JJ, Quattrini A, Wrabetz L, Hartung H. Role of integrins in the peripheral nervous system. *Prog Neurobiol* 2001; 64: 35-49.

[39] Green RJ, Frazier RA, Shakesheff KM, Davies MC, Roberts CJ, Tendler SJB. Surface plasmon resonance analysis of dynamic biological interactions with biomaterials. *Biomaterials* 2000; 21: 1823-1835.

[40] Madison RD, Da Silva CF, Dikkes P. Entubulation repair with protein additives increases the maximum nerve gap distance successfully bridged with tubular prostheses. *Brain Res* 1988; 447: 325-334.

[41] Woolley AL, Hollowell JP, Rich KM. Fibronectin-laminin combination enhances peripheral nerve regeneration across long gaps. *Otolaryngol Head Neck Surg* 1990; 103: 509-518.

[42] Bailey SB, Eichler ME, Villadiego A, Rich KM. The influence of fibronectin and laminin during Schwann cell migration and peripheral nerve regeneration through silicon chambers. *J Neurocytol* 1993; 22: 176-184.

[43] Vleggeert-Lankamp CLAM, Pêgo AP, Deenen M, Lakke EAJF, Poot AA, Grijpma DW, Feijen J, Marani E. Human Schwann cell proliferation on coatings. *(manuscript in preparation).*

CHAPTER 10

Preparation and *in vivo* performance of degradable two-ply nerve guides based on (co)polymers of trimethylene carbonate and ε-caprolactone

A.P. PÊGO[1], C.L.A.M. VLEGGEERT–LANKAMP[2], E.A.J.F. LAKKE[2], E. MARANI[1,2], R.T.W.M. THOMEER[2], A.A. POOT[1], D.W. GRIJPMA[1] and J. FEIJEN[1]

[1] *Institute for Biomedical Technology (BMTI) and Department of Polymer Chemistry and Biomaterials, Faculty of Chemical Technology, University of Twente, P.O. Box 217, 7500 AE Enschede, The Netherlands*
[2] *Neuroregulation Group, Department of Neurosurgery, Leiden University Medical Center (LUMC), P.O. Box 9604, 2300 RC Leiden, The Netherlands*

ABSTRACT

Two-ply tubes consisting of an inner layer based on poly(1,3-trimethylene carbonate), poly(TMC) and an outer layer based on a copolymer TMC and ε-caprolactone (CL) with 11 mol% TMC were prepared for guided nerve tissue regeneration. A microporous inner layer (pore size range 1-13 μm) was obtained by dip-coating techniques used in combination with porosifying agents. A macroporous outer layer (pore size range 15-265 μm) was prepared by winding of fibers spun from solution. The mechanical properties and *in vivo* performance of these conduits in the correction of 6 mm gaps in the rat sciatic nerve model were compared to two-ply tubes with a non-porous inner layer. Both these two-ply nerve guides bent easily without kinking and showed excellent handling characteristics during surgery. Electrophysiological examinations revealed that the contact between the proximal and distal nerve ends was reestablished in both animal groups treated with the two-ply nerve guides. The nerve fibers regenerated through the artificial grafts showed mean conduction velocities similar to nerve fibers regenerated through autografts. These results indicate that two-ply nerve guides based on TMC and CL (co)polymers can serve as a support for axonal guidance. The use of a microporous poly(TMC) inner layer instead of a non-porous layer had no effect on the outcome of the nerve regeneration process.

INTRODUCTION

The use of autologous nerve grafts in the repair of extensive peripheral nerve injuries results in donor-site morbidity and eventually pain at the donor site. Furthermore, autografting techniques are limited by the availability of donor tissue. Despite these drawbacks, nerve autografting is still considered the treatment of choice in nerve restoration when a nerve gap cannot be repaired by end-to-end suture without tension. So far, the use of off-the-shelf substitutes for autologous nerve grafts resulted in lower levels of nerve regeneration and functional recovery than the use of autografts.

Silicone nerve guides have been successfully applied in the clinic in the reconstruction of different peripheral nerves[1]. However, this approach has been criticized due to reports of inflammation and chronic nerve compression after longer implantation periods[2]. In these cases a second operation was required to remove the non-degrading nerve conduits. Nerve guides that degrade upon nerve regeneration and maturation are, therefore, a preferred alternative. Several bioresorbable materials have been used in preparing artificial nerve guides[3-8]. Some of these systems proved to be promising alternatives to autologous grafts in the repair of short and medium length nerve gaps. However, for the repair of nerve gaps over clinically relevant distances refinement of these systems is required[9,10].

Considering the graft material, the polymer should not show a too high degree of swelling or too rapid degradation[5,11]. The conduits should keep their shape and mechanical properties during the time required for nerve regeneration and maturation[12,13]. Furthermore, the resorption process should not induce a strong inflammatory tissue response[14] that can lead to unrestricted macrophage invasion and fibrosis. The nerve guide should be flexible, since it will be subjected to flexing during the grafting procedure and during the implantation period, but relatively strong and easy to handle in microsurgery. Non-kinking behavior is another important requirement, as upon bending the graft should not occlude and compress the regenerating nerve[9,11,15].

Several studies showed that nerve regeneration and reinnervation were considerably improved in semi-permeable tubes when compared to impermeable ones[10,16,17]. Porous nerve guides allow the exchange of metabolites between the regeneration environment and the surrounding tissue[16] and avoid the building up of pressure due to fluid retention[18]. Pore size and porosity seem to be important factors in determining nerve regeneration. Previous studies revealed that nerves regenerated in

macroporous, open tubular structures contain high levels of connective tissue and dispersed neural elements[19].

The use of artificial nerve grafts also allows the enhancement of the nerve regeneration process by including various matrices containing appropriate cells, growth factors or other stimulating factors in the lumen of the nerve guide[19,20].

In the development of an effective artificial nerve graft, the guide should have a two-ply structure[21]. A microporous inner layer will serve as a barrier to minimize the invasion of fibrous scar tissue while still allowing the exchange of fluids. A macroporous outer layer can provide the nerve guide with dimensional stability and should assure the strength and toughness of the graft, without compromising its flexibility. This outer layer should be highly porous with interconnected pores to provide a low resistance to in- and out-flowing fluids. The outer layer will also allow the ingrowth of capillaries and a better integration of the graft with the surrounding tissue[21-24]. Often these macroporous structures were prepared by particulate leaching methods. We found, however, that preparation methods involving fiber-spinning yielded conduits with much improved flexing properties (Appendix A).

We have previously reported on the potential use of 1,3-trimethylene carbonate (TMC) and ε-caprolactone (CL) based (co)polymers in the preparation of porous conduits for nerve reconstruction in the peripheral nervous system[25]. Poly(TMC) and TMC-CL (co)polymers with high CL content are very flexible and tough materials. These polymers are biocompatible and their degradation rates can be tuned by adjusting the comonomer content[26,27]. After 3 weeks of subcutaneous implantation in the rat, poly(TMC) films had been nearly totally resorbed. In contrast, films of a TMC-CL copolymer with 10 mol% of TMC degraded much slower, keeping their shape and strength during the one-year period of the *in vivo* study. The degradation of both polymers occurs with minimum swelling of the polymer and a mild tissue reaction.

The aim of the present study was to prepare permeable two-ply nerve guides based on TMC-CL (co)polymers and test the effectiveness of the selected model in the improvement of nerve regeneration over the performance of non-permeable comparable conduits. Two-ply nerve guides were prepared by combination of dip-coating and fiber winding techniques. The conduits were characterized in terms of morphology and their *in vivo* performance was evaluated in the correction of 6 mm gaps in the rat sciatic nerve model. Axonal regeneration and functional recovery were assessed by means of an *in vitro* electrophysiological method[28].

MATERIALS AND METHODS

Materials

Polymer grade 1,3-trimethylene carbonate (TMC) was obtained from Boehringer Ingelheim, Germany. ε-Caprolactone (CL) (Acros Organics, Belgium) was purified by drying over CaH_2 (Acros Organics, Belgium) and distillation under reduced argon pressure. Stannous octoate ($SnOct_2$) (stannous 2-ethylhexanoate) was used as received from Sigma, USA. Powdered sugar (Suiker Unie, The Netherlands) used as a porosifying agent was sieved to a particle size smaller than 20 μm using standard test sieves (Endecotts, UK). Solvents (Biosolve, The Netherlands) were of analytical grade.

Polymer Synthesis

Poly(TMC) and poly(TMC-CL) with 11 mol% of TMC were synthesized as previously described[25]. Briefly, the polymerizations were conducted by ring-opening polymerization in an evacuated and sealed glass ampoule using $SnOct_2$ as catalyst. All polymerizations were carried out for a period of 3 days at 130°C±2°C. The obtained polymers were purified by dissolution in chloroform and subsequent precipitation into a ten-fold volume of isopropanol. The precipitated polymers were recovered, washed with fresh isopropanol and dried under reduced pressure at room temperature until constant weight.

Polymer Characterization

Polymers were characterized with respect to chemical composition by nuclear magnetic resonance (NMR). 300 MHz ^{1}H-NMR (Varian Inova 300 MHz) spectra were recorded using solutions of polymer in $CDCl_3$ (Sigma, USA).

Weight average ($\overline{M}w$) and number average ($\overline{M}n$) molecular weights, polydispersity index (PDI) and intrinsic viscosity ($[\eta]$) were determined by gel permeation chromatography (GPC) using a Waters Model 510 pump (USA), a HP Ti-Series 1050 autosampler (USA), a Waters Model 410 Differential Refractometer and a Viscotek H502 Viscometer Detector (USA) with Waters Styragel HR5-HR4-HR2-HR1 columns placed in series. Chloroform was used as eluent at a flow rate of 1.5 ml/min. Narrow polystyrene standards were used for calibration. Sample concentrations of approximately 0.5 wt/vol% and injection volumes of 30 μl were used. All determinations were performed at 25°C.

The thermal properties of the purified polymers were evaluated by differential scanning calorimetry (DSC). Samples (5-15 mg) placed in aluminum pans were analyzed with a Perkin Elmer Pyris1 (USA) at a heating rate of 10°C/min. All samples were heated to 40°C above their melting temperature (when present) or glass transition temperature. The samples were then quenched rapidly (300°C/min) to 40°C below their glass transition temperature and after 5 min a second scan was recorded. The glass transition temperature (Tg) was taken as the midpoint of the heat capacity change and the peak melting temperature (Tm) was determined from the melting endotherm. The crystallinity (w_c) of the semi-crystalline TMC-CL copolymer was determined assuming proportionality to the experimental heat of fusion (ΔH) according to the expression: $w_c = \Delta H / \Delta H°$, where $\Delta H°$ is the heat of fusion of 100% crystalline poly(CL) reported to be 139.4 J/g[29]. Cyclohexane, indium, gallium and tin were used as standards for temperature calibration.

The molar composition, molecular weights and thermal properties of the prepared polymers are compiled in Table 1.

Table 1. Characterization of the prepared CL and TMC (co)polymers.

Polymer	$\overline{M}_n \times 10^{-5}$	PDI	$[\eta]^a$ (dl/g)	Tg^b (°C)	Tm^b (°C)	w_c^b (%)
Poly(TMC)	3.3	1.5	4.20	-19	-	-
Poly(TMC-CL) (11:89 mol%)	1.3	1.7	3.8	-64	37	33

[a] In CHCl$_3$, at 25°C.

[b] Second heating scan (DSC).

Preparation of Two-ply Nerve Guides

Non-porous poly(TMC) inner layer and macroporous poly(TMC-CL) outer layer.

To prepare the inner layer, a glass mandrel ($\phi=1.5\pm0.1$ mm) was immersed (5 mm/s) in a 4 wt/vol% solution of poly(TMC) in chloroform. After 10 seconds in the solution the mandrel was pulled out (5 mm/s) and the chloroform was allowed to evaporate at room temperature for 10 min. This procedure was repeated one more time and the tube was dried overnight in air. The outer layer fibers were spun from 10 wt/vol% poly(TMC-CL) solutions in chloroform containing 0.16 wt/vol% poly(ethylene oxide) (PEO, $\overline{M}_w = 8\times10^6$, Aldrich-Chemie, Germany). The polymer solution was pumped through a needle ($\phi=0.5$ mm) moving up and down (30 mm/s) along the rotating (790 rpm) previously dip-coated tube, onto which the solidifying polymer fiber was wound. Variation of these speeds allows good control of the

resulting winding angles. The distance between the needle and the rotating mandrel was set at 6 mm. Fiber spinning and winding were carried out over a length of 30 mm for 50 minutes and subsequently the graft was dried in air overnight. The nerve guides were removed from the glass mandrels after 5-20 min of immersion in ethanol, dried in a vacuum oven at room temperature and stored at -20°C till further use.

Microporous poly(TMC) inner layer and macroporous poly(TMC-CL) outer layer.

To prepare the inner layer a 3 wt/vol% solution of poly(TMC) in chloroform was prepared and sugar crystals (<20µm) in a 15/85 (wt/wt) polymer/sugar ratio were added under vigorous stirring. The obtained mixture was subsequently degassed for 45 min. A glass mandrel (ϕ=1.5±0.1 mm) was immersed (5 mm/s) in this suspension, pulled out (5 mm/s) and the chloroform was allowed to evaporate at room temperature for 15 min. This procedure was repeated one more time and the tube was dried in air overnight. The outer layer fibers were spun as previously described. Fiber spinning and winding were carried out over a length of 25 mm for 40 min and subsequently the graft was dried in air overnight. The grafts were removed from the glass mandrels after 5-20 min of immersion in cold (-30°C) ethanol and dried overnight in a vacuum oven at room temperature. The sugar was leached out for 2 wks in distilled water (the water was renewed several times) and the remaining structures were dried at room temperature under reduced pressure and stored at -20°C till further use.

Nerve Guide Characterization

Morphology.

The inside and outside surfaces of the prepared guides, as well as their cross-sectional areas, were examined by scanning electron microscopy (SEM). Cross sections were prepared by breaking the tubes in liquid nitrogen. The samples were dried overnight under vacuum and coated with a gold layer using a Polaron E5600 sputter-coater (UK). SEM analyses were carried out using a Hitachi S800 (Japan) field emission scanning electron microscope at voltages of 3-5 kV.

Kinking resistance.

The kinking resistance of the prepared nerve guides was evaluated in a semi-guided bending test. In accordance with the terminology described in ASTM norm E6-89, the bending radius and bending angle are defined as shown in Figure 1.
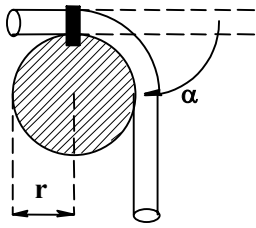
Bending angle (α): change in angle between both legs of the tube during the bend test, before release of the force.

Bending radius (r): radius of the rod around which the tube is bent.

Figure 1. Set-up for the semi-guided bend test.

The nerve guides were bent around rods of decreasing diameter (30, 22, 16, 15, 10 and 6 mm). The bending angle ranged between 45-135° depending on the length of the nerve guide.

The kinking resistance of the nerve guides was rated according to the following scoring system:

(+) non-kinking: the cross-sectional area of the conduit stays intact during bending;

(±) moderate kinking: the cross-sectional area of the conduit decreases slightly at one or more positions;

(-) strong kinking: the cross-sectional area of the conduit is completely constricted at one or more positions.

In Vivo Implantation

Prior to implantation, the nerve guides were cut into the desired dimensions (in liquid nitrogen) and sterilized by rinsing for 10 s in a 70 vol% ethanol solution, followed by rinsing during 30 s in sterile water. Female Wistar rats (weighing 220-240 g) were anaesthetized and the left sciatic nerve was isolated at the midthigh level via a dorsal approach and a 2 mm nerve segment was dissected. The nerve stumps were inserted into 10 mm nerve guides over a distance of 2 mm at each side, so that a 6 mm gap remained. Tissucol® (Immuno AG, Austria) was used to glue the nerve ends to the tube. The wound was closed in layers. The rats were divided in three groups according to the graft used:

Group I (n=6): two-ply nerve guides consisting of a non-porous poly(TMC) inner layer and a macroporous poly(TMC-CL) outer layer;

Group II (n=6): two-ply nerve guides consisting of a microporous poly(TMC) inner layer and a macroporous poly(TMC-CL) outer layer;

Group III (n=12): autografts (used as a control).

After 12 weeks, the grafted sciatic nerve was resected, cleaned and mounted in a nerve chamber developed to measure propagating action potentials[28]. Increasing stimulus voltages were applied to the regenerated nerve fibers and the resulting

compound action currents were measured. In this way the maximum charge displaced (Q_{max}), the mean conduction velocity (MCV) and the mean voltage threshold (V_{50}) were determined. A Chi-square test was performed to identify the regenerated nerve fibers that show electrophysiological response within each of the groups. For the positive responses, values for Q_{max}, MCV and V_{50} were analyzed using one-way ANOVA, followed by Tukey's least significant differences multiple comparisons test to investigate differences between the groups. Differences were considered significant when $p < 0.05$.

RESULTS AND DISCUSSION

In a previous study (see Appendix A) we have reported that the use of two-ply poly(CL) nerve guides consisting of a microporous inner layer and a fibrous macroporous outer layer in the correction of 6 mm nerve defects in the rat sciatic nerve gap model resulted in significantly better nerve regeneration than that observed with nerves grafted with similar conduits with a non-porous inner layer. Despite the fact that the outer layer of the two-ply guides has excellent flexing and handling characteristics, the higher stiffness of the thin inner layer results in a relatively low flexibility of the conduits and strong kinking behavior at small bending radii. Such behavior resulted in lower handling capabilities during surgery, making the telescoping of the nerve stumps into the nerve guides sometimes difficult. This might also have had a detrimental effect on the nerve regeneration process. Furthermore, the relative stiffness and the less than optimal flexibility of the conduits may result in a poorer regeneration outcome as, due to the animal limb movement, pressure exerted by the rim of the relatively rigid tubes may lead to nerve damage[11].

In the present study we prepared two-ply nerve guides consisting of a poly(TMC) microporous inner layer and non-woven macroporous outer layer based on a copolymer of TMC and CL with 10 mol% of TMC. With the TMC based inner layer we intend to improve the flexing characteristics and biological behavior of the conduits. Poly(TMC) is an amorphous (see Table 1) elastomeric material[25] and in a series of TMC and CL (co)polymers, was found to provide the best surface for Schwann cell adhesion and proliferation[30]. This copolymer is less crystalline than poly(CL)[25] and by using it in the preparation of the outer layer we expect to further improve the flexing and kinking resistance of the outer layer.

Nerve Guide Preparation and Characterization

In the fabrication of the two-ply nerve grafts dip-coating techniques were combined with fiber winding techniques for the preparation of the inner and outer layers of the conduit, respectively.

The preparation of porous tubular structures using dip-coating techniques is based on the principle of phase inversion. As the inner layer of the nerve guide has as function to allow the exchange of fluids but also to establish a barrier for the ingrowth of fibrous tissue, the pore size should be in the order of a few micrometers[21].

The dimensions of the pores in the outer layer should be in the range of approximately 25 to 150 μm. Previous studies have shown that this pore size range facilitates vascularization and fibrous tissue ingrowth, which can have a positive effect on the process of regeneration and maturation of the nerve[21,23]. In this study, a non-woven layer of helically wound fibers around the dip-coated inner layer will constitute the outer layer of the grafts. The fibers were spun from solution in a similar procedure to the one described by Leidner et al[31]. This method was chosen as the obtained structures have excellent flexing characteristics, bending with a minimal reduction of the cross-sectional area of the graft lumen. The spinning of fibers from the polymer increases the strength of the wall of the nerve guide by orientation of the polymer fibers. In order for a polymer to be processable by dry-spinning and winding, the polymer solution needs to form fibers that can be stretched without breaking.

Figure 2 shows a cross-section of one of the prepared two-ply nerve guides consisting of a non-porous poly(TMC) inner layer. The inner layer was obtained by evaporation of the solvent (chloroform) after dip-coating (Figure 2.B).

As previously observed in the preparation of two-ply poly(CL) nerve guides, fibers could not be spun from pure poly(TMC-CL) solutions, but were only obtained after the addition of a small amount (1.5% of the total polymer weight) of high molecular weight PEO to the copolymer solutions. By winding fibers spun from the copolymer solutions containing PEO a regular macroporous outer layer was obtained (Figure 3), which was firmly attached to the inner layer (Figure 2.B). Such firm bonding between layers is necessary to prevent the collapse of the thin inner layer of the conduit. The first spun fibers bind to the dip-coated layer as at the moment of contact the polymer fiber still contains solvent. A similar process is responsible for the observed fiber confluence (fiber-to-fiber bonding), which is an essential feature to guarantee the dimensional stability of these structures[32]. The

pore size determined by SEM of the outer layer of the two-ply nerve guides ranged between 15 and 265 μm, with an average value of approximately 60 μm. The pore size was defined as the distance between two fibers located on the same plane[31]. The fiber diameter varied between 5 to 10 μm and the angle of winding (angle between the fiber and the longitudinal axis of the conduit) was approximately 64°.
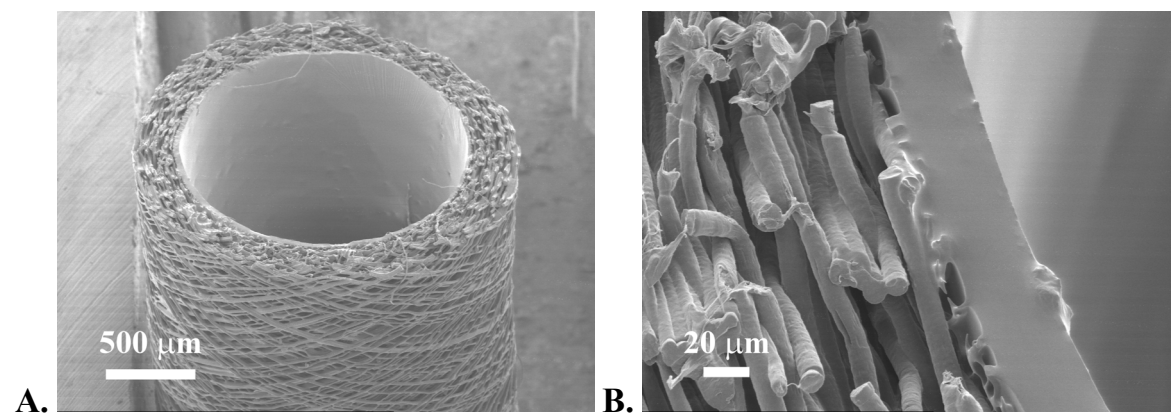

Figure 2. Scanning electron micrographs of cross-sections of a two-ply nerve guide consisting of a non-porous poly(TMC) inner layer and a macroporous poly(TMC-CL) outer layer. (A) Overview. (B) Detail of the connection between the two layers.
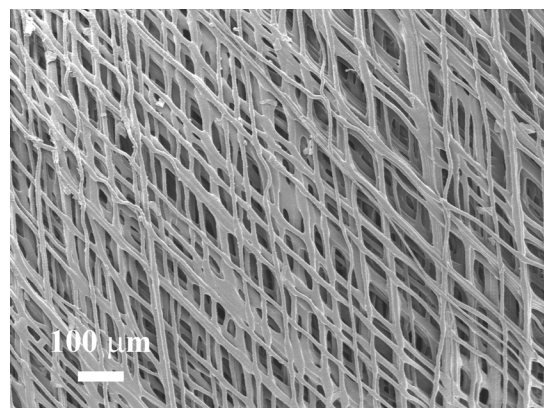

Figure 3. Scanning electron micrograph of the outer surface of the two-ply nerve guides poly(TMC-CL) macroporous outer layer.

A microporous inner layer was obtained by combining phase inversion and particulate leaching techniques. A suspension of the polymer and sugar particles was cast onto a glass rod by dip-coating. Evaporation of the solvent induces polymer solidification and the sugar particles remain entrapped in the polymer matrix. When these particles are extracted with water they leave behind an interconnected network of pores. Figure 4 shows a section of one of the prepared two-ply nerve guides. The inner layer consists of an interconnected network of pores in the size range of 1-13 μm, which is open both at the inner and outer surface (see Figure 5 – nerve guide inner surface). The outer layer was firmly connected to

the inner layer (Figure 4.B) so that the latter attained an optimal resilience. In this case this firm connection between layers is of even more importance. We have previously found that porous poly(TMC) films prepared by the combined use of immersion precipitation and particulate leaching techniques show extensive shrinking and collapse of pores during extraction of the porosifying agents[25]. Therefore, in the present study the leaching of the sugar particles was only performed after the outer layer of fibers was wound to impede collapsing and shrinking of the inner porous structure. The two-week period allowed for leaching of the sugar particles was sufficient to guaranty complete removal of the porosifying agent.
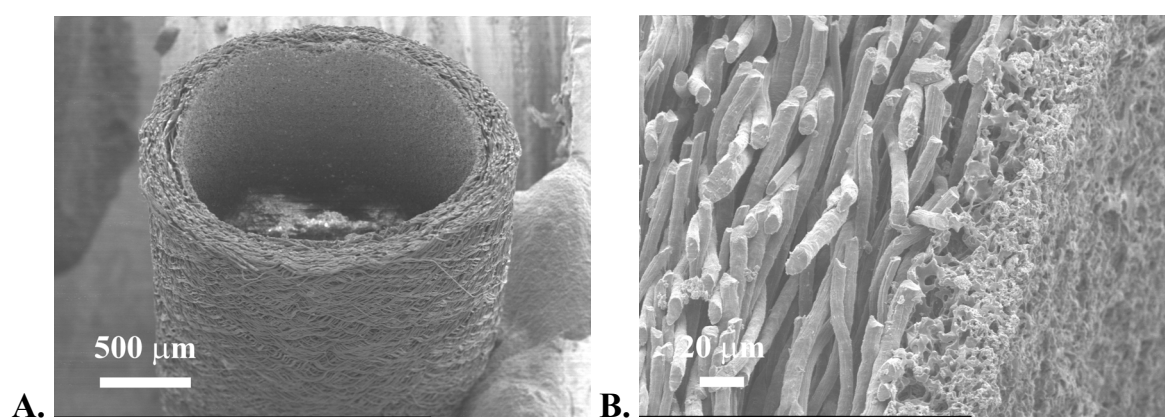
Figure 4. Scanning electron micrographs of cross-sections of a two-ply nerve guide consisting of a microporous poly(TMC) inner layer and a macroporous poly(TMC-CL) outer layer. (A) Overview. (B) Detail of the connection between the two layers.

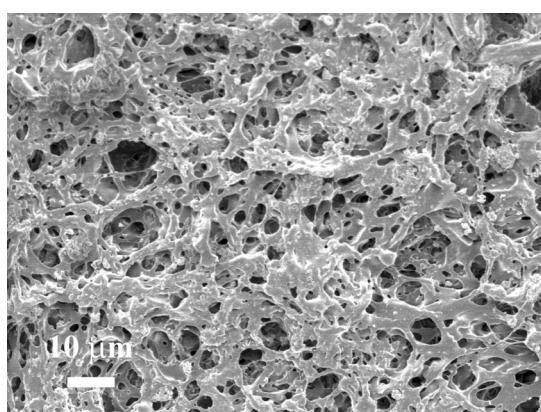**Figure 5.** Scanning electron micrograph of the inner surface of the two-ply nerve guides with a poly(TMC) microporous inner layer.

The average dimensions and pore characteristics of the prepared two-ply conduits and their flexing characteristics are summarized in Table 2.

Table 2. Characterization of two-ply nerve guides based on TMC and CL (co)polymers.

Tube features	Inner diameter (mm)	Wall thickness (µm)		Pore size (µm)		Kinking resistance at different bending radii (mm)					
		Inner layer	Outer layer	Inner layer	Outer layer	15	11	8	7.5	5	3
Non-porous inner layer	1.5	27	235	-	57 (15-265)	+	+	+	+	±	±
Microporous inner layer	1.5	30	179	5 (1-13)	40 (15-80)	+	+	+	+	+	+

Note: Average values of all parameters are presented. Additionally the pore size variation range is presented in brackets.

(+) non-kinking: the cross-sectional area of the conduits stays intact during bending;

(±) moderate kinking: the cross-sectional area of the conduits decreases slightly at one or more positions;

(-) strong kinking: the cross-sectional area of the conduits is completely constricted at one or more positions.

The inner diameter of the conduits and the average pore size of the inner layer of the permeable two-ply conduit were in accordance with the mandrel and sugar particle dimensions, respectively.

Although an optimal thickness has not been defined for nerve guides, thin non-collapsible tubes tend to perform best[5,15]. Therefore, the overall thickness of the nerve guides was minimized provided that the thickness of the inner layer would not compromise the flexibility of the conduits and that the outer layer assured sufficient strength and dimensional stability to prevent the lumen of the tube to collapse.

An important property of a flexible nerve guide, often disregarded, is its ability to bend with minimal reduction in (internal) cross-sectional area. In the present study the bending properties of the nerve guides were evaluated by determining their kinking resistance upon bending.

Silicone tubes are commonly used as nerve grafts in nerve regeneration studies in animal models[14] as well as in clinical practice as an alternative to autografts[1]. Although silicone conduits are non-degradable, which is a major drawback of these systems, they show good mechanical performance in the nerve grafting procedure. Therefore, silicone tubing of similar dimensions as the nerve guides described in this study (inner diameter: 1.47 mm and wall thickness: 245 µm; Helix Medical, CA, USA) was also tested, and used as a reference. For all tested bending radii, silicone tubing showed non-kinking behavior.

The two-ply tube with a microporous inner layer showed the best performance, behaving in a similar manner to the silicone tubing. The conduits with a non-porous inner layer were also very flexible, but at the smallest bending radius showed weaker resistance to kinking with the cross-sectional area of the conduit decreasing slightly at one or more positions. Both types of two-ply tubes showed improved flexing characteristics over comparable poly(CL) conduits (Appendix A).

The good flexing properties of the conduits are the result of the anisotropic properties of the macroporous outer layer[31]. Due to the angle of 64° at which the fibers are wound, the tubes are stiffer in the hoop than in the longitudinal direction. This allows the lumen of the conduits to remain open during flexing.

Nerve Guide Implantation

The TMC and CL (co)polymer based conduits described in the previous paragraphs were evaluated as nerve grafts in the correction of 6 mm gaps in the rat sciatic nerve. In line with their flexing properties, two-ply nerve guides with non-porous or microporous poly(TMC) inner layers exhibited good handling characteristics in surgery. The telescoping of the nerve stumps into the nerve guide could be done with ease. The grafts were smooth and embraced the nerve like a 'soft sleeve'. The nerve ends could be easily secured to the nerve guides with Tissucol®.

Nerve Regeneration Evaluation

At 12 wks post-implantation it was possible to observe that in all groups of animals a bundle of tissue had grown through the nerve graft and bridged the nerve gap. Although the site of implantation could be easily identified for the groups operated with the artificial conduits (groups I and II) the conduits could not be retrieved intact as they had degraded to some extent.

The results of electrophysiological evaluations of the nerve fibers regenerated through the different grafts are presented in Figures 6, 7 and 8.

Q_{max} is a measure of the maximum charge displaced through the nerve fibers and is dependent on the diameter as well as on the number of regenerated and pulse-conducting axons. The MCV is mainly determined by the diameter of the regenerated axons[33]. Higher MCV is observed for axons with a larger diameter. The extra-cellular firing threshold of nerve fibers is inversely proportional to the fiber diameter[34]. Therefore, V_{50} (the voltage at 50% Q_{max}, a parameter for the voltage needed to stimulate the excitable axons) is expected to be smaller for axons with a larger diameter[28].

The Q_{max} determined for nerve fibers regenerated through the artificial nerve grafts was significantly lower than the value obtained for nerve fibers regenerated through autografts (Figure 6). Q_{max} observed for both groups treated with the artificial grafts was not significantly different. MCV (Figure 7) and V_{50} (Figure 8) were not significantly different for the two-ply nerve guide (non-porous or microporous inner layer) and autograft groups.
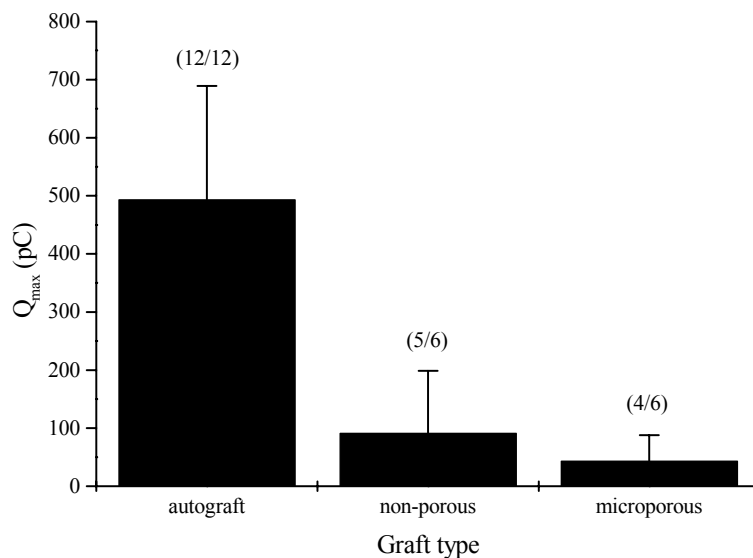

Figure 6. Maximum charge displacement (Q_{max}) for the different groups of animals subjected to nerve grafting with, respectively, nerve autografts and two-ply poly(TMC)/poly(TMC-CL) nerve guides (non-porous and microporous poly(TMC) inner layers). Mean ± standard deviation of the results for the individuals that show electrophysiological response (the number of positive responses over the number of implanted grafts is presented in brackets).

Although Q_{max} of the nerves grafted with the two-ply conduits was still significantly smaller compared to the values found for the autografted nerves, MCV and V_{50} were not significantly different between the three groups, suggesting that the individual diameter of the regenerated axons in the two-ply grafts is in a similar range compared to the diameter of the regenerated axons in the autografts[28].
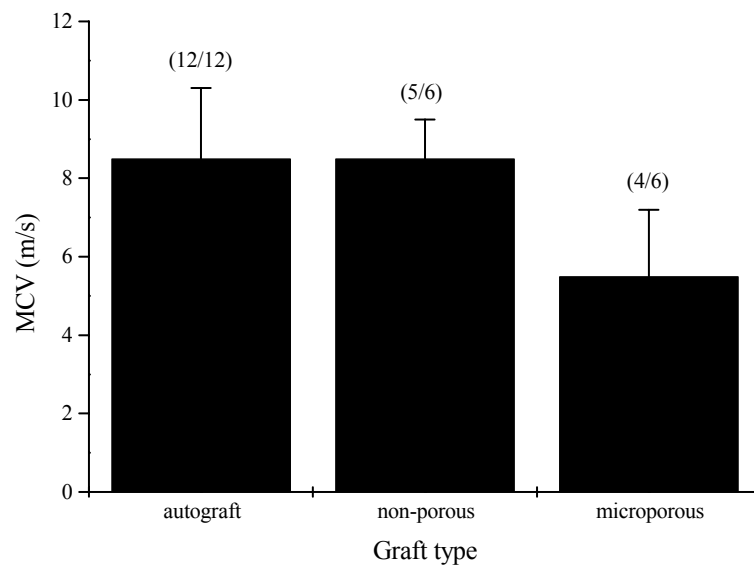
Figure 7. Mean conduction velocity (MCV) for the different groups of animals subjected to nerve grafting with, respectively, nerve autografts and two-ply poly(TMC)/poly(TMC-CL) nerve guides (non-porous and microporous poly(TMC) inner layers). Mean ± standard deviation of the results for the individuals that show electrophysiological response (the number of positive responses over the number of implanted grafts is presented in brackets).

Figure 8. Mean voltage threshold (V_{50}) for the different groups of animals subjected to nerve grafting with, respectively, nerve autografts and two-ply poly(TMC)/poly(TMC-CL) nerve guides (non-porous and microporous poly(TMC) inner layers). Mean ± standard deviation of the results for the individuals that show electrophysiological response (the number of positive responses over the number of implanted grafts is presented in brackets).
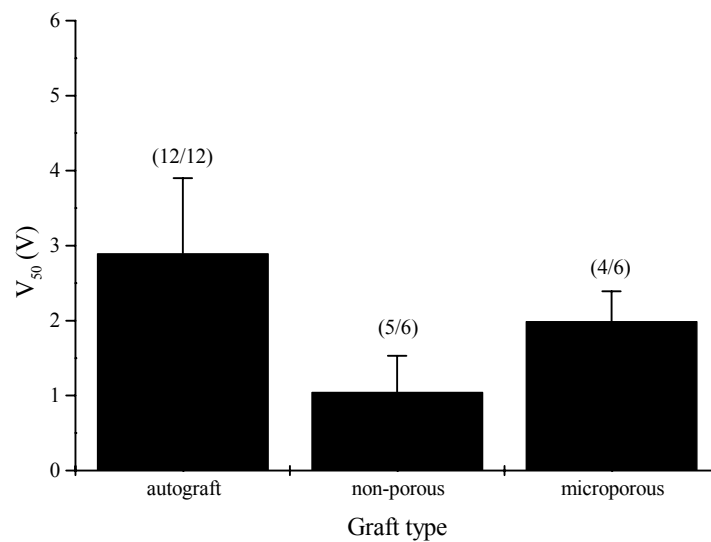
215

When comparing the results obtained with the TMC and CL (co)polymer based nerve guides with the ones obtained with the poly(CL) microporous two-ply conduits (Appendix A), a better outcome in terms of nerve regeneration (higher number of positive electrophysiological responses) was observed when the former conduits were used. This may be the result of a combination of factors such as a better surgical handling performance of the conduits during the grafting procedure, improved flexing properties and the more favorable surface to cell-material interactions provided by the poly(TMC) inner layer[30]. However, in the present study no significant improvement in nerve regeneration was found when a two-ply conduit with a microporous inner layer was used instead of a non-permeable conduit. In subcutaneous implantations of poly(TMC) films enzymatic erosion leads to pitting of the surface[27]. Small pores may, therefore, have been formed within a few days after implantation of the guides. This may lead to increased permeability of the initially non-porous poly(TMC) inner layer. In fact, the described mechanism of resorption of poly(TMC) *in vivo*, which does not involve encapsulation of the implant, may have further implications for the nerve regeneration process, as the cells involved in the phagocytosis of the polymer particles are inflammatory cells like macrophages[35]. In the natural process of nerve repair, macrophages are recruited into the peripheral nerves at the site of the injury and have an important role in initiating Schwann cell and fibroblast mitosis and inducing these cells to produce nerve growth factors[36-38].

The degradation of the nerve conduits we observed, is in line with the previously reported degradation rates *in vivo* for poly(TMC) and the TMC-CL copolymer[27]. Histological examination of the regenerated tissue and target muscles is presently under way and will give us further insight into the regeneration process. These studies will also allow the assessment of the extent of resorption of the conduits *in situ* and to determine if the degradation rates were as required.

CONCLUSIONS

Pliable two-ply nerve conduits of adequate dimensions and pore sizes, comprising a poly(TMC) inner layer and a poly(TMC-CL) (11:89 mol%) macroporous outer layer were reproducibly prepared.

Their good handling characteristics during surgery and the electrophysiological properties of the regenerated nerve fibers indicate that these conduits, independent

of the inner layer structure, can serve as support for axonal guidance. However, the results obtained for regenerated nerve fibers through autografts were still better than the results obtained with the artificial nerve grafts. This indicates the need to supplement the nerve guides with a nerve regenerating stimulatory agent. The use of cultured Schwann cells as a mean of enhancing nerve regeneration seems logical, as these cells play an important role in the nerve regeneration process by producing extracellular matrix proteins and a range of neurotropic and neurotrophic factors that are essential to the growth of neurons[39-42].

ACKNOWLEDGMENTS

REFERENCES

[1]   Lundborg G, Rosen B, Dahlin L, Danielsen N, Holmberg J. Tubular *versus* conventional repair of median and ulnar nerves in the human forearm: early results from a prospective, randomized, clinical study. *J Hand Surg [Am]* 1997; 22: 99-106.

[2]   Merle M, Dellon AL, Campbell JN, Chang PS. Complications from silicon-polymer intubulation of nerves. *Microsurgery* 1989; 10: 130-133.

[3]   Madison R, Sidman RL, Nyilas E, Chiu T-H, Greatorex D. Nontoxic nerve guide tubes support neovascular growth in transected rat optic nerve. *Exp Neurol* 1984; 86: 448-461.

[4]   Kiyotani T, Teramachi M, Takimoto Y, Nakamura T, Shimizu Y, Endo K. Nerve regeneration across a 25-mm gap bridged by a polyglycolic acid-collagen tube: a histological and electrophysiological evaluation of regenerated nerves. *Brain Res* 1996; 740: 66-74.

[5]   den Dunnen WFA, van der Lei B, Robinson PH, Holwerda A, Pennings AJ, Schakenraad JM. Biological performance of a degradable poly(DL-lactide-ε–caprolactone) nerve guide: Influence of tube dimensions. *J Biomed Mater Res* 1995; 29: 757-766.

[6]   Langone F, Lora S, Veronese FM, Caliceti P, Parnigotto PP, Valenti F, Palma G. Peripheral nerve repair using a poly(organo)phosphazene tubular prosthesis. *Biomaterials* 1995; 16: 347-353.

[7]   Aldini NN, Perego G, Cella GD, Maltarello MC, Fini M, Rocca M, Giardino R. Effectiveness of a bioabsorbable conduit in the repair of peripheral nerves. *Biomaterials* 1996; 17: 959-962.

[8]   Chamberlain LJ, Yannas IV, Hsu H-P, Spector M. Histological response to a fully degradable collagen device implanted in a gap in the rat sciatic nerve. *Tissue Eng* 1997; 3: 353-362.

[9]   Mackinnon SE, Dellon AL. A study of nerve regeneration across synthetic (Maxon) and biologic (collagen) nerve conduits for nerve gaps up to 5 cm in the primate. *J Reconstr Microsurg* 1990; 6: 117-121.

[10]   Rodriguez FJ, Gomez N, Perego G, Navarro X. Highly permeable polylactide-caprolactone nerve guides enhance peripheral nerve regeneration through long gaps. *Biomaterials* 1999; 20: 1489-1500.

[11]   Henry EW, Chiu TH, Nyilas E, Brushart TM, Dikkes P, Sidman RL. Nerve regeneration through biodegradable polyester tubes. *Exp Neurol* 1985; 90: 652-676.

[12]   Navarro X, Kennedy WR. Sweat gland reinnervation by sudomotor regeneration after different types of lesions and graft repairs. *Exp Neurol* 1989; 104: 229-234.

[13]   Evans GRD, Brandt K, Widmer M, Gürlek A, Savel T, Gupta P, Lohman R, Williams J, Hodges J, Nabawi A, Patrick C, Mikos AG, "Tissue engineered conduits: the use of biodegradable poly-DL-lactic-co-glycolic acid (PLGA) scaffolds in peripheral nerve regeneration" In: Stark GE, Horch R, Tanczos E. *Biological matrices and tissue reconstruction*, Berlin: Spinger; 1998. p 225-235.

[14]   Dahlin LB, Lundborg G. Use of tubes in peripheral nerve repair. *Neurosurg Clin N Am* 2001; 12: 341-352.

[15]   Buti M, Verdu E, Labrador RO, Vilches JJ, Fores J, Navarro X. Influence of physical parameters of nerve chambers on peripheral nerve regeneration and reinnervation. *Exp Neurol* 1996; 137: 26-33.

[16]   Aebischer P, Valentini RF, Winn SR, Kunz S, Sasken H, Galletti PM. Regeneration of transected sciatic nerves through semi-permeable nerve guidance channels. Effects of extracellular matrix protein additives. *ASAIO Trans* 1986; 32: 474-477.

[17]   Kim DH, Connolly SE, Zhao S, Beuerman RW, Voorhies RM, Kline DG. Comparison of macropore, semipermeable, and nonpermeable collagen conduits in nerve repair. *J Reconstr Microsurg* 1993; 9: 415-420.

[18]   den Dunnen WF, Meek MF, Grijpma DW, Robinson PH, Schakenraad JM. *In vivo* and *in vitro* degradation of poly[50/50 (85/15 L/D)LA/ε-CL], and the implications for the use in nerve reconstruction. *J Biomed Mater Res* 2000; 51: 575-585.

[19] Valentini RF, "Nerve guidance channels" In: Bronzino JD. *The Biomedical Engineering Handbook*, Boca Raton, FL: CRC Press; 1995. p 1985-1996.

[20] Heath CA, Rutkowski GE. The development of bioartificial nerve grafts for peripheral-nerve regeneration. *Trends Biotechnol* 1998; 16: 163-168.

[21] Hoppen HJ, Leenslag JW, Pennings AJ, van der Lei B, Robinson PH. Two-ply biodegradable nerve guide: basic aspects of design, construction and biological performance. *Biomaterials* 1990; 11: 286-290.

[22] Grijpma DW, Zondervan GJ, Pennings AJ. High molecular weight copolymers of L-lactide and ε-caprolactone as biodegradable elastomeric implant materials. *Polym Bull* 1991; 25: 327-333.

[23] den Dunnen WFA, Schakenraad JM, Zondervan GJ, Pennings AJ, van der Lei B, Robinson PH. A new PLLA/PCL copolymer for nerve regeneration. *J Mater Sci: Mater Med* 1993; 4: 521-525.

[24] den Dunnen WF, van der Lei B, Schakenraad JM, Blaauw EH, Stokroos I, Pennings AJ, Robinson PH. Long-term evaluation of nerve regeneration in a biodegradable nerve guide. *J Microsurg* 1993; 14: 508-515.

[25] Pêgo AP, Poot AA, Grijpma DW, Feijen J. Copolymers of trimethylene carbonate and ε-caprolactone for porous nerve guides: synthesis and properties. *J Biomater Sci Polym Ed* 2001; 12: 35-53. Chapter 3 of this thesis.

[26] Pêgo AP, Poot AA, Grijpma DW, Feijen J. *In vitro* degradation of trimethylene carbonate based (co)polymers. *Macromol Chem Phys (accepted for publication)* Chapter 6 of this thesis.

[27] Pêgo AP, van Luyn MJA, Brouwer LA, van Wachem PB, Poot AA, Grijpma DW, Feijen J. *In vivo* behavior of poly(1,3-trimethylene carbonate) and copolymers of 1,3-trimethylene carbonate with D,L-lactide or ε-caprolactone. Degradation and tissue response. *(submitted to J Biomed Mater Res, 2002)* Chapter 7 of this thesis.

[28] Vleggeert-Lankamp CLAM, van den Berg RJ, Lakke EAJF, Malessy MJA, Thomeer RTWM. Increased firing threshold and refractory period of the Aα- and Aß-fibers in the autografted rat sciatic nerve. *(manuscript in preparation)*.

[29] Crescenzi V, Manzini G, Calzolari G, Borri C. Thermodynamics of fusion of poly-β-propiolactone and poly-ε-caprolactone. Comparative analysis of the melting of aliphatic polylactone and polyester chains. *Eur Polym J* 1972; 8: 449-463.

[30] Pêgo AP, Vleggeert-Lankamp CLAM, Deenen M, Lakke EAJF, Grijpma DW, Poot AA, Marani E, Feijen J. Adhesion and growth of human Schwann cells on trimethylene carbonate (co)polymers. *(submitted to J Biomed Mater Res, 2002)* Chapter 9 of this thesis.

[31] Leidner J, Wong EWC, MacGregor DC, Wilson GJ. A novel process for the manufacturing of porous grafts: process description and product evaluation. *J Biomed Mater Res* 1983; 17: 229-247.

[32] Bots JG. "Polyethers as biomaterials" Ph.D. Thesis. University of Twente, Enschede, The Netherlands. 1988.

[33] Hursh JB. Conduction velocity and diameter of nerve fibers. *Am J Physiol* 1939; 127: 131-139.

[34] Jack JJB, Noble D, Tsien RW, *Electric current flow in excitable cells*. Oxford: Oxford University Press; 1983.

[35] Fansa H, Schneider W, Keilhoff G. Revascularization of tissue-engineered nerve grafts and invasion of macrophages. *Tissue Eng* 2001; 7: 519-524.

[36] Brown MC, Perry VH, Lunn ER, Gordon S, Heumann R. Macrophage dependence of peripheral sensory nerve regeneration: possible involvement of nerve growth factor. *Neuron* 1991; 6: 359-370.

[37] Dahlin LB. Prevention of macrophage invasion impairs regeneration in nerve grafts. *Brain Res* 1995; 679: 274-280.

[38] Miyauchi A, Kanje M, Danielsen N, Dahlin LB. Role of macrophages in the stimulation and regeneration of sensory nerves by transposed granulation tissue and temporal aspects of the response. *Scand J Plast Reconstr Surg Hand Surg* 1997; 31: 17-23.

[39] Terenghi G. Peripheral nerve injury and regeneration. *Histol Histopathol* 1995; 10: 709-718.

[40] Son Y-J, Thompson WJ. Schwann cell processes guide regeneration of peripheral axons. *Neuron* 1995; 14: 125-132.

[41] Fu SY, Gordon T. The cellular and molecular basis of peripheral nerve regeneration. *Mol Neurobiol* 1997; 14: 67-116.

[42] Frostick SP, Yin Q, Kemp GJ. Schwann cells, neurotrophic factors, and peripheral nerve regeneration. *Microsurgery* 1998; 18: 397-405.

CHAPTER 11

Preparation of degradable porous structures based on 1,3-trimethylene carbonate and D,L-lactide (co)polymers for heart tissue engineering*

A.P. PÊGO[1], B. SIEBUM[1], M.J.A. VAN LUYN[2], X.J. GALLEGO y VAN SEIJEN[2], A.A. POOT[1], D.W. GRIJPMA[1], and J. FEIJEN[1]

[1] *Institute for Biomedical Technology (BMTI) and Department of Polymer Chemistry and Biomaterials, Faculty of Chemical Technology, University of Twente, P.O. Box 217, 7500 AE Enschede, The Netherlands*

[2] *Department of Pathology & Lab. Medicine, Medical Biology, Tissue Engineering, Faculty of Medical Sciences, University of Groningen, Hanzeplein 1 - Entrance 25, 9713 GZ Groningen, The Netherlands*

ABSTRACT

Biodegradable porous scaffolds for heart tissue engineering were prepared from amorphous elastomeric (co)polymers of 1,3-trimethylene carbonate (TMC) and D,L-lactide (DLLA). Leaching of salt from compression-molded polymer/salt composites allowed the preparation of highly porous structures in a reproducible fashion. By adjusting the salt particle size and the polymer to particle weight ratio in the polymer/salt composite preparation the pore size and porosity of the scaffolds could be precisely controlled. The thermal properties of the polymers used for the scaffold preparation had a strong effect on the morphology, mechanical properties and dimensional stability of the scaffolds at physiological conditions. Interconnected highly porous structures (porosity 94% and average pore size 100 µm) based on a TMC-DLLA copolymer (19:81 mol%) had suitable mechanical properties and displayed adequate cell-material interactions to serve as scaffolds for cardiac cells. This copolymer is non-cytotoxic and allows the adhesion and proliferation of cardiomyocytes. During incubation in phosphate buffered saline at 37°C, these scaffolds were dimensionally stable and the number average molecular weight ($\overline{M}n$) of the polymer decreased gradually from 2.0×10^5 to 0.3×10^5 in a period up to 4 months. The first signs of mass loss (5%) were detected after 4 months of incubation. The

---

221

degradation behavior of the porous structures was similar to that of non-porous films with similar composition and can be described by autocatalyzed bulk hydrolysis.

INTRODUCTION

Post-ischemic heart failure is a major health issue in Western countries[1]. Therapeutic options for the treatment of end-stage cardiac failure are limited, with cardiac transplantation being the most accepted clinical treatment. Because of the lack of donor organs, alternatives have to be developed. Replacing the damaged tissue with newly grown material from autologous origin can be a very promising treatment to prevent post-ischemic complications[2-6]. Three-dimensional engineered cardiac tissue could also provide an alternative to the currently used grafts for repair of cardiac defects in patients with congenital heart diseases[7-9], as the grafts currently available, made of materials such as expanded polytetrafluoroethylene or glutaraldehyde-treated xenopericardium, lack growth potential and are non-contractile.

In the tissue engineering approach to cardiomyoplasty, cardiomyocytes are incorporated into a scaffold that is implanted in or onto the scar tissue. The scaffold should initially act as an adhesive substrate and a physical support for the cells. During proliferation of the cells and production of extra cellular matrix, the scaffold should degrade leaving in its place a new patch of tissue[8].

In order to allow the development of myocardial tissue, the scaffold should be made from a biocompatible material that can be reproducibly processed into three-dimensional porous structures that are dimensionally stable under physiological conditions. Furthermore, the mechanical properties of the scaffolding material should be adequate to provide the correct micro-stress environment for the cells to develop the required phenotype and orientation. Therefore, the scaffold should be very flexible in order to allow the contraction of the growing tissue and to stand the contractions of the surrounding myocardium after implantation.

A number of natural and synthetic materials are currently being employed as scaffolds in tissue engineering. These include alginates[10], collagen gels and fibers[2], poly(glycolic acid)[11], poly(lactic acid)[12,13], as well as their copolymers[14]. Synthetic, biodegradable polymers are an attractive choice due to the controlled manner in which they can be manufactured and the possibility of tuning their macrostructure, mechanical properties and degradation profile.

Polymers based on glycolide and lactide can have important drawbacks for use in the preparation of scaffolds for heart tissue engineering such as incompatible mechanical properties and too high rates of degradation[9]. The recent development of copolymers with high elasticity and a controllable degradation profile[15-18] opens an entirely new perspective in this field[19].

We have previously reported on the properties of poly(ester carbonate)s based on poly(1,3-trimethylene carbonate) (poly(TMC)) as elastomeric materials with potential use in soft tissue engineering. High molecular weight copolymers of TMC and D,L-lactide (DLLA) with 20 and 50 mol% of TMC are amorphous and relatively strong elastomers under physiological conditions[20]. When subjected to hydrolytic degradation *in vitro* these copolymers maintained suitable mechanical properties up to 3 months and resorbed in less than a year[21]. In a separate study the *in vivo* degradation of the copolymer with 50 mol% of TMC was evaluated by subcutaneous implantation of polymer films in the back of rats. The material showed a similar degradation profile to that observed *in vitro*. During degradation and resorption of the polymer only a mild tissue reaction was observed[22].

The aim of this study was to assess the potential use of copolymers of TMC and DLLA with 20 and 50 mol% of TMC as materials to produce flexible three-dimensional scaffolds for heart tissue engineering. Porous scaffolds were prepared via a process involving the combination of coprecipitation, compression molding and salt-leaching techniques[23]. The dimensional stability and degradation in phosphate buffered saline (PBS) at 37°C of a selection of the prepared porous scaffolds was monitored over a period of 16 weeks. The most promising structures were further tested for the effect of sterilization by gamma-radiation on the morphology and stability of the porous scaffolds and on the extent of degradation of the polymer used in the preparation of the scaffolds.

MATERIALS AND METHODS

Materials

Polymer grade 1,3-trimethylene carbonate (TMC) and D,L-lactide (DLLA) were obtained, respectively, from Boehringer Ingelheim, Germany and Purac Biochem, The Netherlands. Stannous octoate (SnOct$_2$) (stannous 2-ethylhexanoate) was used as received from Sigma, USA. Sodium chloride (NaCl) (Merck, Germany), used as porosifying agent in the preparation of porous structures, was fractionated before

use with standard test sieves (Endecotts, UK) with mesh sizes of 63, 106 and 250 μm. Except for chloroform and pentane that were of analytical grade (Biosolve, The Netherlands), all the other used solvents were of technical grade (Assink BV, The Netherlands).

Polymer Synthesis

Poly(TMC) and copolymers of TMC and DLLA with 20 and 50 mol% of TMC were synthesized as previously described[20]. Briefly, polymerizations were conducted by ring-opening polymerization in evacuated and sealed glass ampoules using $SnOct_2$ as catalyst. All polymerizations were carried out for a period of 3 days at 130°C±2°C. Poly(DLLA) was polymerized under nitrogen atmosphere at 140-150°C for 3 hrs with 0.1 wt% of $SnOct_2$. The polymers were purified by dissolution in chloroform and subsequent precipitation into an excess of isopropanol. The precipitated polymers were recovered, washed with fresh isopropanol and dried under reduced pressure at room temperature.

Polymer Characterization

<u>Nuclear magnetic resonance (NMR) spectroscopy</u>. A Varian Inova 300 MHz spectrometer (USA) was used for molar composition analysis. ^{1}H-NMR spectra were recorded at 300 MHz using solutions of polymers in $CDCl_3$ (Sigma, USA).

<u>Gel permeation chromatography (GPC)</u>. Weight and number average molecular weight ($\overline{M}w$ and $\overline{M}n$, respectively), polydispersity index (PDI) and intrinsic viscosity ([η]) were determined by GPC using a Waters Model 510 pump (USA), a HP Ti-Series 1050 autosampler (USA), a Waters Model 410 Differential Refractometer and a Viscotek H502 Viscometer Detector (USA) with Waters Styragel HR5-HR4-HR2-HR1 columns placed in series. Chloroform was used as eluent at a flow rate of 1.5 ml/min. Narrow polystyrene standards were used for calibration. Sample concentrations of approximately 0.5 wt/vol% and injection volumes of 30 μl were used. All determinations were performed at 25°C.

<u>Differential scanning calorimetry (DSC)</u>. The thermal properties of the purified samples were evaluated by DSC. Samples (5-15 mg) placed in aluminum pans were analyzed with a Perkin Elmer Pyris1 (USA) at a heating rate of 10°C/min. All samples were heated to 40°C above their glass transition temperature. Subsequently, the samples were quenched rapidly (300°C/min) until 40°C below their glass transition temperature and after 5 min a second scan was recorded. The glass

transition temperature (Tg) was taken as the midpoint of the heat capacity change. Indium, gallium and tin were used as standards for temperature calibration.

Film Preparation

Films of the purified polymers were obtained by melt-pressing (Fontijne laboratory press THB008, The Netherlands) at 140°C for 10 min to a final thickness of 200 or 500 μm. The films were rapidly cooled to 15°C under pressure and stored at -20°C until further use.

Cell Culture

Adhesion and proliferation of human umbilical vein endothelial cells (HUVECs). HUVECs were isolated from a single umbilical vein and cultured on the surface of the TMC-DLLA (co)polymers as previously described[24]. Disks with a diameter of 10 mm were punched out of the melt-pressed films (200 μm thickness) and sterilized by incubation in 70 vol% ethanol solution for 15 s, followed by a rinsing step of 30 s in sterile water. After sterilization, individual disks were placed in wells of 48-well tissue culture poly(styrene) plates (TCPS; Costar, USA) and incubated for 30 min with PBS (pH 7.4, NPBI, The Netherlands). After removal of the PBS, the discs were immobilized with sterile rubber rings (Eriks, The Netherlands). HUVECs (passage 2) were seeded on the (co)polymer surface at a density of $4x10^4$ cell/cm^2 in 3 ml of culture medium and incubated at 37°C, in a humidified atmosphere of 5% CO_2 and 95% air. The culture medium consisted of 50 vol% M199 (with Hank's salts) and 50 vol% RPMI 1640 (with 25 mM HEPES) and contained 100 U/ml penicillin, 100 μg/ml streptomycin and 2 mM Glutamax (all from Gibco, UK). Prior to use, the culture medium was supplemented with filter-sterilized pooled human serum (20 vol%). TCPS surfaces were used as positive control. The culture medium was refreshed every two days. Cell numbers were quantified (Bürker chamber) at 6 hrs, 1, 3, 6 and 9 days after seeding.

Cardiomyocyte culture. Rat cardiomyocytes (embryonal rat cardiomyocyte cell line; ATTC: CRL-1446) were cultured using previously described conditions[6] on the surface of poly(TMC-DLLA) (81:19 mol%) copolymer films. Disks with a diameter of 8 mm were punched out of melt-pressed films (200 μm) and sterilized by incubation in 70 vol% ethanol solution as described above. After sterilization, individual disks were placed in tissue culture well-plates. Cardiomyocytes were seeded on the copolymer surface at a density of $5x10^4$ cells/cm^2 and incubated at

37°C, in a humidified atmosphere of 5% CO_2 and 95% air. The culture medium consisted of Dulbecco's Modified Essential Medium (DMEM) enriched with 10 vol% of fetal bovine serum (FBS), 100 U/ml penicillin, 100 μg/ml streptomycin and 1 vol% glutamine (all from Gibco). The status of the cultures was examined for up to 8 days of culture by phase contrast microscopy.

Porous Structure Preparation by a Coprecipitation, Compression Molding and Particulate Leaching Process

Porous structures based on poly(TMC-DLLA) (co)polymers were prepared by leaching of compression molded salt-containing polymer precipitates[23]. The polymers were dissolved in chloroform to a final concentration of 5 wt/vol% and NaCl with a particle size range of 63-106 μm or 106-250 μm was added to the vigorously stirred polymer solutions. The polymer to salt ratio was 5:95 wt/wt%. The salt suspension was precipitated into a ten-fold volume of isopropanol and a fibrous composite was obtained. The precipitated salt/polymer fibers were collected, washed with fresh isopropanol and dried under reduced pressure at room temperature.

The composite materials were melt-pressed in a circular mould (ϕ=14 mm; height=8.4 mm) at 140°C for 11 min and rapidly cooled to 15°C under pressure in the mold. Subsequently, the salt particles were extracted from the disks in gently stirred distilled water for 5 days at 6°C. The water was refreshed each day. Finally, the specimens were freeze-dried overnight and the porous structures were further dried under reduced pressure at room temperature for two more days.

Characterization of the Porous Structures

Morphology. The average pore size and interconnectivity of the porous structures were evaluated by scanning electron microscopy (SEM). Cross-sections of the scaffolds were coated with a gold layer using a Polaron E5600 sputter-coater (UK). SEM analyses were carried out using a Hitachi S800 (Japan) field emission scanning electron microscope at voltages of 5 kV.

Porosity. The porosity of the scaffolds was determined by measuring the dimensions and the mass of the scaffolds. Porosity (p) was defined as follows:

$$p = 1 - \frac{d}{d_p} \tag{1}$$

where d is the density of the scaffolds and d_p is the density of the polymer. The density of the porous scaffolds was calculated according to the following equation:

$$d = \frac{m}{V} \tag{2}$$

where m and V are the mass and volume of the scaffold, respectively. The density of the polymers (d_p) was determined using non-porous blocks of the polymers (ϕ=14 mm; height=8.4 mm) melt-pressed at 140°C for 11 min and rapidly cooled to 15°C under pressure in the mold.

The theoretical porosity (p_t) of the prepared scaffolds was calculated from the salt weight fraction (w), the density of sodium chloride (d_{salt}) reported to be 2.17 g/cm$^{3[25]}$ and the density of the polymer (d_p) as in equation 3.

$$p_t = \frac{\dfrac{w}{d_{salt}}}{\dfrac{w}{d_{salt}} + \dfrac{1-w}{d_p}} \tag{3}$$

Shrinkage. The volume shrinkage (s) of the scaffolds in relation to the mold size was defined as:

$$\text{volume shrinkage} = 1 - \frac{V}{V_0} \tag{4}$$

where V is the volume of the scaffold at the end of the processing steps and V_0 is the volume of the mold.

Mechanical properties. Compressive stress-strain curves for the prepared scaffolds (three-fold) were determined at room temperature using a Zwick Z020 universal testing machine (Germany) operated at a cross-head speed of 2 mm/min and with a 10N load cell.

Water flux. Water flux measurements were carried out with poly(TMC-DLLA) (81:19 mol%) porous scaffolds (ϕ=25 mm and height=4 mm). The pre-wetted scaffolds (three-fold) were placed in a 'dead end' flow cell (ϕ=25 mm) and secured to a glass filter support (P3) by a silicone rubber ring with a 20 mm inner diameter. In this way, a total flux area of 3.14 cm^2 was created. The flow cell was then filled with water and a pressure of 0.1 bar was applied. The water flux was determined gravimetrically over a period of 30 min. The water flow was defined as the average permeated mass of water (in g) per time unit (in min) through the surface area of the scaffold (in cm^2).

In Vitro Degradation

The dimensional stability and degradation of porous scaffolds prepared with salt particles of 106-250 μm were evaluated at 37°C in PBS containing 0.02 wt/vol% of NaN$_3$ (Sigma, USA) to prevent bacterial growth. PBS was changed once a month in the first three months of the study and every two weeks at longer periods of time. At each analysis point duplicate samples were withdrawn and, after blotting the excess of liquid, the dimensions of the samples were measured. The porous structures were subsequently washed with distilled water, dried under vacuum at room temperature and the dry weight as well as the molecular weight of the samples were determined.

Gamma-Irradiation

Poly(TMC-DLLA) (81:19 mol%) porous structures prepared with salt particles of 106-250 μm were exposed under vacuum to 15.8, 24.1 and 37.5 kGy gamma-irradiation from a ^{60}Co source (Gammaster, Ede, The Netherlands). Each irradiation procedure was done on triplicate samples. Analysis of the polymer molecular weight and of the morphology of the porous structures was performed after treatment.

RESULTS AND DISCUSSION

Polymer Synthesis and Characterization

Copolymers of TMC and DLLA are amorphous and non-crystallizable[20] and their degradation profiles can be tuned as a function of the comonomer content[21,22]. From these, copolymers with TMC contents of 20 and 50 mol% were selected for the preparation of porous scaffolds for heart tissue engineering. The selection is based on the expectation that these materials can be processed efficiently into porous structures, have adequate mechanical properties and degrade at the desired rate at physiological conditions. At room temperature these materials are in the glassy state (Tg above room temperature) allowing easy processing and handling. After water uptake, Tg decreases to below body temperature and the materials show rubbery behavior under physiological conditions[20].

The synthesis of statistical TMC and DLLA copolymers with the selected compositions was accomplished through ring-opening polymerization in the melt, using stannous octoate as a catalyst. The respective parent homopolymers were also included in this study and used as a reference. The molar composition, molecular

weights, thermal properties and densities of the synthesized (co)polymers after purification are compiled in Table 1.

Table 1. Characterization of the synthesized TMC-DLLA (co)polymers after purification.

Polymer	$\overline{M}n \times 10^{-5}$	$\overline{M}w \times 10^{-5}$	PDI	$[\eta]^a$ (dl/g)	Tg^b (°C)	Density (g/cm^3)
Poly(TMC)	2.7	5.4	2.0	4.5	-19	1.31
Poly(TMC-DLLA) 46:54 mol%	1.7	3.7	2.2	2.5	21	1.27
Poly(TMC-DLLA) 19:81 mol%	2.2	4.9	2.2	2.9	42	1.23
Poly(DLLA)	0.9	1.6	1.8	1.4	49	1.26

^{a} In CHCl$_3$, 25°C.

^{b} Second heating scan (DSC).

The composition of the obtained copolymers differs slightly from the ratio of monomers charged. This may be explained by a small loss of monomer that sublimated during the evacuation of the ampoules. Under the applied polymerization conditions high molecular weight polymers ($\overline{M}n > 90,000$) were obtained. The polydispersity index of all polymers varied from 1.8 to 2.2. The thermal properties, and consequently the mechanical properties, of the TMC copolymers can be varied to a large extent by adjusting the comonomer composition. TMC and DLLA (co)polymers are amorphous for the whole range of compositions, with a Tg varying between -19°C for poly(TMC) and 49°C for poly(DLLA). Therefore, the polymers obtained vary from rubbers with low Young's moduli, as in the case of poly(TMC) and the copolymer with 46 mol% TMC, to stiff materials with high Young's moduli as for the copolymer with 19 mol% TMC and poly(DLLA)[20]. The density of the copolymers ranged between 1.26 and 1.31 g/cm^3.

Endothelial Cell Culturing on TMC and DLLA (Co)polymer Films

In vitro cytotoxicity assays are the primary biocompatibility screening tests for materials used in medical devices[26]. In the present study, the cytotoxicity of the prepared (co)polymers was assessed by investigating the capability of human umbilical vein endothelial cells (HUVECs) to adhere and proliferate on the surface of these materials. Although most cytotoxicity assays employ permanent cell lines, such as the L-929 mouse fibroblast cell line[26], human endothelial cells also provide a useful cell type to study possible negative effects of the polymers on

cellular metabolism[27]. Furthermore, endothelial cells have biological relevance for the present application. Although endothelial cells do not improve heart function, endothelium does play a key role in promoting vascularization of tissues, a phenomenon that is fundamental for the survival of the hybrid construct *in vivo*. In general, there is one capillary for each muscle fiber[28].

HUVEC adhesion and proliferation on TMC-DLLA copolymers and the parent homopolymers were determined at 6 hrs, 1, 3, 6 and 9 days after seeding (Figure 1). Tissue culture poly(styrene) (TCPS) was used as positive control.
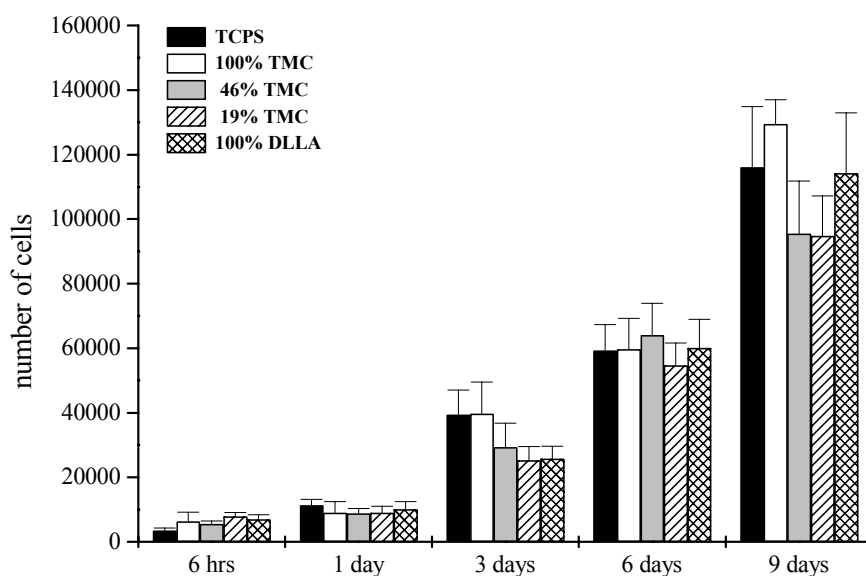

Figure 1. Total number of HUVECs observed on TMC and DLLA (co)polymer films and TCPS at different time points. (n=3, mean ± standard deviation).

All polymer surfaces support endothelial cell adhesion and proliferation. Up to 9 days of culture no signs of cytotoxicity were detected. Both for short and long culture times no significant differences were observed between the total cell numbers on the five different surfaces. The cultures reached confluence between 3 and 6 days after seeding, at which time the cell layers showed the typical "cobblestone-like" morphology of endothelial cells[29,30] (data not shown).

Preparation of Porous Structures

When designing the scaffolds that will host the developing cardiac tissue a processing method should be selected that allows the preparation of three-dimensional porous scaffolds in a reproducible fashion, with good control of pore size, pore interconnectivity and homogeneity of the porous structures. Furthermore,

the scaffolds should keep their shape and dimensions under physiological conditions during the time required for development of the mature tissue structure. There is no optimal pore size established for the culture of cardiomyocytes in three-dimensional porous scaffolds. However, based on previous work we expect that an average pore size of approximately 100 μm will allow homogeneous infiltration of the cells into the scaffold and expression of their contractile phenotype[4,6]. The scaffolds should be highly porous to accommodate a large number of cells and allow neovascularization of the matrix.

The most commonly used techniques developed to construct porous polymer scaffolds are not suited for processing amorphous rubbery materials. Due to their relatively low Tg, TMC-DLLA (co)polymers are difficult to grind even under cryogenic conditions. Therefore, procedures that combine compression molding of salt and polymer particle mixtures with salt leaching are not applicable. Phase inversion by immersion precipitation techniques lead to the formation of non-porous structures[31,32]. The absence of physical cross-links (crystallinity) that could stabilize the structure and the low Tg of the materials, that is further depressed by the plasticizing effect of the solvents, allows relaxation of the polymer chains in time, resulting in collapse of the pores. With freeze-drying techniques highly porous structures can be obtained, but important drawbacks are the poor homogeneity and interconnectivity of the porous network throughout the scaffold. Moreover, often large defects are formed in the structure[33].

Recently, we have described a method that allows the preparation of highly porous structures based on rubbery materials. Poly(ε-caprolactone) scaffolds were obtained by combination of coprecipitation, compression molding and leaching methods, with good control of pore size and porosity[23]. In a first step, salt particles are dispersed in a polymer solution and the obtained dispersion is precipitated in an excess of non-solvent (the solvent and non-solvent for the polymer are non-solvents for the porosifying agent). This yields a fibrous composite in which the entrapped salt particles are homogenously distributed. The composite can be processed by thermal processing techniques into a device of the desired shape and size, which can then be extracted, leaving behind an interconnected structure of pores.

Highly porous, well interconnected structures were obtained by leaching of compression molded, salt-containing TMC-DLLA (co)polymer precipitates (Table 2). All structures shrunk homogeneously during the salt-leaching process. Volume shrinkage was particularly significant for scaffolds based on the copolymers and poly(TMC). This phenomenon is a consequence of the higher mobility of the

polymer chains in the wet state, due to depression of the Tg of the polymer upon water uptake. Leaching the scaffolds in cold water (6°C) prevented shrinkage to a certain extent. At room temperature poly(TMC-DLLA) (46:54 mol%) and poly(TMC) scaffolds shrunk up to 45 and 70%, respectively. Freeze-drying was used to remove the water from the leached scaffolds to avoid more extensive shrinkage of the scaffolds.

The porosity of the prepared scaffolds (Table 2) is in agreement with the expected value (92%) calculated from the polymer to salt ratio used in the coprecipitation process (5:95 wt%). The only exceptions were observed for the poly(TMC) scaffolds prepared with the salt size range between 63 and 106 μm, which had a final porosity of 87%. Due to the lower resistance of these scaffolds to shrinkage, a significant number of pores may have collapsed, which leads to a reduction of the overall porosity.

Table 2. Volume shrinkage[a] after leaching and final porosity of the porous scaffolds (n≥10, average±standard deviation) prepared by leaching (at 6°C) of compression molded salt-containing polymer precipitates with salt particles of different size range.

Polymer	salt size: 63-106 μm		salt size: 106-250 μm	
	Shrinkage (%)	Porosity (%)	Shrinkage (%)	Porosity (%)
P(TMC)	45±6.1	86±4.1	34±6.1	92±0.7
P(TMC-DLLA) 46:54 mol%	27±4.8	91±2.1	22±3.4	94±1.0
P(TMC-DLLA) 19:81 mol%	17±1.8	90±2.9	17±2.8	94±0.9
P(DLLA)	4±1.2	95±0.2	7±1.8	95±0.3

[a] Note that changes in height and radius are much smaller.

Figure 2 shows characteristic SEM images of the different scaffolds based on the two TMC-DLLA copolymers and parent homopolymers. Very regular structures with homogeneously distributed pores were obtained. The five-day period allowed for leaching of the salt particles was sufficient to guarantee complete removal of the porosifying agent as no residual salt was observed.
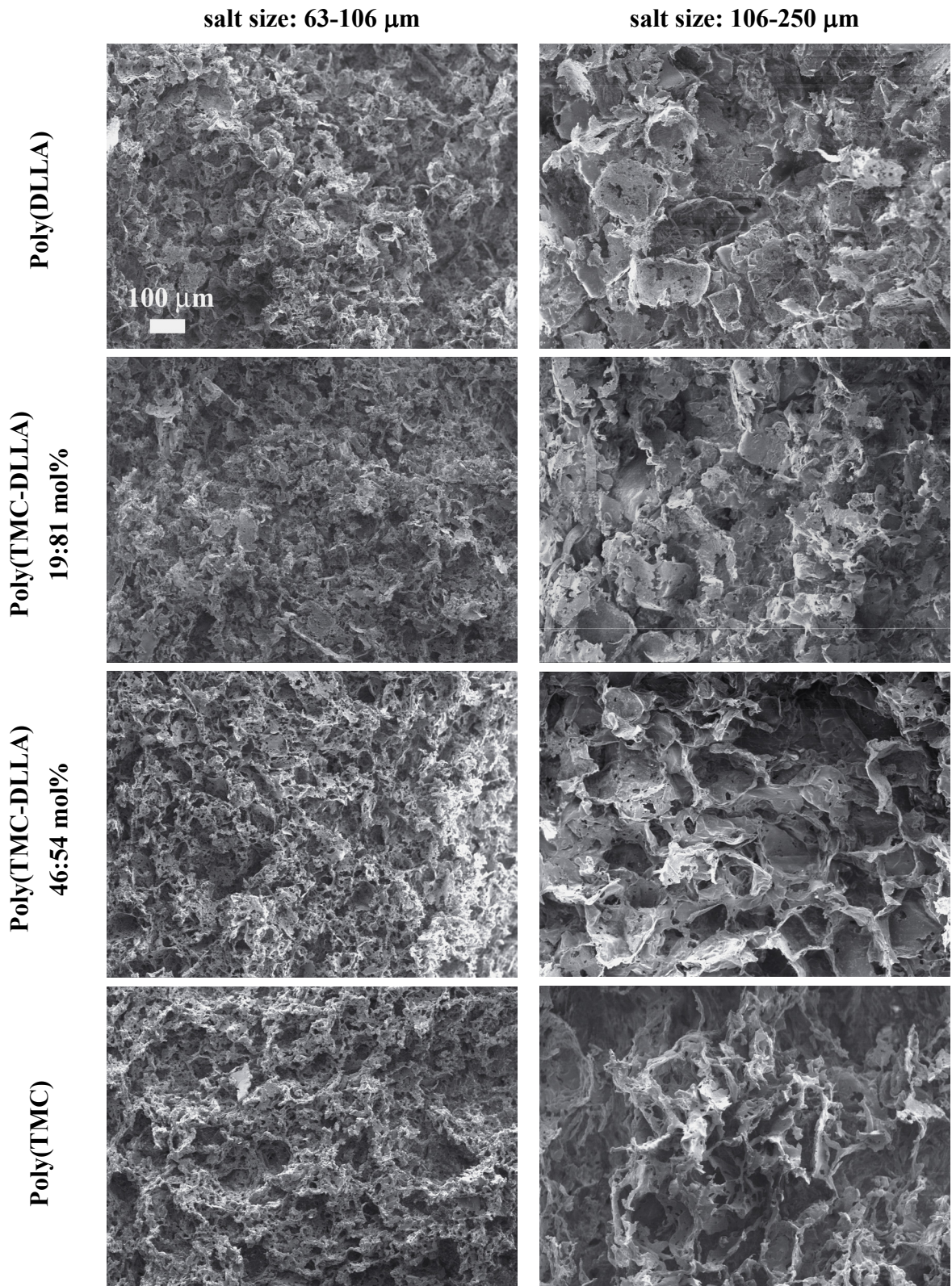
Figure 2. SEM images of TMC-DLLA (co)polymer porous structures prepared by leaching of compression molded salt-containing polymer precipitates with salt particles of different size range.

The pore size of the scaffolds could be easily tuned by variation of the salt particle size range (Table 3). The average pore size derived from SEM is in good agreement with the dimensions of the salt particles used. With an increase in TMC content the scaffolds exhibit pores with a more rounded morphology, what can be ascribed to the same effect that leads to higher shrinkage of these scaffolds during salt-leaching.

Table 3. Average pore size ± standard deviation (μm) of TMC-DLLA (co)polymer porous structures prepared by leaching of compression molded salt-containing polymer precipitates with salt particles of different size range (measurements performed on single scaffolds).

Polymer	salt size: 63-106 μm	salt size: 106-250 μm
P(TMC)	75±27	86±25
P(TMC-DLLA) 46:54 mol%	52±16	110±35
P(TMC-DLLA) 19:81 mol%	68±21	100±27
P(DLLA)	57±12	145±28

Mechanical Properties of TMC-DLLA (Co)polymer Porous Structures

The mechanical properties of the scaffolds were evaluated by determining their compressive stress-strain behavior at room temperature. All scaffolds exhibited the typical compressive stress-strain behavior of flexible foams: linear elasticity at low stresses followed by a collapse plateau that is truncated by a regime of densification in which the stress rises steeply[34].

The compression modulus was determined for scaffolds prepared with both salt size ranges (Table 4).

Table 4. Compression moduli of porous scaffolds prepared by leaching of compression molded salt-containing polymer precipitates with salt particles of different size range.

Polymer	salt size: 63-106 μm		salt size: 106-250 μm	
	Porosity (%)	Compression modulus (kPa)	Porosity (%)	Compression modulus (kPa)
P(TMC)	86±4.1	10±1	92±0.7	6±0.5
P(TMC-DLLA) 46:54 mol%	91±2.1	8±0.8	94±1.0	6±0.4
P(TMC-DLLA) 19:81 mol%	90±2.9	430±40	94±0.9	300±10
P(DLLA)	95±0.2	290±14	95±0.3	150±50

The scaffolds based on the (co)polymers with the highest TMC content had the lowest compression moduli.

The compression modulus of a polymeric scaffold decreases with increasing porosity[34]. As poly(TMC-DLLA) (19:81 mol%) and poly(DLLA) scaffolds had the highest porosity, the differences in flexibility between the scaffolds with high and low TMC content must be mainly determined by the thermal properties of the (co)polymers.

Although the differences were not significant, for each polymer, the porous structures prepared with the smaller salt sizes were more rigid. This is to be expected as these had a smaller average pore size and in general were also less porous[35].

In Vitro Degradation of Poly(TMC-DLLA) (Co)polymer Porous Structures

None of the scaffolds prepared with the smallest salt particle size (63-106 mm) retained their original dimensions when incubated in PBS at 37°C. The highest decrease in volume was observed for the poly (TMC) and poly(TMC-DLLA) (46:54 mol%) scaffolds. These shrunk up to 80% in three weeks. The scaffolds prepared from poly(TMC-DLLA) (19:81 mol%) and poly(DLLA) were more stable, but in three weeks even these shrunk to 45% and 65% of their original volume, respectively.

While poly(TMC) and poly(TMC-DLLA) (46:54 mol%) scaffolds with the larger pores showed a similar behavior to that described above, scaffolds with large pores prepared from polymers with high DLLA content retained their original shape and structure during a 16-week immersion period. The average volume of these scaffolds as a function of incubation time is plotted in Figure 3.

After a small initial decrease in volume (<10%) during the first days of incubation, the dimensions of the poly(TMC-DLLA) (19:81 mol%) and poly(DLLA) scaffolds with larger pore size did not significantly change in time. In contrast, poly(TMC) and poly(DLLA-TMC) (46:54 mol%) scaffolds showed significant shrinkage in one week, with an average volume decrease of 68 and 60%, respectively. In time these scaffolds shrunk further, leading to collapse of the porous structure in 16 weeks.

The differences between the shrinking resistance of the different scaffolds can be ascribed to the thermal properties of the polymers. Despite being in the rubbery state under physiological conditions, the copolymer with 19 mol% of TMC allows the preparation of dimensionally stable structures. As the Tg of this copolymer in

the wet state is just below 37°C[20], the mobility of the polymer chains is still significantly constrained and hinders the shrinkage process.
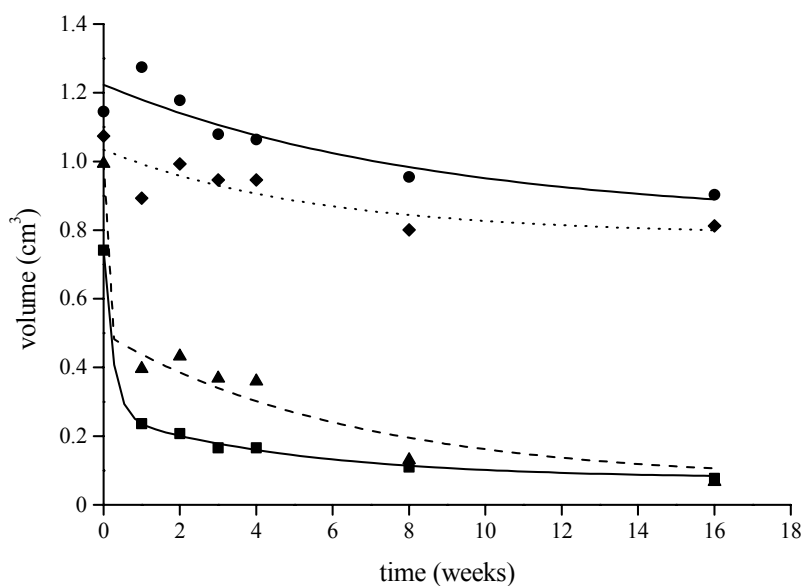

Figure 3. Average volume of the scaffolds (salt size range 106-250 μm) during incubation in PBS at 37°C. (■) 100% TMC; (▲) 46% TMC; (♦) 19% TMC and (●) 100% DLLA.

The *in vitro* degradation of TMC-DLLA (co)polymer porous scaffolds followed a similar trend to that of non-porous (co)polymer films of similar composition[21]. Figure 4 shows the variation of $\overline{M}n$ of the (co)polymers as a function of immersion time in PBS at 37°C. For all samples and at all stages of the degradation monomodal molecular weight distributions were observed. In 16 weeks, poly(TMC) scaffolds did not show a significant decrease in $\overline{M}n$. In contrast, for the DLLA homopolymer scaffolds ($\overline{M}n$=70,000 after melt-pressing) a continuous reduction was observed, in which $\overline{M}n$ decreased to 53% of its initial value. The copolymers degraded at higher rates than both homopolymers.

Mass loss was only detected for the (co)polymers containing DLLA. At 16 weeks a small decrease in mass (between 5 and 6%) of these scaffolds was observed, when $\overline{M}n$ had approached a value of approximately 35,000.

Hydrolysis rates in PBS at 37°C were determined for the DLLA containing (co)polymers, which showed a clear decrease in molecular weight. The kinetics of chain scission of the copolymer scaffolds could be well-fitted to an autocatalytic kinetic model[36]. Poly(DLLA) showed limited degradation in the 16 weeks of the study. Both autocatalytic[36] and a non-catalytic model[37] fitted the experimental

results equally well (data not shown). The rates of hydrolysis for the DLLA containing (co)polymers, based on the autocatalytic model, are presented in Table 5. The previously determined hydrolysis rates of non-porous films are also presented for comparison[21].
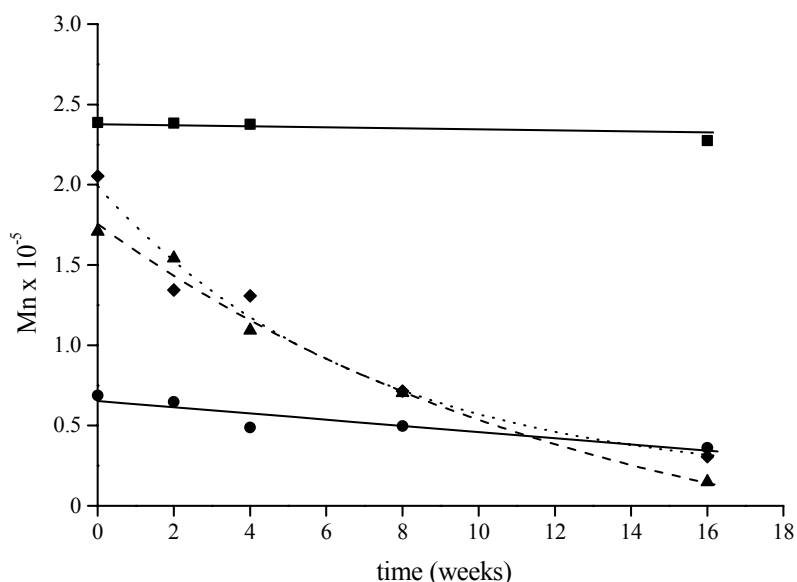

Figure 4. Number average molecular weight ($\overline{M}n$) of the scaffolds (salt size range 106-250 μm) as a function of incubation time in PBS at 37°C. (■) 100% TMC; (▲) 46% TMC; (♦) 19% TMC and (●) 100% DLLA.

Table 5. Hydrolysis rates of TMC-DLLA (co)polymer porous scaffolds (salt size range 106-250 μm) in PBS at 37°C (autocatalytic model).

Polymer	Porous structures ($x10^{-2}$ day^{-1})	Correlation coefficient, r	Non-porous films[21] ($x10^{-2}$ day^{-1})
Poly(TMC-DLLA) 46:54 mol%	2.2	-0.990	3.6^a
Poly(TMC-DLLA) 19:81 mol%	1.7	-0.993	2.1^b
Poly(DLLA)	0.5	-0.947	0.7

^{a} Poly(TMC-DLLA) (50:50 mol%).

^{b} Poly(TMC-DLLA) (20:80 mol%).

The rates of hydrolysis of the polymers in the porous scaffolds were lower than the hydrolysis rates of non-porous polymer films of similar composition. The observations relative to the copolymers are in line with a degradation process involving chain cleavage throughout the bulk, autocatalyzed by generated acidic

end groups. The faster degradation of the non-porous films can be ascribed to a greater autocatalytic effect[38,39]. The surface to volume ratio is much higher in porous structures, leading to a decreased accumulation of carboxylic end groups in the polymer bulk, as polymer degradation products can diffuse in shorter periods of time to the degradation medium[40]. In the same way, the penetration of ions present in PBS may be of higher significance in the porous scaffolds, resulting in a more extensive buffering effect.

The negligible decrease in molecular weight observed for the poly(TMC) scaffolds (Figure 4) is in line with previous findings[21,41,42]. In PBS at 37°C polymeric carbonate linkages are much less susceptible to hydrolysis than polymeric ester linkages. Furthermore, generation of catalytic acid end groups is not expected to occur in poly(TMC). Therefore, the presence of pores is not expected to influence the degradation of poly(TMC) *in vitro*. In contrast to the very slow degradation *in vitro*, poly(TMC) degrades rapidly *in vivo* via surface erosion[22].

Poly(TMC-DLLA) (19:81 mol%) Porous Structures

The previously described results suggest that scaffolds based on the TMC-DLLA copolymer with 19 mol% of TMC with the largest average pore size are the most appropriate for the development of three-dimensional hybrid constructs for heart tissue engineering. These scaffolds are highly porous, consisting of an interconnected network of pores with an average pore size of 100 μm. Furthermore, these structures are very flexible, retaining their shape and dimensions for a period of at least 16 weeks under hydrolytic conditions.

Interconnection of the pore network of these scaffolds was confirmed by water permeation measurements. The average water flux through the large pore scaffolds was 30 ± 5 g/(min·cm^2), while the empty cell allows a water throughput of 47 ± 1 g/(min·cm^2) (in this case the water permeates only through the sintered glass filter support present at the bottom of the cell).

In view of their final application in the clinic, the possibility to sterilize the scaffolds by means of a standard sterilization method for medical devices is an important issue. We investigated the possibility of using ^{60}Co gamma-radiation sterilization, as it is one of the most commonly used methods and does not involve the use of toxic substances[43].

Figure 5 shows the effect of gamma-radiation dosage on the $\overline{M}n$ of copolymer scaffolds prepared with salt particles of 106-250 μm. Even at dosages below 25

kGy, the standard sterilization dose for medical devices[43], a steep decrease in the $\overline{M}_n$ of the scaffolds was observed. The reduction in $\overline{M}_n$ and the linear decrease in the polydispersity index with increasing average radiation dose (Figure 5) suggest that chain scission is the primary mechanism of polymer degradation[44].
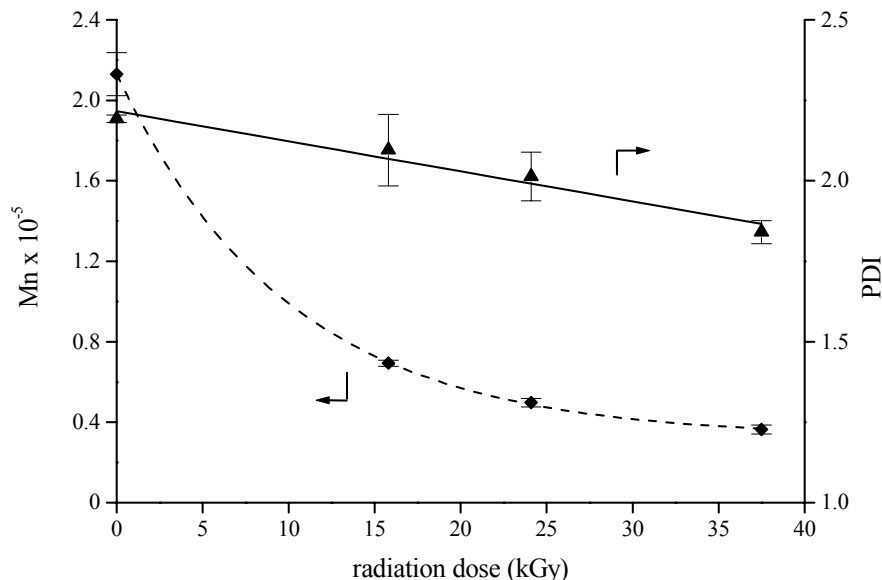

Figure 5. Number average molecular weight ($\overline{M}_n$) and polydispersity index (PDI) of the poly(TMC-DLLA) (19:81 mol%) scaffolds (salt size range 106-250 μm) after gamma-radiation treatment at different average radiation doses. (n=3, mean ± SD).

The handling characteristics and average pore size of the scaffolds as well as the morphology of the porous structure did not change after the gamma-radiation treatments. Additionally, the irradiated scaffolds still retained their shape and dimensions when incubated at physiological conditions. This is an important advantage of these polymeric systems over the commonly used collagen matrices. It has been previously found that gamma-sterilized collagen sponges showed severe shrinkage under cell-culturing conditions[45].

Although gamma-irradiation can be used to sterilize TMC-DLLA copolymer scaffolds, it is important to take the observed decrease in the polymer molecular weight into account, as this parameter may have an impact on the physical properties[20] and resorption time[36] of the materials. This phenomenon stresses the need of using high molecular weight polymers in the preparation of these polymeric structures.

In a preliminary study we investigated the adhesion and proliferation of rat cardiomyocytes (cell line) on the surface of poly(TMC-DLLA) (19:81 mol%) films. Microscopic observations indicate that rat cardiomyocytes attach and proliferate well on the copolymer surface (Figure 6). The growth of primary neonatal rat cardiac cells in three-dimensional scaffolds based on the TMC-DLLA copolymer with 19 mol% of TMC is currently being investigated.
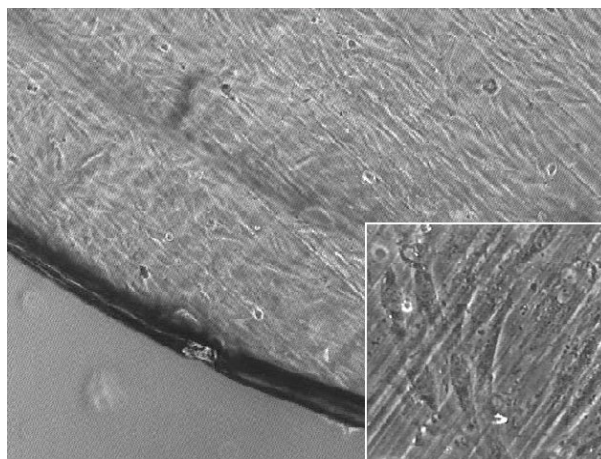

Figure 6. Phase-contrast micrographs (magnification: 50x and 200x) of rat cardiomyocytes (cell line) on the surface of a poly(TMC-DLLA) (19:81 mol%) compression molded film at 8 days of culture.

CONCLUSIONS

Particulate leaching of compression-molded polymer/salt composites was found to be an excellent method to reproducibly prepare interconnected, highly porous structures from amorphous elastomers based on (co)polymers of TMC and DLLA. By adjusting the salt particle size and the polymer to particle ratio, the pore size and porosity of the scaffolds could be precisely controlled. The thermal properties of the polymers have a strong effect on the mechanical properties of the scaffolds and on their dimensional stability at physiological conditions. Scaffolds prepared from polymers with high TMC contents were the most flexible. However, these scaffolds also showed a low resistance to volume shrinkage. In contrast, scaffolds prepared from the (co)polymers with high DLLA contents still showed adequate flexibility and were more dimensionally stable. Particularly, the scaffolds prepared with the largest salt size range (106-250 μm) retained their shape and structure during 16 weeks of incubation in PBS at 37°C.

By selecting a TMC-DLLA copolymer with 19 mol% of TMC, interconnected highly porous structures (94% porosity and average pore size 100 μm) were prepared, which combine suitable mechanical properties and biocompatibility for the development of three-dimensional constructs to host cardiac cells. The copolymer is non cytotoxic and allows the adhesion and proliferation of cardiomyocytes. During incubation in phosphate buffered saline at 37°C, a gradual decrease in molecular weight was observed for a period up to 4 months. The degradation profiles of the porous scaffolds were similar to those of non-porous films, being best described by autocatalyzed hydrolysis in the bulk.

ACKNOWLEDGMENTS

REFERENCES

[1] Hennekens CH. Increasing burden of cardiovascular disease: current knowledge and future directions for research on risk factors. *Circulation* 1998; 97: 1095-1102.

[2] Eschenhagen T, Fink C, Remmers U, Scholz H, Wattchow J, Weil J, Zimmermann W, Dohmen HH, Schafer H, Bishopric N, Wakatsuki T, Elson EL. Three-dimensional reconstitution of embryonic cardiomyocytes in a collagen matrix: a new heart muscle model system. *FASEB J* 1997; 11: 683-694.

[3] Carrier RL, Papadaki M, Rupnick M, Schoen FJ, Bursac N, Langer R, Freed LE, Vunjak-Novakovic G. Cardiac tissue engineering: cell seeding, cultivation parameters, and tissue construct characterization. *Biotechnol Bioeng* 1999; 64: 580-589.

[4] Leor J, Aboulafia-Etzion S, Dar A, Shapiro L, Barbash IM, Battler A, Granot Y, Cohen S. Bioengineered cardiac grafts. A new approach to repair the infarcted myocardium? *Circulation* 2000; 102: III56-61.

[5] Shimizu T, Yamato M, Isoi Y, Akutsu T, Setomaru T, Abe K, Kikuchi A, Umezu M, Okano T. Fabrication of pulsatile cardiac tissue grafts using a novel 3-dimensional

cell sheet manipulation technique and temperature-responsive cell culture surfaces. *Circ Res* 2002; 90: e40-e48.

[6]   van Luyn MJA, Tio RA, Gallego y van Seijen XJ, Plantinga JA, de Leij LFMH, de Jongste MJL, van Wachem PB. Cardiac tissue engineering: Characteristics of in unison contracting two- and three-dimensional neonatal rat ventricle cell (co)-cultures. *Biomaterials* (in press).

[7]   Li RK, Jia ZQ, Weisel RD, Mickle DAG, Choi A, Yau TM. Survival and function of bioengineered cardiac grafts. *Circulation* 1999; 100: 63-69.

[8]   Sakai T, Li RK, Weisel RD, Mickle DA, Kim ET, Jia ZQ, Yau TM. The fate of a tissue-engineered cardiac graft in the right ventricular outflow tract of the rat. *J Thorac Cardiovasc Surg* 2001; 121: 932-942.

[9]   Folliguet TA, Rucker-Martin C, Pavoine C, Deroubaix E, Henaff M, Mercadier JJ, Hatem SN. Adult cardiac myocytes survive and remain excitable during long-term culture on synthetic supports. *J Thorac Cardiovasc Surg* 2001; 121: 510-519.

[10] Shapiro L, Cohen S. Novel alginate sponges for cell culture and transplantation. *Biomaterials* 1997; 18: 583-590.

[11] Papadaki M, Bursac N, Langer R, Merok J, Vunjak-Novakovic G, Freed LE. Tissue engineering of functional cardiac muscle: molecular, structural, and electrophysiological studies. *Am J Physiol Heart Circ Physiol* 2001; 280: H168-178.

[12] Mooney DJ, Park S, Kaufmann PM, Sano K, McNamara K, Vacanti JP, Langer R. Biodegradable sponges for hepatocyte transplantation. *J Biomed Mater Res* 1995; 29: 959-965.

[13] Evans GRD, Brandt K, Widmer MS, Lu L, Meszlenyi RK, Gupta PK, Mikos AG, Hodges J, Williams J, Gurlek A, Nabawi A, Lohman R, Patrick CW. *In vivo* evaluation of poly(L-lactic acid) porous conduits for peripheral nerve regeneration. *Biomaterials* 1999; 20: 1109-1115.

[14] Marler JJ, Upton J, Langer R, Vacanti JP. Transplantation of cells in matrices for tissue regeneration. *Adv Drug Deliv Rev* 1998; 33: 165-182.

[15] Grijpma DW, Zondervan GJ, Pennings AJ. High molecular weight copolymers of L-lactide and ε-caprolactone as biodegradable elastomeric implant materials. *Polym Bull* 1991; 25: 327-333.

[16] Williams SF, Martin DP, Horowitz DM, Peoples OP. PHA applications: addressing the price performance issue. I. Tissue engineering. *Int J Biol Macromol* 1999; 25: 111-121.

[17] Wang Y, Ameer GA, Sheppard BJ, Langer R. A tough biodegradable elastomer. *Nat Biotechnol* 2002; 20: 602-606.

[18] Pêgo AP, Poot AA, Grijpma DW, Feijen J. Biodegradable elastomeric scaffolds for soft tissue engineering. *J Control Release* (in press).

[19] Stock UA, Vacanti JP. Tissue engineering: current state and prospects. *Annu Rev Med* 2001; 52: 443-451.

[20] Pêgo AP, Poot AA, Grijpma DW, Feijen J. Physical properties of high molecular weight 1,3-trimethylene carbonate and D,L-lactide copolymers. *(submitted to J Mater Sci: Mater Med, 2002)* Chapter 5 of this thesis.

[21] Pêgo AP, Poot AA, Grijpma DW, Feijen J. *In vitro* degradation of trimethylene carbonate based (co)polymers. *Macromol Chem Phys (accepted for publication)* Chapter 6 of this thesis.

[22] Pêgo AP, van Luyn MJA, Brouwer LA, van Wachem PB, Poot AA, Grijpma DW, Feijen J. *In vivo* behavior of poly(1,3-trimethylene carbonate) and copolymers of 1,3-trimethylene carbonate with D,L-lactide or ε-caprolactone. Degradation and tissue response. *(submitted to J Biomed Mater Res, 2002)* Chapter 7 of this thesis.

[23] Hou QP, Grijpma DW, Feijen J. Preparation of porous poly(ε-caprolactone) structures. *Macromol Rapid Commun* 2002; 23: 247-252.

[24] van Wachem PB, Reinders JH, van Buul-Wortelboer MF, de Groot PG, van Aken WG, van Mourik JA. von Willebrand factor in cultured human vascular endothelial cells from adult and umbilical cord arteries and veins. *Thromb Haemost* 1986; 56: 189-192.

[25] *CRC Handbook of Chemistry and Physics*. Lide DR Ed-in-Chief, Boca Raton, FL: CRC Press; 2002.

[26] Northup SJ, "*In vitro* assessment of tissue compatibility" In: Ratner BD, Hoffman AS, Schoen FJ, Lemons JE. *Biomaterials science. An introduction to materials in medicine*, San Diego, CA, USA: Academic Press; 1996. p 215-220.

[27] Kirkpatrick CJ, Otto M, Kooten TV, Krump V, Kriegsmann J, Bittinger F. Endothelial cell cultures as a tool in biomaterial research. *J Mater Sci-Mater Med* 1999; 10: 589-594.

[28] Little RC, Little WC, "Physiology of the heart and circulation" In: Chicago: Year Book Medical Publishers, Inc.; 1989. p 37-40.

[29] Akins RE, Boyce RA, Madonna ML, Schroedl NA, Gonda SR, McLaughlin TA, Hartzell CR. Cardiac organogenesis *in vitro*: reestablishment of three-dimensional tissue architecture by dissociated neonatal rat ventricular cells. *Tissue Eng* 1999; 5: 103-118.

[30] Ahluwalia A, Basta G, Chiellini F, Ricci D, Vozzi G. Endothelial cell adhesion on bioerodable polymers. *J Mater Sci-Mater Med* 2001; 12: 613-619.

[31] van de Witte P, Esselbrugge H, Dijkstra PJ, van den Berg JWA, Feijen J. Phase transitions during membrane formation of polylactides.1. A morphological study of membranes obtained from the system polylactide-chloroform-methanol. *J Membr Sci* 1996; 113: 223-236.

[32] Pêgo AP, Poot AA, Grijpma DW, Feijen J. Copolymers of trimethylene carbonate and ε-caprolactone for porous nerve guides: synthesis and properties. *J Biomater Sci Polym Ed* 2001; 12: 35-53. Chapter 3 of this thesis.

[33] Hou Q, Grijpma DW, Feijen J. Porous polymeric structures for tissue engineering prepared by a coagulation, compression moulding and salt leaching technique. *(submitted to Biomaterials, 2002)*.

[34] Gibson LG, Ashby MF, "Cellular Solids: structure and properties" In: Oxford: Pergamon Press; 1988. p 120-168.

[35] Shutov FA. Foamed polymers. Cellular Structure and properties. *Adv Polym Sci* 1983; 51: 155-218.

[36] Pitt CG, Chasalow FI, Hibionada DM, Klimas DM, Schindler A. Aliphatic polyesters. I. The degradation of poly(ε-caprolactone) *in vivo. J Appl Polym Sci* 1981; 26: 3779-3787.

[37] Pitt CG, Gu Z. Modification of the rates of chain cleavage of poly(ε-caprolactone) and related polyesters in the solid state. *J Control Release* 1987; 4: 283-292.

[38] Lu L, Peter SJ, Lyman MD, Lai HL, Leite SM, Tamada JA, Vacanti JP, Langer R, Mikos AG. *In vitro* degradation of porous poly(L-lactic acid) foams. *Biomaterials* 2000; 21: 1595-1605.

[39] Lam KH, Nieuwenhuis P, Molenaar I, Esselbrugge H, Feijen J, Dijkstra PJ, Schakenraad JM. Biodegradation of porous versus nonporous poly(L-lactic acid) films. *J Mater Sci-Mater Med* 1994; 5: 181-189.

[40] Grizzi I, Garreau H, Li S, Vert M. Hydrolytic degradation of devices based on poly(DL-lactic acid) size-dependence. *Biomaterials* 1995; 16: 305-311.

[41] Zhu KJ, Hendren RW, Jensen K, Pitt CG. Synthesis, properties, and biodegradation of poly(1,3-trimethylene carbonate). *Macromolecules* 1991; 24: 1736-1740.

[42] Albertsson A-C, Eklund M. Influence of molecular structure on the degradation mechanism of degradable polymers: *in vitro* degradation of poly(trimethylene carbonate), poly(trimethylene carbonate-co-caprolactone), and poly(adipic anhydride). *J Appl Polym Sci* 1995; 57: 87-103.

[43] Kowalski JB, Morrissey RF, "Sterilization of implants" In: Ratner BD, Hoffman AS, Schoen FJ, Lemons JE. *Biomaterials science. An introduction to materials in medicine*, San Diego, CA: Academic Press; 1996. p 415-420.

[44] Nugroho P, Mitomo H, Yoshii F, Kume T. Degradation of poly(L-lactic acid) by gamma-irradiation. *Polym Degrad Stabil* 2001; 72: 337-343.

[45] Noah EM, Chen J, Jiao X, Heschel I, Pallua N. Impact of sterilization on the porous design and cell behavior in collagen sponges prepared for tissue engineering. *Biomaterials* 2002; 23: 2855-2861.

APPENDIX A

Preliminary study on the preparation and *in vivo* performance of degradable poly(ε-caprolactone) two-ply nerve guides

A.P. PÊGO[1], C.L.A.M. VLEGGEERT–LANKAMP[2], E.A.J.F. LAKKE[2], E. MARANI[1,2], R.T.W.M. THOMEER[2], A.A. POOT[1], D.W. GRIJPMA[1] and J. FEIJEN[1]

[1] *Institute for Biomedical Technology (BMTI) and Department of Polymer Chemistry and Biomaterials, Faculty of Chemical Technology, University of Twente, P.O. Box 217, 7500 AE Enschede, The Netherlands*
[2] *Neuroregulation Group, Department of Neurosurgery, Leiden University Medical Center (LUMC), P.O. Box 9604, 2300 RC Leiden, The Netherlands*

ABSTRACT

Poly(ε-caprolactone) (poly(CL)) was used as a model polymer to set-up the preparation of pliable, two-ply permeable conduits for guided tissue regeneration and to study the effect of the tube structure on the mechanical performance of the conduits. A microporous inner layer (pore size range 1-10 μm) was obtained by dip-coating techniques where phase separation was induced by immersion precipitation. A macroporous outer layer (pore size range 10-70 μm) was prepared by winding of fibers spun from solution. Two-ply tubes consisting of a non-porous inner layer and fiber-wound macroporous single-layer conduits were also prepared. The use of microporous two-ply nerve guides in the correction of 6 mm gaps in the rat sciatic nerve model resulted in significantly better nerve regeneration as established by *in vitro* electrophysiological methods than that observed with nerves grafted with non-porous or macroporous conduits. Despite the fact that the fiber-based outer layer has excellent flexing characteristics due to its anisotropic properties, the higher stiffness of the isotropic inner layer results in a relatively low flexibility of the conduits and poor kinking resistance at small bending radii. Such behavior resulted in less than optimal handling characteristics during surgery.

INTRODUCTION

Poly(CL), a though semi-crystalline polymer with a low glass transition temperature[1], was selected as a starting material for the preparation of the two-ply nerve guides. Poly(CL) degrades very slowly *in vitro* and *in vivo*, and is most suitable for long-term applications[2]. It has been extensively studied for the preparation of delivery systems such as Capronor, a 1-year contraceptive[3].

In the fabrication of the two-ply nerve grafts dip-coating techniques were combined with fiber winding techniques, for the preparation of the inner and outer layers of the conduit, respectively.

In the present study porous tubular structures were prepared using dip-coating techniques followed by phase inversion during immersion precipitation. In this way, highly porous structures with pore sizes in the order of a few micrometers can be prepared[4]. Such pore sizes will allow the exchange of fluids and nutrients but will also minimize the ingrowth of fibrous tissue[5].

The dimensions of the pores in the outer layer should be in the range of approximately 25 to 150 μm. Previous studies have shown that this pore size range allows vascularization and fibrous tissue ingrowth, which can have a positive effect on the regeneration and maturation of the nerve[5,6]. In this study, a layer of fibers wound helically around the dip-coated inner layer constitutes the outer porous layer of the grafts. The fibers were spun from solution in a similar procedure to the one described by Leidner et al[7]. This method was chosen because (1) it allows the preparation of porous tubular structures with a pore size in the desired range; (2) the obtained structures have excellent flexing characteristics, bending with minimal reduction of the cross-sectional area of the graft lumen and (3) the spinning of fibers from the polymer increases the strength of the wall of the nerve guide by orientation of the polymer fibers.

The purpose of this study was to set-up a preparation procedure to obtain permeable two-ply porous conduits made of poly(CL) in a reproducible fashion, with good control of pore size, pore interconnectivity and homogeneity of the porous structure. The effect of the tube structure on its mechanical performance and flexing properties was also investigated. For that purpose two-ply conduits with a non-porous inner layer and single-layer fiber wound macroporous conduits were also prepared. The prepared nerve guides were used to evaluate the effect of pore size on the correction of nerve defects in the rat sciatic nerve gap model[8], by means of a quantitative *in vitro* electrophysiological method[9]. Autografts were used as

positive control. Special attention was given to the effect of the mechanical properties of the nerve guides on the surgical grafting procedure.

MATERIALS AND METHODS

Materials

ε-Caprolactone (CL) (Acros Organics, Belgium) was purified by drying over CaH_2 (Acros Organics, Belgium) and distillation under reduced argon pressure. Stannous octoate ($SnOct_2$) (stannous 2-ethylhexanoate) was used as received from Sigma, USA. Solvents (Biosolve, The Netherlands) were of analytical grade.

Polymer Synthesis

Two batches of poly(CL) were synthesized as previously described[1]. Briefly, the polymerizations were conducted by ring-opening polymerization in evacuated and sealed glass ampoules using $SnOct_2$ as catalyst. Both polymerizations were carried out for a period of 3 days at 130°C±2°C. The obtained polymers were purified by dissolution in chloroform and subsequent precipitation into a ten-fold volume of isopropanol. The precipitated polymers were recovered, washed with fresh isopropanol and dried under reduced pressure at room temperature until constant weight.

Polymer Characterization

Polymers were characterized with respect to residual monomer content by nuclear magnetic resonance (NMR). 300 MHz ^{1}H-NMR (Varian Inova 300 MHz) spectra were recorded using solutions of polymer in $CDCl_3$ (Sigma, USA).

Weight average ($\overline{M}w$) and number average ($\overline{M}n$) molecular weights, polydispersity index (PDI) and intrinsic viscosity ($[\eta]$) were determined by gel permeation chromatography (GPC) using a Waters Model 510 pump (USA), a HP Ti-Series 1050 autosampler (USA), a Waters Model 410 Differential Refractometer and a Viscotek H502 Viscometer Detector (USA) with Waters Styragel HR5-HR4-HR2-HR1 columns placed in series. Chloroform was used as eluent at a flow rate of 1.5 ml/min. Narrow polystyrene standards were used for calibration. Sample concentrations of approximately 0.5 wt/vol% and injection volumes of 30 μl were used. All determinations were performed at 25°C.

The thermal properties of the purified polymers were evaluated by differential scanning calorimetry (DSC). Samples (5-15 mg) placed in aluminum pans were analyzed with a Perkin Elmer Pyris1 (USA) at a heating rate of 10°C/min. The samples were heated to 40°C above their melting temperature, subsequently quenched rapidly (300°C/min) to 40°C below their glass transition temperature and after 5 min a second scan was recorded. The glass transition temperature (Tg) was taken as the midpoint of the heat capacity change and the peak melting temperature (Tm) was determined from the melting endotherm. The crystallinity (w_c) of the CL homopolymers was determined assuming proportionality to the experimental heat of fusion (ΔH) according to the expression: $w_c = \Delta H / \Delta H°$, where $\Delta H°$ is the heat of fusion of 100% crystalline poly(CL) reported to be 139.4 J/g[10]. Cyclohexane, indium, gallium and tin were used as standards for temperature calibration.

The molar composition, molecular weights and thermal properties of the prepared polymers are compiled in Table 1.

Table 1. Characterization of the prepared CL and TMC (co)polymers.

Polymer	$\overline{M}_n \times 10^{-5}$	PDI	$[\eta]^a$ (dl/g)	Tg^b (°C)	Tm^b (°C)	w_c^b (%)
Poly(CL)$_A$	1.6	2.0	3.9	-68	55	45
Poly(CL)$_B$	2.7	2.1	5.8	-67	56	48

^{a} In CHCl$_3$, at 25°C.

^{b} Second heating scan (DSC).

Nerve Guide Preparation

<u>Single layer macroporous nerve guides</u>.

Fibers were spun from 12 wt/vol% poly(CL)$_A$ solutions in chloroform containing 0.12 wt/vol% poly(ethylene oxide) (PEO, $\overline{M}_w = 8 \times 10^6$, Aldrich-Chemie, Germany). The polymer solution was pumped through a needle ($\phi = 0.5$ mm) moving up and down (30 mm/s) along a vertically rotating (790 rpm) glass mandrel ($\phi = 1.5 \pm 0.1$ mm), onto which the solidifying polymer fiber was wound. Variation of these speeds allows good control of the resulting winding angles. The distance between the needle and the rotating mandrel was set at 6 mm. Fiber spinning and winding were carried out for 50 minutes over a length of 70 mm and subsequently the graft was dried in air overnight. The nerve guides were removed from the glass

mandrels after 5-20 min of immersion in ethanol, dried in a vacuum oven at room temperature and stored at -20°C till further use.

Two-ply nerve guides (non-porous inner layer/macroporous outer layer).

To prepare the inner layer, a glass mandrel (ϕ=1.5±0.1 mm) was immersed (12 mm/s) in a 4 wt/vol% solution of poly(CL)$_B$ in chloroform. After 10 seconds in the solution the mandrel was pulled out (12 mm/s) and the chloroform was allowed to evaporate in air overnight. The outer layer fibers were spun, following the procedure described above, from 5 wt/vol% poly(CL)$_B$ solutions in chloroform containing 0.07 wt/vol% PEO and wound on the rotating previously dip-coated tube. Fiber spinning and winding were carried out for 70 min over a length of 60 mm and subsequently the graft was dried in air overnight. The nerve guides were removed from the glass mandrels after 5-20 min of immersion in ethanol, dried in a vacuum oven at room temperature and stored at -20°C till further use.

Two-ply nerve guides (microporous inner layer/macroporous outer layer).

To prepare the inner layer, a glass mandrel (ϕ=1.5±0.1 mm) was immersed (5 mm/s) in a 4 wt/vol% solution of poly(CL)$_B$ in tetrahydrofuran (THF). After 10 seconds in the solution the mandrel was pulled out (5 mm/s) and immersed (5 mm/s) in a coagulation bath consisting of a mixture of ethanol:THF (8:1 vol:vol). After 1 hr the mandrel was removed from the coagulation bath and the solvent allowed to evaporate in air overnight. The outer layer fibers were spun, following the procedure described above, from 5 wt/vol% poly(CL)$_B$ solutions in chloroform containing 0.07 wt/vol% PEO and wound on the rotating previously dip-coated tube. Fiber spinning and winding were carried out for 54 min over a length of 40 mm and subsequently the graft was dried in air overnight. The nerve guides were removed from the glass mandrels after 5-20 min of immersion in ethanol, dried in a vacuum oven at room temperature and stored at -20°C till further use.

Nerve Guide Characterization

Morphology.

The inside and outside surfaces of the prepared guides, as well as their cross-sectional areas, were examined by scanning electron microscopy (SEM). Cross sections were prepared by breaking the tubes in liquid nitrogen. The samples were dried overnight under vacuum and coated with a gold layer using a Polaron E5600 sputter-coater (UK). SEM analyses were carried out using a Hitachi S800 (Japan) field emission scanning electron microscope at voltages of 5 kV.

Kinking resistance.

The kinking resistance of the prepared nerve guides was evaluated in a semi-guided bending test. The nerve guides were sequentially bent around rods of decreasing diameter (30, 22, 16, 15, 10 and 6 mm). The bending radius was defined as the radius of the rod around which the conduit is bent. The bending angle, defined as the change in angle between both legs of the sample during the bend test, ranged between 90-180º depending on the length of the nerve guide and the rod diameter. The kinking resistance of the nerve guides was rated according to the following scoring system:

(+) non-kinking: the cross-sectional area of the conduit stays intact during bending;

(±) moderate kinking: the cross-sectional area of the conduit decreases slightly at one or more positions;

(-) strong kinking: the cross-sectional area of the conduit is completely constricted at one or more positions.

In Vivo Implantation

Prior to implantation, the nerve guides were cut into the desired dimensions (in liquid nitrogen) and sterilized by rinsing for 10 s in a 70 vol% ethanol solution, followed by rinsing during 30 s in sterile water. Female Wistar rats (weighing 220-240 g) were anaesthetized and the left sciatic nerve was isolated at the midthigh level via a dorsal approach and a 2 mm nerve segment was dissected. The nerve stumps were inserted in a 10 mm nerve guide over a distance of 2 mm at each side, so that a 6 mm gap remained. Tissucol® (Immuno AG, Austria) was used to glue the nerve ends to the tube. The wound was closed in layers. The rats were divided in four groups according to the graft used for repair:

Group I (n=8): single-layer macroporous nerve guides;

Group II (n=6): two-ply nerve guides consisting of a non-porous inner layer and a macroporous outer layer;

Group III (n=6): two-ply nerve guides consisting of a microporous inner layer and a macroporous outer layer;

Group IV (n=12): autografts.

After 12 weeks, the grafted sciatic nerve was resected, cleaned and mounted in a nerve chamber developed to measure propagating action potentials[9]. Increasing stimulus voltages were applied to the regenerated nerve fibers and the resulting compound action currents were measured. In this way the maximum charge displaced (Q_{max}), the mean conduction velocity (MCV) and the mean voltage

threshold (V_{50}) were determined. A Chi-square test was performed to identify the regenerated nerve fibers that show electrophysiological response within each of the groups. For the positive responses, values for Q_{max}, MCV and V_{50} were analyzed using one-way ANOVA, followed by Tukey's least significant differences multiple comparisons test to investigate differences between the groups. Differences were considered significant when $p<0.05$.

RESULTS AND DISCUSSION

Nerve Guide Preparation and Characterization

Figure 1 shows a cross-section of a two-ply nerve guide with a microporous inner layer. The inner layer is comprised of an interconnected network of pores in the size range of 1-10 μm, which is open both at the inner and outer surfaces (see Figure 2 – inner surface of the nerve guide). The pores present in the inner layer (Figure 1.B and 2) originate from the demixing process which occurs during the exchange of the solvent (THF) by the non-solvent (ethanol:THF 8:1).
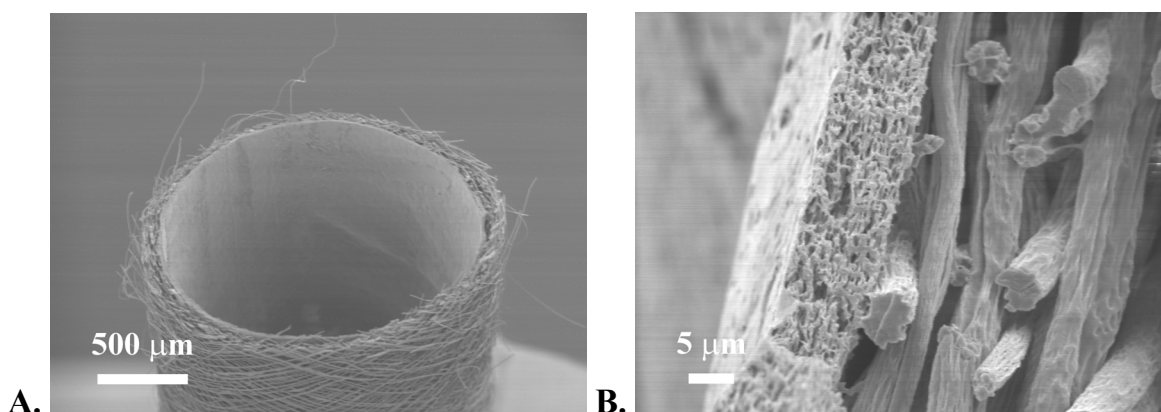

Figure 1. Scanning electron micrographs of cross-sections of a two-ply poly(CL) nerve guide consisting of a microporous inner layer and a macroporous outer layer.
(A) Overview. (B) Detail of the connection between the two layers.

In the preparation of the fiber-based outer layer, fibers could not be formed from pure poly(CL) solutions, but were only obtained after the addition of a small amount (<1% of the total polymer weight) of high molecular weight PEO. The introduction of PEO led to an increase in the viscosity of the solutions. However, the spinnability of these solutions can not only be attributed to increased viscosity, since poly(CL) solutions of higher concentration (25 wt/vol%) could not be spun

either. Spinnability of polymer solutions is a complex phenomenon that depends on many parameters such as polymer characteristics, viscosity, surface tension and viscoelasticity of the liquid and processing conditions[11-14]. The viscoelastic properties of the poly(CL) solutions may have changed upon addition of PEO due to changes in the entanglement network density and formation of physical cross-links.
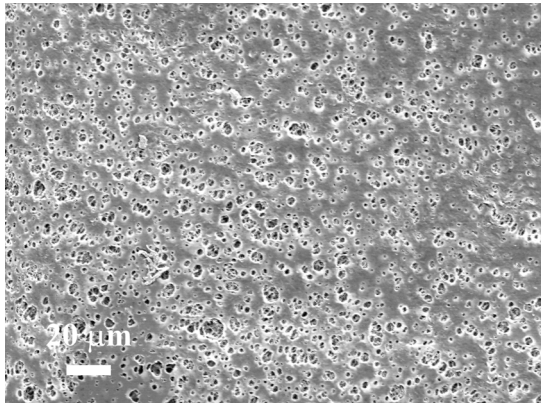

Figure 2. Scanning electron micrograph of the inner surface of the two-ply poly(CL) nerve guides with a microporous inner layer.

A regular macroporous outer layer firmly attached to the inner layer was obtained by fiber winding. Such firm bonding between layers is necessary to prevent the collapse of the thin inner layer of the conduit. The first spun fibers bind to the dip-coated layer as at the moment of contact the polymer fiber still contains some solvent. A similar process is responsible for the observed fiber confluence (fiber-to-fiber bonding), which is an essential feature to guarantee the dimensional stability of these structures[15]. The pore size determined by SEM of the outer layer of the two-ply nerve conduits ranged between 10 and 70 μm, with an average value of approximately 30 μm. The pore size was defined as the distance between two fibers located on the same plane[7]. The fiber diameter varied between 5 to 20 μm, and the angle of winding (angle between the fiber and the longitudinal axis of the conduit) was found to be approximately 64º.

Single-layer macroporous tubes consisting only of a wound layer of fibers were prepared (Figure 3) to characterize further the outer layer in the two-ply conduits. Pore sizes at the inner and outer surfaces of the fiber-wound structures were similar.
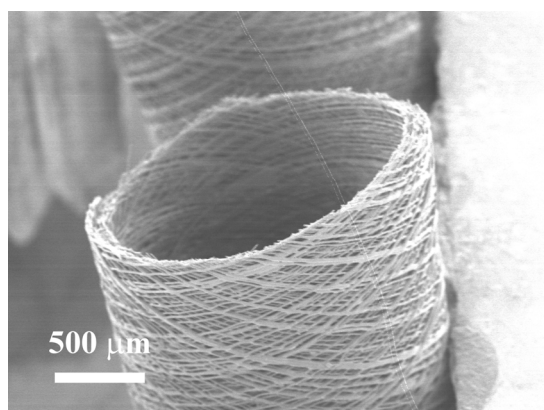
Figure 3. Scanning electron micrograph of a cross-section of a single-layer poly(CL) nerve guide prepared by fiber winding.
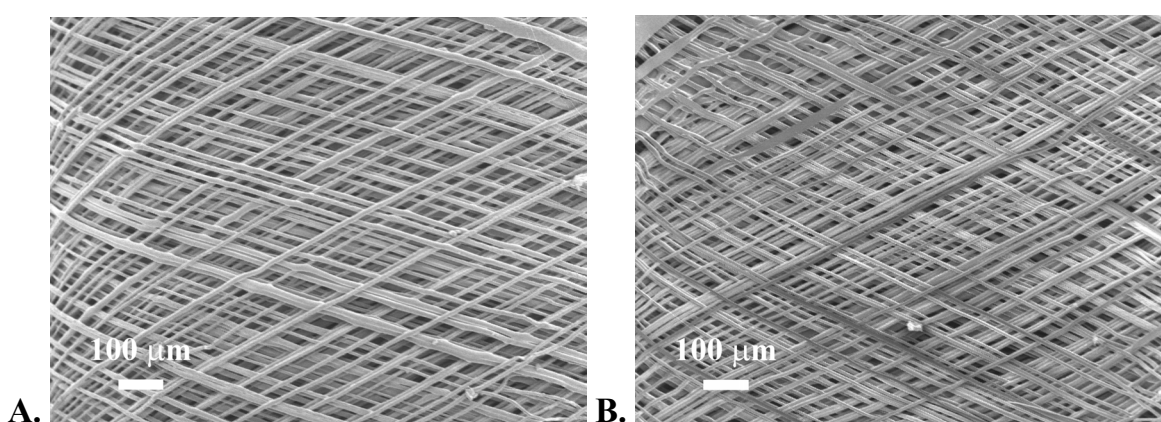

Figure 4. Scanning electron micrographs of the (A) outer and (B) inner surfaces of a single-layer poly(CL) nerve guide prepared by fiber winding.

Two-ply nerve guides with a non-porous inner layer (Figure 5.A) were also prepared. The inner layer was obtained by evaporation of the solvent (chloroform) after deposition of a polymer solution onto the mandrel by dip-coating. During the evaporation of the solvent, the polymer solution solidifies resulting in a non-porous structure (Figure 5.B). Due to the absence of pores, the final thickness of the inner layer of these tubes is smaller than in the case of the microporous inner layer of the previously described two-ply nerve guides.

The average dimensions and pore characteristics of the three-types of conduits prepared, as well as their flexing properties are summarized in Table 2. The inner diameter of the conduits was in accordance with the dimensions of the glass mandrels used in the preparation of the nerve guides and the average pore size of the inner and outer layers were in the range of the targeted values.

Although an optimal thickness has not been defined for nerve guides, thin non-collapsible tubes tend to perform the best[16,17]. Therefore, the overall thickness of

the nerve guides was minimized provided that the thickness of the inner layer would not compromise the flexibility of the conduits and that the outer layer assured sufficient strength and dimensional stability to prevent the lumen of the tube to collapse.
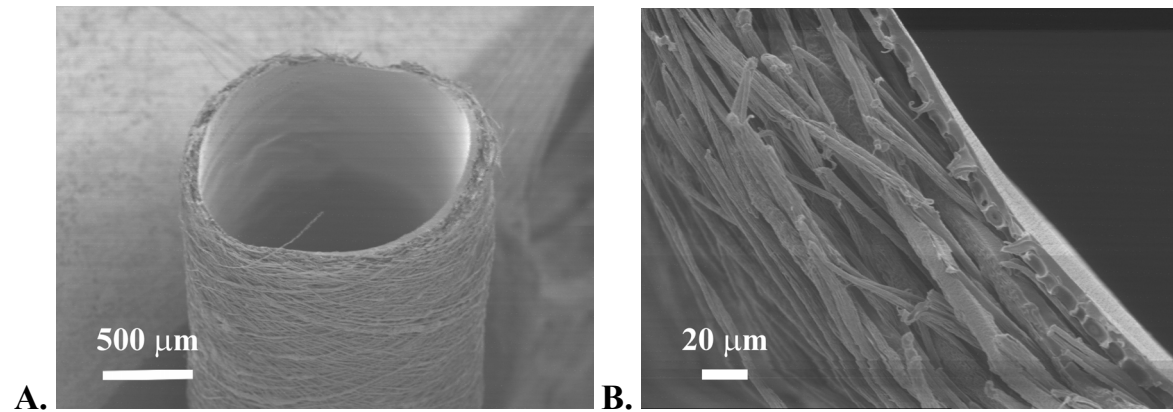

Figure 5. Scanning electron micrographs of cross-sections of a two-ply poly(CL) nerve guide consisting of a non-porous inner layer and a macroporous outer layer.
(A) Overview. (B) Detail of the connection between the two layers.

Table 2. Characterization of the poly(CL) nerve guides.

Tube features	Inner diameter (mm)	Wall thickness (μm)		Pore size (μm)		Kinking resistance at different bending radii (mm)					
		Inner layer	Outer layer	Inner layer	Outer layer	15	11	8	7.5	5	3
Single layer: macroporous	1.6	-	158	-	41 (10-230)	+	+	+	+	+	+
Two-ply: non-porous inner layer	1.7	15	80	-	45 (5-70)	±	±	-	nd	nd	nd
Two-ply: microporous inner layer	1.7	19	101	5 (1-10)	33 (9-74)	±	±	-	nd	nd	nd

Note: Average values (n≥3) of all parameters are given. The pore size variation range is presented in brackets.

nd – Not determined.

(+) non-kinking: the cross-sectional area of the conduits stays intact during bending;

(±) moderate kinking: the cross-sectional area of the conduits decreases slightly at one or more positions;

(-) strong kinking: the cross-sectional area of the conduits is completely constricted at one or more positions.

An important property of a flexible nerve guide, often disregarded, is its ability to bend with a minimal reduction in the tube's (internal) cross-sectional area. In the present study the flexing properties of the nerve guides were evaluated by determining their kinking resistance upon bending.

Silicone tubes are commonly used as nerve grafts in nerve regeneration studies in animal models[18] as well as in clinical practice as an alternative to autografts[19]. Although the fact that silicone-based conduits are non-degradable, which is a major drawback of these systems, they show good mechanical characteristics for use as nerve grafts. Therefore, silicone tubing of similar dimensions to the nerve guides described in this study (inner diameter: 1.47 mm and wall thickness: 245 µm; Helix Medical, CA, USA) was also tested, and used as a reference. For all tested bending radii, silicone tubing showed non-kinking behavior.

Macroporous single-layer nerve guides prepared by means of fiber winding behaved similarly to the silicone tubing. The conduits were found to be very flexible, bending easily without kinking, even at small bending radii.

The two-ply tubes were found to be stiffer, their cross-sectional area already decreasing at several points when the tubes were bent around the rods with the largest diameters. At a bending radius of 8 mm, strong kinking, with total occlusion of the lumen of the tubes, was observed.

The good flexing properties of the single-layer fiber-wound macroporous tubes are the result of the anisotropic properties of these structures[7]. Due to the 64° angle at which the fibers are wound, the tubes are stiffer in the hoop than in the longitudinal direction. This allows the lumen of the tube to remain open during flexing, resulting in non-kinking behavior. The mechanical properties of the inner layers of the two-ply tubes are isotropic and the effect described above is not observed, which leads to a decrease in kinking resistance of these conduits.

Nerve Guide Implantation

The three types of poly(CL) conduits described in the previous paragraphs were evaluated as nerve grafts in the correction of 6 mm gaps in the rat sciatic nerve.

In line with the flexing properties, macroporous poly(CL) nerve guides showed the best handling characteristics during the surgical grafting procedure. The telescoping of the nerve stumps into the nerve guide could be easily done. The graft was smooth and embraced the nerve like a 'soft sleeve'. The two-ply nerve guides, with non-porous and microporous inner layers, were more rigid. This sometimes led to less than optimal positioning of the nerve stumps into the nerve guide. Moreover, the

edges of these conduits were not as smooth as the edges of the macroporous nerve guides, which might have caused some irritation to the nerve stumps.

In all cases the nerve ends could be easily secured to the nerve guide with Tissucol®.

Nerve Regeneration Evaluation

For all groups of animals operated with poly(CL) conduits, at 12 wks post-implantation it was possible to observe that the nerve guides were still present at the implantation site and that a bundle of tissue had grown through the artificial grafts and had bridged the nerve gap. However, in the group grafted with the macroporous nerve guides a significant amount of fibrous tissue was also present and had infiltrated the wall of the conduits.

The results of the electrophysiological evaluation of the nerve fibers regenerated through the different grafts are given in Figures 6, 7 and 8.
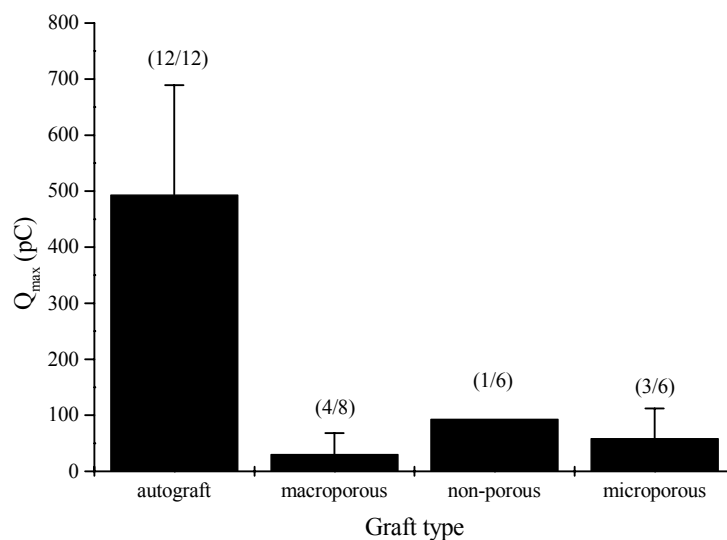
Figure 6. Maximum charge displacement (Q_{max}) for the different groups of animals subjected to nerve grafting with, respectively, nerve autografts and poly(CL) based nerve guides (macroporous single-layer, two-ply with non-porous inner layer and two-ply with microporous inner layer). Mean ± standard deviation of the results for the individuals that show electrophysiological response (the number of positive responses over the number of implanted grafts is presented in brackets).

Figure 7. Mean conduction velocity (MCV) for the different groups of animals subjected to nerve grafting with, respectively, nerve autografts and poly(CL) based nerve guides (macroporous single-layer, two-ply with non-porous inner layer and two-ply with microporous inner layer). Mean ± standard deviation of the results for the individuals that show electrophysiological response (the number of positive responses over the number of implanted grafts is presented in brackets).

Figure 8. Mean voltage threshold (V_{50}) for the different groups of animals subjected to nerve grafting with, respectively, nerve autografts and poly(CL) based nerve guides (macroporous single-layer, two-ply with non-porous inner layer and two-ply with microporous inner layer). Mean ± standard deviation of the results for the individuals that show electrophysiological response (the number of positive responses over the number of implanted grafts is presented in brackets).
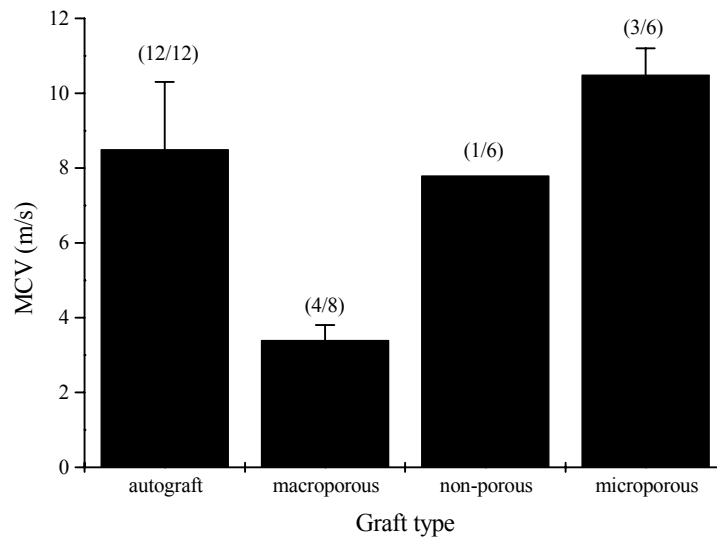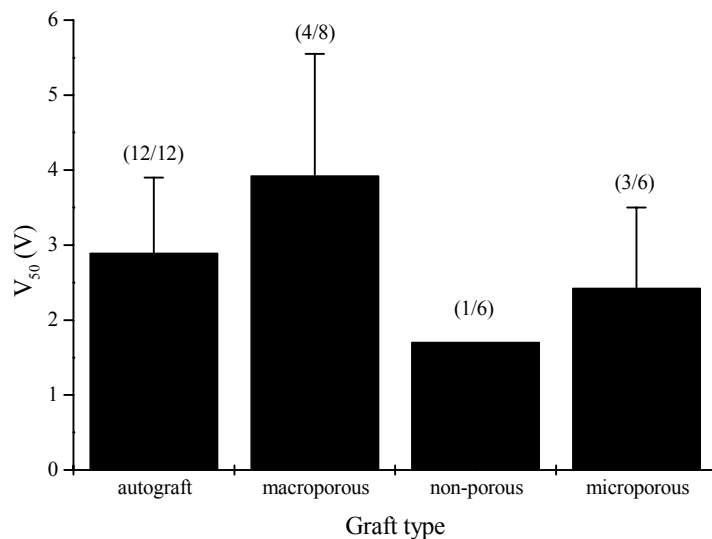
Q_{max} is a measure of the maximum charge displaced through the nerve fibers and is dependent on the diameter as well as on the number of regenerated and pulse-conducting axons. The MCV is mainly determined by the diameter of the regenerated axons[20]. Higher MCV is observed for axons with a larger diameter. The extra-cellular firing threshold of nerve fibers is inversely proportional to the fiber diameter[21]. Therefore, V_{50} (the voltage at 50% Q_{max}, a parameter for the voltage needed to stimulate the excitable axons) is expected to be smaller for axons with a larger diameter[9].

Q_{max} measured for all nerve fibers regenerated through the artificial nerve guides was significantly lower than the value obtained for nerves regenerated through autografts (Figure 6). In 5 out of the 6 animals operated with two-ply grafts with a non-porous inner layer, Q_{max} of the regenerated nerve fibers was too low to be measured and therefore, in terms of nerve regeneration the overall outcome of this group is significantly worse than the groups operated with the macroporous conduits and the two-ply nerve guides with the microporous inner layer. For the groups operated with permeable grafts (groups I and III) there was no significant difference between the Q_{max} values for each group.

Although the differences between Q_{max} for the groups operated with permeable grafts were not significant, significant differences were observed in terms of MCV (Figure 7) and V_{50} (Figure 8). For group I (macroporous graft) MCV was smaller and V_{50} higher than for the group operated with the two-ply microporous tube (group III). This implies a worse performance of the macroporous conduits, which may be explained by infiltration of fibrous tissue into the regeneration area, in line with previous findings[22].

MCV and V_{50} were not significantly different for the group operated with two-ply nerve guides (microporous inner layer) and the autograft group.

The obtained results confirm that compared to non-permeable nerve guides, the use of permeable nerve guides has a beneficial effect on nerve regeneration. The group operated with the two-ply nerve guides with a microporous inner layer showed electrophysiological responses closest to the autograft group. Although Q_{max} of the nerves grafted with the two-ply conduits was still significantly smaller than the values found for the autografted nerves, MCV and V_{50} were not significantly different, suggesting that the individual diameter of the regenerated axons in the porous grafts is in a similar range compared to the diameter of the axons regenerated in the autografts[9].

Histological examination of the regenerated tissue and of the target muscles is presently under investigation and will give us further insight into the regeneration process.

CONCLUSIONS

With the applied process conditions, permeable two-ply tubes of the desired dimensions and pore size could be prepared in a reproducible manner, both layers consisting of homogeneous interconnected pores. The use of these nerve guides in the correction of 6 mm nerve defects in the rat sciatic nerve gap model resulted in significantly better nerve regeneration (as established by electrophysiological methods) than that observed with nerves grafted with similar two-ply tubes with a non-porous inner layer.

Despite the fact that the outer layer of the two-ply guides has excellent flexing and handling characteristics (similar to silicone tubing), the higher stiffness of the thin inner layer results in a relatively low flexibility of the conduits and strong kinking behavior at small bending radii. Such behavior resulted in less suitable handling during surgery, making the telescoping of the nerve stumps into the nerve guides difficult at times. This might also have had a detrimental effect on the nerve regeneration process. The relative stiffness and the less than optimal flexibility of the conduits may result in a poorer regeneration outcome as, due to the animal limb movement, pressure exerted by the rim of the relatively rigid tubes may lead to nerve damage[23].

ACKNOWLEDGMENTS

REFERENCES

[1]   Pêgo AP, Poot AA, Grijpma DW, Feijen J. Copolymers of trimethylene carbonate and ε-caprolactone for porous nerve guides: synthesis and properties. *J Biomater Sci Polym Ed* 2001; 12: 35-53. Chapter 3 of this thesis.

[2]   Pitt CG, "Poly-ε-caprolactone and its copolymers" In: Chasin M, Langer R. *Biodegradable polymers as drug delivery systems*, New York, NY: Marcel Dekker; 1990. p 71-120.

[3]   Pitt CG, Schindler A, "Capronor: A biodegradable delivery system for levonorgestrel" In: Zatuchni GI, Goldsmith A, Shelton JD, Sciarra JJ. *Long-Acting Contraceptive Delivery Systems*, Philadelphia: Harper and Row; 1984. p 48-63.

[4]   Hinrichs W. "Porous polymer structures for tissue engineering" Ph.D. Thesis. University of Twente, Enschede, The Netherlands. 1992.

[5]   Hoppen HJ, Leenslag JW, Pennings AJ, van der Lei B, Robinson PH. Two-ply biodegradable nerve guide: basic aspects of design, construction and biological performance. *Biomaterials* 1990; 11: 286-290.

[6]   den Dunnen WFA, Schakenraad JM, Zondervan GJ, Pennings AJ, van der Lei B, Robinson PH. A new PLLA/PCL copolymer for nerve regeneration. *J Mater Sci: Mater Med* 1993; 4: 521-525.

[7]   Leidner J, Wong EWC, MacGregor DC, Wilson GJ. A novel process for the manufacturing of porous grafts: process description and product evaluation. *J Biomed Mater Res* 1983; 17: 229-247.

[8]   Vleggeert-Lankamp CLAM, Pêgo AP, Lakke EAJF, Marani E, Poot AA, Grijpma DW, Feijen J, Thomeer RTWM. Pores in artificial nerve grafts improve electrophysiological properties of regenerating peripheral nerves. Abstract submitted to the 33rd Annual Meeting of the American Association of Hand Surgery. Kauai, Hawaii, USA (2003).

[9]   Vleggeert-Lankamp CLAM, van den Berg RJ, Lakke EAJF, Malessy MJA, Thomeer RTWM. Increased firing threshold and refractory period of the Aα- and Aß-fibers in the autografted rat sciatic nerve. *(manuscript in preparation)*.

[10]   Crescenzi V, Manzini G, Calzolari G, Borri C. Thermodynamics of fusion of poly-β-propiolactone and poly-ε-caprolactone. Comparative analysis of the melting of aliphatic polylactone and polyester chains. *Eur Polym J* 1972; 8: 449-463.

[11]   Hashimoto K, Imae T. The spinnability of aqueous polymer-solutions. *Polym J* 1990; 22: 331-335.

[12]   Imae T, Hashimoto K, Ikeda S. The spinnability of viscoelastic solutions of tetradecyl-trimethylammonium and hexadecyl-trimethylammonium salicylates. *Colloid Polym Sci* 1990; 268: 460-468.

[13] Hashimoto K, Imae T, Nakazawa K. The viscoelasticity of spinnable solutions of alkyltrimethylammonium salicylates. *Colloid Polym Sci* 1992; 270: 249-258.

[14] Imae T, "Spinnability of viscoelastic surfactant solutions and molecular assembly formation" In: *Structure and flow in surfactant solutions, ACS symposium series, 578*, 1994. p 140-152.

[15] Bots JG. "Polyethers as biomaterials" Ph.D. Thesis. University of Twente, Enschede, The Netherlands. 1988.

[16] Buti M, Verdu E, Labrador RO, Vilches JJ, Fores J, Navarro X. Influence of physical parameters of nerve chambers on peripheral nerve regeneration and reinnervation. *Exp Neurol* 1996; 137: 26-33.

[17] den Dunnen WFA, van der Lei B, Robinson PH, Holwerda A, Pennings AJ, Schakenraad JM. Biological performance of a degradable poly(DL-lactide-ε–caprolactone) nerve guide: Influence of tube dimensions. *J Biomed Mater Res* 1995; 29: 757-766.

[18] Dahlin LB, Lundborg G. Use of tubes in peripheral nerve repair. *Neurosurg Clin N Am* 2001; 12: 341-352.

[19] Lundborg G, Rosen B, Dahlin L, Danielsen N, Holmberg J. Tubular *versus* conventional repair of median and ulnar nerves in the human forearm: early results from a prospective, randomized, clinical study. *J Hand Surg [Am]* 1997; 22: 99-106.

[20] Hursh JB. Conduction velocity and diameter of nerve fibers. *Am J Physiol* 1939; 127: 131-139.

[21] Jack JJB, Noble D, Tsien RW, *Electric current flow in excitable cells*. Oxford: Oxford University Press; 1983.

[22] Valentini RF, "Nerve guidance channels" In: Bronzino JD. *The Biomedical Engineering Handbook*, Boca Raton, FL: CRC Press; 1995. p 1985-1996.

[23] Henry EW, Chiu TH, Nyilas E, Brushart TM, Dikkes P, Sidman RL. Nerve regeneration through biodegradable polyester tubes. *Exp Neurol* 1985; 90: 652-676.

APPENDIX B

First attempts to improve guided nerve regeneration by filling of nerve guides with a Schwann cell-containing ECM-derived protein gel

A.P. PÊGO[1], C.L.A.M. VLEGGEERT–LANKAMP[2], E.A.J.F. LAKKE[2], E. MARANI[1,2], R.T.W.M. THOMEER[2], A.A. POOT[1], D.W. GRIJPMA[1] and J. FEIJEN[1]

[1] *Institute for Biomedical Technology (BMTI) and Department of Polymer Chemistry and Biomaterials, Faculty of Chemical Technology, University of Twente, P.O. Box 217, 7500 AE Enschede, The Netherlands*
[2] *Neuroregulation Group, Department of Neurosurgery, Leiden University Medical Center (LUMC), P.O. Box 9604, 2300 RC Leiden, The Netherlands*

INTRODUCTION

In a previous study we found that two-ply nerve guides comprised of a non-porous inner layer of poly(1,3-trimethylene carbonate) (poly(TMC)) and macroporous outer layer based on a copolymer of TMC and ε-caprolactone (CL) with 10 mol% of TMC can serve as a support for axonal guidance in the correction of peripheral nerve defects in the rat sciatic nerve model[1]. The nerve guides showed good bending properties and excellent handling characteristics during surgery, flexing easily without kinking. Functionality of the regenerated axons was evaluated by an *in vitro* quantitative electrophysiological method[2]. The results showed that the contact between the proximal and distal nerve ends was reestablished and that the conductive velocity of the regenerated axons in the nerve guides did not differ from that of autografts. However, other electrophysiological properties of nerve fibers regenerated through autografts were still better than those of axons regenerated through the artificial nerve guides.

Extracellular matrix (ECM) proteins like fibronectin (FN), laminin (LN) or collagen were found to stimulate the outgrowth of neurites and enhance nerve

regeneration[3-7]. With rare exceptions[8], the incorporation of Schwann cells (SCs) into a nerve guide also proved to have a positive effect on the overall regeneration process, increasing peripheral nerve growth, myelination and functional recovery[9-14]. SCs play a vital role in the natural nerve regeneration process, producing ECM proteins and a range of neurotropic and neurotrophic factors essential for axonal growth[15-18].

The aim of the present study was to evaluate the effect of heterologous SCs seeded in a gel consisting of a mixture of LN, FN and collagen type I incorporated in the previously developed and tested nerve guides, on the enhancement of nerve regeneration and recovery of electrophysiological properties in the rat sciatic nerve gap model.

MATERIALS AND METHODS

Polymer Synthesis and Characterization

Poly(TMC) and poly(TMC-CL) with 11 mol% of TMC were synthesized and characterized as previously described[19]. Briefly, the polymerizations were conducted by ring-opening polymerization in evacuated and sealed glass ampoules using $SnOct_2$ as catalyst. All polymerizations were carried out for a period of 3 days at 130°C±2°C. The obtained polymers were purified by dissolution in chloroform and subsequent precipitation into a ten-fold volume of isopropanol. The precipitated polymers were recovered, washed with fresh isopropanol and dried under reduced pressure at room temperature until constant weight. The molar composition, molecular weights and thermal properties of the polymers were evaluated after processing and are compiled in Table 1.

Table 1. Characterization of the prepared TMC and CL (co)polymers.

Polymer	$\overline{M}_n \times 10^{-5}$	PDI	$[\eta]^a$ (dl/g)	Tg^b (ºC)	Tm^b (ºC)	w_c^b (%)
Poly(TMC)	3.3	1.5	4.20	-19	-	-
Poly(TMC-CL) (11:89 mol%)	1.3	1.7	3.8	-64	37	33

$\overline{M}_n$: average number molecular weight; PDI: polydispersity index; $[\eta]$: intrinsic viscosity; Tg: glass transition temperature; Tm: melting temperature and w_c: crystallinity.

^{a} In $CHCl_3$, at 25ºC.

^{b} Second heating scan (DSC).

Nerve Guide Preparation

Two-ply nerve guides consisting of a non-porous poly(TMC) inner layer and a macroporous poly(TMC-CL) outer layer were prepared by a combination of dip-coating (inner layer) and fiber winding (outer layer) techniques and subsequently characterized as previously described[1]. To prepare the inner layer, a glass mandrel (ϕ=1.5±0.1 mm) was immersed in a 4 wt/vol% solution of poly(TMC) in chloroform. After 10 seconds in the solution the mandrel was pulled out and the chloroform was allowed to evaporate at room temperature for 10 min. This procedure was repeated and the tube was dried overnight in air. The outer layer fibers were spun from 10 wt/vol% poly(TMC-CL) solutions in chloroform containing 0.16 wt/vol% poly(ethylene oxide) (PEO, $\overline{M}w$=8x10^6, Aldrich-Chemie, Germany) and wound on a rotating previously dip-coated tube. Fiber spinning and winding were carried out over a length of 30 mm for 40 min and subsequently, the grafts were dried overnight in air. The nerve guides were removed from the glass mandrels after 5-20 min of immersion in ethanol, dried in a vacuum oven at room temperature and stored at -20°C until further use.

The structure of the prepared porous scaffolds was evaluated using a Hitachi S800 field emission scanning electron microscope (SEM) operating at 5 kV. Prior to microscopical evaluation the structures were coated with a gold layer using a Polaron E5600 sputter-coater.

The characteristics of the nerve guides are summarized in Table 2.

Table 2. Characterization of two-ply nerve guides based on TMC and CL (co)polymers.

Inner diameter (mm)	Wall thickness (μm)		Pore size (μm)	
	Inner layer	Outer layer	Inner layer	Outer layer
1.5	27	235	non porous	57 (15-265)^a

^{a} Pore size range.

Isolation and Purification of Rat Schwann Cells (RSC)

Pieces of rat sciatic nerve and brachial plexus (adult Wistar rats) were used to establish RSC cultures by means of a sequential explantation technique[20]. After careful stripping of the epineurium and connective tissue, the nerve explants were cut into pieces of approximately 1 mm^3. These were placed in gelatin-coated culture flasks (Greiner, The Netherlands) and covered with a thin layer of culture medium

consisting of Dulbecco's modified Eagle's medium (DMEM; Bio-Whittaker Europe, Belgium), 10% fetal calf serum (FCS; Gibco BRL, Life Technologies, Germany), 0.225% NaHCO$_3$ (Sigma, USA), 1 mM sodium pyruvate (Sigma), 0.03% L-glutamine (Sigma), 0.6% D(+)-glucose (Sigma), 0.12% tryptose phosphate (Sigma), 100 IU/ml penicillin (Gist-Brocades, The Netherlands) and 50 µg/ml streptomycin (Gist-Brocades). SCs and fibroblasts migrate out of the nerve pieces and adhere to the bottom of the gelatin-coated culture flasks. When the outgrowth around the explants reached a near-confluent monolayer, the explants were transferred and placed in new flasks with fresh medium. This procedure was repeated for approximately 4-5 weeks. As fibroblasts migrate faster than SCs[20], after a few transfer rounds most of the cells migrating out of the nerve pieces are SCs.

Gelatin coatings on the culture flasks were prepared by incubating a 0.5 wt/vol% solution of gelatin (Difco Laboratories) for 45 min at room temperature, followed by 15 min incubation with 0.5 wt/vol% glutaraldehyde (Merck, Germany) solution. The coated flasks were then thoroughly rinsed with distilled water and dried overnight in a laminar flow chamber.

Immunocytostaining of Rat Schwann Cells

In order to differentiate between RSCs and fibroblasts, cell cultures were made on gelatin-coated coverslips (same coating procedure as described above for the coating of culture flasks), fixed with Cryofix® (Merck, Germany), rinsed 3 times with PBS and incubated with antibodies appropriately diluted in PBS containing 0.1% bovine serum albumin (BSA) and 1% normal goat serum (NGS; CLB, The Netherlands). To identify Schwann cells, antibodies directed against S100 and glial fibrillary associated protein (GFAP; Boehringer Mannheim Biochemica, Germany) were added in a dilution of 1:1,000 and 1:500, respectively. For fibroblast identification, antibodies directed against Thy 1.1 (Serotec, UK) and smooth muscle actin (SMA; Sigma) were used in a dilution of 1:10,000 and 1:200, respectively. After overnight incubation at 4°C and 100% humidity, cultures were again rinsed 3 times with PBS and subsequently stained with GAM/FITC (Molecular Probes, The Netherlands) appropriately diluted in PBS containing 0.1% BSA and 1% NGS. After extensive rinsing with PBS, sections were mounted, dehydrated and coverslipped with Fluoromount® (Merck) and viewed with a fluorescence microscope (Olympus, The Netherlands).

Seeding of the Nerve Guides

Before filling with the ECM protein gel (with and without RSCs), the nerve guides were cut to the desired lengths (in liquid nitrogen) and sterilized by rinsing for 10 s in a 70 vol% ethanol solution, followed by rinsing during 30 s in sterile water. Subsequently, the nerve guides were blotted with sterile filter paper, placed in a Petri dish and left drying for a few minutes in a laminar flow chamber.

Meanwhile, RSCs were collected from the gelatin-coated culture flasks, by incubation for approximately 1 min at room temperature with a solution of 0.25% trypsin (Difco Laboratories, USA) and 10 mM ethylenediaminetetraacetic acid (EDTA) in DMEM, followed by the addition of an equal amount of culture medium. A small cell sample was stained with True Blue (Janssen Chimica, Belgium) to evaluate cell viability. The cell number was estimated using a Bürker-Türk chamber and subsequently the cell suspension was centrifuged for 5 min at 1,600 rpm. The cell pellet was washed with culture medium and after a second centrifugation step (5 min, 1,600 rpm) the cells were resuspended in a mixture containing 10 μl of LN (0.5 mg/ml, Boehringer Mannheim Biochemica), 5 μl of FN (1 mg/ml, Boehringer Mannheim Biochemica), 10 μl $NaHCO_3$/NaOH buffer (3.79 g $NaHCO_3$ in 100 ml 0.1N NaOH) in 80 μl of collagen type I (3 mg/ml, Vitrogen®, Cohesion, California, USA) to a final concentration of 2.5 x 10^6 RSC/ml. Five 10 mm nerve guides were filled with 17 μl aliquots of the RSC suspension and five other nerve guides were filled with similar gel-forming mixtures without RSCs and used as control. The nerve guides were placed in a Petri dish and incubated for 2 hrs at 37ºC in humidified air containing 5% CO_2. After this time, gelation was complete and the conduits were covered with a thin layer of medium and incubated at 37ºC in humidified air containing 5% CO_2 for 24 hrs prior to implantation.

Nerve Guide Implantation and Electrophysiological Evaluation

Female Wistar rats (weighing 220-240 g) were anaesthetized and the left sciatic nerve was isolated at the midthigh level via a dorsal approach and a 2 mm nerve segment was dissected. The nerve stumps were inserted in a 10 mm nerve guide over a distance of 2 mm at each side, so that a 6 mm gap remained. Tissucol® (Immuno AG, Austria) was used to glue the nerve ends to the tube. The wound was closed in layers. The rats were divided into two groups according to the graft used for repair:

Group I (n=5): nerve guides with ECM protein gel;

Group II (n=5): nerve guides with ECM protein gel+RSC;

Group III (n=12): autografts (positive control).

After 12 weeks, the grafted sciatic nerve was resected, cleaned and mounted in a nerve chamber developed to measure propagating action potentials[2]. Increasing stimulus voltages were applied *in vitro* to the regenerated nerve fibers and the resulting compound action currents were measured. In this way the maximum charge displaced (Q_{max}), the mean conduction velocity (MCV) and the mean voltage threshold (V_{50}) were determined.

RESULTS

Purification and Characterization of Rat Schwann Cell Cultures

Purification by the sequential explantation method resulted in cultures that stained almost exclusively with S100 and GFAP antibodies, and only sporadically with Thy1.1 and SMA antibodies, indicating highly purified (95-98%) RSC cultures. 99-100% of the cells that were to be seeded stained with True Blue, indicating high RSC viability.

Surgical Procedure

After filling of the tubes with the ECM protein mixture (with and without RSCs) and subsequent gelation of this suspension, no changes in the aspect and dimensions of the nerve guides was observed. During surgery the tubes could be handled well, flexing and bending without kinking. The telescoping of the nerve stumps into the nerve guide could be done with ease. The grafts were smooth and embraced the nerve like a 'soft sleeve'. The nerve ends could be easily secured to the nerve guides with Tissucol®.

Electrophysiological Properties of the Regenerated Nerve

In each group one animal showed automutilation a few days after surgery and eventually died before the scheduled explantation date. At 12 wks post-implantation, in the remaining animals of both groups treated with an artificial graft, a bundle of tissue had grown through the graft and had bridged the nerve gap (Figure 1). Although the site of implantation could be easily identified, the conduits could not be retrieved intact as they had degraded to some extent. The target muscles showed signs of

atrophy. The autografted nerves exhibited a good graft in continuity. The muscles innervated by the nerve were only slightly atrophic.
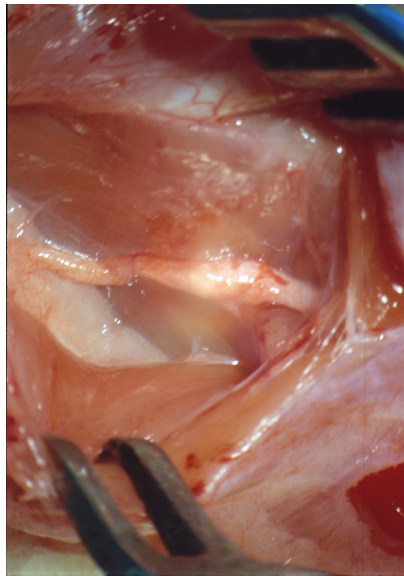

Figure 1. Photograph showing the appearance of the tissue regenerated through a nerve guide seeded with heterologous RSCs in an ECM protein gel (12-week implantation period).

The electrophysiological properties of the nerve fibers regenerated through both kinds of artificial grafts and the autografts is presented in Table 1. For sake of comparison, previously obtained results with similar nerve guides without an ECM protein gel (empty tubes) are also shown[1].

Q_{max} is a measure of the maximum charge displaced through the nerve fibers and is dependent on the diameter as well as on the number of regenerated and pulse-conducting axons. The MCV is mainly determined by the diameter of the regenerated axons[21]. Higher MCV values are observed for axons with a larger diameter. The extra-cellular firing threshold of nerve fibers is inversely proportional to the fiber diameter[22]. Therefore, V_{50} (the voltage at 50% Q_{max}, a parameter for the voltage needed to stimulate the excitable axons) is expected to be smaller for axons with a larger diameter[2].

In 2 of the 4 animals operated with grafts filled only with the ECM protein gel that survived the 12-week implantation period, an electrophysiological response was detected in the regenerated nerve fibers. However, even in these two cases, Q_{max} was significantly lower than the response observed in the autograft group. Furthermore, although the electrophysiological responses observed in the former group were in the same order of magnitude as the response of axons regenerated

through an empty nerve guide, the percentage of responses was much lower (2/5 versus 5/6). For none of the nerve fibers regenerated through grafts seeded with SCs a significant electrophysiological response could be detected.

Table 1. Electrophysiological response of nerves regenerated after grafting with two-ply nerve guides based on TMC and CL (co)polymers.

Nerve guide features	Rat nr.	Q_{max} (pC)	MCV (m/s)	V_{50}
ECM protein gel	1 (dam.)	No response		
	2 (dam.)	109	7.1	1.9
	3	Animal died before 12 wks		
	4	41	4.3	2.0
	5	No response		
ECM protein gel with RSCs	6 (dam.)	No response		
	7 SC	No response		
	8 SC	Animal died before 12 wks		
	9 SC	No response		
	10 SC	No response		
Empty nerve guide[a]	n=6 (average ± SD of 5/6)	92 ± 107	8.5 ± 1.0	1.3 ± 0.4
Autograft	n=12 (average ± SD of 12/12)	494 ± 195	8.5 ± 1.8	2.9 ± 1.0

dam.: damaged tubes (shrunk during conditioning of the nerve guides+gel(+SCs) in the operating theater due to overshooting of the oven temperature).

[a] Data from reference[1].

DISCUSSION

The obtained results indicate that there was no evident improvement in terms of nerve regeneration and functional recovery when the poly(TMC-CL) copolymer based nerve guides were supplemented with RSCs seeded in a gel matrix based on LN, FN and collagen type I. In each group one animal showed automutilation, what did not occur when empty nerve guides were used as grafts.

In the animals that survived the 12-week implantation period, it was observed that a bundle of tissue had grown through the nerve guides. Supposedly, some neurites grew through the guide, as the surrounding muscle was not completely atrophied, but the charge displaced through the regenerated axons was too small to be detected. Histological examination of the regenerated nerve and the target muscles will be performed to further evaluate and characterize the regenerated tissue.

The poor results obtained appear to be related to the protein-based three-dimensional matrix and not to a detrimental effect of the seeded RSCs. Although in previous reports SCs have been shown to enhance the nerve regeneration process, the used gel might have hindered the positive effect of their presence.

ECM components, such as LN, FN and collagen, localized in the endoneurium and basal membrane of the peripheral nerve are presumptive tropic factors that guide the elongation of nerve growth cones during the regeneration process[17,23]. However, the applied ECM protein gel, even though containing neurite-promoting factors, could have impaired nerve regeneration by physically impeding the diffusion of critical factors, the migration of non-neuronal cells, or the elongation of regenerating axons[24,25]. Additionally, the gel could have physically impaired the formation of the initial regenerative cable[26]. Receptor-mediated interactions may also have played an important role in influencing cell migration. Although the different ECM proteins present in the gel may improve cell-cell interactions and cell migration, binding of the cells to the distinct ECM protein domains may trigger intracellular responses that inhibit cell motility[27].

Previous studies have shown the dependence of nerve regeneration upon the density, viscosity and concentration of the applied gels[26,28,29]. While the concentration of collagen in the used gel was similar or lower than previous reported values[3,10] for gels that did not hinder nerve regeneration, the gel resulting from the mixture of the three proteins probably has a different final structure. For example, it was reported[27] that the addition of LN or FN to a collagen type I gel leads to an increase in the diameter of the fibers within the gel and to the formation, at high concentrations of LN or FN, of web-like structures between fibers. Furthermore, the gelation times were found to increase with the amount of LN or FN added, what may reflect changes in assembly of the gel matrix. The observed differences in the gel structures resulted in differing patterns of neurite extension *in vitro*, even with inhibition of the growth of neurites under certain conditions[27].

In the future, if such a gel is to be used as a support matrix for the seeding of SCs, the gel composition needs to be optimized. The testing of a range of compositions is then required. A gel matrix based on LN, FN and collagen type I mixtures has been previously used in the repair of a 10 mm nerve gap in the rat sciatic nerve model with silicone tubes[30]. The nerve guides were found to improve nerve regeneration in comparison to empty silicone tubes. In that study the concentration of collagen was approximately 2 times lower than used in the present study and the concentrations of LN and FN were 5 times higher.

Further improvement can be achieved by using matrices that are longitudinally oriented and provide wide enough guiding channels for cellular and axonal migration[31]. In a similar manner as successfully attained for collagen[32,33], the alignment of gels based on mixtures of LN, FN and collagen by exposure to high-strength magnetic fields could be investigated.

Another approach might involve the filling of the nerve guide with a SC suspension in a mixture of only LN and FN[4], which do not form a gel. In this manner an eventual detrimental effect of a dense gel can be avoided. In a previous study we have shown that TMC and CL based (co)polymers, either coated or non-coated with FN, allow the adhesion and proliferation of human SCs[34]. This is important, as in such systems the initial survival of the SCs will depend on their capability to attach to the nerve guide inner surface.

REFERENCES

[1] Pêgo AP, Vleggeert-Lankamp CLAM, Lakke EAJF, Marani E, Thomeer RTWM, Poot AA, Grijpma DW, Feijen J. Preparation and *in vivo* performance of degradable two-ply nerve guides based on (co)polymers of trimethylene carbonate and ε-caprolactone. Chapter 10 of this thesis.

[2] Vleggeert-Lankamp CLAM, van den Berg RJ, Lakke EAJF, Malessy MJA, Thomeer RTWM. Increased firing threshold and refractory period of the Aα- and Aß-fibers in the autografted rat sciatic nerve. *(manuscript in preparation)*.

[3] Madison RD, Da Silva CF, Dikkes P. Entubulation repair with protein additives increases the maximum nerve gap distance successfully bridged with tubular prostheses. *Brain Res* 1988; 447: 325-334.

[4] Woolley AL, Hollowell JP, Rich KM. Fibronectin-laminin combination enhances peripheral nerve regeneration across long gaps. *Otolaryngol Head Neck Surg* 1990; 103: 509-518.

[5] Bailey SB, Eichler ME, Villadiego A, Rich KM. The influence of fibronectin and laminin during Schwann cell migration and peripheral nerve regeneration through silicon chambers. *J Neurocytol* 1993; 22: 176-184.

[6] Toba T, Nakamura T, Shimizu Y, Matsumoto K, Ohnishi K, Fukuda S, Yoshitani M, Ueda H, Hori Y, Endo et a. Regeneration of canine peroneal nerve with the use of a polyglycolic acid-collagen tube filled with laminin-soaked collagen sponge: a comparative study of collagen sponge and collagen fibers as filling materials for nerve conduits. *J Biomed Mater Res* 2001; 58: 622-630.

[7]   Yoshii S, Oka M. Collagen filaments as a scaffold for nerve regeneration. *J Biomed Mater Res* 2001; 56: 400-405.

[8]   Bryan DJ, Holway AH, Wang KK, Silva AE, Trantolo DJ, Wise D, Summerhayes IC. Influence of glial growth factor and Schwann cells in a bioresorbable guidance channel on peripheral nerve regeneration. *Tissue Eng* 2000; 6: 129-138.

[9]   Guénard V, Kleitman N, Morrissey TK, Bunge RP, Aebischer P. Syngeneic Schwann cells derived from adult nerves seeded in semipermeable guidance channels enhance peripheral nerve regeneration. *J Neurosci* 1992; 12: 3310-3320.

[10]   Keeley R, Atagi T, Sabelman E, Padilla J, Kadlcik P, Agras J, Eng L, Wiedman T-W, Nguyen K, Sudekum A, Rosen J. Synthetic nerve graft containing collagen and synthetic Schwann cells improves functional, electrophysiological, and histological parameters of peripheral nerve regeneration. *Restor Neurol Neurosci* 1993; 5: 353-366.

[11]   Kim DH, Connolly SE, Kline DG, Voorhies RM, Smith A, Powell M, Yoes T, Daniloff JK. Labeled Schwann cell transplants *versus* sural nerve grafts in nerve repair. *J Neurosurg* 1994; 80: 254-260.

[12]   Bryan DJ, Wang RR, Chakalis-Haley DP. Effect of Schwann cells in the enhancement of pheripheral-nerve regeneration. *J Recon Microsurg* 1996; 12: 439-446.

[13]   Ansellin AD, Fink T, Davey DF. Peripheral nerve regeneration through nerve guides seeded with adult Schwann cells. *Neuropathol Appl Neurobiol* 1997; 23: 387-398.

[14]   Rodriguez FJ, Verdu E, Ceballos D, Navarro X. Nerve guides seeded with autologous Schwann cells improve nerve regeneration. *Exp Neurol* 2000; 161: 571-584.

[15]   Terenghi G. Peripheral nerve injury and regeneration. *Histol Histopathol* 1995; 10: 709-718.

[16]   Son Y-J, Thompson WJ. Schwann cell processes guide regeneration of peripheral axons. *Neuron* 1995; 14: 125-132.

[17]   Fu SY, Gordon T. The cellular and molecular basis of peripheral nerve regeneration. *Mol Neurobiol* 1997; 14: 67-116.

[18]   Frostick SP, Yin Q, Kemp GJ. Schwann cells, neurotrophic factors, and peripheral nerve regeneration. *Microsurgery* 1998; 18: 397-405.

[19]   Pêgo AP, Poot AA, Grijpma DW, Feijen J. Copolymers of trimethylene carbonate and ε-caprolactone for porous nerve guides: synthesis and properties. *J Biomater Sci Polym Ed* 2001; 12: 35-53. Chapter 3 of this thesis.

[20]   Morrissey TK, Kleitman N, Bunge RP. Isolation and functional characterization of Schwann cells derived from adult peripheral nerve. *J Neurosci* 1991; 11: 2433-2442.

[21]   Hursh JB. Conduction velocity and diameter of nerve fibers. *Am J Physiol* 1939; 127: 131-139.

[22] Jack JJB, Noble D, Tsien RW, *Electric current flow in excitable cells*. Oxford: Oxford University Press; 1983.

[23] Chernousov MA, Carey DJ. Schwann cell extracellular matrix molecules and their receptors. *Histol Histopath* 2000; 15: 593-601.

[24] Aebischer P, Valentini RF, Winn SR, Kunz S, Sasken H, Galletti PM. Regeneration of transected sciatic nerves through semi-permeable nerve guidance channels. Effects of extracellular matrix protein additives. *ASAIO Trans* 1986; 32: 474-477.

[25] Valentini RF, Aebischer P, Winn SR, Galletti PM. Collagen- and laminin-containing gels impede peripheral nerve regeneration through semipermeable nerve guidance channels. *Exp Neurobiol* 1987; 98: 350-356.

[26] Labrador RO, Buti M, Navarro X. Influence of collagen and laminin gels concentration on nerve regeneration after resection and tube repair. *Exp Neurol* 1998; 149: 243-252.

[27] Baldwin SP, Krewson CE, Saltzman WM. PC12 cell aggregation and neurite growth in gels of collagen, laminin and fibronectin. *Int J Dev Neurosci* 1996; 14: 351-364.

[28] Labrador RO, Buti M, Navarro X. Peripheral-nerve repair - Role of agarose matrix density on functional recovery. *NeuroReport* 1995; 6: 2022-2026.

[29] Wells MR, Kraus K, Batter DK, Blunt DG, Weremowitz J, Lynch SE, Antoniades HN, Hansson H-A. Gel matrix vehicles for growth factor application in nerve gap injuries repaired with tubes: a comparison of Biomatrix, collagen, and methylcellulose. *Exp Neurol* 1997; 146: 395-402.

[30] Chen YS, Hsieh CL, Tsai CC, Chen TH, Cheng WC, Hu CL, Yao CH. Peripheral nerve regeneration using silicone rubber chambers filled with collagen, laminin and fibronectin. *Biomaterials* 2000; 21: 1541-1547.

[31] Ceballos D, Navarro X, Dubey N, Wendelschafer-Crabb G, Kennedy WR, Tranquillo RT. Magnetically aligned collagen gel filling a collagen nerve guide improves peripheral nerve regeneration. *Exp Neurol* 1999; 158: 290-300.

[32] Dubey N, Letourneau PC, Tranquillo RT. Guided neurite elongation and schwann cell invasion into magnetically aligned collagen in simulated peripheral nerve regeneration. *Exp Neurol* 1999; 158: 338-350.

[33] Wonder M, Shklyarevskiy IO, Dijkstra PJ, Poot AA, Rutten WLC, Feijen J. Orientation of collagen by exposure to high magnetic fields. Proceedings of the Dutch Annual Conference on Biomedical Engineering. Papendal, The Netherlands (2002), p. 155.

[34] Pêgo AP, Vleggeert-Lankamp CLAM, Deenen M, Lakke EAJF, Grijpma DW, Poot AA, Marani E, Feijen J. Adhesion and growth of human Schwann cells on trimethylene carbonate (co)polymers. *(submitted to J Biomed Mater Res, 2002)* Chapter 9 of this thesis.

PART IV

CONCLUDING REMARKS

"We have a habit in writing articles published in scientific journals to make the work as finished as possible, to cover all the tracks, to not worry about the blind alleys or to describe how you had the wrong idea first, and so on. So there isn't any place to publish, in a dignified manner, what you actually did in order to get to do the work, although, there has been in these days, some interest in this kind of thing."
Richard Feynman (1918-1988) - Nobel Lecture, 1966

Prospects

The main aim of this thesis was to develop biodegradable elastomeric porous structures for use as scaffolds in (soft) tissue engineering. Poly(1,3-trimethylene carbonate) (poly(TMC)), a rubbery polymer, was used as a starting point in the design of synthetic materials that can serve as a viable alternative to the most commonly used polymers in the field - poly(lactide), poly(glycolide) and their copolymers. In order to obtain materials with different mechanical properties and degradation rates, TMC has been copolymerized with either D,L-lactide (DLLA) or ε-caprolactone (CL).

The good physical, mechanical and degradation characteristics of these materials and their processablity into porous scaffolds, as well as their suitability for the culturing of different cell types, make TMC-based copolymers promising candidates for use in tissue engineering. However, several topics still need to be addressed along with the investigation of the potential use of these materials in other applications in medicine:

Polymers
- Determination of the (cyclic) creep behavior of the different copolymers of interest and respective scaffolds. This issue is of particular interest in applications where the scaffolds are subjected to long-term cyclic loading as in the case of heart tissue engineering. In engineering cardiac muscle, a porous structure is seeded with cardiac cells and the scaffold should not only sustain and recover from the contractions of the growing tissue but also of the surrounding myocardium after implantation.
- Determination of the effect of cross-linking on the *in vivo* degradation behavior of poly(TMC) networks.
- Investigation of the use of these materials for other soft tissue engineering applications where an elastomer is desirable, as for example in vascular tissue engineering.

Artificial Nerve Guides
- Improvement of the nerve guide design with optimization of the Schwann cell seeding procedure.

- Investigation of the nerve guide degradation profile *in situ*.

Cardiac Muscle Tissue Engineering
- Culture of cardiac cells on three-dimensional scaffolds based on a TMC-DLLA copolymer containing 20 mol% of TMC, both under static and dynamic conditions.
- Investigation of the effect of cardiac cell cultures on the degradation profile of the three-dimensional scaffolds based on a TMC-DLLA copolymer containing 20 mol% of TMC.

Summary

In the field of tissue engineering, the search for suitable materials for use in the preparation of scaffolds to host the developing tissue represents a major subject of study. Biodegradable materials show great potential in this area as, by resorbing upon performing their function, they obviate long-term biocompatibility concerns. The selection of synthetic, biodegradable polymers over natural materials, like collagen, is an attractive choice due to the controlled manner in which they can be manufactured and the possibility of tuning their macrostructure, mechanical properties and degradation profile. The most commonly used biodegradable polymers for implants in the biomedical field have been poly(lactide) (poly(LA)), poly(glycolide) (poly(GA)) and their copolymers. However, these can have important drawbacks for use in certain applications such as incompatible mechanical properties (stiffness and brittleness) and unsuitable degradation rates. When engineering tissues for soft-tissue applications, synthetic elastic scaffolds with tunable degradation properties are desirable. Such constructs should perform well under long-term cyclic deformation conditions. Degradation at a controlled rate to match cell and tissue growth *in vitro* and/or *in vivo* of such an elastic scaffold would provide the gradual substitution of the scaffold by the regenerated tissue.

In this work poly(1,3-trimethylene carbonate) (poly(TMC)) – a rubbery and amorphous polymer – has been taken as a starting point in the design of alternative synthetic polymers with tailor-made characteristics. It was the aim of this investigation to evaluate the potential of (co)polymers of TMC with either D,L-lactide (DLLA) or ε-caprolactone (CL) as degradable elastomers for soft tissue engineering applications. In particular we focused on the tissue engineering approach to correct peripheral nerve defects and to treat heart failure or heart defects. This alternative approach overcomes some of the pitfalls of the presently used clinical strategies to treat these conditions (**Chapter 2**). By copolymerization we expect to modulate the rates of polymer degradation as well as modify the physical properties of the material to suit the requirements for the preparation of scaffolds for cardiac muscle engineering and nerve regeneration (nerve guides).

The first experimental part of this work concerns the description of the synthesis and characterization of the different (co)polymers of TMC.

High molecular weight statistical (co)polymers ($\overline{M}n$ above 93,000) were prepared in the melt by ring-opening polymerization with stannous octoate (SnOct$_2$). In **Chapter 3** and **Chapter 5** the synthesis of TMC-CL and TMC-DLLA (co)polymers is described, respectively. The nature of the comonomer and the copolymer composition were found to have a significant effect on the thermal and mechanical properties of the copolymers. All TMC-CL copolymers are in the rubbery state at room temperature. At TMC contents higher than 25 mol% no crystallinity is detected. For these materials a decrease in crystallinity results in loss of strength and decrease in toughness. Amorphous poly(TMC), however, shows excellent ultimate mechanical properties due to strain-induced crystallization. In contrast, TMC-DLLA copolymers are amorphous over the entire range of compositions. The polymers vary from rubbers to stiff materials as the content of TMC decreases. Significant improvement of the mechanical performance of these high molecular weight materials was observed in comparison to that previously reported for TMC-DLLA copolymers of lower molecular weight. TMC-CL and TMC-DLLA copolymers are hydrophobic, showing very low equilibrium water absorption (<1.5 wt%).

The polymerization conditions were also found to have a pronounced effect on the microstructure and physical properties of TMC and CL copolymers (**Chapter 4**). Statistical copolymers of equimolar amounts of TMC and CL were synthesized in the presence of SnOct$_2$ (in the bulk at 80 and 130°C) and yttrium isopropoxide (in solution at room temperature and in the bulk at 80°C). Both catalysts yielded polymers with shorter average monomer sequence lengths at higher reaction temperatures. For the polymerizations with SnOct$_2$ a similar effect was observed when the reactions were allowed to proceed for longer periods of time, which points to the occurrence of transesterification reactions. Independent of the catalyst/initiator system, the copolymers prepared in the bulk at 80°C or 130°C are amorphous. The copolymer prepared in solution at room temperature with yttrium isopropoxide has a more blocky structure, with CL sequences long enough to crystallize. In accordance with its thermal behavior, the semi-crystalline copolymer is much stiffer and tougher than the amorphous copolymers prepared at higher temperatures.

The effect of comonomer type and copolymer composition on the *in vitro* hydrolytic degradation of selected TMC-CL and TMC-DLLA copolymers was also investigated. The degradation of melt-pressed copolymer films in phosphate buffered saline at pH 7.4 and 37°C has been followed for a period of over two years

(**Chapter 6**). The degradation profiles of TMC-DLLA and TMC-CL based copolymers are similar, being best described by autocatalyzed bulk hydrolysis, preferentially of ester bonds. The hydrolysis rates varied by 2 orders of magnitude, depending on polymer composition and physical characteristics at the degradation conditions. In two years poly(TMC) showed a negligible change in molecular weight and only a relatively small decrease in mechanical properties. Copolymers of TMC-DLLA can undergo complete degradation *in vitro*. Poly(DLLA) was resorbed in 2 years, while copolymers with 20 and 50 mol% of TMC were resorbed in less than a year. In contrast (semi-crystalline) TMC-CL copolymers degraded much slower. These materials maintained suitable mechanical properties for more than 1 year and no mass loss was observed for any of the TMC-CL (co)polymers during the study. For both series of copolymers an $\overline{M}_n$ of 25,000 was found to be a limiting value below which tensile properties are lost.

The degradation of poly(TMC-CL) (11:89 mol%), poly(TMC-DLLA) (48:52 mol%) and poly(TMC) were also evaluated *in vivo* upon subcutaneous implantation of polymers disks in a rat model (**Chapter 7**). While the degradation behavior of the copolymers was similar to that observed *in vitro*, poly(TMC) degraded much faster *in vivo* than *in vitro*. Only a few polymer particles could be detected extracellularly in the tissue after 3 weeks of implantation and histological evaluation showed that the polymer disks were resorbed totally in less than a year. The degradation of poly(TMC), from the early stages of implantation, was associated with infiltration of macrophages and formation of giant cells which were found to be involved in the phagocytosis of particles of the degrading implant. The evidence gathered in this study points to the conclusion that *in vivo*, poly(TMC) is degraded via surface erosion involving cellular activity. All three tested polymers were well tolerated by the tissue upon subcutaneous implantation.

Poly(TMC) has often been regarded as a rubbery polymer that can not be applied in the biomedical field due to its poor dimensional stability, tackiness and inadequate mechanical properties. In the present work we found evidence of the contrary (**Chapters 3, 5** and **6**). Very high molecular weight poly(TMC), besides being very flexible, is tough and shows rubber-like properties despite being totally amorphous and not cross-linked. The mechanical performance of poly(TMC) was found to be dependent on the molecular weight of the polymer (**Chapter 8**). An $\overline{M}_n$ of 100,000 was determined to be a critical value below which the polymer has negligible mechanical properties and poor dimensional stability. In view of the potential use of poly(TMC) based implants in the clinic, the possibility to sterilize the scaffolds by

means of a standard method has also been investigated. Poly(TMC) cross-links upon gamma-irradiation, resulting in the formation of an insoluble network. The extent of cross-linking was found to increase with the radiation dose. This can be highly advantageous as the mechanical properties of high molecular weight poly(TMC) rubbers were found to improve upon irradiation. Especially the creep resistance increased, enhancing the elastomeric character of the polymer.

When considering the preparation of nerve guides for nerve reconstruction, it is desirable that the conduits keep their shape and mechanical properties during the time required for nerve regeneration and maturation. Therefore, for the conduit preparation it is preferable to use slowly degrading materials, like the TMC and CL based (co)polymers, as in the clinical situation most often large nerve defects have to be corrected. Based on this selection, the next step was to evaluate how variations in the polymer composition affect the adhesion, proliferation and morphology of human Schwann cells (SCs) on TMC and CL (co)polymer substrates, with the final goal of using these materials in the preparation of artificial nerve grafts seeded with SCs (**Chapter 9**). These cells play a vital role in the natural nerve regeneration process, producing extracellular matrix proteins and a range of neurotropic and neurotrophic factors essential for neuron growth. The adhesion, proliferation and morphology of human SCs on copolymers containing 10 and 82 mol% of TMC and on the respective homopolymers were investigated. The results indicate that all tested materials support the adhesion and proliferation of human SCs, although cells adhered faster and in greater numbers on the (co)polymers with higher TMC content.

In the development of an effective artificial nerve graft, we proposed that the guide should have a two-ply structure. A microporous inner layer will serve as a barrier to minimize the ingrowth of fibrous scar tissue but still allowing the exchange of fluids. A macroporous outer layer can provide the nerve guide with dimensional stability, strength and toughness while allowing a good integration of the graft with the surrounding tissue. In a pilot study, poly(CL) was used as a model polymer to set-up the preparation methods of pliable, two-ply permeable conduits and to study the effect of the tube structure on their mechanical performance (**Appendix A**). Based on the developed procedures, two-ply tubes consisting of an inner layer based on poly(TMC) (a good substrate for SC adhesion) and an outer layer based on a copolymer of TMC and CL with 11 mol% of TMC (which combines adequate mechanical properties with reduced crystallinity in comparison to poly(CL)) were prepared (**Chapter 10**). A microporous inner layer was obtained by dip-coating

techniques used in combination with porosifying agents. A macroporous outer layer was prepared by winding of fibers spun from solution. The mechanical properties and the *in vivo* performance of these conduits in the correction of 6 mm defects in the rat sciatic nerve gap model were compared to two-ply tubes with a non-porous inner layer. Both two-ply nerve guides flex easily without kinking and showed excellent handling characteristics during surgery. Electrophysiological examinations revealed that the contact between the proximal and distal nerve ends was reestablished in both animal groups treated with the two-ply nerve guides. But no clear effect, in terms of electrophysiological properties, was detected on the outcome of the nerve regeneration process when nerve conduits with a microporous inner layer were used instead of a non-porous layer. The nerve fibers regenerated through the artificial grafts showed mean conduction velocities similar to nerve fibers regenerated through autografts (the use of which is regarded as the "gold standard" for the repair of large peripheral nerve lesions). The results seem promising, but other electrophysiological properties of nerve fibers regenerated through autografts were still better than those of axons regenerated through the artificial nerve guides.

The first attempts to improve the performance of the developed nerve guides are described in **Appendix B**. In that study the effect on the enhancement of nerve regeneration and functional recovery of heterologous SCs seeded in a gel consisting of a mixture of laminin, fibronectin and collagen type I incorporated in the previously developed nerve guides was evaluated. No evident improvement was observed when the poly(TMC-CL) copolymer based nerve guides were supplemented with rat SCs seeded in the selected protein-based gel matrix. The poor results obtained appear to be related to the characteristics of the protein-based three-dimensional matrix and not to a detrimental effect of the seeded rat SCs. The importance of the gel composition on the regeneration outcome has been addressed.

As mentioned above, TMC-DLLA copolymers were found to degrade faster than TMC-CL copolymers. They can be totally resorbed in approximately one year, fitting the requirements for the preparation of scaffolds for heart tissue engineering better than TMC-CL copolymers. Biodegradable porous scaffolds for heart tissue engineering were prepared from amorphous elastomeric copolymers of TMC and DLLA (**Chapter 11**). Leaching of salt from compression-molded polymer/salt composites allowed the preparation of highly porous structures in a reproducible fashion. The thermal properties of the polymers used for the scaffold preparation proved to have a strong effect on the morphology, mechanical properties and

dimensional stability of the scaffolds at physiological conditions. Interconnected highly porous structures based on a TMC-DLLA copolymer with 19 mol% TMC showed the most suitable mechanical properties and displayed adequate cell-material interactions to serve as a scaffold for cardiac muscle cells. Such scaffolds are dimensionally stable under physiological conditions and their *in vitro* degradation behavior is similar to that of non-porous films with similar composition.

The research conducted in this thesis showed promising results allowing to speculate that the use of TMC-based materials may find wide application in (soft) tissue engineering as well as in other biomedical applications. Many questions still need to be addressed though. These and future lines of research are addressed in the last section of this thesis - **Prospects**.

Samenvatting

Tissue engineering is een betrekkelijk nieuwe technologie, die gebruik maakt van medische, biologische en materiaalkundige principes in de (re)generatie van nieuw, functioneel weefsel. Een belangrijk onderzoeksgebied in *tissue engineering* is de ontwikkeling van geschikte materialen, die gebruikt kunnen worden in de vervaardiging van dragers voor de uitgroei van cellen tot nieuw weefsel. Biodegradeerbare materialen zijn veelbelovend, aangezien ze zorgen over de biocompatibiliteit op lange termijn wegnemen. De keuze van synthetische, biodegradeerbare polymeren in plaats van natuurlijke materialen (zoals collageen) is een aantrekkelijke, gezien de gecontroleerde manier waarop ze gemaakt kunnen worden en de mogelijkheid tot het sturen van hun macrostructuur, mechanische eigenschappen en afbraakprofiel. De meest gebruikte biodegradeerbare polymeren voor biomedische implantaten zijn poly(lactide) (poly(LA)), poly(glycolide) (poly(GA)) en hun copolymeren. Zij kunnen echter belangrijke nadelen hebben bij bepaalde toepassingen, zoals niet-compatibele mechanische eigenschappen (stijfheid en brosheid) en degradatiesnelheid. Voor het maken van zachte weefsels zijn synthetische, elastische dragers met controleerbare degradatie-eigenschappen gewenst. Zulke dragers moeten bestand zijn tegen condities van langdurige cyclische deformatie. Gecontroleerde afbraak van zulke elastische dragers, die overeenkomt met de snelheid van cel- en weefselingroei *in vitro* en/of *in vivo*, zou moeten zorgen voor een geleidelijke vervanging van de drager door nieuw geregenereerd weefsel.

In dit proefschrift is poly(1,3-trimethyleen carbonaat) (poly(TMC)) – een rubberachtig en amorf polymeer – als uitgangspunt genomen in het ontwerp van alternatieve synthetische polymeren met de gewenste karakteristieken. Het doel van dit onderzoek is de evaluatie van (co)polymeren van TMC met of D,L-lactide (DLLA) of ε-caprolacton (CL) als afbreekbare elastomeren voor toepassing in de (re)generatie van zachte weefsels. In het bijzonder hebben wij ons gericht op het herstellen van perifere zenuwdefecten en de behandeling van hartfalen of hartdefecten middels *tissue engineering*. Deze alternatieve benadering vermijdt een aantal problemen van de hedendaagse klinische behandelingen (**Hoofdstuk 2**). Door copolymerisatie verwachten wij de afbraaksnelheid van het polymeer te reguleren en de fysische eigenschappen aan te passen aan de eisen, die gesteld

worden aan dragers in *tissue engineering* van hartweefsel en zenuwregeneratie (zenuwgeleiders).

Het eerste experimentele deel van dit werk richt zich op de synthese en karakterisering van verscheidene (co)polymeren van TMC. Statistische (co)polymeren van hoog moleculair gewicht ($\overline{M}_n$ >93,000) zijn in de smelt gemaakt door ringopeningspolymerisatie met tin(II)octoaat (SnOct$_2$). In **Hoofdstuk 3** en in **Hoofdstuk 5** zijn de syntheses van TMC-CL en TMC-DLLA (co)polymeren respectievelijk beschreven. De aard van het comonomeer en de copolymeersamenstelling blijken een belangrijke invloed te hebben op de thermische en mechanische eigenschappen van de copolymeren. Bij kamertemperatuur zijn alle TMC-CL copolymeren rubberachtig. Bij TMC gehaltes hoger dan 25 mol% is geen kristalliniteit waargenomen. Voor deze materialen resulteert een afname in kristalliniteit in een verlies van sterkte en een afname in de taaiheid. Amorf poly(TMC) daarentegen vertoont uitstekende mechanische eigenschappen door rek-geïnduceerde kristallisatie. TMC-DLLA copolymeren daarentegen zijn over de hele reeks van samenstellingen amorf. De materialen variëren van rubbers tot stijve glasachtige materialen met afnemend TMC gehalte. In vergelijking met eerder gerapporteerde resultaten van TMC-DLLA copolymeren van lager molgewicht, nemen wij een aanzienlijke verbetering van de mechanische eigenschappen van hoogmoleculaire materialen waar. TMC-CL en TMC-DLLA copolymeren zijn hydrofoob met een zeer lage waterabsorptie (<1.5 wt%).

De polymerisatieomstandigheden hebben eveneens een sterke invloed op de microstructuur en fysische eigenschappen van TMC en CL copolymeren (**Hoofdstuk 4**). Statistische copolymeren van equimolaire hoeveelheden TMC en CL zijn gesynthetiseerd in aanwezigheid van SnOct$_2$ (in bulk bij 80 en 130 °C) en yttriumisopropoxide (in oplossing bij kamertemperatuur en in bulk bij 80 °C). Beide katalysatoren leveren polymeren met kortere gemiddelde monomeersequentie-lengtes bij hogere reactietemperaturen. Voor polymerisaties met SnOct$_2$ is een vergelijkbaar effect waargenomen wanneer de reacties werden uitgevoerd over een langere tijdsduur, hetgeen wijst op het optreden van transesterificatiereacties. Onafhankelijk van het gebruikte katalysator/initiator systeem zijn alle copolymeren, gemaakt in bulk bij 80 of 130 °C, amorf. Het copolymeer gemaakt in oplossing bij kamertemperatuur met yttriumisopropoxide heeft een meer blokachtige structuur, met CL sequenties die lang genoeg zijn om te kristalliseren. In overeenstemming met zijn thermisch gedrag is dit semi-kristallijne copolymeer veel stijver en taaier dan de amorfe copolymeren gemaakt bij hogere temperaturen.

Het effect van comonomeertype en copolymeersamenstelling op de *in vitro* hydrolytische afbraak van geselecteerde TMC-CL en TMC-DLLA copolymeren is eveneens onderzocht. De degradatie van geperste copolymeerfilms in fosfaat-gebufferde zoutoplossing bij pH 7.4 en 37°C is onderzocht gedurende een periode van twee jaar (**Hoofdstuk 6**). De afbraakprofielen van TMC-DLLA en TMC-CL copolymeren zijn vergelijkbaar en kunnen het best beschreven worden door autogekatalyseerde bulkhydrolyse, bij voorkeur van de esterbindingen. Afhankelijk van de polymeersamenstelling en de fysische eigenschappen bij de degradatieomstandigheden variëren de hydrolysesnelheden twee ordegroottes. Poly(TMC) vertoonde gedurende twee jaar slechts een verwaarloosbare verandering in molgewicht en een relatief kleine afname van de mechanische eigenschappen. Copolymeren van TMC-DLLA kunnen volledige afbraak *in vitro* ondergaan. In twee jaar was poly(DLLA) geresorbeerd, terwijl copolymeren met 20 en 50 mol% TMC in minder dan een jaar geresorbeerd waren. (Semi-kristallijne) TMC-CL copolymeren daarentegen degradeerden veel langzamer. Deze materialen behielden geschikte mechanische eigenschappen gedurende meer dan één jaar. Voor alle TMC-CL (co)polymeren is gedurende één jaar geen massaverlies waargenomen. Voor beide series copolymeren is waargenomen dat een $\overline{M}_n$ van 25,000 een grenswaarde is, waaronder de mechanische eigenschappen verloren gaan.

De afbraak van poly(TMC-CL) (11:89 mol%), poly(TMC-DLLA) (48:52 mol%) en poly(TMC) is ook *in vivo* geëvalueerd door middel van subcutane implantaties van polymeerschijfjes in ratten (**Hoofdstuk 7**). Het degradatiegedrag van de copolymeren was vergelijkbaar met dat *in vitro*, poly(TMC) daarentegen brak sneller af *in vivo* dan *in vitro*. Slechts enkele polymeerdeeltjes konden na drie weken implantatie extracellulair in het weefsel worden waargenomen. Histologische evaluatie toonde dat de polymeerschijfjes volledig geresorbeerd waren in minder dan een jaar. Vanaf de eerste stadia van implantatie ging de degradatie van poly(TMC) gepaard met infiltratie van macrofagen en vorming van reuzencellen, welke betrokken waren bij de fagocytose van deeltjes van het degraderende implantaat. De in deze studie verkregen bewijzen ondersteunen de conclusie dat *in vivo*, poly(TMC) afbreekt via oppervlakte-erosie, waarbij cellulaire activiteit betrokken is. Alle drie de geteste polymeren werden tijdens subcutane implantatie goed verdragen door het weefsel.

Poly(TMC) is vaak beschouwd als een rubberachtig polymeer, dat vanwege zijn slechte stabiliteit, kleverigheid en onvoldoende mechanische eigenschappen niet toegepast kan worden in het biomedische veld. In dit proefschrift hebben we bewijs

gevonden van het tegenovergestelde (**Hoofdstuk 3,5** en **6**). Poly(TMC) van zeer hoog molgewicht is, behalve flexibel, ook taai en vertoont rubberachtige eigenschappen, ondanks het feit dat het volledig amorf en niet vernet is. Het is gebleken dat de mechanische eigenschappen van poly(TMC) afhankelijk zijn van het molgewicht van het polymeer (**Hoofdstuk 8**). Een $\overline{M}_n$ van 100,000 is de grenswaarde waaronder het polymeer te verwaarlozen mechanische eigenschappen en slechte stabiliteit heeft. Met het oog op het potentiële gebruik van op poly(TMC) gebaseerde implantaten in het ziekenhuis, is de mogelijkheid tot sterilisatie door middel van een standaardsterilisatiemethode onderzocht. Poly(TMC) vernet onder invloed van gammastraling, waarbij een onoplosbaar netwerk wordt gevormd. De mate van vernetting blijkt toe te nemen met de stralingsdosis. Dit kan grote voordelen hebben, aangezien de mechanische eigenschappen van poly(TMC) rubbers van hoog molgewicht verbeterden onder invloed van straling. Met name de weerstand tegen kruip nam toe, waarbij het elastomere karakter van het polymeer versterkt werd.

In de fabricage van zenuwgeleiders voor het herstel van zenuwen is het wenselijk, dat de geleiders hun vorm en mechanische eigenschappen behouden gedurende de tijd, die nodig is voor zenuwregeneratie en –ontwikkeling. Aangezien in de klinische situatie meestal grote zenuwdefecten hersteld moeten worden, is het wenselijk in de vervaardiging van de geleider langzaam afbrekende materialen, als TMC en CL (co)polymeren te gebruiken. Gebaseerd op deze selectie was de volgende stap na te gaan hoe de polymeersamenstelling de adhesie, proliferatie en morfologie van humane Schwanncellen op TMC en CL (co)polymeersubstraten beïnvloedt. Het uiteindelijke doel is het gebruik van deze materialen in de vervaardiging van kunstmatige zenuwgeleiders gezaaid met Schwanncellen (**Hoofdstuk 9**). Deze cellen spelen een essentiële rol in het natuurlijke zenuwregeneratieproces, zij produceren extracellulaire matrixeiwitten en een reeks neurotrope en neurotrofe factoren, die essentieel zijn voor de groei van neuronen. De adhesie, proliferatie en morfologie van humane Schwanncellen op copolymeren met 10 en 82 mol% TMC en op de respectievelijke homopolymeren is onderzocht. De resultaten tonen dat alle onderzochte materialen de adhesie en proliferatie van humane Schwanncellen ondersteunen, hoewel de cellen sneller hechtten en in grotere aantallen op de (co)polymeren met een hoger TMC-gehalte.

In de ontwikkeling van een effectieve, kunstmatige zenuwgeleider, zullen wij een geleider bestaande uit twee lagen gebruiken. Een microporeuze binnenlaag zal dienst doen als barrière om de ingroei van fibreus littekenweefsel te minimaliseren,

waarbij de uitwisseling van vloeistoffen nog steeds mogelijk is. Een macroporeuze buitenlaag kan de zenuwgeleider stabiliteit, sterkte en taaiheid geven, terwijl het een goede integratie met het omliggende weefsel toestaat. In een proefstudie is poly(CL) als modelpolymeer gebruikt om de vervaardigingsmethoden van dergelijke buigzame, tweelagige, doorlaatbare geleiders te ontwikkelen en om het effect van de geleiderstructuur op de mechanische eigenschappen te bestuderen (**Appendix A**). Op basis van de ontwikkelde methoden zijn tweelagige buisjes, bestaande uit een binnenste laag op basis van poly(TMC) (een goed substraat voor Schwannceladhesie) en een buitenste laag op basis van een copolymeer van TMC en CL met 11 mol% TMC (vanwege de goede mechanische eigenschappen en gereduceerde kristalliniteit in vergelijking met poly(CL)) vervaardigd (**Hoofdstuk 10**). Een microporeuze binnenlaag is verkregen door dip-coating technieken in combinatie met water oplosbare kristallen, waarmee poriën gemaakt kunnen worden. Een macroporeuze buitenlaag is vervaardigd door het wikkelen van oplossing-gesponnen vezels. De mechanische eigenschappen en de *in vivo* eigenschappen van deze geleiders in het herstel van een 6 mm defect in de sciatische zenuw van de rat is vergeleken met tweelagige buisjes met een niet-poreuze binnenkant. Beide zenuwgeleiders buigen makkelijk zonder te knikken en hebben een uitstekende hanteerbaarheid voor gebruik in operaties. Elektrofysiologisch onderzoek liet zien dat het contact tussen de proximale en distale zenuweinden in beide behandelde groepen hersteld werd. In termen van elektrofysiologische eigenschappen werd geen duidelijk effect waargenomen op het uiteindelijke zenuwregeneratieproces, wanneer zenuwgeleiders met een microporeuze binnenlaag gebruikt werden in plaats van geleiders met een niet-poreuze binnenlaag. De zenuwvezels, die hersteld werden door de kunstmatige zenuwgeleider, hadden gemiddelde geleidbaarheidsnelheden die vergelijkbaar waren met zenuwvezels hersteld door autotransplantatie (een methode die gezien wordt als de gouden standaard voor het herstel van grote perifere zenuwbeschadigingen). De resultaten lijken veelbelovend, maar andere elektrofysiologische eigenschappen van zenuwvezels hersteld door autotransplantatie, waren nog steeds beter dan voor de axonen hersteld door kunstmatige zenuwgeleiders.

Eerste pogingen tot verbetering van de functie van de ontwikkelde zenuwgeleiders staan beschreven in **Appendix B**. In deze studie is het effect van zaaien van heterologe Schwanncellen in een gel bestaande uit een mengsel van laminine, fibronectine en collageen type I onderzocht. Deze gel werd ingebracht in de eerder

ontwikkelde en geteste zenuwgeleiders. Geen duidelijke verbetering werd waargenomen toen de op poly(TMC-CL) gebaseerde zenuwgeleiders, voorzien van de gekozen gelmatrix, gezaaid werden met ratten-Schwanncellen. De magere resultaten lijken verband te hebben met de eigenschappen van de driedimensionale eiwitmatrix en niet met een nadelig effect van de gezaaide ratten-Schwanncellen. Het belang van de gelsamenstelling op het uiteindelijke herstel is besproken.

Zoals eerder vermeld, blijken TMC-DLLA copolymeren sneller te degraderen dan TMC-CL copolymeren. Zij kunnen volledig geresorbeerd worden in ongeveer één jaar, waarmee ze beter voldoen aan de eisen die gesteld worden aan *tissue engineering* van hartweefsel dan de TMC-CL copolymeren. Bioafbreekbare poreuze dragers voor het maken van hartweefsel zijn gemaakt van amorfe, elastomere copolymeren van TMC en DLLA (**Hoofdstuk 11**). Het uitlogen van zout uit de geperste polymeer/zout composieten maakt het mogelijk om hoog poreuze structuren op een reproduceerbare manier te maken. De thermische eigenschappen van de polymeren, gebruikt voor de vervaardiging van de dragers, blijkt een sterke invloed te hebben op de morfologie, mechanische eigenschappen en stabiliteit van de dragers onder fysiologische omstandigheden. Doorverbonden hoog poreuze structuren op basis van een TMC-DLLA copolymeer met 19 mol% TMC hebben de meest geschikte mechanische eigenschappen en bleken goede cel-materiaal interacties te vertonen om te dienen als drager voor hartcellen. Deze dragers zijn stabiel onder fysiologische omstandigheden en hun degradatiegedrag is vergelijkbaar met die van niet-poreuze films van vergelijkbare samenstelling.

Het onderzoek beschreven in dit proefschrift toont veelbelovende resultaten. Het gebruik van materialen op basis van TMC vindt mogelijk brede toepassing in de *tissue engineering* van zachte weefsels, alsook in andere biomedische toepassingen. Vele vragen dienen echter nog beantwoord te worden. Huidige en toekomstige onderzoekslijnen worden besproken in het laatste deel van dit proefschrift – **Vooruitzichten**.

Curriculum Vitae

Ana Paula Pêgo was born on the 30th of September 1973 in Porto, Portugal. In 1991 she graduated in the field of Natural Sciences at the high school *Garcia de Orta* in Porto. In the same year she started her studies in Food Engineering at the Biotechnology School of the Portuguese Catholic University. During the last year of her studies she spent six months at the Chemistry and Biochemistry Engineering Department of the University of Maryland - Baltimore County, USA, where she was involved in a project of purification of proteins produced by bacteria fermentation. In 1996 she obtained her engineering degree with honors, receiving the Portuguese Engineering Association Award for the highest classification in Food Engineering studies for the year of 1996. During 1997 she worked as research assistant at the *Centro de Estudos de Paramiloidose* of the *Santo António* Hospital in Porto, in a project involving the production of recombinant proteins by yeast fermentation. In February 1998 she joined the Polymer Chemistry and Biomaterials Group at the University of Twente, The Netherlands as a Ph.D. student. The results of her research are described in this thesis.